


**Physiochemical Characterization of  
Phosphatidylinositol-4,5-Bisphosphate and its Interaction  
with PTEN-Long**

A dissertation submitted to  
the faculty of the  
Worcester Polytechnic Institute  
in partial fulfillment of the requirements for the  
Degree of Doctor of Philosophy  
in  
Biochemistry  
by  
Anne-Marie Bryant

November 6, 2019

© Copyright

All rights reserved



Physiochemical Characterization of Phosphatidylinositol-4,5-Bisphosphate  
and its Interaction with PTEN-Long

by

Anne-Marie Bryant

A Dissertation

Submitted to the Faculty

of the

WORCESTER POLYTECHNIC INSTITUTE

in partial fulfillment of the requirements for the

Degree of Doctor of Philosophy

in

Biochemistry

APPROVED:

\_\_\_\_\_ Arne Gericke, PI, WPI CBC Department Head

\_\_\_\_\_ Alonzo Ross, Co-PI, WPI CBC Department

\_\_\_\_\_ Joseph Duffy, WPI BBT Department Head

\_\_\_\_\_ Carissa Olsen, WPI Assistant Professor

## Table of Contents

List of Figures.....	7
List of Tables .....	11
Dissertation Summary .....	13
1. Chapter 1: Introduction .....	19
1.1 Importance of Lipids in the Biological Membrane .....	19
1.2 Phosphoinositides Provide Spatiotemporal Control of Signaling Events .....	21
1.3 Phosphoinositide Cluster Formation.....	25
1.4 Cellular Evidence of Phosphoinositide Cluster Formation.....	27
1.5 Physical Basis For Phosphoinositide Cluster Formation .....	28
1.6 Phosphoinositide Clustering in PI3K Pathway .....	34
1. Chapter 2: Methodologies & Techniques .....	37
1.7 Lipid Sample Preparation .....	37
1.8 Buffer Preparation.....	37
1.9 Phosphate Assay.....	38
1.10 Thin Layer Chromatography (TLC) .....	39
1.11 Dynamic Light Scattering (DLS).....	39
1.12 Synthesis of Bis(cyclohexylamine) Monomethyl Phosphate .....	40
1.13 Infrared Spectroscopy of Monomethyl Phosphate Methodology .....	40
1.14 Langmuir Trough Experiments.....	41
1.1.1 Principle of Langmuir Trough Monolayer Technique.....	41
1.1.2 Experimental Procedure of Langmuir Trough Experiments .....	46

<b>1.15</b>	<b>Attenuated Total Reflection (ATR) Fourier Transform Infrared (FTIR)</b>	
	<b>Spectroscopy .....</b>	<b>47</b>
<b>1.1.3</b>	<b>Experimental Procedure for ATR-FTIR .....</b>	<b>50</b>
<b>1.16</b>	<b>Protein Purification Methodology .....</b>	<b>51</b>
<b>1.1.4</b>	<b>Amplification of the Alternative Translated Region (ATR) peptide of PTEN-L..</b>	<b>51</b>
<b>1.1.5</b>	<b>Cloning ATR-Domain of PTEN-L into pET30b Vector .....</b>	<b>52</b>
<b>1.1.6</b>	<b>Transformation of ATR/pET30b into BL21 DE3 pLys Competent Cells .....</b>	<b>55</b>
<b>1.1.7</b>	<b>ATR/pET30b in <i>Escherichia coli</i> Shaker Flask Expression.....</b>	<b>55</b>
<b>1.1.8</b>	<b>ATR-Domain of PTEN/pET30b in <i>Escherichia coli</i> Bioreactor Expression .....</b>	<b>57</b>
<b>1.1.9</b>	<b>Purification of ATR/pET30b .....</b>	<b>59</b>
<b>1.1.10</b>	<b>Analysis of ATR-Domain Purity, Concentration, and Aggregation .....</b>	<b>61</b>
<b>2.</b>	<b>Chapter 3: The Effects of Cations on PI(4,5)P<sub>2</sub> Clustering .....</b>	<b>64</b>
<b>1.17</b>	<b>Introduction.....</b>	<b>64</b>
<b>1.18</b>	<b>Results:.....</b>	<b>70</b>
<b>2.1.1</b>	<b>Monomethyl Phosphate Interaction with Ca<sup>2+</sup> and K<sup>+</sup>.....</b>	<b>70</b>
<b>2.1.2</b>	<b>Investigating the Role of Calcium on PI(4,5)P<sub>2</sub> Clustering in Langmuir Films....</b>	<b>74</b>
<b>2.1.3</b>	<b>Investigating the Role of Physiological Calcium Concentrations on PI(4,5)P<sub>2</sub></b>	
	<b>Clustering in Langmuir Films .....</b>	<b>79</b>
<b>2.1.4</b>	<b>Investigating the Role of Cations on PI(4,5)P<sub>2</sub> Clustering in Langmuir Films.....</b>	<b>83</b>
<b>2.1.5</b>	<b>The Synergistic Cation Effects on PI(4,5)P<sub>2</sub> Clustering in Langmuir Monolayers</b>	
	<b>89</b>	
<b>1.19</b>	<b>Conclusion: .....</b>	<b>93</b>
<b>3.</b>	<b>Chapter 4: Role of Cholesterol in PI(4,5)P<sub>2</sub> Cluster Formation.....</b>	<b>95</b>

1.20	Introduction.....	95
1.21	Results:.....	98
3.1.1	Effects of cholesterol on PI(4,5)P <sub>2</sub> clustering .....	98
1.22	Conclusion .....	106
4.	Chapter 5: The Effect of Calcium on Mixed PI/ PI(4,5)P <sub>2</sub> and PS/ PI(4,5)P <sub>2</sub> Langmuir Films .....	108
1.23	Introduction: .....	108
1.24	Results:.....	111
4.1.1	The Effect of Ca <sup>2+</sup> on Individual PI or PS $\pi$ /A-Isotherms .....	111
4.1.2	Effect of Ca <sup>2+</sup> on Mixed PI/ PI(4,5)P <sub>2</sub> .....	116
4.1.3	Effect of Ca <sup>2+</sup> on Mixed PS/ PI(4,5)P <sub>2</sub> .....	119
4.1.4	Comparing PI and PS interaction with PI(4,5)P <sub>2</sub> .....	122
1.25	Conclusion .....	126
5.	Chapter 6: ATR-Domain of PTEN-Long Membrane Binding Preferences .....	128
1.26	Introduction.....	128
1.27	Results:.....	132
5.1.1	ATR-Domain Protein Expression and Purification.....	132
5.1.2	Investigation of ATR-Domain Secondary Structure .....	133
5.1.3	Investigation of ATR-Domain Lipid Binding Preferences.....	137
5.1.4	Investigation of the Effect of ATR-Domain on Membrane Integrity.....	145
1.28	Conclusion: .....	148
6.	Chapter 7: Summation of Dissertation .....	150
1.29	Discussion.....	150

<b>1.30</b>	<b>Future Work.....</b>	<b>155</b>
<b>7.</b>	<b>References.....</b>	<b>157</b>

## List of Figures

Figure 1. Aims to Understand Factors that Affect Phosphoinositide Clustering. ....	18
Figure 2. The Composition of Lipids in the Plasma Membrane. ....	19
Figure 3: The Fluid-Mosaic Model of the Plasma Membrane. ....	20
Figure 4. Chemical Structures of 7 Naturally Occurring Members of the Phosphoinositide Family. ....	22
Figure 6. PI(4,5)P <sub>2</sub> H-Bond Network .....	32
Figure 7. Spatiotemporal Activation in the PI3K/Akt Signaling Pathway. ....	35
Figure 12. Schematic of a Langmuir Trough. ....	43
Figure 13. Schematic Representation of Surface Pressure/Area Isotherm. ....	45
Figure 14. Schematic Diagram of Attenuated Total Reflectance Accessory. ....	48
Figure 15. Flow-Chart of Plasmid Purification for ATR Domain. ....	53
Figure 16. BLAST Sequence Alignment of ATR-Domain .....	54
Figure 17. Flow-Chart of Tested Conditions for ATR Domain Expression. ....	56
Figure 18. Upscale of ATR-domain Expression in 10-L Biofermentor. ....	58
Figure 19. Biofermentor Run Data Analysis. ....	58
Figure 20. Flow-Chart of ATR Domain Column Chromatography Purification Conditions. ....	59
Figure 22. LC-MS/MS Results Confirming ATR-Domain Amino Acid Identity. ....	62
Figure 21. A.) Western Blot and B.) SDS-PAGE of ATR-Domain. ....	62
Figure 23. Chemical Structure of Phosphatidylinositol-4,5-bisphosphate [PI(4,5)P <sub>2</sub> ]. ....	65
Figure 24 : Structure of the monomethyl phosphate dianion (MMP <sup>2-</sup> ). ....	70

<b>Figure 25 : Spectra for monomethyl phosphate in the pH range 1.5–10.0.....</b>	<b>71</b>
<b>Figure 26 : Infrared spectra of MMP<sub>2</sub>- in the presence of K<sup>+</sup> (2.5 M) with increasing [Ca<sub>2+</sub>].</b>	
.....	<b>72</b>
<b>Figure 27. PI(4,5)P<sub>2</sub> <math>\pi</math>/A-Isotherm in the Presence of High Molar Concentration of</b>	
<b>Calcium .....</b>	<b>75</b>
<b>Figure 28. Comparing PI(4,5)P<sub>2</sub> <math>\pi</math>/A-Isotherm in the Presence of Several Calcium</b>	
<b>Concentrations. ....</b>	<b>77</b>
<b>Figure 29. PI(4,5)P<sub>2</sub> <math>\pi</math>/A-Isotherm in the Presence of Various Calcium Concentrations. .</b>	<b>78</b>
<b>Figure 30. PI(4,5)P<sub>2</sub> <math>\pi</math>/A-Isotherm in the Presence of Low Molar Calcium Concentrations.</b>	
.....	<b>81</b>
<b>Figure 31. Structural Model Depicting Ca<sub>2+</sub> Interaction with PI(4,5)P<sub>2</sub> Monolayers .....</b>	<b>82</b>
<b>Figure 32. PI(4,5)P<sub>2</sub> <math>\pi</math>/A-Isotherm in the Presence of Sodium. ....</b>	<b>84</b>
<b>Figure 33. PI(4,5)P<sub>2</sub> <math>\pi</math>/A-Isotherm in the Presence of Potassium.....</b>	<b>85</b>
<b>Figure 34. Comparing the Specific Ion Effect on PI(4,5)P<sub>2</sub> <math>\pi</math>/A-Isotherm Behavior.....</b>	<b>86</b>
<b>Figure 35. Structural Model Depicting Na<sup>+</sup> (A) &amp; K<sup>+</sup> Interaction with PI(4,5)P<sub>2</sub> Monolayers</b>	
.....	<b>88</b>
<b>Figure 36. The Synergistic Effects of Ca<sub>2+</sub>, Na<sup>+</sup>, K<sup>+</sup> on PI(4,5)P<sub>2</sub> <math>\pi</math>/A-Isotherm at Bulk</b>	
<b>375mM. ....</b>	<b>90</b>
<b>Figure 37. The Synergistic Effects of Ca<sub>2+</sub>, Na<sup>+</sup>, K<sup>+</sup> on PI(4,5)P<sub>2</sub> <math>\pi</math>/A-Isotherm at Bulk</b>	
<b>200mM (A) and 125mM (B). ....</b>	<b>92</b>
<b>Figure 38. PI(4,5)P<sub>2</sub> <math>\pi</math>/A-Isotherm in the Presence of High Molar Concentration of</b>	
<b>Calcium .....</b>	<b>100</b>



<b>Figure 39. PI(4,5)P<sub>2</sub> <math>\pi</math>/A-Isotherm in the Presence of High Molar Concentration of Sodium. ....</b>	<b>102</b>
<b>Figure 40. PI(4,5)P<sub>2</sub> <math>\pi</math>/A-Isotherm in the Presence of High Molar Concentration of Potassium.....</b>	<b>103</b>
<b>Figure 41. Comparing 125mM PI(4,5)P<sub>2</sub> <math>\pi</math>/A-Isotherm with Calcium (A), Sodium (B), or Potassium (C) in the Presence and Absence of Cholesterol. ....</b>	<b>105</b>
<b>Figure 42. Model of Cholesterol Participating in PI(4,5)P<sub>2</sub> Hydrogen Bond Network. ....</b>	<b>107</b>
<b>Figure 43. PI <math>\pi</math>/A-Isotherm in the Presence of Low Molar Calcium Concentrations. ....</b>	<b>112</b>
<b>Figure 44. POPS <math>\pi</math>/A-Isotherm in the Presence of Low Molar Calcium Concentrations. ....</b>	<b>113</b>
<b>Figure 45. Structural Model of A.) PI interaction with Ca<sub>2+</sub> and B.)PS Interaction with Ca<sub>2+</sub>.....</b>	<b>115</b>
<b>Figure 46. Surface <math>\pi</math>/A-Isotherm of Mixed PI:PI(4,5)P<sub>2</sub> Monolayers at a 1:1 Ratio in the Presence of Low Molar Calcium Concentrations. ....</b>	<b>116</b>
<b>Figure 47. Surface <math>\pi</math>/A-Isotherm of Mixed PI:PI(4,5)P<sub>2</sub> Monolayers at a 2:1 Ratio in the Presence of Low Molar Calcium Concentrations. ....</b>	<b>117</b>
<b>Figure 48. Surface <math>\pi</math>/A-Isotherm of Mixed PS:PI(4,5)P<sub>2</sub> Monolayers at a 1:1 Ratio in the Presence of Low Molar Calcium Concentrations. ....</b>	<b>120</b>
<b>Figure 49. Structural Model of A.) PI interaction with PI(4,5)P<sub>2</sub> and B.)PS Interaction with PI(4,5)P<sub>2</sub>.....</b>	<b>121</b>
<b>Figure 50. Comparison of Surface <math>\pi</math>/A-Isotherm of PI and PS Monolayers in the Presence of Low Molar Calcium Concentrations. ....</b>	<b>123</b>
<b>Figure 51. Comparison of Surface <math>\pi</math>/A-Isotherm of PI or PS with PI(4,5)P<sub>2</sub> Monolayers in the Presence of Low Molar Calcium Concentrations.....</b>	<b>125</b>

<b>Figure 52. Schematic Representation of PTEN-L Protein Domains.....</b>	<b>129</b>
<b>Figure 53. Upscaled Expression of ATR-Domain in Biofermentor.....</b>	<b>132</b>
<b>Figure 54. CD spectra of the ATR-Domain.....</b>	<b>134</b>
<b>Figure 55. IR spectrum of the ATR-Domain.....</b>	<b>134</b>
<b>Figure 56. ATR Domain Sequence (A) and Amino Acid Distribution (B). .....</b>	<b>135</b>
<b>Figure 57. Thermal Denaturation (A) and Thermal Renaturation (B) CD Spectra for ATR-Domain .....</b>	<b>136</b>
<b>Figure 59. IR spectra of ATR-Domain in the Presence of 5% PI(4,5)P<sub>2</sub> Vesicles.....</b>	<b>138</b>
<b>Figure 58. Avanti Inositol Snoopers® were used to preliminarily investigate ATR-Domain Interactions with 13 Different Lipids Species. ....</b>	<b>138</b>
<b>Figure 60. IR spectra of ATR Domain in the Presence of Either PI or PS Vesicles. ....</b>	<b>140</b>
<b>Figure 61. IR spectra of ATR Domain in the Presence of Either PI/PI(4,5)P<sub>2</sub> or PS/PI(4,5)P<sub>2</sub> Vesicles.....</b>	<b>141</b>
<b>Figure 62. CD spectra of the ATR-Domain and MBH Peptide of PTEN-L .....</b>	<b>142</b>
<b>Figure 63. IR spectra of MBH peptide of PTEN-L in the Presence of 30% PS.....</b>	<b>142</b>
<b>Figure 64. IR spectra of MBH peptide of PTEN-L in the Presence of 100% PS.....</b>	<b>143</b>
<b>Figure 66. Titration of ATR-Domain in the Presence of 100% POPC Vesicles. ....</b>	<b>145</b>
<b>Figure 67. Titration of ATR-Domain in the Presence of 30% POPC Vesicles. ....</b>	<b>146</b>
<b>Figure 68. Titration of ATR-Domain in the Presence of 5% PI(4,5)P<sub>2</sub>/10% PI Vesicles. ....</b>	<b>147</b>

## List of Tables

<b>Table 1: Comparison of Experimental &amp; Computationally Derived Surface Tension Data</b>	<b>93</b>
<b>Table 2: Comparison of Experimental &amp; Computational Derived Surface Tension Data in Presence of Cholesterol.....</b>	<b>104</b>
<b>Table 3: FTIR Amide I Peaks for ATR-Domain (A) &amp; MBH Peptide (B) in the Presence of Anionic Lipid Vesicles .....</b>	<b>144</b>

Dedication

To my family, especially

Landyn Michael James (BoBo, Monkey Boy)

&

Carlee Anne-Marie (Monkey Girl)

*Always remember that you can do anything you set your mind to.*

*It just takes perseverance, action and facing your fears.*

## Dissertation Summary

The focus of this dissertation is to understand the physicochemical factors that affect the spatiotemporal control of phosphoinositide signaling events. Despite their low abundance in cellular membranes ( ~ 1% of total lipids) phosphoinositides are assuming major roles in the spatiotemporal regulation of cellular signaling, therefore making this group of lipids an attractive area of study, especially for identifying drug targets. The main phosphoinositide studied in this dissertation is phosphatidylinositol-4,5-bisphosphate [PI(4,5)P<sub>2</sub>], which regulates various intracellular signaling pathways, notably the PI3K/AKT pathway. The PI3K/AKT pathway plays a critical role in regulating diverse cellular functions including metabolism, growth, proliferation, and survival. Thus, dysregulation of the PI3K/AKT pathway is implicated in a number of human diseases including cancer, diabetes, cardiovascular disease and neurological diseases. PI(4,5)P<sub>2</sub> regulates phosphoinositide signaling in the PI3K/AKT pathway through interaction of its highly anionic headgroup with polybasic proteins. The highly specific manner that allows hundreds of structurally diverse proteins to interact with lipid species found in such low supply may require the local formation of PI(4,5)P<sub>2</sub> clusters (domains).

Although a significant amount of evidence has accumulated over the past decade that supports the notion of PI(4,5)P<sub>2</sub>-rich clusters, our understanding regarding the structural determinants required for cluster formation remains limited. Studies have shown that PI(4,5)P<sub>2</sub>

clustering is induced by cellular cations interacting with PI(4,5)P<sub>2</sub> via electrostatic interactions, suggesting that non-clustering/clustering transitions are particularly sensitive to ionic conditions. However, why some ions are more effectively cluster PI(4,5)P<sub>2</sub> than others remains to be understood. For our first research aim, we investigated the effects of divalent (Ca<sub>2+</sub>) and monovalent cations (Na<sup>+</sup>, K<sup>+</sup>) on PI(4,5)P<sub>2</sub> clustering to understand the ionic environment required for electrostatic PI(4,5)P<sub>2</sub> cluster formation. We used monolayers at the air/water interface (Langmuir films) to monitor PI(4,5)P<sub>2</sub> molecular packing in the presence of each cation. Our results indicated that Ca<sub>2+</sub> individually and Ca<sub>2+</sub> along with K<sup>+</sup> had a greater effects on PI(4,5)P<sub>2</sub> cluster formation than Na<sup>+</sup> and K<sup>+</sup>, individually and combined. We hypothesize that the cations shield the negatively charged headgroups, allowing adjacent PI(4,5)P<sub>2</sub> molecules to interact via H-bonding networks. The analysis of the electrostatic environment required for stable PI(4,5)P<sub>2</sub> clustering will help us understand important aspects of PI(4,5)P<sub>2</sub> mediated signaling events, such as the temporal control of protein binding to PI(4,5)P<sub>2</sub> clusters to enhance their function.

Another important spatiotemporal modulator that affects the local concentration of PI(4,5)P<sub>2</sub> clusters is cholesterol, a steroid present in large quantities (30-40 mole%) in the plasma membrane. Cholesterol has been shown to induce the formation of liquid-ordered domains when interacting with an otherwise gel phase forming lipid, however, the interaction of cholesterol with an inner leaflet lipid species that favors more of a disordered environment to form clusters is poorly understood. We hypothesize that cations along with cholesterol work synergistically to induce PI(4,5)P<sub>2</sub> clustering. Thus, our second research aim was to investigate the role of cholesterol on PI(4,5)P<sub>2</sub> clustering by monitoring the molecular packing of PI(4,5)P<sub>2</sub> in the presence of both cholesterol and cations. This aim was investigated similarly to the first aim with Langmuir trough monolayer film experiments. Our results showed that cholesterol in the presence of Ca<sub>2+</sub> had an

additive effect leading to the strongest condensation of the monolayer (increase in PI(4,5)P<sub>2</sub> packing). Our hypothesis is that Ca<sup>2+</sup> significantly reduces the negative electron density of the phosphate groups, allowing the cholesterol hydroxyl group to interact with PI(4,5)P<sub>2</sub> headgroup through hydrogen-bond formation. To confirm our hypothesis, we collaborated with a computational group at the NIH that performed all-atom molecular dynamics (MD) simulations that closely agreed with our experimental data. Thus we were able to determine that the cholesterol hydroxyl group directly interacts via hydrogen-bonding with the phosphodiester group as well as the PI(4,5)P<sub>2</sub> hydroxyl groups in the 2- and 6-position. The insight into the structural positioning of cholesterol moving closer to the PI(4,5)P<sub>2</sub> headgroup region suggests this unique interaction is important for PI(4,5)P<sub>2</sub> cluster formation.

Other anionic lipid species are suspected to interact with PI(4,5)P<sub>2</sub> and strengthen PI(4,5)P<sub>2</sub> clustering. We were particularly interested in the interaction of PI(4,5)P<sub>2</sub> with phosphatidylinositol (PI) and phosphatidylserine (PS) because both are abundant in the plasma membrane, ~6-10% and ~10-20% respectively, and both electrostatically bind to peripheral proteins. Therefore, the third research aim analyzed the capacity of PI and PS to form stable clusters with PI(4,5)P<sub>2</sub>. We hypothesize that a mixed PI/PI(4,5)P<sub>2</sub> or PS/PI(4,5)P<sub>2</sub> domains are ideal for protein binding, since in combination PI or PS with PI(4,5)P<sub>2</sub> would provide the necessary negative electrostatic environment, while PI(4,5)P<sub>2</sub> would provide the high specificity and additional electrostatics for protein binding. Langmuir trough monolayer films were used to investigate the stabilization of PI/PI(4,5)P<sub>2</sub> and PS/PI(4,5)P<sub>2</sub> monolayers in the presence of Ca<sup>2+</sup>. Our results showed a condensation of the monolayer for both PI/PI(4,5)P<sub>2</sub> and PS/PI(4,5)P<sub>2</sub> with an increase in Ca<sup>2+</sup> concentrations, which suggests that Ca<sup>2+</sup> shields the highly negatively charged phosphomonoester groups of PI(4,5)P<sub>2</sub> allowing PI and PS to participate in PI(4,5)P<sub>2</sub>'s hydrogen-

bond network. Interestingly, both PI and PS equally stabilized PI(4,5)P<sub>2</sub> cluster formation, therefore it is highly likely that these lipids interact *in vivo* to form large stable electrostatic domains required for protein binding.

The first three aims provided us with information about the physiological relevant environments required for PI(4,5)P<sub>2</sub> cluster formation, while the last aim was geared towards understanding the temporal control of protein association with phosphoinositides in the plasma membrane. Specifically, we analyzed the plasma membrane association of PTEN-L, a translation variant protein of PTEN, that has the ability to exit and enter back into cells, unlike classical PTEN. The ability of PTEN-L to facilitate entry across the anionic and hydrophobic layers of the plasma membrane (in the case of direct transport of PTEN-L across the membrane) or into phospholipid transport vesicles (in the case of vesicular transport of PTEN-L across cells) is likely due to the addition of the 173 N-terminal amino acids, the alternative translated region (ATR-domain). Thus, our fourth research aim focused on the biophysical role of the ATR-domain to associate with inner leaflet plasma membrane lipids. Using attenuated total reflection-Fourier transform infrared (ATR-FTIR) spectroscopy to monitor secondary structural changes of the ATR-domain upon lipid binding, it was revealed that both PS and PI(4,5)P<sub>2</sub> induced conformational change towards a slight increase in  $\beta$ -sheet content in an otherwise unstructured domain suggesting these lipids are required for ATR-domain interaction with the PM. Further studies revealed that the ATR-domain affects the integrity of PS lipid vesicles, further indicating the presence of PS is required to drive ATR-domain across the membrane. This aim provides information on ATR-domain lipid binding preferences aiding in our understanding of the biological and functional role of PTEN-L as a deliverable tumor suppressor protein.



The overall goal of the research in this dissertation is to understand factors that fine-tune PI(4,5)P<sub>2</sub> cluster formation in space and time. Our first three research aims were designed to understand the synergistic effects of spatiotemporal modulators (cations, cholesterol, and anionic lipids) on local concentration of PI(4,5)P<sub>2</sub> clusters. Our results indicate that Ca<sup>2+</sup>, cholesterol, and the presence of anionic lipids PI and PS all induce stable domains, thus it is highly likely this is part of the biological environment required *in vivo* for cationic proteins to bind. The last aim, the association of the ATR-domain with phospholipids in the plasma membrane, provided evidence that PS is likely required to drive the ATR-domain across the plasma membrane. This dissertation unifies nearly two decades worth of research by shedding light on synergistic modulators of PI(4,5)P<sub>2</sub> cluster formation (**Figure 1**). Thus, this work has potentially far reaching consequences for understanding temporal control of the spatially resolved protein activity.

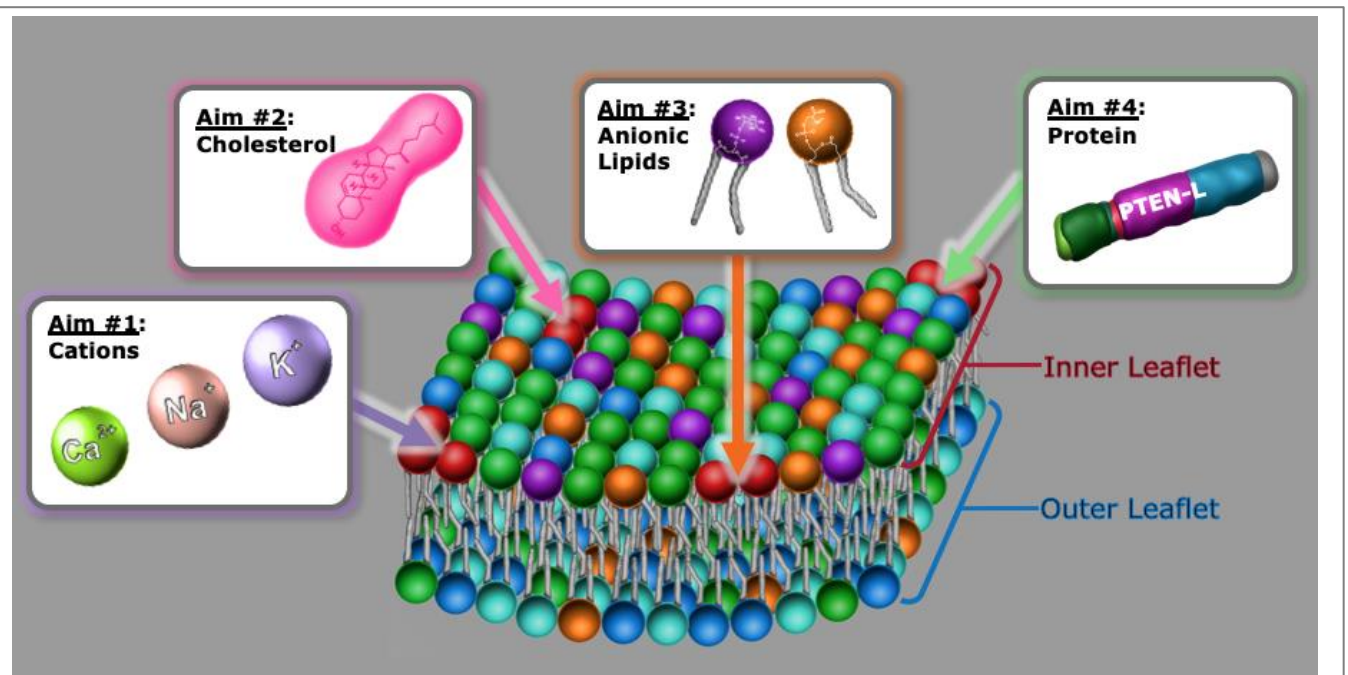


**Figure 1. Aims to Understand Factors that Affect Phosphoinositide Clustering.**

Phosphoinositides (PIPs), in particular PI(4,5)P<sub>2</sub> (red), are not uniformly distributed throughout the inner leaflet of the plasma membrane, but instead can be found enriched in domains. PIPs clustering has been proposed to originate from electrostatic interactions between proteins with basic peptide residues (aim #4, green). However, recent studies have suggested that the interaction with divalent cations such as Ca<sub>2+</sub> (aim #1, purple), cholesterol (aim #2, pink), and other anionic lipids (aim #3, orange) may stabilize PI(4,5)P<sub>2</sub> clusters. The mechanisms that lead to the formation of PIP enriched domains remains a mystery. This dissertation further explores factors that lead to PI(4,5)P<sub>2</sub> clustering.

# Chapter 1: Introduction

## 1.1 Importance of Lipids in the Biological Membrane

At the infancy in understanding lipid function, it was thought that lipids merely provided structural support for bilayer formation and membrane protein function; however, decades of research have revealed that lipids regulate nearly all cellular processes. Thanks to sophisticated techniques we have a detailed model

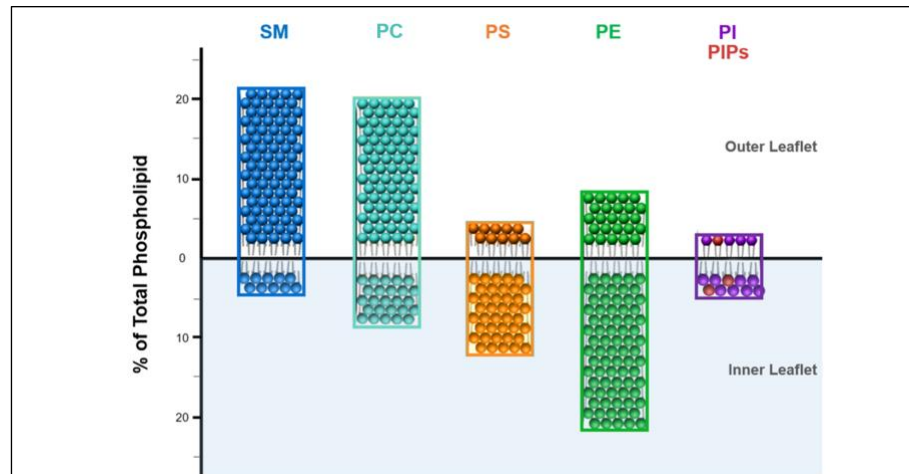


**Figure 2. The Composition of Lipids in the Plasma Membrane.**

Phosphatidylcholine (PC, teal) a zwitterionic lipid is the most abundant phospholipid making up ~ 43% total lipids in the plasma membrane (a majority is found in outer leaflet). Sphingomyelin (SM, blue), the second most abundant lipid at ~23 % of total lipids, is also predominately found in the outer leaflet. The third most abundant lipid in the phosphatidylethanolamine (PE, green) comprises ~21 % of total phospholipids, with a majority located in the inner leaflet. Comprising the rest of the inner leaflet lipids are the anionic phospholipids: phosphatidylserine (PS, orange) at ~ 4% , phosphatidylinositol (PI, purple) at ~ 7%, and the phosphatidylinositol derivatives at ~2% (PIPs, red).

of the lipids present in the biological membranes, which include an astounding >1,000 different lipid species due to aliphatic chain and head group chemistry (Fahy, Sud et al. 2007, Sud, Fahy et al. 2007, van Meer, Voelker et al. 2008). The membrane lipids are amphipathic in nature where the hydrophobic acyl tails of the lipids self-associate shielding themselves from water, while the polar hydrophilic head groups interact with one another and their aqueous environment. The exoplasmic leaflet of the plasma membrane is composed primarily of phosphatidylcholine (PC)

and sphingomyelins, while the cytosolic facing leaflet is enriched in amino-phospholipids phosphatidylethanolamine (PE) and negatively charged phosphatidylserine (PS) and phosphatidylinositol (PI). Other minor phospholipids, such as phosphatidic acid (PA) and phosphoinositides (PIPs) are also enriched on the cytofacial side of the membrane (**Figure 2**). The lipid bilayer provides the solvent for proteins, where intrinsic proteins are integral to the bilayer (transmembrane proteins) and extrinsic proteins are on the periphery of the bilayer (surface residing proteins) as represented in the Fluid Mosaic Model (**Figure 2**) (Escriba and Nicolson

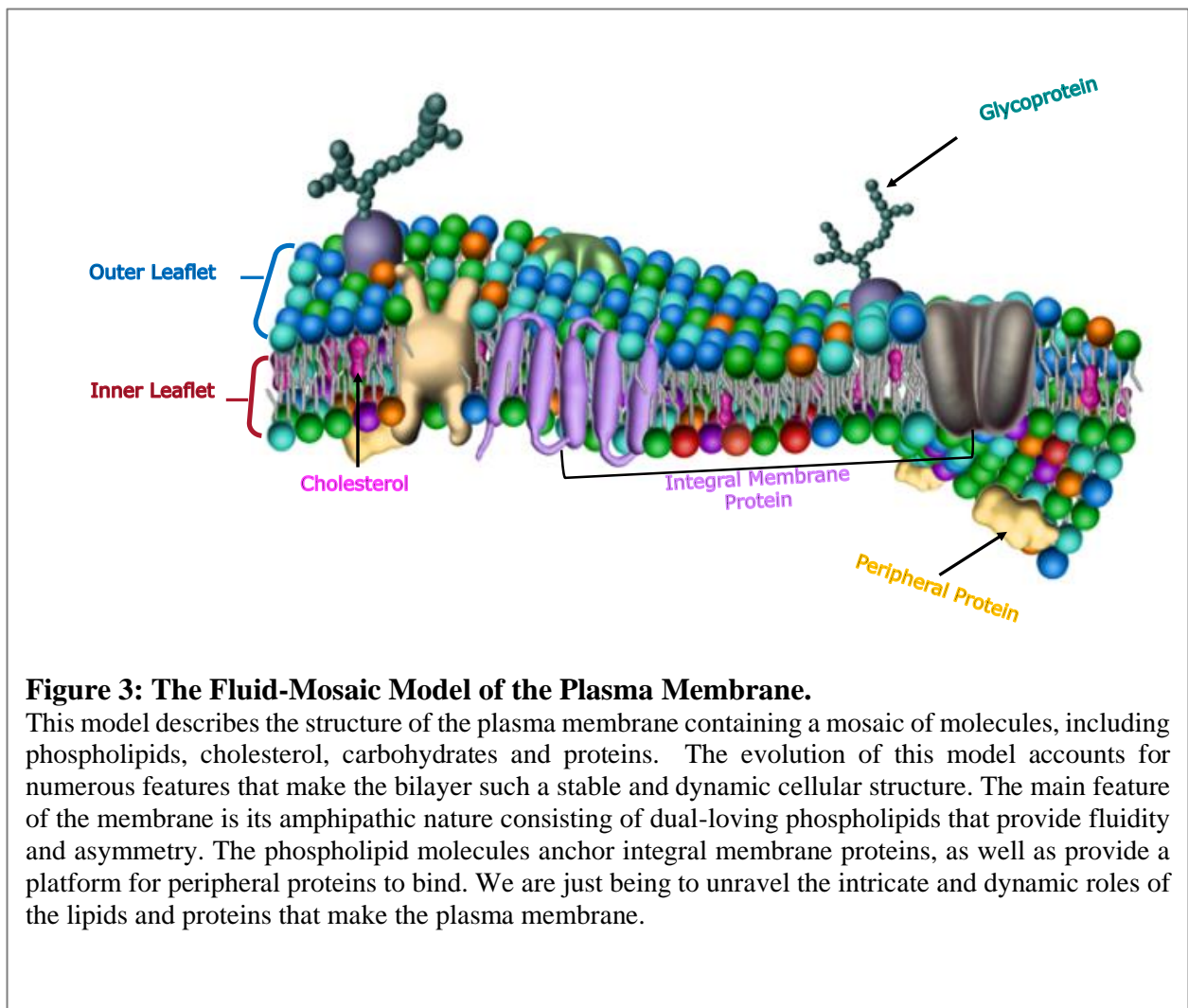


**Figure 3: The Fluid-Mosaic Model of the Plasma Membrane.**

This model describes the structure of the plasma membrane containing a mosaic of molecules, including phospholipids, cholesterol, carbohydrates and proteins. The evolution of this model accounts for numerous features that make the bilayer such a stable and dynamic cellular structure. The main feature of the membrane is its amphipathic nature consisting of dual-loving phospholipids that provide fluidity and asymmetry. The phospholipid molecules anchor integral membrane proteins, as well as provide a platform for peripheral proteins to bind. We are just being to unravel the intricate and dynamic roles of the lipids and proteins that make the plasma membrane.

2014, Goni 2014, Nicolson 2014, Demchenko 2012). The differences in the charge and size of the head group, especially with bulky headgroups like PC and PIPs directly influence lipid-lipid and lipid-protein interactions within the bilayer adding to its complexity.

## **1.2 Phosphoinositides Provide Spatiotemporal Control of Signaling Events**

Phosphoinositides (PIPs) are an essential class of phospholipids with direct involvement in almost every aspect of cellular physiology including membrane trafficking, signal transduction, cell growth, cytoskeletal dynamics, lipid transport/exchange between organelles, and the regulation of transmembrane proteins. (Lemmon 2003). Despite their low abundance in the plasma membrane (~ 1% of total lipids), PIPs have emerged as key regulators of cellular signaling, cytoskeletal rearrangement, acquisition of cellular polarity and regulation of cellular adhesion, motility, and cytokinesis (Carney 1995, Di Paolo and De Camilli 2006, Balla 2013, Schink, Tan et al. 2016, Dickson and Hille 2019). The ability of PIPs to regulate signaling events is rooted in the reversible phosphorylation at hydroxyl positions 3, 4 or 5 of the inositol ring by cytoplasmic lipid kinases. The phosphorylation gives rise to monophosphorylated derivatives: PI(3)P, PI(4)P and PI(5)P, bisphosphorylated derivatives: PI(3,4)P<sub>2</sub>, PI(3,5)P<sub>2</sub> and PI(4,5)P<sub>2</sub> and trisphosphorylated derivative: PI(3,4,5)P<sub>3</sub> (

**Figure 4).**

Like other phospholipids they have a glycerol backbone esterified to two fatty acid chains. The acyl chain on the *sn*-1 position of glycerol backbone is predominately stearyl, while the *sn*-2 chain is enriched in arachidonic acid a distinctive feature of PIPs. The arachidonoyl chain, which has four double bonds, can cause disruption of dense membrane packing due to the chain

being kinked. Therefore PIPs have a preference for fluid membrane regions, but this does not mean that PIPs cannot accumulate into *fluid* domains (see section 1.17). The phosphate group is attached to a polar head group, cyclic polyol *myo*-inositol (CHOH)<sub>6</sub>, which assumes a “chair” conformation with five of its six –OH groups being equatorial and the one at position 2 being axial (

**Figure 4)** (Luckey 2014). These seven interconvertible PIPs are amphiphilic in nature with their polar inositol head group facing toward the cytoplasm and non-polar hydrophobic fatty acid tails embedded in the lipid bilayer.

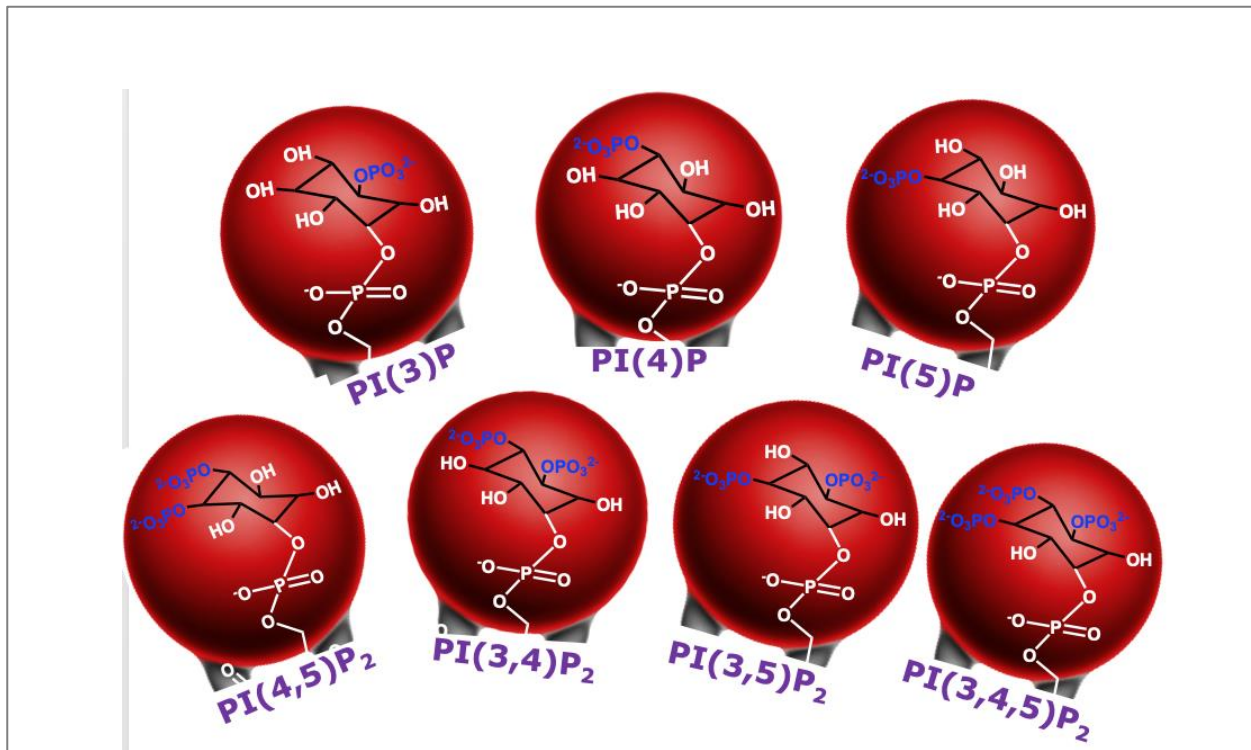


**Figure 4. Chemical Structures of 7 Naturally Occurring Members of the Phosphoinositide Family.**

They are derived from the precursor phosphatidylinositol (PI) by a reversible phosphorylation at hydroxyl positions 3, 4 or 5 of the inositol ring through specific kinases. Phosphatidylinositol monophosphates are PI(3)P, PI(4)P, and PI(5)P. The phosphatidylinositol bisphosphates are PI(3,4)P<sub>2</sub>, PI(3,5)P<sub>2</sub>, and PI(4,5)P<sub>2</sub>. The phosphatidylinositol trisphosphate is PI(3,4,5)P<sub>3</sub>.

The spatiotemporally regulated production and turnover of PIPs is crucial for localized PIP signaling and function. Depending on the membrane compartment, there are groups of highly specific kinases and phosphatases that modify the phosphate group substitution pattern at the inositol ring providing “temporal control” of signaling events. The concerted action of phosphatases and kinases regulate the generation and turnover of PIPs, thus affecting the local concentration and the production of distinct pools (domains/clusters) (Balla 2013). These distinct phosphoinositide pools have been shown to be dynamically regulated, leading to intricate “spatial control” of signaling events. PIPs regulation of “spatial control” manifests itself in several ways. One direct way of regulation is through the unique differences in lipid compositions among membrane organelles where individual PIPs can then serve as a code for cellular organelle identity membranes (Di Paolo and De Camilli 2006, Kutateladze 2010). For instance PI(4)P is enriched in the Golgi, whereas PI(3)P marks the early endosome and is then converted to PI(3,5)P<sub>2</sub> at the level of the sorting endosome (Balla 2013). The interconversion of one PIP isoform to another providing the accumulation of different species is also directly related to their role in vesicular trafficking including endocytosis and exocytosis (Picas, Gaits-Iacovoni et al. 2016).

Another way that PIPs demonstrate “spatial control” is through a gradient distribution, which is essential for generating and maintaining polarized gradients for cell migration. A lateral non-uniform distribution of PIPs has been observed in in the amoeba *Dictyostelium discoideum* and neutrophils, where a high concentration of PI(4,5)P<sub>3</sub> accumulate at the leading edge of the cell inducing actin cytoskeleton rearrangement (Shi 2003, Saarikangas, Zhao et al. 2010, Cauvin and Echard 2015, Devreotes and Horwitz 2015, Viaud, Mansour et al. 2016). In contrast, PI(4,5)P<sub>2</sub> is

concentrated at the trailing membrane of migrating cells to suppress lateral pseudopod formation, thus maintaining directional cell migration. PIPs also play essential roles in the establishment and maintenance of epithelial polarity, in which the apical side of epithelial cells show increased PI(4,5)P<sub>2</sub> concentrations, while the basolateral side exhibits increased PI(3,4,5)P<sub>3</sub> concentrations (Cain and Ridley 2009, Tahirovic and Bradke 2009, Saarikangas, Zhao et al. 2010, Cauvin and Echard 2015, Viaud, Mansour et al. 2016). The spatial localization of PI(4,5)P<sub>2</sub> and PI(3,4,5)P<sub>3</sub> to distinct compartments in epithelial cells is crucial for the proper differentiation, proliferation, and morphogenetic processes of many cell types (Tahirovic and Bradke 2009, Cauvin and Echard 2015, Schink, Tan et al. 2016). Additionally, PI(4,5)P<sub>2</sub> and PI(3,4,5)P<sub>3</sub> play fundamental roles during cytokinesis where PI(3,4,5)P<sub>3</sub> concentrates to the opposing poles of the newly forming daughter cells activating actin polymerization to generate the force that drives daughter cells apart. At the same time PI(4,5)P<sub>2</sub> concentrates to the cleavage furrow, where it further regulates the spindle orientation, mitotic cell shape and bridge stability after furrow ingression; thereby establishing and maintaining epithelial polarization (Barr and Gruneberg 2007, Saarikangas, Zhao et al. 2010).

But by far the most intricate way PIPs provide “spatial control” is by acting as membrane targets for protein recruitment and assembly, triggering downstream signaling cascades. Cytosolic proteins are attracted to PIPs usually with initial low affinity, thus cooperative association with one or more additional proteins and/or lipids amplifies the interaction resulting in enhanced membrane protein affinity (Di Paolo and De Camilli 2006, Saarikangas, Zhao et al. 2010). The proteins that interact with PIP-rich domains are most often peripheral proteins that reversibly translocate to cellular membranes. These PIP-binding proteins contain regions rich in



cationic amino acids, also known as phosphoinositide binding motifs, that provide a “PI code” based on the stereospecific recognition of the unique phosphate group positions around the inositol ring. More than 10 PIP binding domains have been identified including pleckstrin homology (PH), bin-amphiphysin-Rvs (BAR), epsin n-terminal homology (ENTH), phox (PX), C2 and FYVE domains (Lemmon 2003, Lemmon 2007, Stahelin, Scott et al. 2014). The highly selective interaction of proteins containing one or more PIP binding motifs is the foundation of PIPs involvement in regulating many cellular processes, including membrane trafficking, cell growth and survival, cytoskeletal dynamics, and chemotaxis (Di Paolo and De Camilli 2006, Balla 2013, Falke and Ziemba 2014). PIP-protein interactions in combination with PIPs unique subcellular distribution generates a robust mechanism responsible for the spatiotemporal fine-tuning at the plasma membrane–cytosol interface, thus providing intricate control of cellular signaling. This makes PIPs and PIP-binding proteins an attractive area of study, especially for identifying drug targets, therefore it is imperative that we fully understand the driving force(s) behind PIP cluster formation.

### **1.3 Phosphoinositide Cluster Formation**

A significant amount of evidence suggests that PIPs, mainly PI(4,5)P<sub>2</sub> is enriched in clusters (domains, pools) thereby increasing its local concentration and creating a distinct PIP environment (**Figure 4**). It has been suggested that PIP domains, a region in the membrane that is chemically, compositionally and functionally distinct from its surroundings, are necessary for the high specificity binding of >280 intracellular proteins to lipids found in such low supply. However, the exact mechanism that leads to the formation of PIP enriched domains has not been pinpointed. Recent studies have shown that PI(4,5)P<sub>2</sub> can co-cluster with polybasic peptides from the PIP

interactome, as observed with BAR proteins requiring PI(4,5)P<sub>2</sub> clusters (McLaughlin 2005, Saarikangas 2009, Zhao 2013, Slochower, Wang et al. 2014). Interestingly, after the initial PIP domain formation, the BAR protein can dissociate leaving behind a pool of PIPs, suggesting the formed PIP clusters could sequentially interact with different effectors. The ability of proteins to interact with PIP-enriched areas regardless of their ability to polymerize has been shown with epsin N-terminal homology (ENTH) and AP180 N-terminal homology (ANTH) domains (Picas 2014). Based on these studies PIP clustering seems to be a general property required for proteins to localize to the membrane. Now comes the chicken or the egg argument: Do proteins cluster PIPs in the membrane? Or do PIP-clusters attract the proteins to the membrane?

Much of the research in the past decade has aimed to understand alternative or complementary mechanisms that lead to PIP clustering. Especially considering the PIP diffusion coefficient within the membrane plane ( $D \sim 2.6 \times 10^{-7} \text{ cm}^2 \cdot \text{s}^{-1}$ ), it is highly likely other mechanisms are needed in order to spatially preserve the turnover of different PIP subdomains (Koldso, Shorthouse et al. 2014). Three models have recently been proposed that may lead to the formation of PIP-protein complexes (Hammond 2016). The difference between the three models is whether concentration of PIPs is a prerequisite (“platform model”), a driving force (“selfish model”), or a by-product (“megapool model”). In the “platform model”, PIP domain formation is a requirement for the association of the protein with the lipid, as observed with the myristoylated alanine-rich C-kinase substrate (MARCKS) protein. The unstructured basic domain in the MARCKS protein electrostatically interacts with PI(4,5)P<sub>2</sub> translocating MARCKS to the PM allowing the hydrophobic insertion of its myristate chain into the bilayer (McLaughlin 2005). In the “selfish” model, kinases drive the synthesis of PIPs consequently making a PIP pool that

associates with the appropriate PIP-binding domain. One example where this is observed is with the Sec14 family of proteins that specifically couple inositol lipid kinases to individual protein complexes (Grabon, Khan et al. 2015). Lastly, the “megapool model” occurs serendipitously because of the recruitment of a PIP effector protein, thus leading to an electrostatic attraction of additional PIP molecules and formation of PIP pools. This multitasking of PIP clustering could regulate clathrin-mediated endocytosis (CME), where the central players F-BAR, ANTH, ENTH, and N-BAR domains are shown to local segregate PI(4,5)P<sub>2</sub> suggesting PIP clusters regulate protein intermediates of CME (McMahon and Boucrot 2011, Picas, Gaits-Iacovoni et al. 2016). There is a lack of definitive evidence for any of these models based on the technical challenges present with detecting, labeling, and observing the nanoscopic spatial organization of the PIPs and PIP-binding proteins. However, the current evidence of PI clustering in trafficking and signal transduction opens up exciting perspectives of PIP-cluster formation.

#### **1.4 Cellular Evidence of Phosphoinositide Cluster Formation**

At the cellular level we are still learning how PI(4,5)P<sub>2</sub> clustering happens. Studies have shown that PI(4,5)P<sub>2</sub> clusters occurs in cells and in unfixed or rapidly frozen membrane sheets prepared from cells. (Fujita 2009, van den Bogaart, Meyenberg et al. 2011, Honigmann, van den Bogaart et al. 2013). The most common method to map cellular localization of PIP pools in live cells is to fuse a fluorescent protein, such as GFP, to a protein that has high affinity and selectivity to the PIP of interest like PH , ENTH, C2 domains. Whether PI(4,5)P<sub>2</sub> forms clusters in cells without the influence of binding proteins or antibodies is an unexplored field due to lack of resolution of microcopy at the nanometer scale. (Varnai and Balla 2006; Yeung et al. 2006; Yeung et al. 2008; Fairn et al. 2011) (Stauffer et al, 1998; Varnai and Balla, 1998). Thus experiments

manipulating the cellular levels of PIPs such as overexpression of PIP phosphatases or kinases, PIP kinase selective inhibitors and direct chemical analysis of PIP levels have been used to study PIP accumulation (Suh and Hille 2007). However, most studies in cells have focused on the association of PIP-binding proteins. A study of syntaxin1 in PC12 cells showed that clustered cell-surface proteins led to the formation of PI(4,5)P<sub>2</sub> clusters by electrostatic interactions with juxta-membrane basic residues (van den Bogaart, Meyenberg et al. 2011). The behavior of protein clustering occurs during signaling, focal adhesion formation, and early steps in formation of endocytosis. Endocytosis is actually a great example of the recruitment of proteins, such as F-BAR which assembles with each other into polymers that bend membranes and recruit and cluster PI(4,5)P<sub>2</sub> (Heath and Insall 2008). Another example of PI(4,5)P<sub>2</sub> association driven by cellular PI(4,5)P<sub>2</sub>-binding proteins is with myristoylated alanine-rich C-kinase substrate that modulates PI(4,5)P<sub>2</sub> distribution at the inner leaflet during various cellular events. The accumulation of PI(4,5)P<sub>2</sub> serves as a docking site for cytosolic proteins that bind electrostatically and specifically to PI(4,5)P<sub>2</sub> (Gambhir 2004) (Laux 2000, McLaughlin 2005, Brown 2015) (Glaser 1996, McLaughlin, Wang et al. 2002, Gambhir 2004, Brown 2015). Because the PI(4,5)P<sub>2</sub> clusters are smaller than the diffraction limit, we have heavily relied on model membrane experiments to understand factors that affect PI(4,5)P<sub>2</sub> clustering.

## **1.5 Physical Basis For Phosphoinositide Cluster Formation**

Most biophysical studies have used PI(4,5)P<sub>2</sub>, or cholesterol with PI(4,5)P<sub>2</sub> to investigate PIP clustering. (Koreh 1986, Hope 1996, Pike 1996, Pike 1998, Redfern 2004, Redfern and Gericke 2005, Levental, Christian et al. 2009, Kwiatkowska 2010, Gao, Lowry et al. 2011, Wang, Collins et al. 2012, Jiang, Redfern et al. 2014, Salvemini, Gau et al. 2014). In model membranes,

PI(4,5)P<sub>2</sub> has been reported to form clusters, but whether the conditions used in these experiments induce distinct pools of unclustered and clustered PI(4,5)P<sub>2</sub> *in vivo* unclear. Even though previous studies were based on non-physiological conditions, for instance in many studies the inner leaflet compositions don't reflect cellular PI(4,5)P<sub>2</sub> concentrations and bulk lipid compositions, they have provide us with insight on PI(4,5)P<sub>2</sub> cluster formation (Redfern and Gericke 2005, Levental, Christian et al. 2009, Sarmiento, Coutinho et al. 2014).

Even though the inner leaflet of the plasma membrane is void of lipids that form gel phases at physiological temperatures, model membrane studies have shown that cholesterol induces PIP domain formation (Jiang, Redfern et al. 2014). The stabilization of PIP-enriched phases by cholesterol is so pronounced, that even lower than physiological concentrations of cholesterol (20%) are sufficient to stabilize phosphoinositide vesicles (important to note: PIPs by themselves do not form vesicles). The authors of this study also showed that the hydroxyl (OH) group of cholesterol was essential for this domain formation (Jiang, Redfern et al. 2014). Considering the importance of the cholesterol OH-group in domain formation, the authors hypothesized that this interaction involves hydrogen bond (H-bond) formation between the cholesterol OH-group and functional groups at the inositol ring. The observation that cholesterol promotes clustering of PIPs in simple model membrane systems provides a first glimpse of cholesterol-dependent inner leaflet plasma membrane domain formation, thus in this dissertation we will further investigate the role of cholesterol by introducing cation-induced PI(4,5)P<sub>2</sub> clusters.

Cholesterol depletion studies show impaired hormone-stimulated phosphatidylinositol turnover due to PI(4,5)P<sub>2</sub> delocalization (Pike 1998). The initial studies suggested that PI(4,5)P<sub>2</sub>

is enriched in raft domains. A key feature of raft domains are sphingolipid and cholesterol-based structures raft-like liquid ordered (Lo) phase domains, which are floating in a liquid-disordered (Ld) phase that is enriched in lipids that have at least one acyl chain with a cis unsaturation. Since phospholipids in the inner leaflet of the plasma membrane have kinked unsaturated acyl chains that disrupts tight lipid packing, this PIP-raft theory poses several problems 1.) the study utilizing cholesterol depletion may have disrupted PI(4,5)P<sub>2</sub> signaling by changing the structural and physical properties of the membrane (van Rheenen, Achame et al. 2005) 2.) raft domains are ordered phases, while the PI(4,5)P<sub>2</sub> is found in fluid phases due to its highly disordered arachidonoyl chain. This makes it extremely unlikely that PI(4,5)P<sub>2</sub> partitions into raft domains, unless there is some undiscovered driving force.

An alternative hypothesis is that PI(4,5)P<sub>2</sub> forms clusters independently through hydrogen bond (H-bond) formation between PI(4,5)P<sub>2</sub> headgroups (**Figure 6**). Several biophysical studies in model membranes, have observed that PI(4,5)P<sub>2</sub> molecules can form clusters independent of external factors, such as the absence of cholesterol (Redfern and Gericke 2005, Kooijman, King et al. 2009, Jiang, Redfern et al. 2014). The first study to show this with a binary PI(x)P/PC model membrane system that formed phosphoinositide monophosphate (PI(x)P) micro-domains (Redfern 2004). The authors suggested that the hydroxyl groups of the inositol ring participate in the H-bond network by acting as hydrogen donors, while the phosphomonoester, phosphodiester and other hydroxyl groups from adjacent lipid molecules act as hydrogen bond acceptors (**Figure 6**). To further strengthen this argument, the authors showed that phosphoinositide polyphosphates were also able to form domains. However, it was interesting that PI(4,5)P<sub>2</sub> had less of a tendency than PI(x)P to form domains. This strongly suggests that the presence of another molecule and/or lipid may be important for domain formation (Redfern and Gericke 2005). This idea was further

supported in another study in which the degree of PI(4,5)P<sub>2</sub> cation clustering showed that six phosphoinositide species co-clustered suggesting the composition of the surrounding lipids, with cholesterol enhances this behavior (Wen, Vogt et al. 2018). Another study built upon these findings using magic angle spinning <sup>31</sup>P nuclear magnetic resonance spectroscopy (NMR). Their data showed a “smearing” out of the phosphomonoester group charge suggesting that PIPs must participate in an H-bond network through both inter- and intramolecular interactions (Kooijman, King et al. 2009).

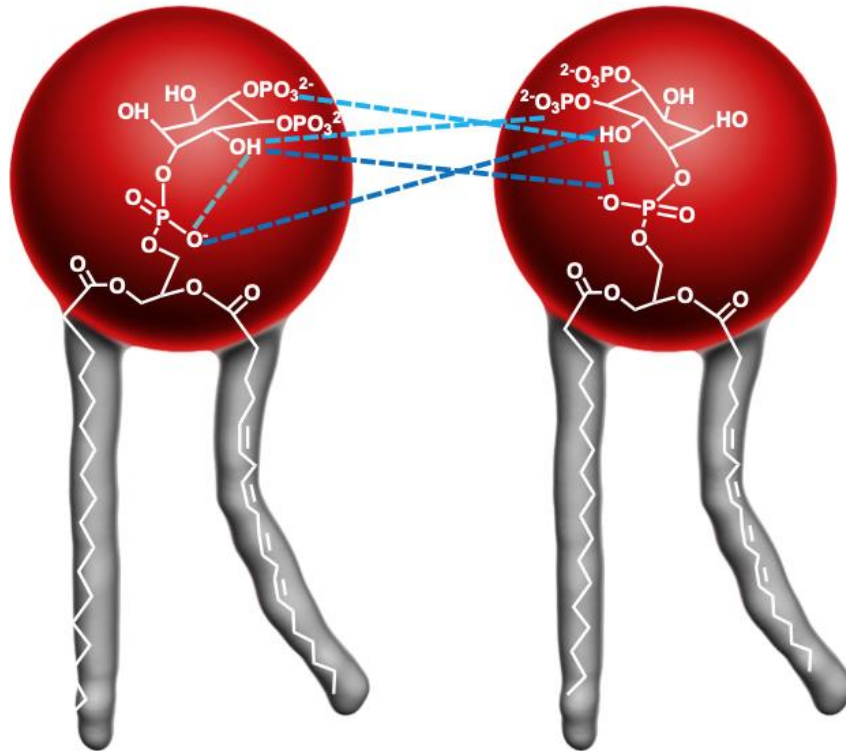


**Figure 5. PI(4,5)P<sub>2</sub> H-Bond Network**

Several studies have strongly suggested that intramolecular hydrogen bond forms between the hydroxyl and phosphomonoester groups and intermolecular bonds from the hydroxyl groups of the inositol ring acting as hydrogen donors, while the phosphomonoester, phosphodiester and other hydroxyl groups from adjacent lipid molecules act as hydrogen bond acceptors. (---- H-bond between phosphomonoester and OH-group, - - - - H-bond between phosphodiester and OH-group; intramolecular ..... H-bond).

Even though there is expanding evidence supporting an H-bond network formation for the stabilization of PIP enriched phases, these studies have drawn opposition from researchers who insist that electrostatic repulsion between the highly charged PI(4,5)P<sub>2</sub> molecules is strong enough to prevent cluster formation (Fernandes, Loura et al. 2006) (Gamper and Shapiro 2007, Blin, Margeat et al. 2008). This lead to an alternative hypothesis that PI(4,5)P<sub>2</sub> clustering is induced by



cellular cations electrostatically interacting with PI(4,5)P<sub>2</sub>. There have been a few *in vitro* studies exploring the impact of divalent cations on H-bond networks, showing that Ca<sup>2+</sup> is capable of clustering PI(4,5)P<sub>2</sub> molecules (Golebiewska, Gambhir et al. 2006, Dasgupta 2009, Graber, Jiang et al. 2012, Wang, Collins et al. 2012, Graber, Gericke et al. 2014, Jiang, Redfern et al. 2014, Sarmiento, Coutinho et al. 2014, Wang, Slochower et al. 2014, Wen, Vogt et al. 2018). It has been suggested that cations Ca<sup>2+</sup>, as well as Mg<sup>2+</sup>, bridge headgroup phosphates through shielding the phosphomonoester groups, allowing highly negative PI(4,5)P<sub>2</sub> molecules to come close together and form domains. The PI(4,5)P<sub>2</sub> clustering effect of Ca<sup>2+</sup> is independent of the PIP acyl chain composition, underscoring the headgroup-driven nature of this clustering (Carvalho, Ramos et al. 2008, Levental 2008, Levental, Christian et al. 2009, Wang, Collins et al. 2012, Sarmiento, Coutinho et al. 2014, Slochower, Wang et al. 2014, Wang, Slochower et al. 2014, Wen, Vogt et al. 2018) A revealing study using fluorescence resonance energy transfer (FRET) showed that micromolar Ca<sup>2+</sup> concentrations trigger the formation of nanosized PI(4,5)P<sub>2</sub> domains (Wen, Vogt et al. 2018). This study provided us with the first evidence that PI(4,5)P<sub>2</sub> forms clusters at physiologically relevant concentrations. Complementing these experimental approaches, molecular dynamics simulations also showed that Ca<sup>2+</sup> altered PI(4,5)P<sub>2</sub> properties and induced PI(4,5)P<sub>2</sub> cluster formation. (Ellenbroek, Wang et al. 2011, Slochower, Huwe et al. 2013).

Another important factor that may affect PI(4,5)P<sub>2</sub> domain formation is the “threshold” PI(4,5)P<sub>2</sub> concentration (Wen, Vogt et al. 2018). This concept is analogous to “critical micelle concentration (CMC),” where higher order aggregation forms micelles (Davis, Richens et al. 2011). This idea was investigated using sensitive assays of self-quenching FRET revealing the “critical PIP concentration (CPC)” was remarkably low (0.02–0.05 mol% of total lipid) (Wen,

Vogt et al. 2018). This means that below the CPC ( $<0.02$  mol%), PI(4,5)P<sub>2</sub> exists essentially as individual molecules, however above this concentration PI(4,5)P<sub>2</sub> clusters form. Interestingly but not surprising, in these studies multivalent metal ions were required for PI(4,5)P<sub>2</sub> cluster formation. Although physiological concentrations of PI(4,5)P<sub>2</sub> are well above the CPC value, this is not certainly the case for the other PIP isoforms. For example, the concentration of PI(3,4,5)P<sub>3</sub> is  $\sim 0.02$ – $0.05\%$ , which is in the exact concentration range where Ca<sup>2+</sup>-induced clustering occurs (Stahelin, Scott et al. 2014), thus suggesting PI(3,4,5)P<sub>3</sub> forms clusters when activating downstream signaling pathways.

## 1.6 Phosphoinositide Clustering in PI3K Pathway

PI(3,4,5)P<sub>3</sub> plays a major role in the phosphatidylinositol 3-kinase (PI3K)/Akt pathway which regulates cell metabolism, growth, and apoptosis. Defects in its signaling have been implicated in many diseases, including cancer, type 2 diabetes, and heart-related diseases (Fruman, Chiu et al. 2017) (**Figure 6**). The activation of this pathway is initiated at the plasma membrane, where phosphoinositide-3-kinase (PI3K) phosphorylates the 3-position on the inositol ring of PI(4,5)P<sub>2</sub> to produce PI(3,4,5)P<sub>3</sub>. The PI3K enzyme must first be activated by a receptor like the receptor tyrosine kinase (RTK) upon ligand binding (Stokoe 1997, Datta 1999). The resulting PI(3,4,5)P<sub>3</sub> recruits pleckstrin homology (PH) domain-containing proteins Akt (also known as protein kinase B) and the phosphoinositide-dependent kinase 1 (PDK1) to the plasma membrane. Once at the membrane, Akt is phosphorylated and activated by PDK1. Akt adopts an open conformation and inhibits several members of the apoptotic pathway through phosphorylation of multiple proteins on serine and threonine residues (Brunet 1999, Lucic, Rathinaswamy et al. 2018). Through phosphorylation of these target proteins Akt promotes cellular growth, proliferation,

extracellular matrix interactions, and motility (Figure 7) (Brunet 1999, Lemmon and Schlessinger 2010, Szymonowicz, Oeck et al. 2018). However, an unresolved question is how does PI(3,4,5)P<sub>3</sub>, which is present in a low concentration below the CPC (~0.02–0.05%) act as a signaling molecule for

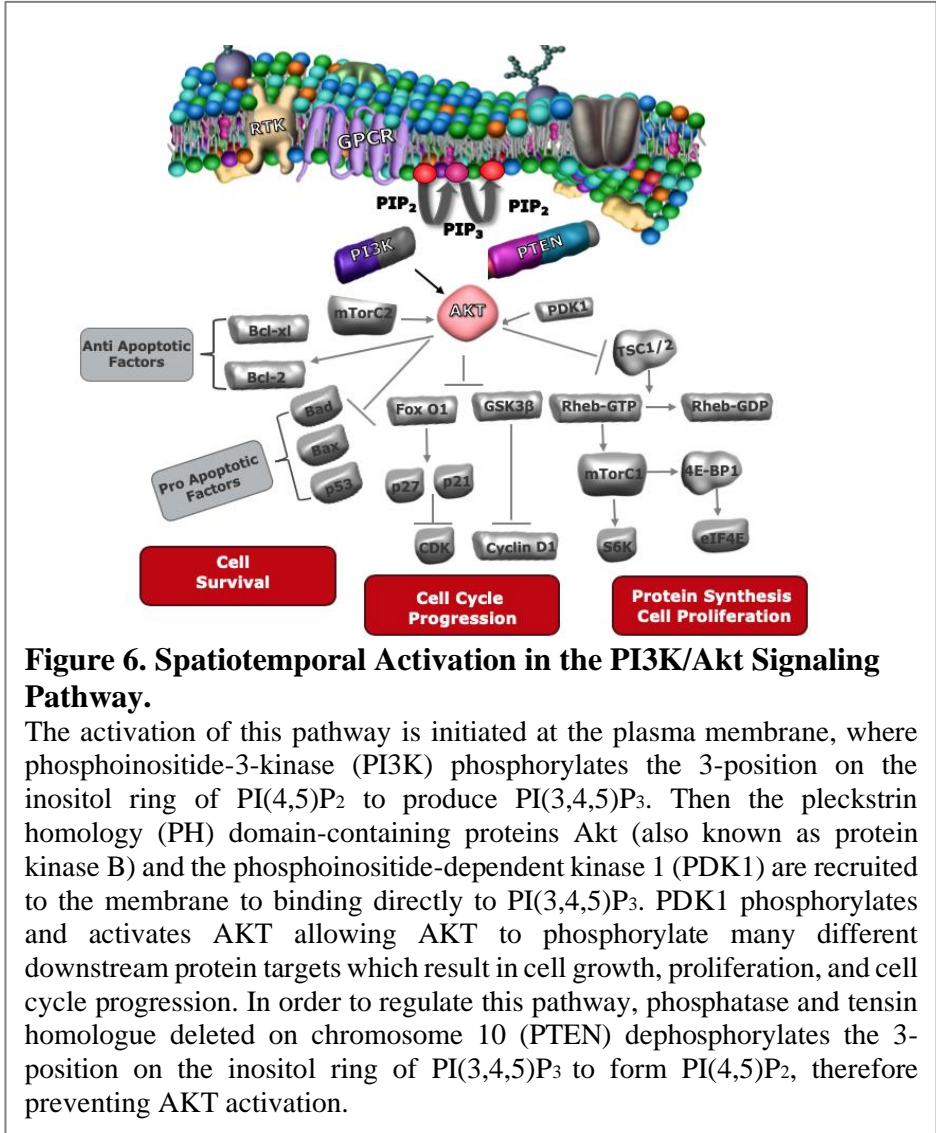


**Figure 6. Spatiotemporal Activation in the PI3K/Akt Signaling Pathway.**

The activation of this pathway is initiated at the plasma membrane, where phosphoinositide-3-kinase (PI3K) phosphorylates the 3-position on the inositol ring of PI(4,5)P<sub>2</sub> to produce PI(3,4,5)P<sub>3</sub>. Then the pleckstrin homology (PH) domain-containing proteins Akt (also known as protein kinase B) and the phosphoinositide-dependent kinase 1 (PDK1) are recruited to the membrane to binding directly to PI(3,4,5)P<sub>3</sub>. PDK1 phosphorylates and activates AKT allowing AKT to phosphorylate many different downstream protein targets which result in cell growth, proliferation, and cell cycle progression. In order to regulate this pathway, phosphatase and tensin homologue deleted on chromosome 10 (PTEN) dephosphorylates the 3-position on the inositol ring of PI(3,4,5)P<sub>3</sub> to form PI(4,5)P<sub>2</sub>, therefore preventing AKT activation.

this pathway. It is highly likely that a local enrichment of PI(3,4,5)P<sub>3</sub> is likely required for downstream signaling proteins to bind. It has been suggested that PI3K pushes PI(3,4,5)P<sub>3</sub> levels to the higher end of this concentration range thus leading to the formation of Ca<sup>2+</sup> induced PI(3,4,5)P<sub>3</sub> clusters (Gericke 2018). This type of mechanism would be an example of the “selfish” model (Hammond 2016), in which PI3K locally produces PI(3,4,5)P<sub>3</sub> and the accumulation leads to clustering once the CPC is reached. Another study has shown that PDK1 is activated in domains

enriched in sphingolipid and cholesterol, suggesting that membrane rafts may also be important regulators. (Gao, Lowry et al. 2011).

This pathway is controlled by phosphatase and tensin homologue deleted on chromosome 10 (PTEN), which dephosphorylates the 3-position on the inositol ring of PI(3,4,5)P<sub>3</sub> to form PI(4,5)P<sub>2</sub> preventing AKT activation (Myers 1997, Tonks 1998). PTEN's action on PI(3,4,5)P<sub>3</sub> requires that PTEN must first be dephosphorylated at its C-terminal tail, which leads to an open conformation that is competent for membrane binding (Campbell, Liu et al. 2003, Das, Dixon et al. 2003, Wang and Jiang 2008, Ross and Gericke 2009, Shenoy, Shekhar et al. 2012, Lumb and Sansom 2013, Iijima 2015). PTEN dephosphorylation of PI(3,4,5)P<sub>3</sub> may cause PI(3,4,5)P<sub>3</sub> levels to drop below CPC, thus possibly dissolution of the Ca<sup>2+</sup>/PI(3,4,5)P<sub>3</sub> clusters (Gericke 2018). As a result, this leads us to believe that the turn-on and -off signal of the PI3K pathway would be more robust with variations in the “threshold” CPC levels than with solely relying on the enzymatic action of P13K and PTEN to affect PI(3,4,5)P<sub>3</sub> concentrations (Gericke 2018).

In order to understand the direct regulation of PI(4,5)P<sub>2</sub>-binding proteins and their association with signaling pathways, such as PI3K, we need to address the players that fine-tune the signaling. The physical characteristics of PIP domain formation such as stability, fluidity, and electrostatic potential are potentially important factors for the selection of PIP-binding proteins. Thus, the overall goal of this dissertation is to further understand spatial (i.e., cations and cholesterol) and temporal (protein binding) factors that lead to phosphoinositide clustering (**Figure 1**). There is also a need to increase the complexity of PIP model membrane systems in order to understand the predominant interactions of PIPs in biological membranes. Thus, we will also explore PI(4,5)P<sub>2</sub> cluster formation in the presence of other inner leaflet anionic lipids (see chapter **Error! Reference source not found.**).

## Chapter 2: Methodologies & Techniques

This chapter describes the various methodologies and techniques that were used to conduct the studies in this dissertation.

### 1.7 Lipid Sample Preparation

The following are the lipids used for the experiments presented in this dissertation: 1.) L- $\alpha$ -phosphatidylinositol-4,5-bisphosphate (PI(4,5)P<sub>2</sub>, brain porcine) 2.) L- $\alpha$ -phosphatidylinositol (Liver PI, bovine) 3.) 1-palmitoyl-2-oleoyl-sn-glycero-3-phospho-L-serine (POPS) 4.) 1-palmitoyl-2-oleoyl-glycero-3-phosphocholine (POPC) and 5.) Cholesterol (ovine, wool). All lipid samples were obtained in powder form from Avanti Polar Lipids, Inc. (Alabaster, AL). Lipid stock solutions were prepared by dissolving the appropriate phospholipid (~1 mg), typically with a mixture of 20:9:1 chloroform:methanol:water (~1 mL). To ensure the purity of the lipid samples TLC was performed (methodology section: 1.10) and phosphate assays were performed to determine the accurate concentration (methodology section: 1.9). The PI(4,5)P<sub>2</sub>/cholesterol samples were prepared with PI(4,5)P<sub>2</sub> as 80% of total moles and cholesterol as 20% of total moles.

### 1.8 Buffer Preparation

All buffers used contained either 10mM HEPES (high purity grade, Amresco) or 10 mM Tris (VWR) along with corresponding salts: KCl (VWR), NaCl (VWR), or CaCl<sub>2</sub> (99%, Alfa Aesar) and stored in borosilicate volumetric flasks. The pH for each buffer was adjusted to 7.4 using the corresponding solutions: K<sup>+</sup> buffers were adjusted with 1 M KOH, Ca<sub>2</sub><sup>+</sup> buffers were adjusted with 1 M Ca(OH)<sub>2</sub>, and Na<sup>+</sup> buffers were adjusted with 1 M NaOH. The number of moles required to adjust the pH was subtracted from total amount of moles needed for each experiment.

The water was purified to 7.4 M $\Omega$ \*cm passage through Hydro Picopure 3 Ultrapure system (Hydro). All buffers void of Ca<sub>2+</sub> contained 0.1 mM disodium EDTA (VWR).

## 1.9 Phosphate Assay

To determine the total phosphorus content of each freshly prepared lipid sample a phosphate assay was run. The lipid sample (0.5  $\mu$ moles phosphorus) was added to the bottom of a glass tube and solvent was gently removed with a N<sub>2</sub> stream. The phosphorus standard was added into six separate tubes: 0  $\mu$ moles (0  $\mu$ l) blank, 0.01625  $\mu$ moles (25  $\mu$ l), 0.0325  $\mu$ moles (50  $\mu$ l), 0.0570  $\mu$ moles (88  $\mu$ l), 0.0815  $\mu$ moles (125  $\mu$ l), and 0.1114  $\mu$ moles (175  $\mu$ l). The phosphate concentration for all lipid samples and standards were determined in triplicate. To each of the standard and sample tubes 0.225 mL of 8.9 M H<sub>2</sub>SO<sub>4</sub> was added and the samples were heated in the hood on an aluminum block at 215 °C for 40 minutes. The sample tubes were removed from the aluminum block and allowed to cool for 5 minutes. Then 75  $\mu$ L of 30 % H<sub>2</sub>O<sub>2</sub> was added and the tubes were heated for 40 minutes at 215 °C. Subsequently, the tubes were removed and cooled down for 5-10 minutes (room temperature). Then 1.95 mL of deionized water was added, and each tube was vortexed. Following was the addition of 0.25 mL 2.5 % (w/v) ammonium molybdate (VI) tetrahydrate to all tubes and vertexing each tube 3x. Finally, 0.25 mL 10 % (w/v) ascorbic acid solution to all tubes and each tube was vortexed for 3x. All the tubes were heated at 100 °C for 7 minutes (until observable color change). Then 250  $\mu$ L of each sample was added to a micro-titer plate and the absorbance was measured at 600 nm (Bartlett 1958).

## **1.10 Thin Layer Chromatography (TLC)**

To verify the purity of the lipid samples a thin layer chromatography (TLC) analysis was performed. For PIP lipid samples, the silica gel plate was pre-coated with 5 % (w/v) potassium oxalate in a mixture of 2/3 (v/v) methanol/water. The coated plate was dried and activated at 100 °C for 20-30 minutes before use. The PIP lipid samples were spotted lightly on the potassium oxalate coated silica plates and were placed in a chamber with the following mobile phase: chloroform:methanol:water:acetic acid (10:10:3:1, v/v). The spots were visualized with an iodine vapor chamber, where the  $R_f$  of PI(4,5)P<sub>2</sub> is typically ~0.3-0.4 and PI(3,4,5)P<sub>3</sub>: ~0.2.

## **1.11 Dynamic Light Scattering (DLS)**

Dynamic light scattering (DLS), also known as photon correlation spectroscopy (PCS) or quasi-elastic light scattering, is used to measure the diffusion of macromolecules in solution. The technique primarily measures the Brownian motion of macromolecules in solution that arises due to bombardment from solvent molecules, and relates this motion to the size of particles. In a dynamic light-scattering instrument, the sample is exposed to a laser light and when the monochromatic wave of light encounters macromolecules the incident light scatters in all directions and scattering intensity is recorded by a detector. The scattering intensity of the light is directly related to the size and shape of the macromolecules. The movement of particles is monitored over a range of time, therefore the time averaged intensity provides information on the size of macromolecules; since large particles diffuse more slowly, resulting in similar positions at different time points, compared to small particles, which move faster, consequently not adopting a specific position (Kaszuba, McKnight et al. 2007, Stetefeld, McKenna et al. 2016). The DLS was used in our analysis since it is a non-invasive technique that requires comparatively low amounts

of sample, thus providing us with reliable estimates of the size distribution of lipid and protein samples. To perform all the experiments, we used a Zetasizer Nano-S from Malvern Instruments Ltd. along with Zetasizer software version 7.11.

## **1.12 Synthesis of Bis(cyclohexylamine) Monomethyl Phosphate**

According to the literature (Modro 1992) dichloromethyl phosphate 1 (1 mol equiv) in acetonitrile (0.5 mL per mmol of 1) was added dropwise to a solution of AgNO<sub>3</sub> (2 mol equiv) in water/acetonitrile (1:1, v/v, 1.5 mL per g of AgNO<sub>3</sub>) with stirring at 0 °C. The mixture was stirred overnight in a refrigerator and filtered several times to remove the AgCl precipitate. The solvent was evaporated under reduced pressure. Ethanol was added to the residue to complete precipitation of AgCl. After filtration, the ethanol was removed under reduced pressure and the resulting residue was placed under high vacuum. Monomethyl phosphate 2 was obtained as a colorless oil with white crystals (confirmed with <sup>31</sup>P NMR and <sup>1</sup>H NMR). Cyclohexylamine was added to 2 in excess at 0 °C to form insoluble bis(cyclohexylamine) monomethyl phosphate 3. Excess cyclohexylamine was removed via filtration, and 3 was sonicated in hexane, resulting in a white solid. The white solid 3 was dried overnight under vacuum. The monomethyl phosphate salt 3 was characterized by <sup>31</sup>P NMR H decoupling (chemical shift: 4.84 ppm in D<sub>2</sub>O) and <sup>1</sup>H NMR (chemical shifts: 1.18 (m), 1.32 (m), 1.65 (m), 1.79 (m), 1.87 (m), 3.08 (m), and 3.46 (d) ppm in D<sub>2</sub>O) and FTIR bands in the spectral region 900–1600 cm<sup>-1</sup>.

### **1.13 Infrared Spectroscopy of Monomethyl Phosphate Methodology**

In situ FTIR measurements were performed on a Mettler Toledo ReactIR 15 instrument using a 6.3 mm AgXDi Comp probe and iC IR software. A pH- dependent titration was performed



with 400 mg of monomethyl phosphate (MMP) dissolved in 4 mL of high-performance liquid-chromatography-grade water by adding HCl dropwise to obtain spectra over the desired pH range. On the basis of this titration, a titration of  $\text{Ca}^{2+}$  ions into monomethyl phosphate dissolved in an excess  $\text{K}^+$  was performed at pH 7.5, the deprotonated state of monomethyl phosphate. To have an excess of  $\text{K}^+$  ions, 400 mg of bis(cyclohexylamine) MMP salt was dissolved in 4 mL of 2.5 M KCl solution ( $\sim 1:7$  ( $\text{MMP}^{2-}:\text{K}^+$ ) molar ratio, which is consistent with simulations). The pH was adjusted to 7.5 using HCl and stirred at room temperature. Then, 200  $\mu\text{L}$  additions of 0.5 M  $\text{CaCl}_2$  were titrated into the solution at 3 min intervals. For each  $\text{Ca}^{2+}$  concentration, a spectrum of 250 scans was obtained with a  $4\text{ cm}^{-1}$  resolution. Peak positions were determined from the 2<sup>nd</sup> derivative of the respective spectrum using a center of mass algorithm.

## **1.14 Langmuir Trough Experiments**

### **1.1.1 Principle of Langmuir Trough Monolayer Technique**

Biological membranes are highly complex systems with hundreds of variations in lipid species headgroup structures and acyl-chain lengths and saturation. This complexity puts constraints on studying membranes in their natural state; therefore, we must rely on techniques that allow us to study aspects of the biological membrane, such as using a Langmuir trough. The Langmuir-trough is a convenient way to study several membrane-specific parameters, such as molecular packing, physical states, lateral pressure and lipid composition at the air/water interface. The surface pressure/area isotherms obtained from these experiments provide valuable information about the

thermodynamic properties of the monolayer making it an ideal technique to study the impact of chemical and physical conditions on the lipid monolayer characteristics.

The difference in environment between the surface molecules and those in the bulk is the excess free energy at the air/water interface. This interfacial free energy is accessible by measurements of the surface tension. The surface tension of pure water ( $\gamma_0$ ) is  $\sim 73$  mN/m at  $20^\circ\text{C}$ , which is an exceptionally high value compared to other solvents, making water a very good subphase for monolayer studies. The water subphase is placed into rectangular Teflon trough that consists of two movable barriers on the sides of the trough. Then the lipid mixture of interest is dissolved in an organic solvent which is spread on the subphase. As the organic solvent evaporates, the lipid monolayer is formed on the subphase. At the start of the experiment, there is a large available area for the monolayer to spread, therefore the distance between adjacent molecules is large and their interactions are weak (monolayer regarded as a two-dimensional gas). Under these conditions, the monolayer has little effect on the surface tension of water. When the available surface area of the monolayer is reduced by sweeping the movable barriers over the surface of the trough, the molecules start to exert a repulsive force and the surface tension decreases (surface pressure increases).

The surface pressure is measured with a Wilhelmy plate, a thin plate made of platinum, glass, quartz, mica or filter paper that is suspended so that it is partially immersed in the subphase. The force due to surface tension on a Wilhelmy plate is measured, which is converted into surface pressure ( $\pi$ , mN/m).

The surface pressure ( $\pi$ ) of the lipid monolayer can be described by the following equation:

$$\pi = \gamma_0 - \gamma$$

Where  $\pi$  denotes the surface pressure,  $\gamma_0$  is the surface tension of the subphase in the absence of the monolayer, and  $\gamma$  is the surface pressure in the presence of the lipid monolayer at the air/water interface. The change in surface pressure during the compression (reducing the area with the barriers) is continuously monitored by using a Wilhelmy plate. As the monolayer is compressed, the reduction in the area leads to an increased surface density of the lipid molecules, resulting in a decrease in  $\gamma$  and an increase in  $\pi$ .

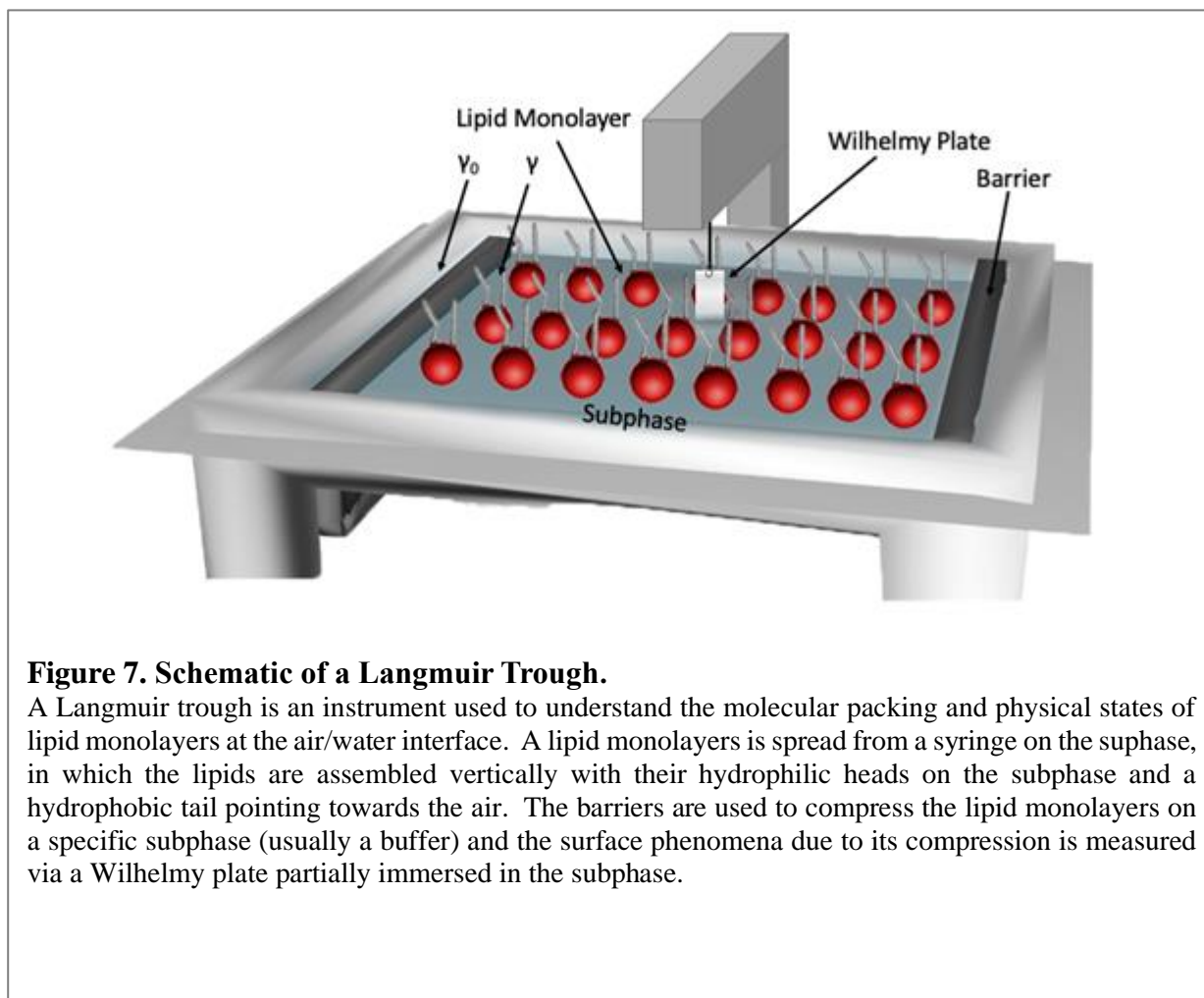


**Figure 7. Schematic of a Langmuir Trough.**

A Langmuir trough is an instrument used to understand the molecular packing and physical states of lipid monolayers at the air/water interface. A lipid monolayers is spread from a syringe on the subphase, in which the lipids are assembled vertically with their hydrophilic heads on the subphase and a hydrophobic tail pointing towards the air. The barriers are used to compress the lipid monolayers on a specific subphase (usually a buffer) and the surface phenomena due to its compression is measured via a Wilhelmy plate partially immersed in the subphase.

The collected data is generated in the form of an isotherm plot, which is the surface pressure ( $\pi$ ) versus the mean molecular area ( $\text{\AA}^2/\text{molecule}$ ). The mean molecular area ( $\text{\AA}^2/\text{molecule}$ ) is determined by monitoring the distance between the barriers. Each specific region of an isotherm gives information regarding the phase state of the monolayer (

**Figure 13).** The phase behavior of the monolayer is mainly determined by the physical and chemical properties of the lipid monolayer, the subphase temperature and the subphase composition. For example, various monolayer states exist depending on the length of the hydrocarbon chain and the magnitude of other cohesive and repulsive forces existing between head groups. An increase in the chain length increases the attraction between molecules, condensing the  $\pi$ -A-isotherm. After spreading the lipids, the monolayer exists in the gaseous state (G) where the area/molecule is large with a low molecular density, hence a low surface pressure. Upon compression, the monolayer enters a liquid-expanded/gaseous (LE/G) coexistence phase, which is characterized by a surface pressure  $< \sim 0.2 \text{ mN/m}$ . Upon further compression, a phase transition occurs to liquid-expanded/liquid-condensed (LE/LC) coexistence region, and finally at even higher densities the monolayer finally reaches the solid state (S). If the monolayer is further compressed after reaching the S-state the monolayer will collapse into three-dimensional structures. This collapse is generally seen as a rapid decrease in the surface pressure (Oy 2013). It should be noted not all Langmuir films will go through all of the states described here during compression of the monolayer. Variations in the thermodynamic behavior of the monolayer

affects the shape of the  $\pi/A$ -isotherm, providing information about the molecular packing of the lipid interactions between the lipid molecules.

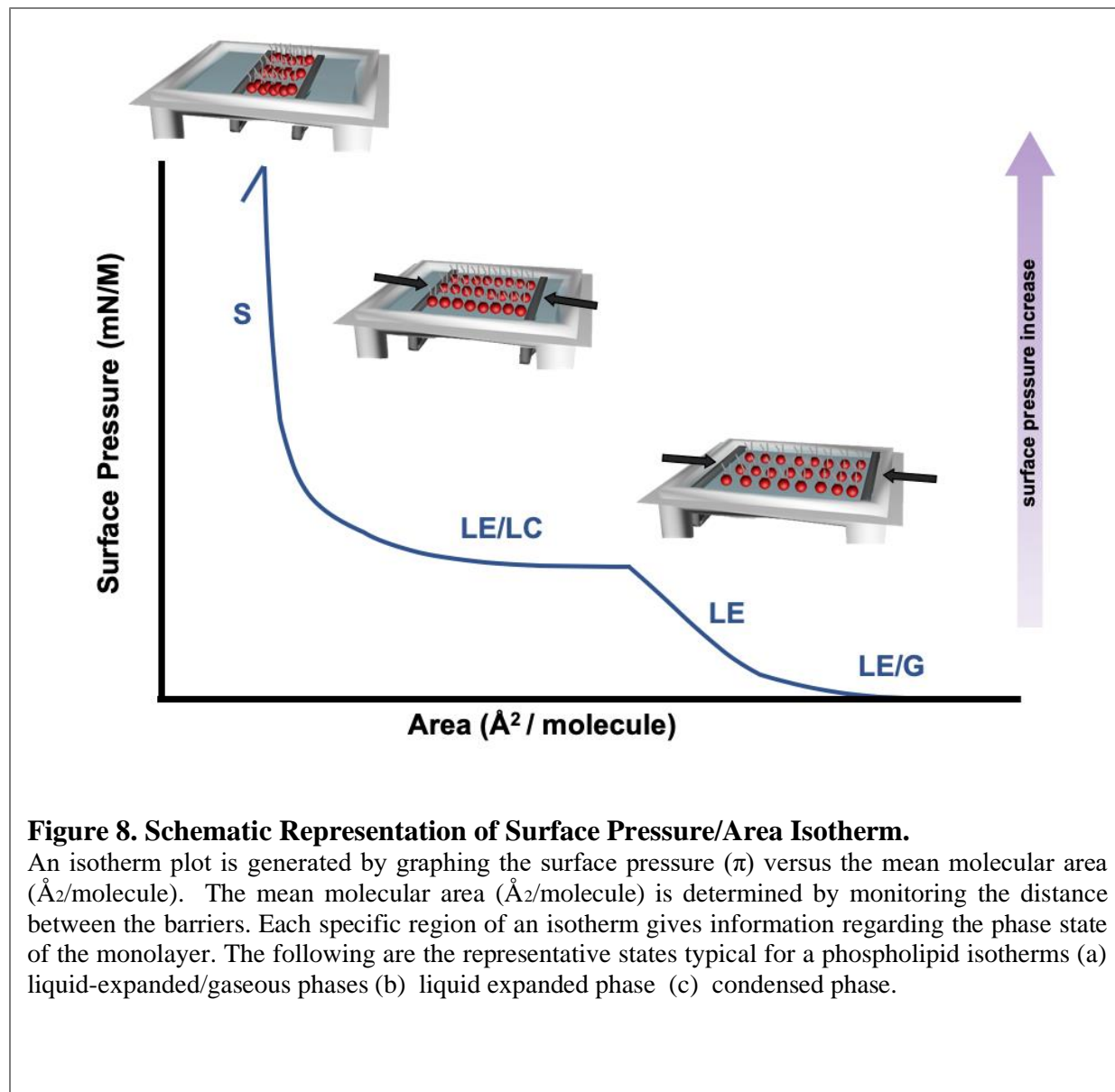


**Figure 8. Schematic Representation of Surface Pressure/Area Isotherm.**

An isotherm plot is generated by graphing the surface pressure ( $\pi$ ) versus the mean molecular area ( $\text{\AA}^2/\text{molecule}$ ). The mean molecular area ( $\text{\AA}^2/\text{molecule}$ ) is determined by monitoring the distance between the barriers. Each specific region of an isotherm gives information regarding the phase state of the monolayer. The following are the representative states typical for a phospholipid isotherms (a) liquid-expanded/gaseous phases (b) liquid expanded phase (c) condensed phase.

### 1.1.2 Experimental Procedure of Langmuir Trough Experiments

The experiments were performed on a Nima 112D trough (Coventry, UK) that was temperature controlled for all experiments (refer to each experiment for specific temperature). The trough and barriers were cleaned thoroughly before experimental runs. The barriers were removed from trough and soaked overnight in hexane:ethanol (9:1) mixture, then the following day they were thoroughly rinsed with deionized water. The trough was cleaned with the following solvents: hexane, a hexane: ethanol mixture (9:1), ethanol, then deionized water. Each solvent stayed in the trough for ~10mins and the Teflon was cleaned with lint-free Kimtech wipes W4 before the addition of the subsequent solvent. Once the trough was thoroughly rinsed with water, the trough was filled with the buffer subphase of interest (refer to each experiment for specific buffer). Before the start of the experiment, the barriers were subjected to a series of compression/expansion cycles to ensure that there was not an increase in pressure upon compression. An increase of surface pressure upon compression may result from surface active impurities. If the pressure increased, any particulates present on the surface were removed by vacuum suction until the pressure reached ~zero. Once the compression of the barriers ceased to increase pressure, the barriers were moved to the fully open position, and the initial surface pressure was recorded. The calculated volume of lipid solution was deposited onto the subphase, then after a 10 minute wait for the organic solvent to evaporate, the barriers were compressed at a rate of 20 cm<sup>2</sup>/min (10.74 Å<sup>2</sup>/min). For cholesterol containing isotherms, the input of molecular weight was for PI(4,5)P<sub>2</sub> only and the concentration input was for the PI(4,5)P<sub>2</sub> only (diluted concentration), the cholesterol molecular weight and concentration were ignored. Therefore, the area/molecule in the  $\pi$ /A-isotherms does not include the area for cholesterol, which is typical for

monolayer studies since the cholesterol molecule takes a smaller space than PI(4,5)P<sub>2</sub> in the monolayer and causes condensations, thus cholesterol was ignored for the calculations. For the 1:1 mixed systems, the input of molecular weight was the average molecular weight and the average concentration of the lipid samples. Therefore, the area/molecule in these  $\pi$ /A-isotherms include the two anionic lipids present. The surface pressure readings were logged at 0.5 seconds with 5 samples per reading and the resulting surface pressure/area isotherm was recorded. These experiments were repeated a minimum of three times for each lipid composition, and the area of the isotherms had to be within 1-2 Ångstroms squared to be considered reproducible.

### **1.15 Attenuated Total Reflection (ATR) Fourier Transform Infrared (FTIR) Spectroscopy**

Attenuated Total Reflection (ATR) Fourier Transform Infrared (FTIR) spectroscopy is a label-free, non-destructive analytical technique that can be used extensively to study a wide variety of different biological molecules. In fact, ATR-FTIR is one of the most valuable methods used to understand proteins and lipids in the biological membrane (Martin, Goormaghtigh et al. 2003, Glassford, Byrne et al. 2013, Kazarian and Chan 2013). The technique provides information about the secondary structure, the orientation and the tertiary structure changes of a protein in an oriented system, such as in the presence of lipids. The environment of the protein molecules can be modulated so that their conformation can be studied as a function of temperature, pressure and pH, as well as in the presence of specific ligands (Barth and Zscherp 2003).

ATR-FTIR spectroscopy involves directing the infrared light at an interface between an infrared transparent material that has a high refractive index (such as a prism made of ZnSe, diamond, silicon or germanium) and a sample on the prism. The angle of incidence of the IR beam

is greater than the critical angle leading to the occurrence of total internal reflection. At the reflecting surface, a standing wave of radiation known as an evanescent wave interacts with the sample, attenuating the infrared beam of light exiting the prism (**Figure 14**). The depth to which the evanescent wave penetrates a sample is dependent on the angle of incidence and the refractive indices of both the prism and the sample, however it is typically in the range of 0.5–2  $\mu\text{m}$ . The penetration depth of the evanescent wave is advantageous for studying molecules in aqueous solutions, in particular proteins. It is also an ideal technique for lipids due to the virtually nonexistent light scattering, especially since light scattering from lipids makes other spectroscopy methods impossible, such as circular dichroism (CD) spectroscopy.

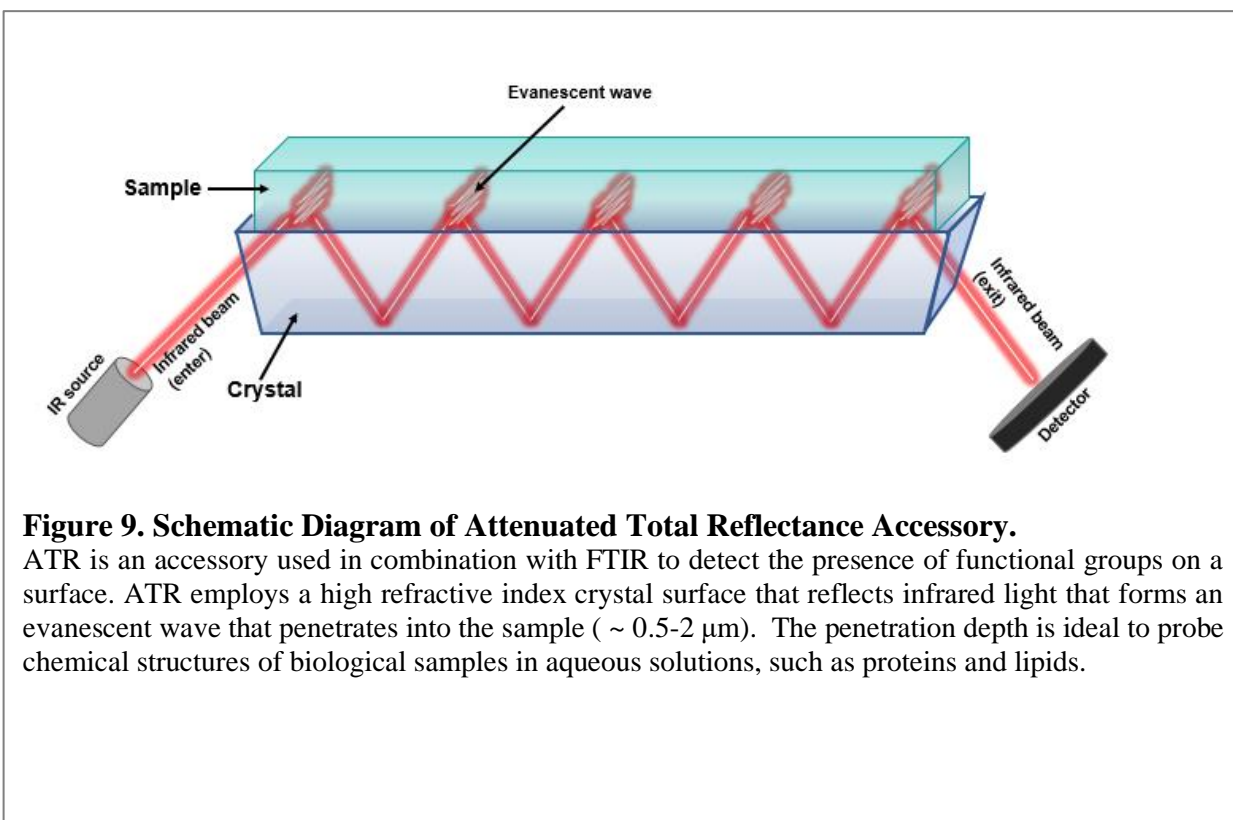


**Figure 9. Schematic Diagram of Attenuated Total Reflectance Accessory.**

ATR is an accessory used in combination with FTIR to detect the presence of functional groups on a surface. ATR employs a high refractive index crystal surface that reflects infrared light that forms an evanescent wave that penetrates into the sample ( $\sim 0.5\text{-}2\ \mu\text{m}$ ). The penetration depth is ideal to probe chemical structures of biological samples in aqueous solutions, such as proteins and lipids.



The use of ATR-FTIR spectroscopy allows us to gain insight into a protein's structure and behavior through monitoring 5 characteristic proteins bands, three of which are known as amide bands. The most notable band is the Amide I band, which for proteins has the strongest absorption of infrared light and is found between 1600 and 1700  $\text{cm}^{-1}$ . This band is primarily caused by stretching vibrations of C=O coupled weakly with C-N stretch and N-H bending. The exact band position is determined by the backbone conformation and the H-bond pattern within the protein molecule (Haris 1999). The other amide bond commonly used to monitor protein structure is the Amide II band, which occurs at 1500–1600  $\text{cm}^{-1}$  and is mainly the result of the C-N stretch along with N-H in-plane bending. Lastly, the Amide III band is found at 1200–1300  $\text{cm}^{-1}$ , which is the result of complex mixture of vibrations from N-H bending and C-N stretching along with deformation vibrations of C-H and N-H (Arrondo 1992, Surewicz 1992, Haris 1999, Barth and Zscherp 2003, Martin, Goormaghtigh et al. 2003).

Although all three bands can be useful to elucidate the secondary structure of a protein, the Amide I band is the most sensitive to structural changes. Thus, it is commonly used as an indicator for secondary structure changes. Furthermore, the amide I band is not greatly affected by changes in the amino acid side groups due to fact that most of its vibrations occur in the protein's amide backbone. Protein conformations affect the amide I band vibrations, which can be easily monitored. Using the amide I band, the secondary structure of a peptide can be determined. In general,  $\alpha$ -helical structures have a band peak at wavenumbers 1650–1658  $\text{cm}^{-1}$ ;  $\beta$ -sheet structures tend to have bands between 1620 and 1640  $\text{cm}^{-1}$  and between 1670 and 1695  $\text{cm}^{-1}$ ; random coil structures occur at around 1644  $\text{cm}^{-1}$  (Arrondo 1992, Surewicz 1992, Surewicz 1993, Haris 1999). The study of aqueous protein requires  $\text{D}_2\text{O}$  buffer because of the overlap of the water scissoring mode with the Amide-I band at 1600  $\text{cm}^{-1}$ . Additionally, water vapor bands between 1800 and

1500  $\text{cm}^{-1}$  may need to be subtracted to ensure a straight baseline between 2000 and 1750  $\text{cm}^{-1}$  (Dong 1990). Lipids in the presence of proteins can be monitored by their ester carbonyl stretching ( $\nu\text{C}=\text{O}$ ) band at  $\sim 1730 \text{ cm}^{-1}$  (Lewis and McElhaney 2013).

### 1.1.3 Experimental Procedure for ATR-FTIR

FTIR experiments were carried out using a Bruker Tensor Spectrometer (Billerica, MA) equipped with a narrow band MCT detector and a Bruker Bio ATRII unit. Interferograms were collected at 2  $\text{cm}^{-1}$  resolution (512 scans, 20 °C), apodization with a Blackman- Harris function, and Fourier transformed with one level of zero-filling to yield spectra encoded at 1  $\text{cm}^{-1}$  intervals. Protein samples (concentration  $\sim 10 \text{ mg/mL}$ ) were dialyzed against buffer (20 mM MOPS pH 7.4, 150 mM NaCl, 1 mM DTT) made in deuterium oxide ( $\text{D}_2\text{O}$ ) adjusted to pH 7.4 with sodium deuterioxide 40 wt. % solution in  $\text{D}_2\text{O}$ . The dialysis was performed three times for 30 minutes each. To determine the secondary structure of the protein,  $\sim 150 \text{ ug}$  of the  $\text{D}_2\text{O}$ -exchanged protein was placed in the ATR unit and analyzed with the Bruker OPUS software. For the protein-lipid samples, the multilamellar vesicles were formed in the presence of the dialyzed protein, so that all aqueous compartments included protein. After adding the protein solution to the dried lipids, they were vortexed for 60 seconds, three times, waiting 5 minutes between vortexing cycles. The resulting protein/vesicle solutions were placed in the BioATR II unit and analyzed with the Bruker OPUS software. The vesicles did not form an anisotropic, ordered film on the ATR crystal but remained isotropic, as checked by IR measurements using polarized radiation. We obtained buffer spectra using the exchange buffer. The  $\text{D}_2\text{O}$  buffer samples were adjusted with respect to their  $\text{H}_2\text{O}$  (HOD) content so that the intensities of the  $\text{H}_2\text{O}$  and HOD bands matched between the

respective protein and buffer solutions. Subsequently, the buffer spectra were subtracted from the protein/lipid samples to yield a flat baseline between 1600 and 1900  $\text{cm}^{-1}$ . All subtraction values were  $1.0000 \pm 0.0005$ . The resulting spectra were exported to Origin software, where the lipid/protein spectra were normalized to the protein only spectrum, using the maximum value of the amide I band ( $\sim 1638 \text{ cm}^{-1}$ ).

## **1.16 Protein Purification Methodology**

We are the first group to bacterially clone, express and purify ATR-domain of PTEN-L despite many scientific challenges like low-yield protein expression and difficulty obtaining >90% pure protein. We have established a reproducible protocol to purify ATR-domain in high concentrations needed for *in-vitro* characterizations of its lipid binding preferences ( $\sim 10\text{mg/mL}$  needed for biophysical studies, such as FTIR). We were able to successfully upscale the expression in a 10-L biofermentor reactor, which allowed us to obtain much higher yields of protein (5mg per 1L cell paste).

### **1.1.4 Amplification of the Alternative Translated Region (ATR) peptide of PTEN-L**

A cDNA fragment encoding the human PTEN-Long (amino acids 1-577) sub-cloned into pET30b was obtained from Ramon Parsons at Icahn School of Medicine at Mount Sinai (ISMMS) (Hopkins, Fine et al. 2013). The construct encoded a truncated form of PTEN-Long that begins with an ATG in front of amino acid 22 (MSES), thereby removing the signal sequence and cleavage site. The ATR-domain was generated from this construct using polymerase chain reaction

(PCR). The primers used for ATR amplification were the following: PTEN-Long (NdeI) forward primer 5'-ATAATGCATATGAGCGAGTCCCCAGTCACCATCAGCAGAG-3' and Long ATR (XhoI) reverse primer 5'-TATACACTCGAGATCCGGCAGACGGTGGCTGAAAAAGAAGC-3'. The amplification condition was performed in a 50µL reaction volume consisting of 1.5 µL template PTEN-Long DNA (~ 160 ng/µL), 1µL of 100 ng/µL forward and reverse primers, 1 µL dNTPs, 1 µL Pfu Turbo DNA polymerase (2.5 U/µL), 0.5 µL DMSO, 39 µL nuclease free water. The PCR cycle was run for 10 minutes at 95 °C as initial denaturation, followed by 40 cycles of 45 seconds at 95 °C for denaturation, 45 seconds at 55 °C for annealing, 60 seconds at 72 °C for extension, and final extension for 5 minutes at 72 °C.

### **1.1.5 Cloning ATR-Domain of PTEN-L into pET30b Vector**

A protocol to successfully clone the ATR-domain of PTEN-L into bacterial expression vector, pET30b was established (**Figure 15**). The amplified PTEN-L ATR products were run on a 1 % agarose gel containing 100X ethidium bromide, then excised and purified using a PCR cleanup kit (Macherey-Nagel). The gel purified PCR products were restriction digested using XhoI and Nde I restriction enzymes for 1 hour at 37 °C, then the digested products were purified using a PCR cleanup kit (Macherey-Nagel). The PCR products were inserted into the *NdeI/XhoI* sites of the bacterial expression vector pET-30b, 5.4 kb (Novagen). A 6-Histag was added on the carboxy terminal of the domains when sub-cloned into the pET30b vector. The PCR products were ligated with the pET30b vector in a 4:1 ratio respectively at room temperature for 5 minutes.

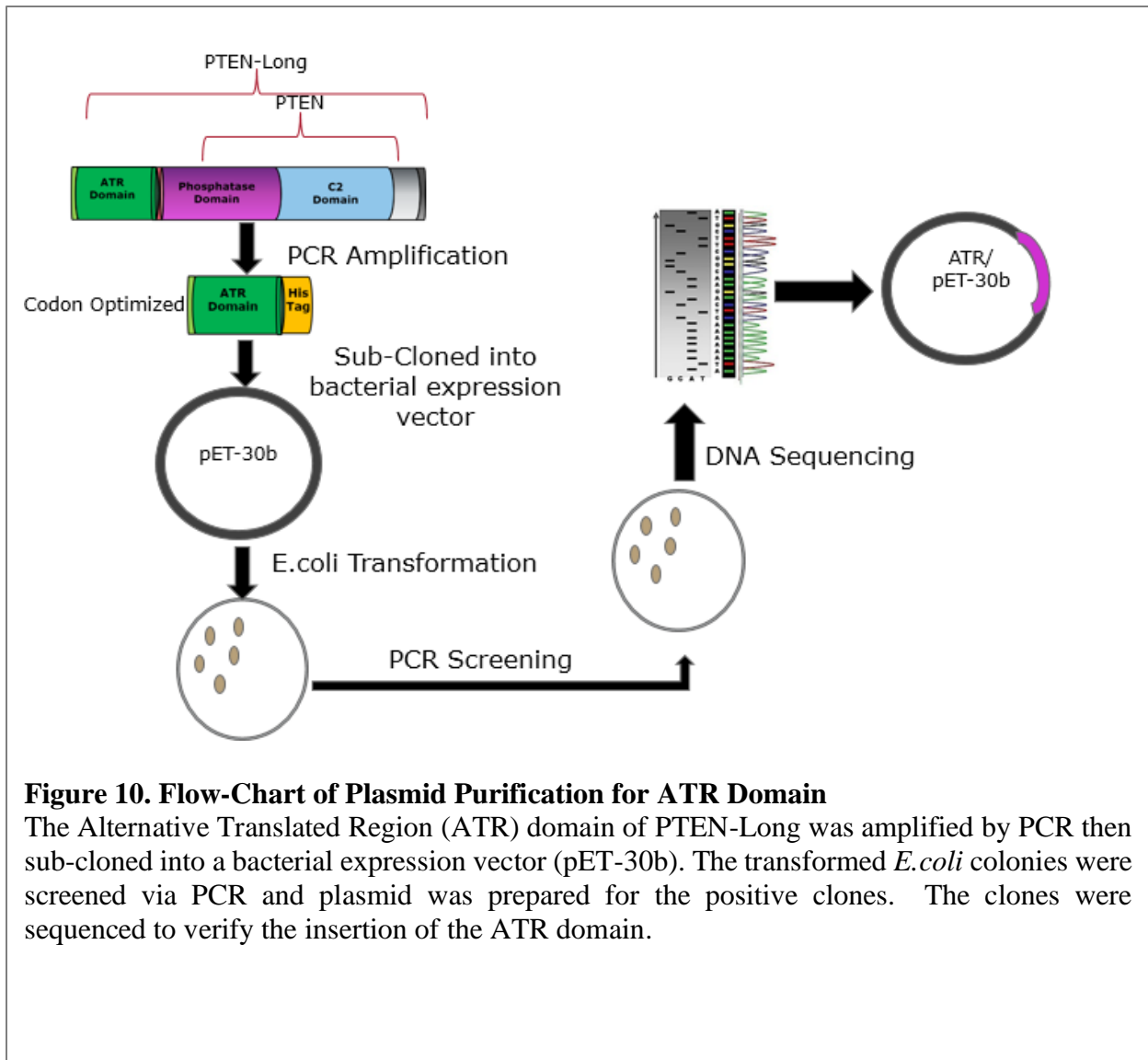


**Figure 10. Flow-Chart of Plasmid Purification for ATR Domain**

The Alternative Translated Region (ATR) domain of PTEN-Long was amplified by PCR then sub-cloned into a bacterial expression vector (pET-30b). The transformed *E. coli* colonies were screened via PCR and plasmid was prepared for the positive clones. The clones were sequenced to verify the insertion of the ATR domain.

Following ligation, 5  $\mu$ L of ligation product was transformed into XL-1 Blue component cells (Stratagene).

To verify the PCR constructs, PCR screening was performed. The transformed colonies were patched on a kanamycin agar plate. A minute amount of each patched colony was added to 100  $\mu$ L of autoclaved water and boiled at 100  $^{\circ}$ C for 10 minutes. Next, the colonies were centrifuged at 14,000 rpm for 10 minutes and 10  $\mu$ L of the supernatant was added to the reaction mixture consisting of 10  $\mu$ L template DNA , 1 $\mu$ L of 100 ng/ $\mu$ L T7 forward and reverse primers, 1  $\mu$ L

dNTPs, 1 μL Taq DNA polymerase, 0.5 μL DMSO, 10 μL nuclease free water and PCR was performed. After the PCR cycle, the products were screened on a 1 % agarose gel. The clones that showed positive for pET30b/ATR were inoculated in 12 mL of LB media (30 mg/mL of kanamycin) overnight at 37 °C. The plasmid was prepared using a plasmid preparation kit (Macherey-Nagel). The clones were then sequenced by Eton Bioscience, Inc. and NCBI BLAST was used to verify the identity of the ATR insert (**Figure 16**).

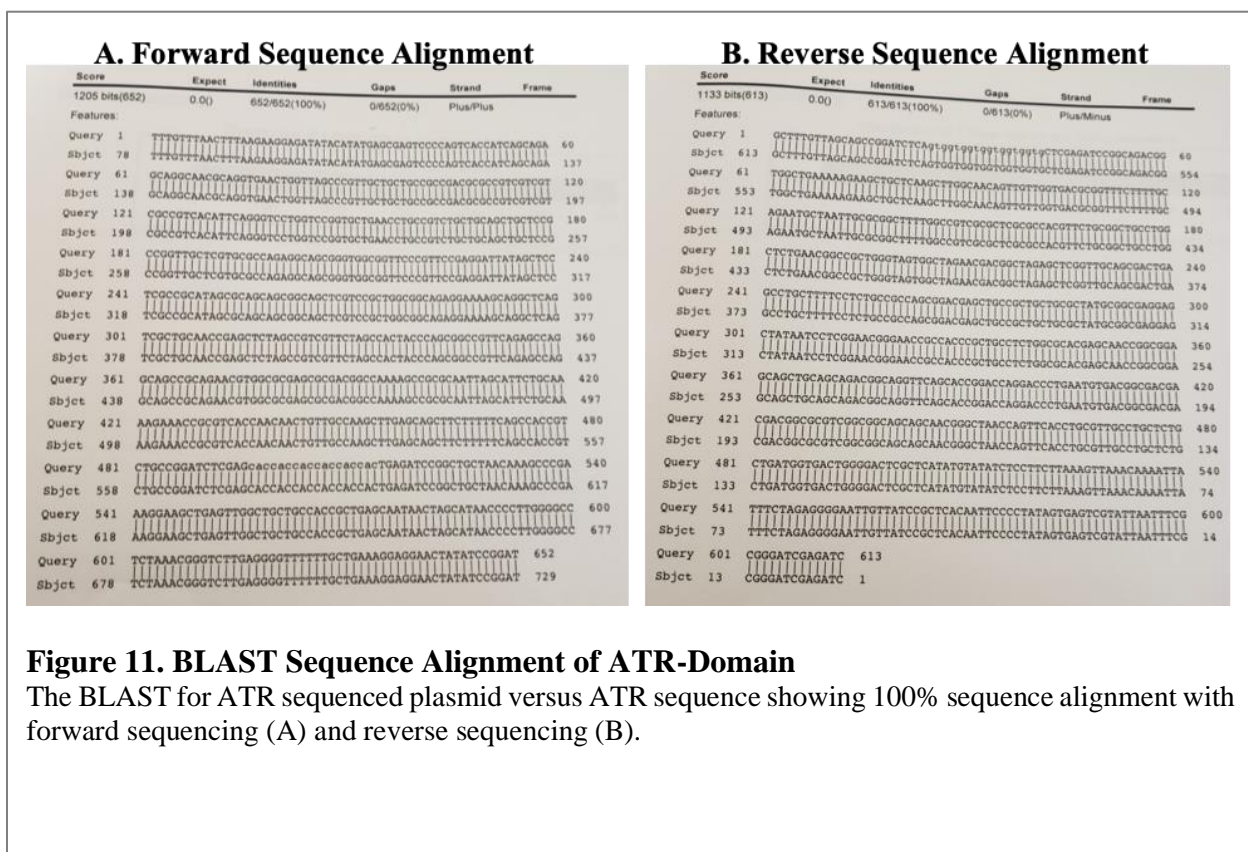


**Figure 11. BLAST Sequence Alignment of ATR-Domain**  
 The BLAST for ATR sequenced plasmid versus ATR sequence showing 100% sequence alignment with forward sequencing (A) and reverse sequencing (B).

### **1.1.6 Transformation of ATR/pET30b into BL21 DE3 pLys Competent Cells**

Approximately 1  $\mu$ L of ATR of PTEN-Long/pET30b codon optimized with C-terminal 6-histidine tag plasmid ( $\sim$  200 ng/ $\mu$ L) was added to *E. coli* strain Rosetta (DE3) competent cells (Novagen). The tube was gently flicked several times and the competent cell/DNA mixture was incubated on ice for 30 minutes. The transformation was heat shocked at 42  $^{\circ}$ C for 42 seconds, then placed back on ice for 2 minutes. 400  $\mu$ L of SOC recovery media was added to the bacteria and grown at 37  $^{\circ}$ C on a rotating incubator for 1 hour. 50  $\mu$ L and 100  $\mu$ L of the transformation was plated on kanamycin agar plates and incubated at 37  $^{\circ}$ C overnight. A single colony for the transformation was grown in 100 mL of autoclaved Luria-Bertani (LB, 1 g tryptone, 0.5 g yeast extract, and 1 g NaCl) containing kanamycin (30 mg/mL) and incubated at 37  $^{\circ}$ C at 200 rpm for approximately 20 hours. A fresh transformation was performed for each expression, except in the case of the large-scale fermentation glycerol stocks were made. After the bacterial growth, 500  $\mu$ L of the overnight culture was added to 500  $\mu$ L of 50 % glycerol in a 2 mL cryo-vial, gently mixed, then flash froze and stored at -80  $^{\circ}$ C.

### **1.1.7 ATR/pET30b in *Escherichia coli* Shaker Flask Expression**

Numerous expression conditions, such as competent cell type, media-type, isopropyl  $\beta$ -D-1-thiogalactopyranoside (IPTG) concentration, induction temperature, and induction length expression conditions were optimized for the expression of ATR-domain (**Figure 17**). The OD<sub>600nm</sub> was taken for the each freshly prepared ATR/pET30b transformation. Then enough of

the culture to bring to ~0.1 OD<sub>600nm</sub> was added to 1 L of autoclaved 2XYT media (16 g tryptone, 10 g yeast extract, 5 g NaCl) containing kanamycin (30 mg/mL) to 0.05 OD<sub>600nm</sub> ( normally ~10 mL of O/N culture). To a 1 L shaker flask culture, 200 µL of antifoaming agent (antifoam 204, Sigma Aldrich) was added and the culture was grown at 37 °C with a 180 rpm shaker speed until culture reached a 0.6-0.8 OD<sub>600nm</sub>. When the culture reached an OD<sub>600nm</sub> of 0.6-0.8, the protein expression was induced with 1 mM isopropylthiogalactoside (IPTG). Then cultures were grown

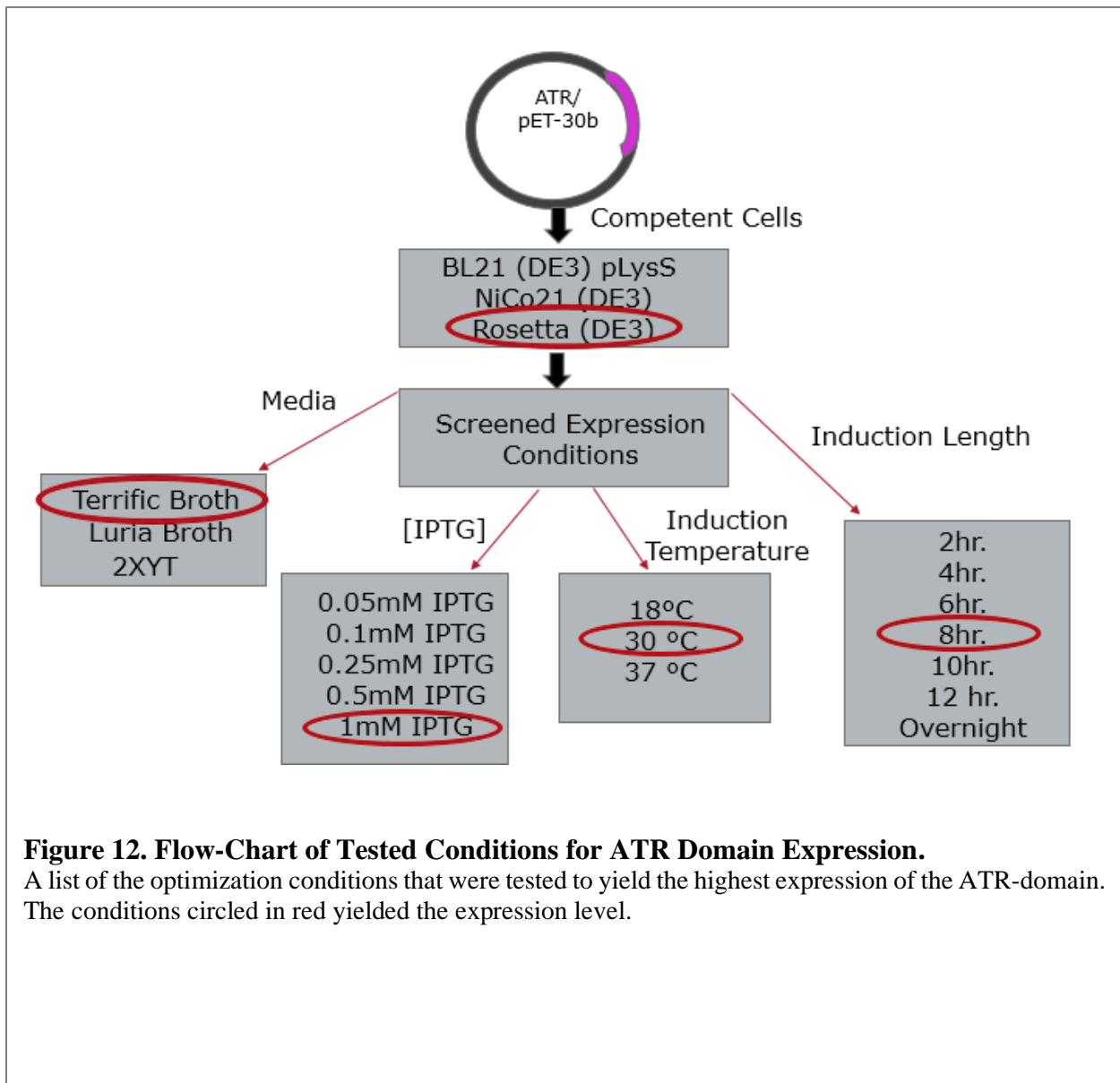


**Figure 12. Flow-Chart of Tested Conditions for ATR Domain Expression.**

A list of the optimization conditions that were tested to yield the highest expression of the ATR-domain. The conditions circled in red yielded the expression level.



for 8 hours at 30 °C. The cells were pelleted by centrifugation at 6,000xg for 10 minutes at 4 °C using a Beckman Coulter JA-10 rotor. The pellets were stored at -20 °C for downstream purification. The pellets (enough to purify from 6 L of culture) were thawed on ice for approximately 30 minutes and then re-suspended in lysis buffer (20 mM Hepes, pH 7.4, 500 mM NaCl, 10 mM  $\beta$ -ME, 1 mM PMSF, 1 mM benzamidine HCl (serine protease inhibitor), 25 U DNase I, 5 mM imidazole) and lysed by French press three times. The lysates were next clarified by centrifugation at 18,000 rpm at 4 °C for 30 minutes using Beckman JA-10. The supernatant was further clarified by ultra-centrifugation at 50,000xg at 4 °C for 45 minutes using Beckman Coulter Type 70Ti rotor.

### **1.1.8 ATR-Domain of PTEN/pET30b in *Escherichia coli* Bioreactor**

#### **Expression**

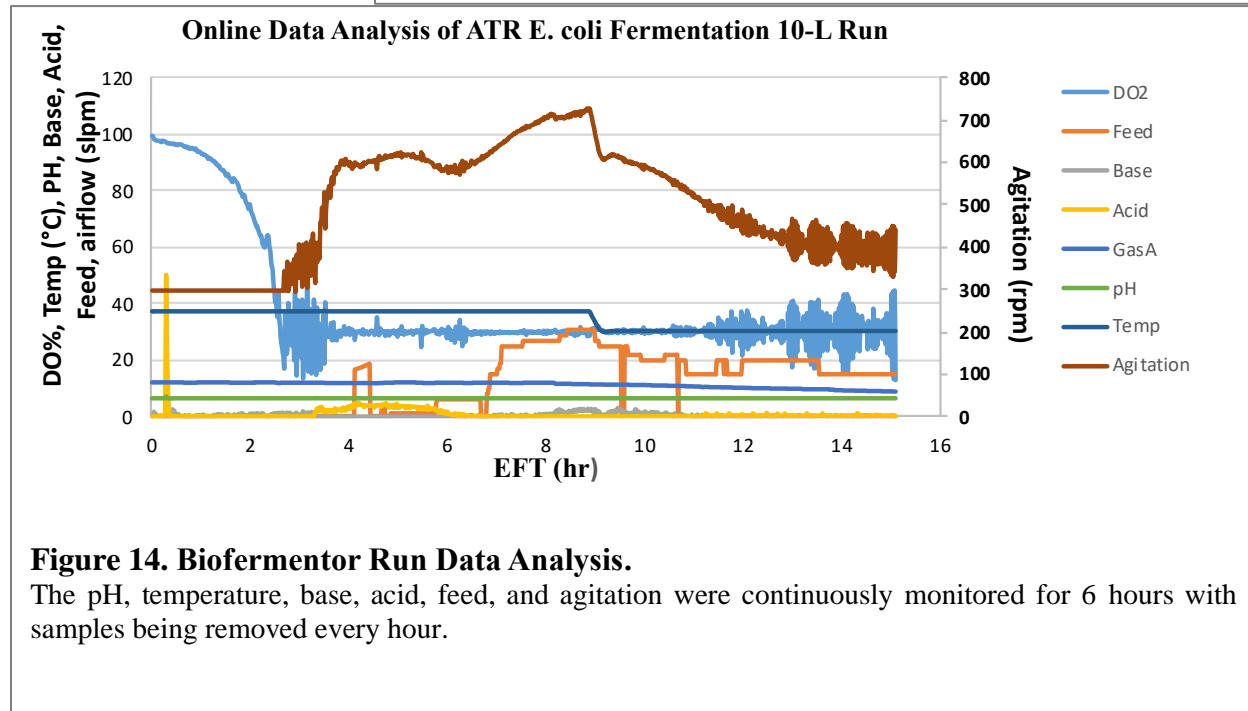
The ATR-domain of PTEN-Long is a low expressing protein. Therefore, expression was upscaled using a 10-L bioreactor. Terrific medium was inoculated with ATR/pet30b glycerol stock and incubated at 37.0 °C and 250 rpm overnight until the optical density (OD<sub>600nm</sub>) was 2-4. The following day, 8.0 L of TB batch medium was transferred into a 10 L Bioflo 3000 vessel (**Figure 18**). After connection of all the hoses, probes (pH, temperature, DO) and inlet tubing (**Figure 18**), 50 mg/mL of kanamycin (8 mL) was added into the fermenter to a final concentration of 50  $\mu$ g/mL. The fermentation run was monitored every hour by measuring OD<sub>600nm</sub>. Once the OD reached ~25-30, 10 mL of 1M IPTG was added for final concentration of 0.1 M IPTG. The pH, temperature, base, acid, feed, and agitation were continuously monitored for 6 hours (**Figure 19**), additionally samples were removed every hour to check the expression levels. The 10 L bacterial

culture was pelleted down by centrifugation at 8000xg and 4 °C for 20 minutes, then the bacterial paste was stored at -20 °C until ready for purification. The upscale of ATR-domain expression in the 10 L biofermentor reactor was successful and a higher yield of protein was obtained (~5mg per 1L of cell paste).



**Figure 13. Upscale of ATR-domain Expression in 10-L Biofermentor.**

In the 10 L Bioflo 3000 vessel, 8.0 L of TB batch medium along with ATR/pet30b and kanamycin (50 µg/mL) was added, then all the hoses, probes (pH, temperature, DO) and inlet tubing were connected before starting the fermentation.



### 1.1.9 Purification of ATR/pET30b

The purification of ATR-domain was successfully optimized to a 2-column purification; the details are described below (**Figure 20**). The PTEN-Long/pET30b contains a carboxy-terminal hexa-histidine (His-6) tag, thus immobilized metal affinity chromatography (IMAC) was used to obtain the highest yield of purified protein. At 4 °C, the supernatant was added 1 mL of HisPur Co-NTA agarose resin (Thermo Fisher Scientific) that had been previously equilibrated with equilibration buffer (20 mM Hepes pH 7.4, 500 mM NaCl, 10 mM imidazole, 10 mM β-ME). Once the protein solution had flowed through the column (approx. 0.5 mL/min), about 40 mL of wash buffer-1 (20 mM HEPES pH 7.4, 500 mM NaCl, 10 mM β-ME, 20 mM imidazole) was added to remove any non-specific bound proteins. To further remove non-specific bound proteins, another wash was performed with 40 mL of wash buffer-2 containing Triton X-100 (20 mM HEPES pH 7.4, 500 mM NaCl, 10 mM β-ME, 10 mM imidazole and 0.75 % Triton-X 100). Then another 20 mL of wash buffer-1 followed by 10 mL of wash buffer-3 containing ATP (20 mM HEPES pH 7.4, 500 mM NaCl, 10 mM β-ME, 20 mM imidazole, 5 mM ATP and 10 mM MgSO<sub>4</sub>). Finally, the his-tagged protein was

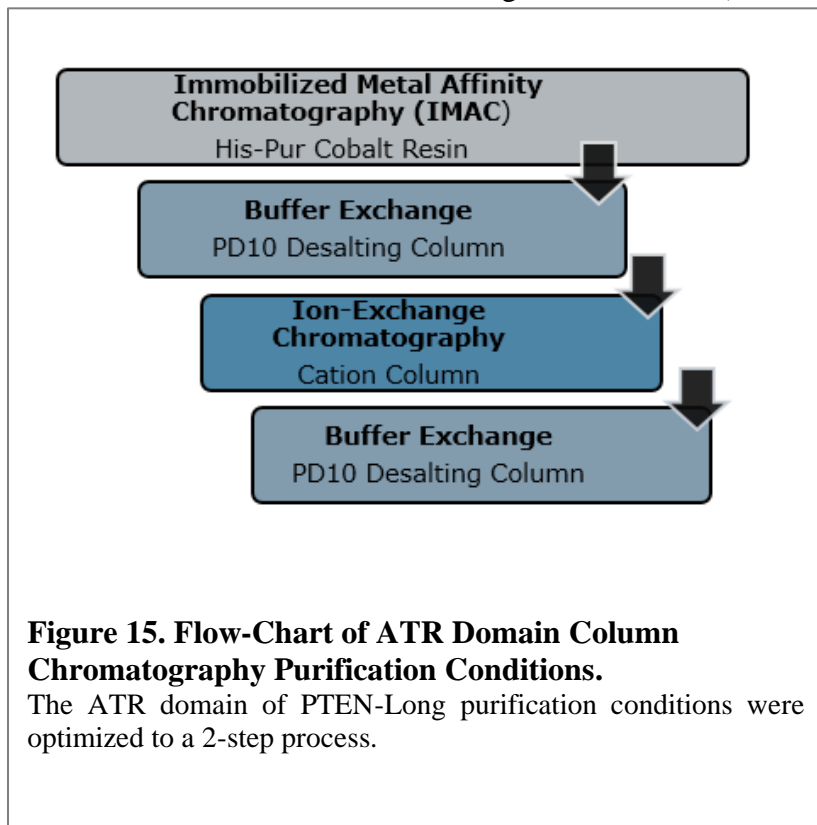


**Figure 15. Flow-Chart of ATR Domain Column Chromatography Purification Conditions.**

The ATR domain of PTEN-Long purification conditions were optimized to a 2-step process.

eluted from the column with 10 mL of elution buffer (20 mM HEPES pH 7.4, 500 mM NaCl, 10 mM  $\beta$ -ME, and 400 mM imidazole) at a flow rate of 0.5 ml/min. The high concentration of imidazole dissociated the his-tagged protein, which was collected in 0.5 mL fractions. The fractions were run on an 15% SDS-PAGE gel. The fractions containing ATR-domain were pooled together and then buffer exchanged using a PD-10 desalting column (20 mM MOPS pH 7.4, 100 mM NaCl, 1 mM DDT).

Next, the ÄKTA FLPC system was used to further purify the protein using cation-exchange column chromatography based on ATR-domain having a isoelectric point (PI) of  $>10$ . The buffer exchanged protein was run at 0.5 mg/mL on a cation column (HiTrap SP FF, GE Healthcare) that was previously equilibrated with low salt buffer (20 mM MOPS pH 7.4, 100 mM NaCl, 1 mM DDT). A gradient of low salt buffer (20 mM MOPS pH 7.4, 50 mM NaCl, 1mM DDT) to high salt buffer (20 mM MOPS pH 7.4, 1 M NaCl, 1 mM DDT) was run at flow rate of 0.5 mL/min. The fractions collected were run on a 15% SDS-PAGE gel and the samples containing the purified ATR-domain were pooled. The purified ATR-domain was buffer exchanged using the PD-10 desalting columns (10 mM MOPS pH 7.4, 150 mM NaCl, and 1 mM DDT). The protein was further analyzed for purity, concentration and aggregation (see section 1.1.10). We have established a reproducible protocol to purify ATR-domain in high concentrations needed for *in-vitro* characterizations (~10 mg/mL needed for FTIR spectroscopy studies).

### **1.1.10 Analysis of ATR-Domain Purity, Concentration, and Aggregation**

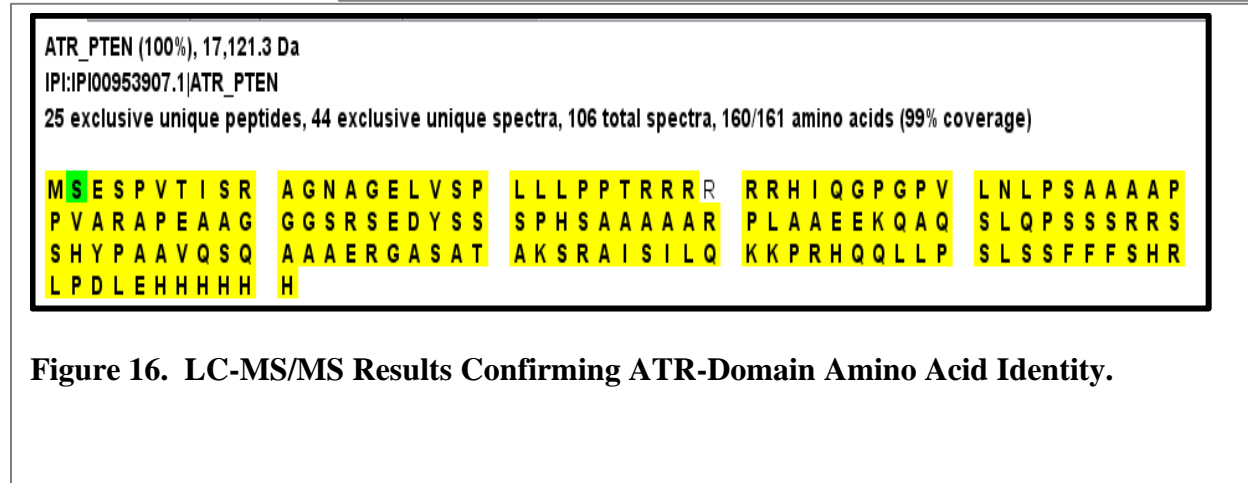
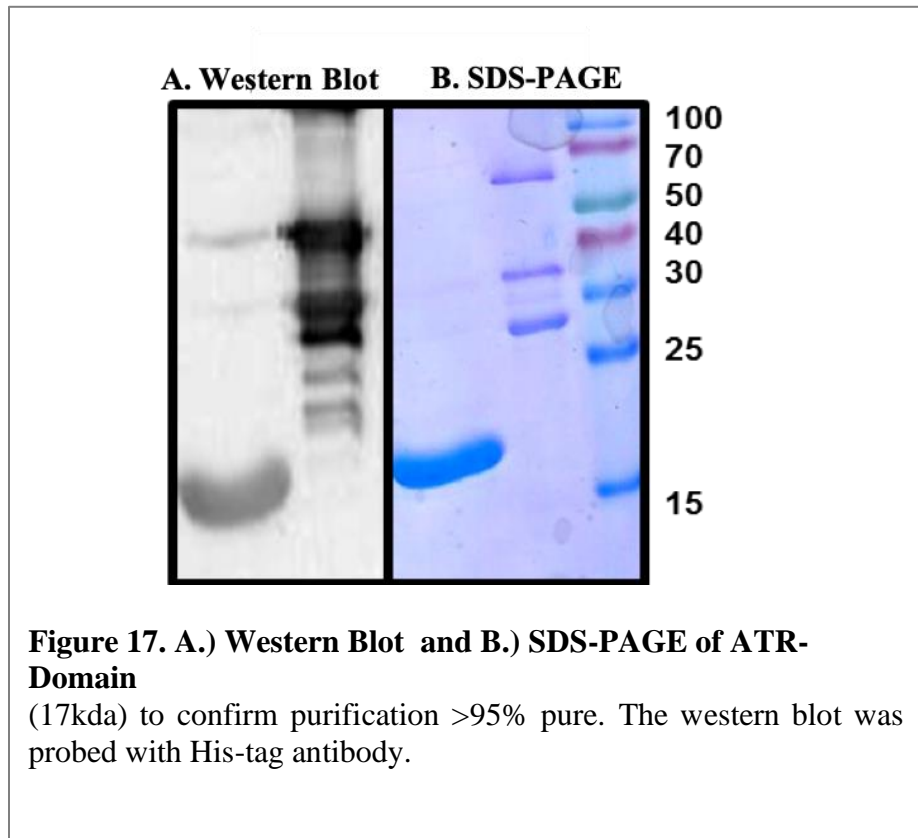
The ATR-domain (~ 17 kDa) was checked for purity using sodium dodecyl sulfate-polyacrylamide gel electrophoresis (SDS-PAGE). The 20  $\mu$ L protein sample with 5  $\mu$ L of loading dye was run on a 15% polyacrylamide gel along with broad range molecular weight marker (New England Biolabs) using the Mini Protean III system from BioRad. The gel was run at room temperature with a voltage of 60V for stacking and 120V for resolving gel with freshly prepared 1X SDS running buffer (25 mM Tris-base, 192 mM glycine, and 0.1 % SDS). The protein bands were visualized by staining the SDS-gel with Fairbanks stains A-C for 10 minutes followed by de-staining with Fairbanks stain D. Next, to further confirm the purification of the ATR-domain a western blot was run. After the protein samples were analyzed on SDS-PAGE gel (following above procedure), the protein sample was transferred from the SDS-PAGE gel to polyvinylidene difluoride (PVDF) membrane (pre-wet in methanol) using a wet-transfer setup at 4 °C and 110minutes at 100 volts. The membrane was blocked with 3% fatty acid free BSA in TBS and shook for 1 hour at room temperature. Then the blot was incubated with His-tag anti-rabbit (Genscript) (100 $\mu$ L of 0.1 $\mu$ g/mL in 25mL of 1% dry milk) and shook for 1 hour at room temperature. The membrane was washed 3x with tris-buffered saline and tween-20 (TBST) buffer and incubated with secondary antibody goat anti-rabbit IgG (Genscript) (100  $\mu$ L of 0.1  $\mu$ g/mL in 25 mL of 1% dry milk ) for 1 hour at room temperature. Following a wash 3x with TBST, the membrane was rinsed with water and developed using enhanced chemiluminescence (ECL) plus western blotting substrate kit (Pierce) and imaged with a BioRad universal II gel-doc imager. The western blot and SDS-PAGE analysis confirmed the ATR-domain was >95% pure (**Figure 21**).

To further verify that the purified protein was indeed ATR-domain, LC-MS/MS was performed at UMass Medical School Spectrometry Facility (**Figure 22**).

The protein concentration was determined using Bradford assay. For the Bradford assay, 25  $\mu$ L of protein sample or 25  $\mu$ L of BSA standard was added to a 96-well u-bottom micro-titer

plate, along with 250  $\mu$ L of Coomassie plus protein assay reagent (Thermo Scientific).

The samples were mixed thoroughly, and the micro-titer plate was read at 595 nm on Perkin Elmer Victor multilabel plate reader using Wallac 1420



Manager software. The concentration was determined from the standard curve with known BSA concentration using the mean and standard deviation of the triplicate set. The Protein sample was checked for aggregation using Zetasizer nano-ZS dynamic light scattering instrument (DLS) at 4 °C (Malvern Instruments) and a monodisperse distribution at ~ 10 nm was found.

## Chapter 3: The Effects of Cations on PI(4,5)P<sub>2</sub> Clustering

### 1.17 Introduction

Cell signaling pathways often involve recruitment of peripheral proteins to the plasma membrane, an association that is classically described as an electrostatically driven approach due to the interaction with anionic headgroups of phospholipids, frequently with PI(4,5)P<sub>2</sub>. PI(4,5)P<sub>2</sub> interaction with proteins regulates a wide variety of cellular processes including endocytosis and exocytosis, endosomal trafficking, cytoskeleton assembly, cell polarization, cell migration (Brown and London 2000, De Matteis 2004, Rheenen 2005, Mengistu 2009). The protein's polybasic residues interact with the highly negative anionic head-group of PI(4,5)P<sub>2</sub>, which includes two phosphomonoesters at the 4- and 5- position, and a phosphodiester in the 1-position securing the headgroup to the glycerol backbone (**Figure 23**) (McLaughlin, Wang et al. 2002, Golebiewska, Gambhir et al. 2006, Lemmon 2007, James, Khodthong et al. 2008, Lemmon 2008, van den Bogaart, Meyenberg et al. 2011, Li, Shi et al. 2014). The ever growing list of PI(4,5)P<sub>2</sub>-regulated proteins (currently >280 proteins) has risen to the point that the cellular concentration of PI(4,5)P<sub>2</sub>-binding proteins is greater than the cellular concentration of PI(4,5)P<sub>2</sub> (Yin 2003, Lemmon 2007, Holmes 2008). While electrostatic interactions with PI(4,5)P<sub>2</sub> may drive proteins to the membrane, how can hundreds of structurally diverse proteins interact with a lipid species found in such low supply (<1% of the total lipids in the PM)? The main hypothesis is that under appropriate conditions PI(4,5)P<sub>2</sub> can cluster into domains that are spatially, structurally, and functionally different from their surroundings providing a highly electrostatic environment for proteins to bind (Do Heo 2006, Fujita 2009, Kwiatkowska 2010, Salvemini, Gau et al. 2014, Brown 2015, Picas, Gaits-Iacovoni et al. 2016). In many cases, the proteins interact with more than one type of anionic



lipid species. This coincidence binding provides for fine tuning of the respective signaling as it requires a distinct environment composed of different lipid species.

It is proposed that small transient clusters of PI(4,5)P<sub>2</sub>, as well as large stable PI(4,5)P<sub>2</sub> lipid domains, affect the lateral organization regulating where and when the protein binds to its target lipid (McLaughlin 2005, Kwiatkowska 2010, Slochower, Wang et al. 2014). Although a significant amount of evidence has accumulated for these PI(4,5)P<sub>2</sub>-rich domains, our understanding regarding the structural determinants required for domain formation is limited.

We are currently struggling to understand the physiological relevant environments required for PI(4,5)P<sub>2</sub> cluster formation. Some researchers believe that the formation and stability of PI(4,5)P<sub>2</sub> clusters is dependent on electrostatic interactions between anionic lipids and polybasic protein domains, as demonstrated with the MARCKS protein (Laux 2000, McLaughlin, Wang et al.

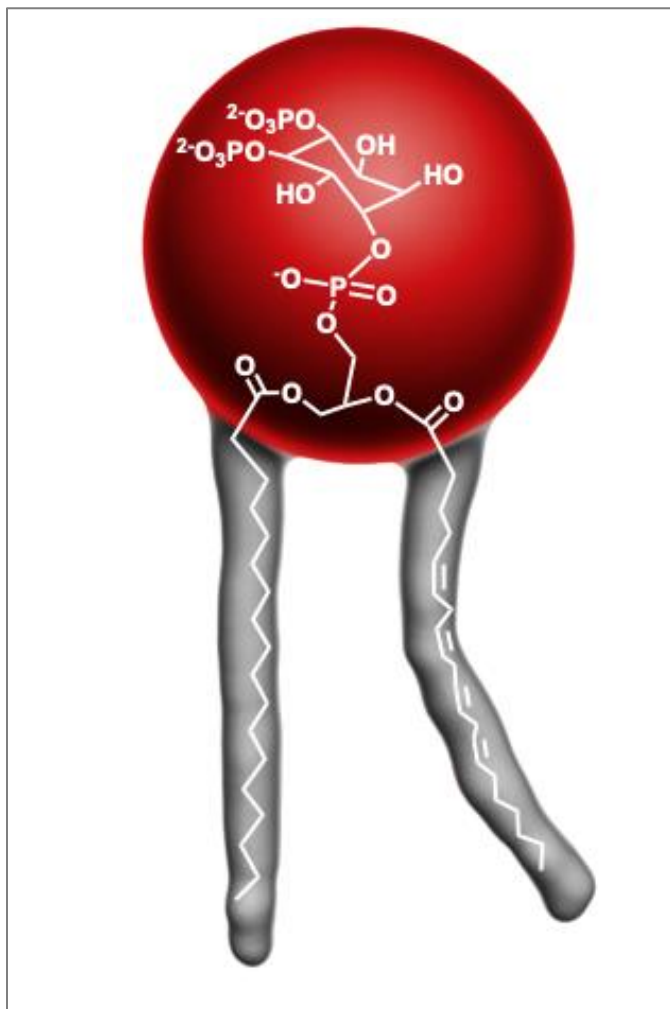


**Figure 18. Chemical Structure of Phosphatidylinositol-4,5-bisphosphate [PI(4,5)P<sub>2</sub>].**

The chemical structure of natural porcine brain PI(4,5)P<sub>2</sub>. The predominant esterified to two fatty acid chains are composed of stearoyl in the *sn*-1 position and arachidonoyl *sn*-2 position of the glycerol backbone. The highly negative headgroup has phosphomonoesters at the 4- and 5-position of the inositol ring.

2002). While other researchers believe that the presence of raft-lipid component, cholesterol, promotes compartmentalization of PI(4,5)P<sub>2</sub> into raft-domains; however, PI(4,5)P<sub>2</sub> does not accumulate in the liquid-ordered phases, which puts PI(4,5)P<sub>2</sub> raft association into question (discussed in Chapter **Error! Reference source not found.**). Interestingly, several studies have shown that PI(4,5)P<sub>2</sub> clusters by itself, suggesting the formation of a H-bonding network. This also suggests that structural determinates, besides proteins, may stabilize lateral PI(4,5)P<sub>2</sub> domains (Ellenbroek, Wang et al. 2011) (Redfern 2004, Redfern and Gericke 2005, Fernandes, Loura et al. 2006). The results from a <sup>31</sup>P NMR study strongly suggested that a hydrogen-bonded networks forms between PI(4,5)P<sub>2</sub> head groups, which is unlike almost all other PIPs (Redfern and Gericke 2005, Levental, Cebers et al. 2008). For intermolecular hydrogen-bonds to lead to PI(4,5)P<sub>2</sub> clusters, PI(4,5)P<sub>2</sub> headgroups must overcome the electrostatic repulsion from their highly negatively charged headgroups. One possible mechanism is to shield the phosphate groups with local cellular cations, which suggests that clustering transitions are sensitive to ionic conditions, not just electrostatic protein interactions (Flanagan 1997, Parekh 2008, Tobias 2008, Kunz 2010, Sarmiento, Coutinho et al. 2014). This assumption has been supported by recent studies showing that the formation of PI(4,5)P<sub>2</sub> clusters are highly dependent on the local cation concentrations in lipid monolayers, large unilamellar vesicles (LUVs), and giant unilamellar vesicles (GUVs) (Lemmon 2008, Ellenbroek, Wang et al. 2011, Slochower, Wang et al. 2014, Graber, Wang et al. 2015, Bilkova, Pleskot et al. 2017, Wen, Vogt et al. 2018). The positive charge of divalent cations reduces the electrostatic repulsion and may act as a bridge between two adjacent lipids (Wen, Vogt et al. 2018) .

The electrostatic potential produced by the charge of the PI(4,5)P<sub>2</sub> headgroup depends directly on the concentration of ions in the cytoplasm (Graber, Wang et al. 2015). PI(4,5)P<sub>2</sub> would

have four negative charges if no cations were bound to it, but the PI(4,5)P<sub>2</sub> is constantly exposed to divalent cations, in particular free cytosolic Ca<sup>2+</sup> (concentration is approximately 100 nM in resting cell). Other ions, such as hydrogen, potassium, magnesium, calcium, and spermine ions in the cytoplasm have also been found to significantly bind to this lipid (Slochower, Wang et al. 2014, Wang, Slochower et al. 2014). It has been proposed that the binding of ions to PI(4,5)P<sub>2</sub> molecules not only depends on the local charge, but also on average electrostatic potential implying that the binding of an ion to one phosphomonoester group on PI(4,5)P<sub>2</sub> may also affect the binding of ions to the adjacent monoester phosphate (Toner, Vaio et al. 2002). In order to understand the binding of cations to the phosphate monoester groups of PI(4,5)P<sub>2</sub>, the characterization of the PI(4,5)P<sub>2</sub> ionization state has been extensively studied.

The electrostatic potential of the PI(4,5)P<sub>2</sub> headgroup under various pH and ion conditions has provided us important information about how PI(4,5)P<sub>2</sub> interacts with chemical species and other membrane resident proteins and lipids. One of the first studies performed was electrophoretic mobility measurements of PI(4,5)P<sub>2</sub>/PC vesicles in the presence of 100 mM KCl, in which the charge was approximated as  $-3$  at pH 7 using the Gouy-Chapman theory (Toner 1988). The Gouy-Chapman theory accounts for the average potential produced by charges at a surface, however the phosphate monoester groups in PI(4,5)P<sub>2</sub> extends  $\sim 0.5$ - $1.0$  nm into the aqueous phase. Therefore, in this case the Gouy-Chapman theory provides us with a theoretical insight into the charge; however, the fact that the distance of PI(4,5)P<sub>2</sub> from the bilayer surface is not considered should not be ignored when considering the surface potential. Another approach monitored the change in zeta potential of PI(4,5)P<sub>2</sub> vesicles at a variety of pH values estimating the charge to be  $-4$  at pH 7 (Ohki 2018). While, an alternative study calculated the charge by combining the first ionization pK<sub>a</sub> values of PI(4,5)P<sub>2</sub> from <sup>31</sup>P NMR studies and second ionization pK<sub>a</sub> values from

phosphatidic acid (PA). The pKa values were within a biologically relevant range for pKa values, with 4-phosphate determined as 6.7 and 5-phosphate as 7.7, which provided an overall negative charge as roughly -4 at pH 7.2. However, it should be noted that the high curvature of the micelles and SUVs used in these studies may have a significant effect on the charge of PI(4,5)P<sub>2</sub> (van Paridon 1986, Swairjo 1994, Levental, Cebers et al. 2008) (Kooijman 2005). This led to another study using multilamellar vesicles that monitored changes in phosphorus chemical shift through <sup>31</sup>P-NMR as the pH was varied. The overall charge of PI(4,5)P<sub>2</sub> calculated from the degree of protonation on the 4- and 5- phosphate was approximately - 4.0 (in a buffer containing 100 mM NaCl, 2 mM EDTA and 50 mM Tris at pH 7.0). In this study it was also further revealed that the degree of deprotonation for PI(4,5)P<sub>2</sub> is inhibited by the presence of the anionic lipids, such as PS and PI. The presence of these anionic lipids increased the negative surface potential, thus decreasing interfacial pH suggesting that PI(4,5)P<sub>2</sub> can overcome the mutual electrostatic repulsion and form intermolecular hydrogen-bonds. Additionally, the ability of PI(4,5)P<sub>2</sub> to hydrogen bond with other anionic lipids significantly increases the deprotonation of PI(4,5)P<sub>2</sub> (Graber, Jiang et al. 2012). Therefore, the net negative charge of PI(4,5)P<sub>2</sub> (ranging from -3 to -5) directly controls interactions with polybasic stretches proteins, as well as other anionic lipids and cations present in the microenvironment of the membrane.

Recent studies have shown that PI(4,5)P<sub>2</sub> clusters can be induced simply by ions; however, why some ions are more effective at affecting PI(4,5)P<sub>2</sub> clustering remains to be understood. Some studies have shown that ions affect domain formation differently. For instance, Ca<sup>2+</sup> and Mg<sup>2+</sup> have similar binding constants for PI(4,5)P<sub>2</sub> but only Ca<sup>2+</sup> is able to induce local PI(4,5)P<sub>2</sub> clustering (Wang, Collins et al. 2012). In order to understand the cation binding effects of PI(4,5)P<sub>2</sub>

clustering, all biologically relevant ions need to be explored. To understand clustering of PI(4,5)P<sub>2</sub> in membranes, our group along with our collaborators investigated clustering of monomethyl phosphate dianion (MMP<sub>2</sub><sup>-</sup>) in solutions of K<sup>+</sup> and Ca<sup>2+</sup>, as well as a mixture of both cations. Using Fourier transform infrared (FTIR) spectroscopy, we observed that Ca<sup>2+</sup> promotes MMP<sub>2</sub><sup>-</sup> clustering in the presence of K<sup>+</sup>, which was confirmed with all-atom molecular dynamics (MD) simulations (Han, Venable et al. 2018). The MMP<sub>2</sub><sup>-</sup> cluster experiments provided a starting point for us to understand cation-dependent clustering of lipids with phosphomonoester groups like phosphoinositides or phosphatidic acid (PA) theoretically and experimentally.

In this study we will systematically investigate PI(4,5)P<sub>2</sub> cluster stabilization in the presence of cations (Ca<sup>2+</sup>, K<sup>+</sup>, Na<sup>+</sup>). We will compare relative effects of these cations on PI(4,5)P<sub>2</sub> condensation using Langmuir trough monolayer studies. Several cation concentrations, as well as mixed cation systems will be explored to determine how PI(4,5)P<sub>2</sub> monolayer packing is electrostatically influenced. We will also use our experimental system to validate all-atom molecular dynamics (MD) simulations performed by our collaborators (Richard Pastor & Kyugreem Han, NIH). We hope our work will explain characteristic ion distributions and clustering patterns of PI(4,5)P<sub>2</sub> allowing us to better understand the spatiotemporal regulation of cell membrane signaling pathways.

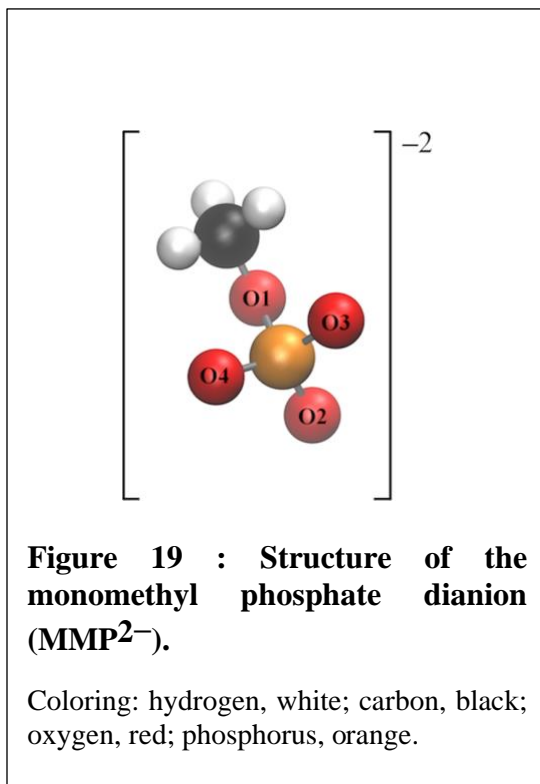
## 1.18 Results:

### 2.1.1 Monomethyl Phosphate Interaction with $\text{Ca}^{2+}$ and $\text{K}^+$

Before we began investigating the effects of cations on PI(4,5)P<sub>2</sub> clustering, we investigated cation-dependent clustering of monomethyl phosphate dianion ( $\text{MMP}^{2-}$ ) (**Figure 24**).

$\text{MMP}^{2-}$  in the presence of  $\text{K}^+$  and  $\text{Ca}^{2+}$  and a mixture of both cations was studied experimentally and theoretically as an entry point to modeling PI(4,5)P<sub>2</sub> clustering in membranes (Han, Venable et al. 2018).

Based on the biphasic pH-dependent ionization of PI(4,5)P<sub>2</sub> and the binding of cations to the more negatively charged oxygen atoms of the phosphate dianions, the completely deprotonated  $\text{MMP}^{2-}$  was used for this study; even though both completely deprotonated and single deprotonated phosphomonoester (monomethyl phosphate anion,  $\text{MMP}^-$ ) exist at pH 7.0. Therefore, we began our studies by monitoring the FTIR bands (1250-950  $\text{cm}^{-1}$ ) over a pH range of 1.5-10.0 to determine the completely deprotonated pH of monomethyl phosphate (**Figure 25**). At low pH, the MMP was single deprotonated, while at  $\text{pH} > 7.0$  the MMP is doubly deprotonated, which was monitored by the band at 981  $\text{cm}^{-1}$  due to the  $\nu_s(\text{PO}_3^{2-})$  vibration. The band at 1181  $\text{cm}^{-1}$  was assigned to the anti-symmetric  $\text{PO}_2^-$  stretching vibration, while the corresponding symmetric stretching vibration was found at 1082  $\text{cm}^{-1}$ . The assignment of the overlapping bands at 1014 and 1046  $\text{cm}^{-1}$  is unclear at this point. Upon further



70

deprotonation, a doublet at 1087 and 1108  $\text{cm}^{-1}$  develops, which can be assigned to the  $\nu_a(\text{PO}_3^{2-})$

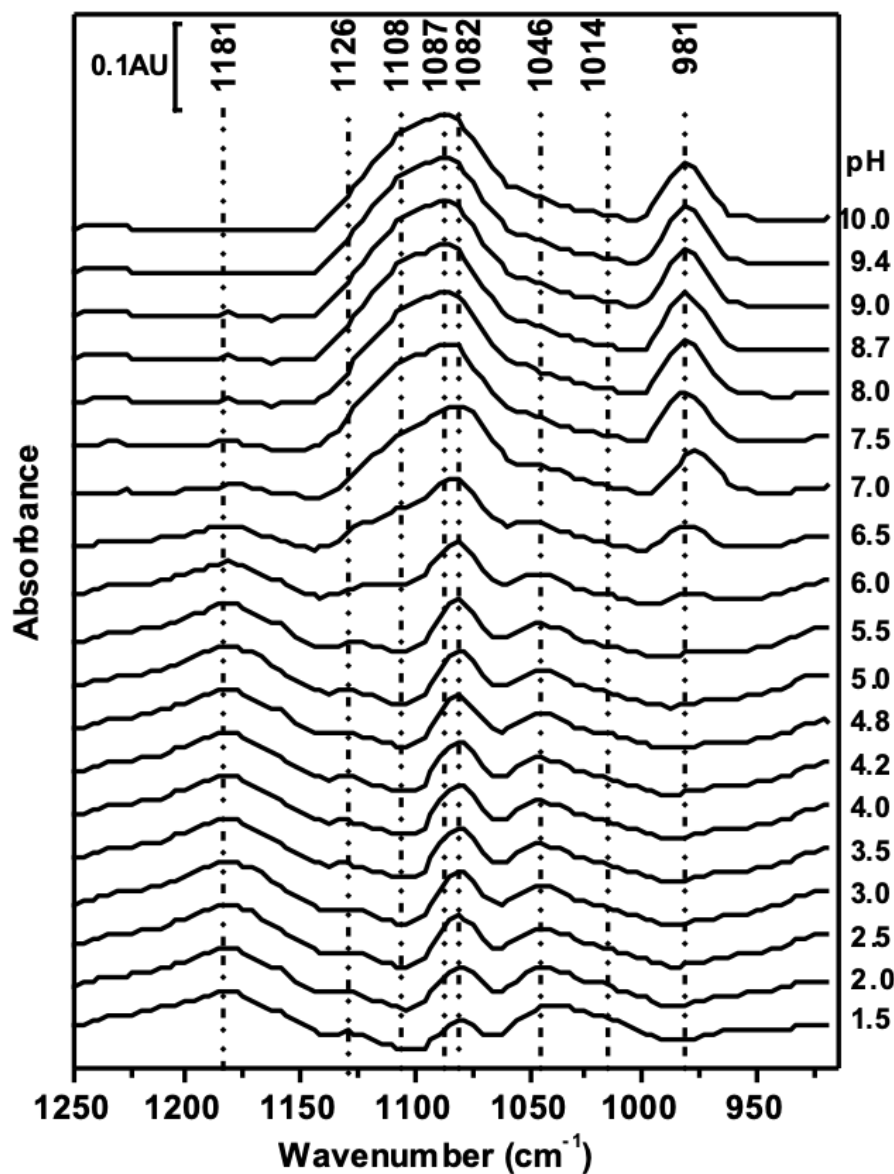
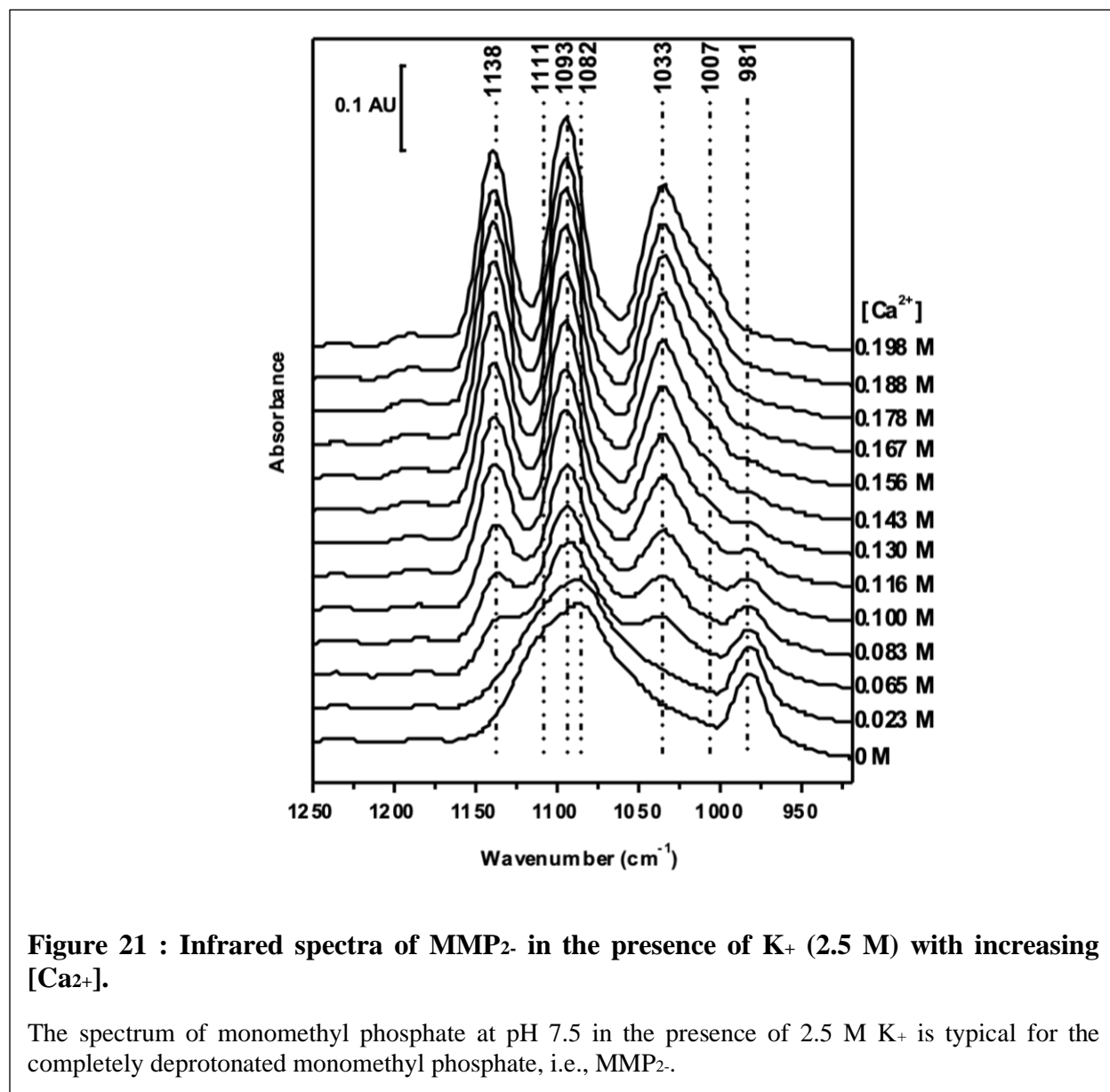


**Figure 20 : Spectra for monomethyl phosphate in the pH range 1.5–10.0.**

At low pH, the MMP is single deprotonated. The band at  $1181\text{cm}^{-1}$  can be assigned to the anti-symmetric  $\text{PO}_2^-$  stretching vibration, while the corresponding symmetric stretching vibration is found at  $1082\text{ cm}^{-1}$ . The assignment of the overlapping bands at  $1014$  and  $1046\text{ cm}^{-1}$  is unclear at this point. Upon further deprotonation, a doublet at  $1087$  and  $1108\text{ cm}^{-1}$  develops, which can be assigned to the  $\nu_a(\text{PO}_3^{2-})$  and  $\nu(\text{C-O-P})$  vibrations, respectively. The band at  $981\text{ cm}^{-1}$  is due to the  $\nu_s(\text{PO}_3^{2-})$  vibration.

and  $\nu(\text{C}-\text{O}-\text{P})$  vibrations, respectively (Laroche, Dufourc et al. 1991).

Next, we investigated the effect of  $\text{Ca}^{2+}$  on the clustering behavior of  $\text{MMP}_2^-$ . Based on deprotonation data (**Figure 25**), monomethyl phosphate at pH 7.5 in the presence of  $\text{K}^+$  (2.5 M) was used to study the completely deprotonated monomethyl phosphate ( $\text{MMP}_2^-$ ) in the presence of  $\text{Ca}^{2+}$ .  $\text{Ca}^{2+}$  was titrated at a concentration range of 0-200mM and for each  $\text{Ca}^{2+}$  concentration a spectrum was obtained (**Figure 26**). Upon addition of  $\text{Ca}^{2+}$  ions, a white precipitate was





observed, indicating the formation of  $\text{Ca}^{2+}/\text{MMP}^{2-}$  crystals. This crystallization was characterized by a marked shift of the  $\text{MMP}^{2-}$  band positions. In the higher wave number region, two strong bands develop at 1093 and 1138  $\text{cm}^{-1}$ , respectively. The  $\nu_s(\text{PO}_3^{2-})$  band found in the absence of  $\text{Ca}^{2+}$  at 981  $\text{cm}^{-1}$  loses intensity with increasing  $\text{Ca}^{2+}$  concentration and instead, a band at 1033  $\text{cm}^{-1}$  with a shoulder at 1007  $\text{cm}^{-1}$  develops. It has been proposed that the binding of  $\text{Ca}^{2+}$  to  $\text{MMP}^{2-}$  reduces the symmetry group from  $\text{C}_{3v}$  (symmetric and asymmetric  $\text{PO}_3^{2-}$  stretching vibrations doubly degenerate) to a low symmetry group, where the degeneracy is removed. Therefore, the 1138 and 1093  $\text{cm}^{-1}$  bands have been assigned to the asymmetric stretching vibrations of the  $\text{PO}_3^{2-}$  group, whereas the bands at 1033 and 1007  $\text{cm}^{-1}$  are due to the  $\text{PO}_3^{2-}$  symmetric stretching mode in the  $\text{MMP}^{2-}/\text{Ca}^{2+}$  complex (Laroche, Dufourc et al. 1991).

Overall, this demonstrated that the interaction of  $\text{Ca}^{2+}$  with  $\text{MMP}^{2-}$  was significantly stronger than the interaction of  $\text{K}^{+}$  with  $\text{MMP}^{2-}$  and that  $\text{Ca}^{2+}$  bridges two or more  $\text{MMP}^{2-}$  molecules for a broad  $\text{Ca}^{2+}$  concentration range. The pronounced  $\text{MMP}^{2-}$  clustering effect of  $\text{Ca}^{2+}$  in the presence of  $\text{K}^{+}$  was confirmed with all-atom molecular dynamics (MD) simulations combined with graph-theoretic analysis (performed by Richard Pastor and Kyugreem Han). The experiment with low and high  $\text{Ca}^{2+}$  concentrations will more likely correspond to the simulations with two cations and only  $\text{Ca}^{2+}$  respectively, in terms of local cation concentration around  $\text{MMP}^{2-}$ . With the high  $\text{Ca}^{2+}$  concentrations (e.g., 0.198 M [ $\text{Ca}^{2+}$ ]), the first coordination shell of  $\text{MMP}^{2-}$  can be mostly occupied by  $\text{Ca}^{2+}$ . The simulation data also showed that this “synergistic” effect depends sensitively on the Lennard-Jones interaction parameters between  $\text{Ca}^{2+}$  and the phosphorus oxygen and correlates with the hydration of the clusters, thus providing us with parameters to understand cation-dependent clustering of lipids with phosphomonoester groups like phosphoinositides or phosphatidic acid. The success of characterizing the cation-dependent

clustering of MMP<sub>2</sub> provided a starting point for us to investigate the clustering of phosphoinositides in cell membranes.

### **2.1.2 Investigating the Role of Calcium on PI(4,5)P<sub>2</sub> Clustering in Langmuir Films**

The success of this study in identifying MMP<sub>2</sub> clusters gave us confidence in our experimental methods and the all-atom simulations by our collaborators, allowing us to understand cation-dependent clustering. In the MMP<sub>2</sub> clustering study, high concentrations of K<sup>+</sup> and Ca<sup>2+</sup> ions (250-500mM) were used to understand the effects of these ions on clustering, which are the typical concentrations used when studying inorganic phosphate clustering. Additionally, for all-atom molecular dynamics (MD) simulations, a higher concentration of ions makes all aspects of sampling easier in the current size of the simulation box (~64 lipids). When moving to understand ion effects on PI(4,5)P<sub>2</sub> clustering, we wanted to stay in line with the experimental parameters of our previous work; thus, we began running our PI(4,5)P<sub>2</sub> monolayer experiments at high cation concentrations (250-500 mM).

Several studies have shown that cations such as calcium can cause PI(4,5)P<sub>2</sub> clustering, but whether this is a purely electrostatic, ion-mediated interaction remains unclear. Therefore, we first investigated the purely electrostatic role of Ca<sup>2+</sup> on PI(4,5)P<sub>2</sub> monolayer packing using Langmuir trough experiments. Please note here these Ca<sup>2+</sup> concentrations were exceedingly higher than physiological concentrations, which are typically ~100 nM in the cytosol and ~2 mM in extracellular fluid and blood plasma. The physical restraints of the all-atom molecular dynamics (MD) simulations required high concentrations, since lower concentrations of Ca<sup>2+</sup> ions do not

provide a fair competition for the negatively charged phosphates. In other words, in the simulations if the amount of  $\text{Ca}^{2+}$  ions is less than the amount required for neutralizing the negative charges of  $\text{PI}(4,5)\text{P}_2$  headgroup, then it would be impossible to distinguish if the interaction was a result of preferential binding or due to a lack of  $\text{Ca}^{2+}$  ions. Therefore, we began our studies with the same  $\text{Ca}^{2+}$  concentration used in the  $\text{MMP}_2^-$  studies (250 mM  $\text{Ca}^{2+}$ ).

The  $\pi/A$ -isotherms of  $\text{PI}(4,5)\text{P}_2$  in the presence of 250 mM  $\text{Ca}^{2+}$  showed a transition from a LE/G state at low surface pressures to an LE state at higher surface pressures (**Figure 27**). Based on previous studies showing that the formation of  $\text{PI}(4,5)\text{P}_2$  clusters was highly dependent on  $\text{Ca}^{2+}$ ,

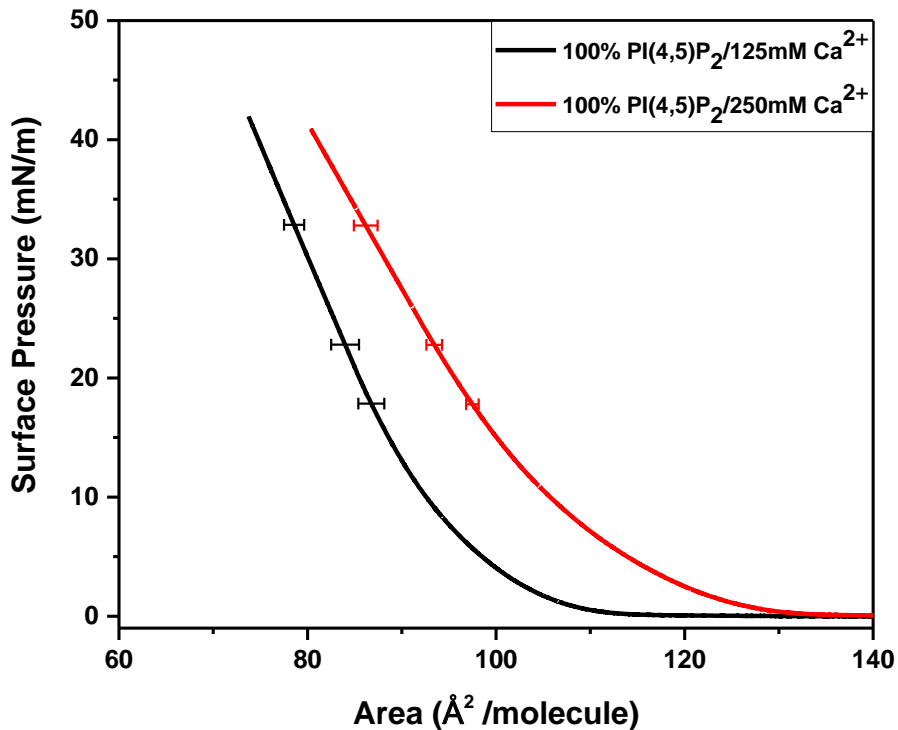


**Figure 22.  $\text{PI}(4,5)\text{P}_2$   $\pi/A$ -Isotherm in the Presence of High Molar Concentration of Calcium**

Monolayers consisted of either 125mM  $\text{Ca}^{2+}$  (black) or 250mM  $\text{Ca}^{2+}$  (red) in 10mM HEPES buffer, pH7.4 at  $T=20.0 \text{ }^\circ\text{C} \pm 0.2$ . Please note that in the presence of high  $\text{Ca}^{2+}$  concentrations the monolayer becomes very stiff, resulting in incorrect surface tension measurements of the Wilhelmy plate in the highly compressed state (low surface tensions).

we expected the  $\pi/A$ -isotherms to be condensed in the presence of such a high  $\text{Ca}_{2+}$  concentrations. The reason for an expansion of the monolayer at sufficiently high concentrations of  $\text{Ca}_{2+}$  is most likely the result of steric effects of the excess  $\text{Ca}_{2+}$  hindering the compressibility of membrane (high  $\text{Ca}_{2+}$  causes a very stiff film) and causing inaccurate surface pressure reading. Therefore, the  $\text{Ca}_{2+}$  concentration in the subphase was lowered to 125 mM, a concentration that could still be tested in all-atom MD simulations. When comparing the 125 mM  $\text{Ca}_{2+}$   $\pi/A$ -isotherm to the 250 mM  $\text{Ca}_{2+}$ , there is a condensation of the monolayer at the lower concentration; however, the characteristics of the isotherm still represent an expanded monolayer, suggesting that even a concentration of 125 mM  $\text{Ca}_{2+}$  leads to a stiff PI(4,5)P<sub>2</sub> monolayer (**Figure 27**). In order to understand the effects of  $\text{Ca}_{2+}$  concentrations, monolayer studies were performed at physiological relevant  $\text{Ca}_{2+}$  concentrations.

Physiological relevant concentrations of  $\text{Ca}_{2+}$  are considered to be 100 nM to ~2 mM; however, a rise of cytosolic  $\text{Ca}_{2+}$  has been observed in microdomains that are involved in cellular signaling ( 0.5  $\mu\text{M}$  to several hundred  $\mu\text{M}$   $\text{Ca}_{2+}$ ) (La Rovere, Roest et al. 2016). The lowest concentration of  $\text{Ca}_{2+}$  that could be experimentally tested was 5 mM. This was because the amount of  $\text{Ca}(\text{OH})_2$  moles required to adjust the pH of the buffer to 7.4 was approximately equivalent to the amount of moles required for a 2.5 mM  $\text{Ca}_{2+}$  concentration. The investigation of the lowest  $\text{Ca}_{2+}$  concentration (5 mM) showed a condensation of the PI(4,5)P<sub>2</sub> monolayer in comparison to 125 mM and 250 mM  $\text{Ca}_{2+}$  concentrations (**Figure 28**). This result confirmed our suspicion that the presence of high  $\text{Ca}_{2+}$  concentrations caused the monolayer to become very stiff, resulting in incorrect surface tension measurements of the Wilhelmy plate in the highly compressed state (low surface tensions).

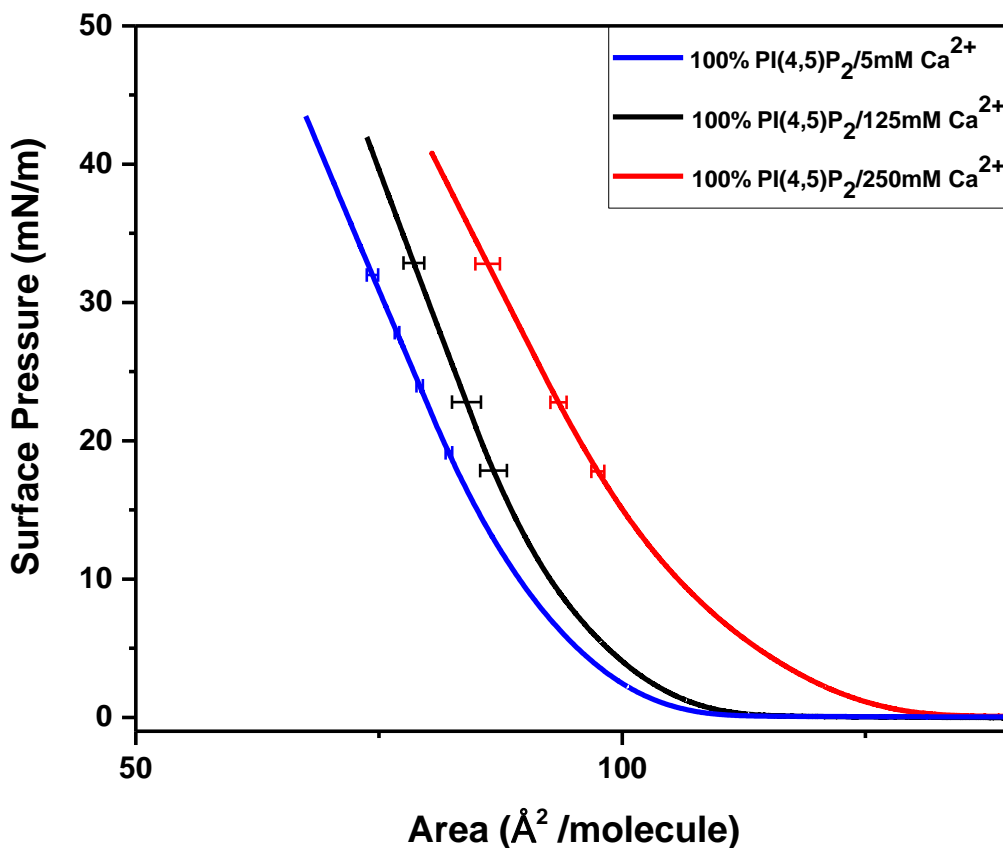


**Figure 23. Comparing PI(4,5)P<sub>2</sub>  $\pi/A$ -Isotherm in the Presence of Several Calcium Concentrations.**

Monolayers consisted of either 5 mM Ca<sub>2+</sub> (navy) 125 mM Ca<sub>2+</sub> (black) or 250 mM Ca<sub>2+</sub> (red) in 10 mM HEPES buffer, pH 7.4 at T=20.0 °C ± 0.2.

Therefore, in order to fully explore the role of low Ca<sub>2+</sub> concentration on PI(4,5)P<sub>2</sub> monolayer stability, we performed the monolayer experiments in the presence of a 125 mM bulk cation concentration, where Na<sup>+</sup> and K<sup>+</sup> concentrations were kept constant, and Ca<sub>2+</sub> concentrations were varied (1 mM, 5 mM, 10 mM, 25 mM, 50 mM and 70 mM). As a control  $\pi/A$ -isotherm in the absence of Ca<sub>2+</sub> but in the presence of 62.5 mM Na<sup>+</sup> and 62.5 mM K<sup>+</sup> (bulk 125 mM) was performed (**Figure 29**). This  $\pi/A$ -isotherm showed an expanded monolayer with a transition from a LE/G state at low surface pressures to an LE/LC state at higher surface pressures,

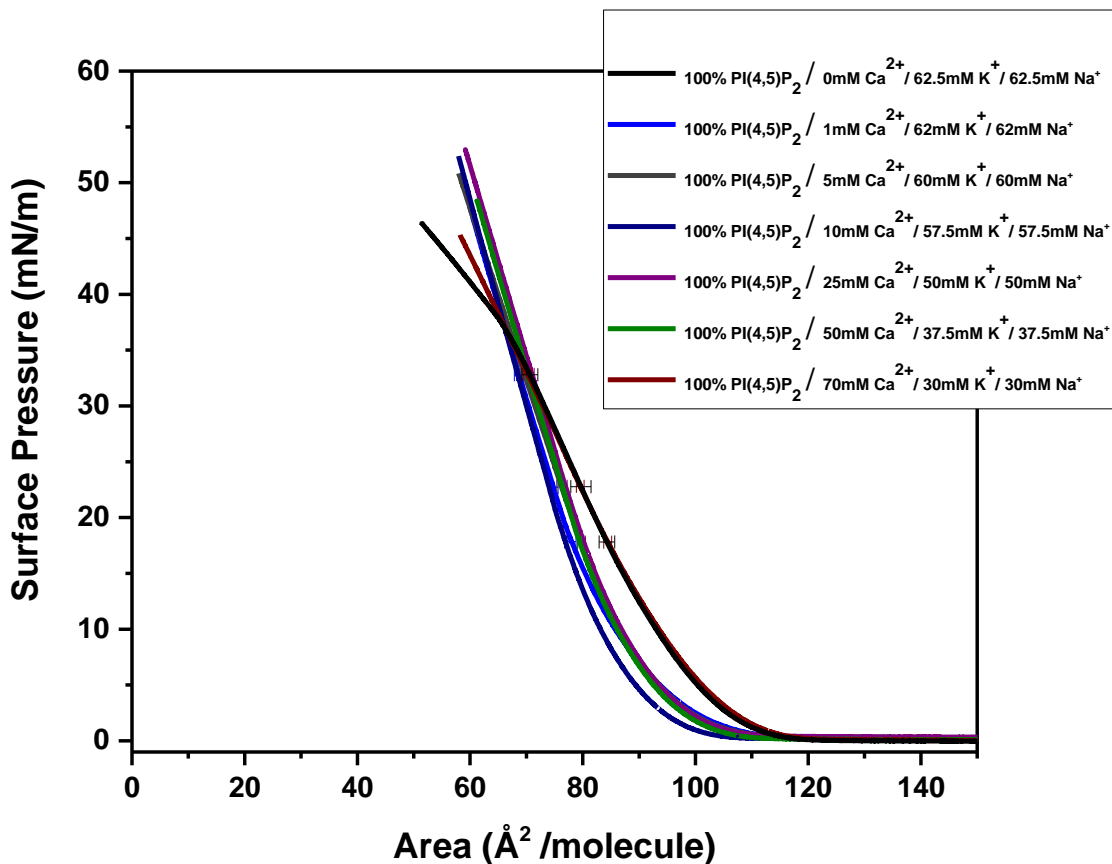


**Figure 24. PI(4,5)P<sub>2</sub>  $\pi$ /A-Isotherm in the Presence of Various Calcium Concentrations.**

The [Ca<sub>2+</sub>] was varied 0 mM Ca<sub>2+</sub> (black), 1 mM Ca<sub>2+</sub> (blue), 5 mM Ca<sub>2+</sub> (gray), 10 mM Ca<sub>2+</sub> (navy), 25 mM Ca<sub>2+</sub> (purple), 50 mM Ca<sub>2+</sub> (green), 70 mM Ca<sub>2+</sub> (wine), while keeping the total bulk concentration 125 mM with molar equivalents Na<sub>+</sub> and K<sub>+</sub>, in 10 mM HEPES buffer, pH 7.4 at T=20.0 °C ± 0.

reaching a collapse at ~45 mN/m. The first addition of Ca<sub>2+</sub> to the subphase was the lowest concentration at 1 mM, which showed relative to the Ca<sub>2+</sub> free subphase experiment, a condensation of the monolayer at surface pressures < 35 mN/m. This unmistakable condensation of the monolayer suggests that Ca<sub>2+</sub> at physiological relevant concentrations does indeed stabilize PI(4,5)P<sub>2</sub> monolayers. The lower area/molecule at surface pressure > 35 mN/m for the PI(4,5)P<sub>2</sub>  $\pi$ /A-isotherm in the absence of Ca<sub>2+</sub> was likely the result of barrier leakage and/or partial monolayer collapse due to PI (4,5)P<sub>2</sub> monolayer instability .

This led us to want to understand the threshold  $\text{Ca}_{2+}$  concentration before it intercalates between the headgroup of PI(4,5)P<sub>2</sub>. To begin to understand what  $\text{Ca}_{2+}$  concentration leads to an expansion of the monolayer, we kept the bulk concentration the same (125 mM) while increasing the  $\text{Ca}_{2+}$  concentration. The  $\pi/A$ -isotherms for 5 mM, 10 mM, 25mM, and 50 mM  $\text{Ca}_{2+}$  all resembled the 1mM  $\text{Ca}_{2+}$   $\pi/A$ -isotherms at surface pressures  $< 20\text{mN/m}$ . There was a slight expansion difference between the 1mM and the 5-50 mM  $\text{Ca}_{2+}$  concentrations at surface pressures greater than  $>20 \text{ mN/m}$ ; however, the expansion was within error limits of the other isotherms. It was not until 70 mM  $\text{Ca}_{2+}$  was added to the subphase that an obvious expansion of the monolayer was observed. Interestingly, the 70 mM  $\text{Ca}_{2+}$   $\pi/A$ -isotherm expanded to resemble a nearly identical  $\pi/A$ -isotherm in the absence of  $\text{Ca}_{2+}$ . This data proves that high  $\text{Ca}_{2+}$  concentrations ( $\geq 70 \text{ mM}$ ) leads to an expansion of the monolayer due to the excess  $\text{Ca}_{2+}$  creating a stiff film (resembling a crystalline-like structure) that results in incorrect surface tension measurements of the Wilhelmy plate in the highly compressed state (low surface tensions).

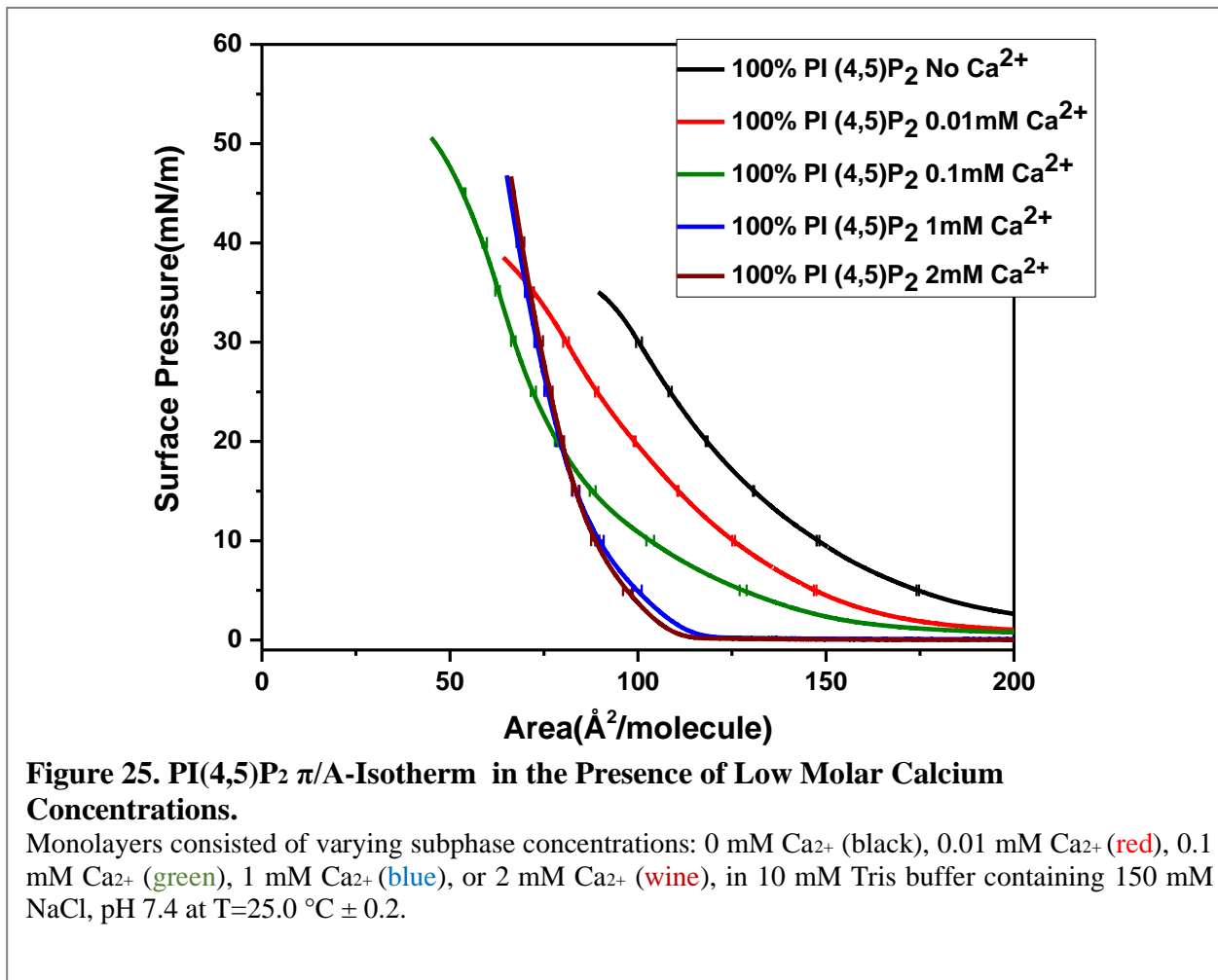
### **2.1.3 Investigating the Role of Physiological Calcium Concentrations on PI(4,5)P<sub>2</sub> Clustering in Langmuir Films**

To continue exploring the role of physiologically relevant  $\text{Ca}_{2+}$  concentrations, we measured  $\pi/A$ -isotherms, mimicking previously performed epifluorescence experiments that showed changes in the morphology of PI(4,5)P<sub>2</sub> monolayers in the presence of  $\text{Ca}_{2+}$  (King 2016).  $\pi/A$ -isotherms studies were performed under the same conditions as the previous epifluorescence experiments to further confirm observed morphological changes. The monolayer subphase conditions were kept the same, with a buffer composed of 10mM Tris along with 150 mM NaCl

and varying physiological concentrations of  $\text{Ca}^{2+}$  (0.01 mM  $\text{Ca}^{2+}$ , 0.1 mM  $\text{Ca}^{2+}$ , 1 mM  $\text{Ca}^{2+}$  or 2 mM  $\text{Ca}^{2+}$ ). As a control, the PI(4,5)P<sub>2</sub> monolayers were also determined in the absence of added  $\text{Ca}^{2+}$  with 0.1 mM EDTA, to chelate any  $\text{Ca}^{2+}$  ions leached from the glassware. Additionally, to remain consistent with epifluorescent experiments, the subphase was maintained at pH 7.4 and a temperature of  $25.0 \pm 0.2^\circ \text{C}$ . Based on previous epifluorescent data exhibiting domains at these low concentrations of  $\text{Ca}^{2+}$  (King 2016), we hypothesized a condensation of the monolayer resulting from  $\text{Ca}^{2+}$  shielding and bridging the PI(4,5)P<sub>2</sub> headgroups.

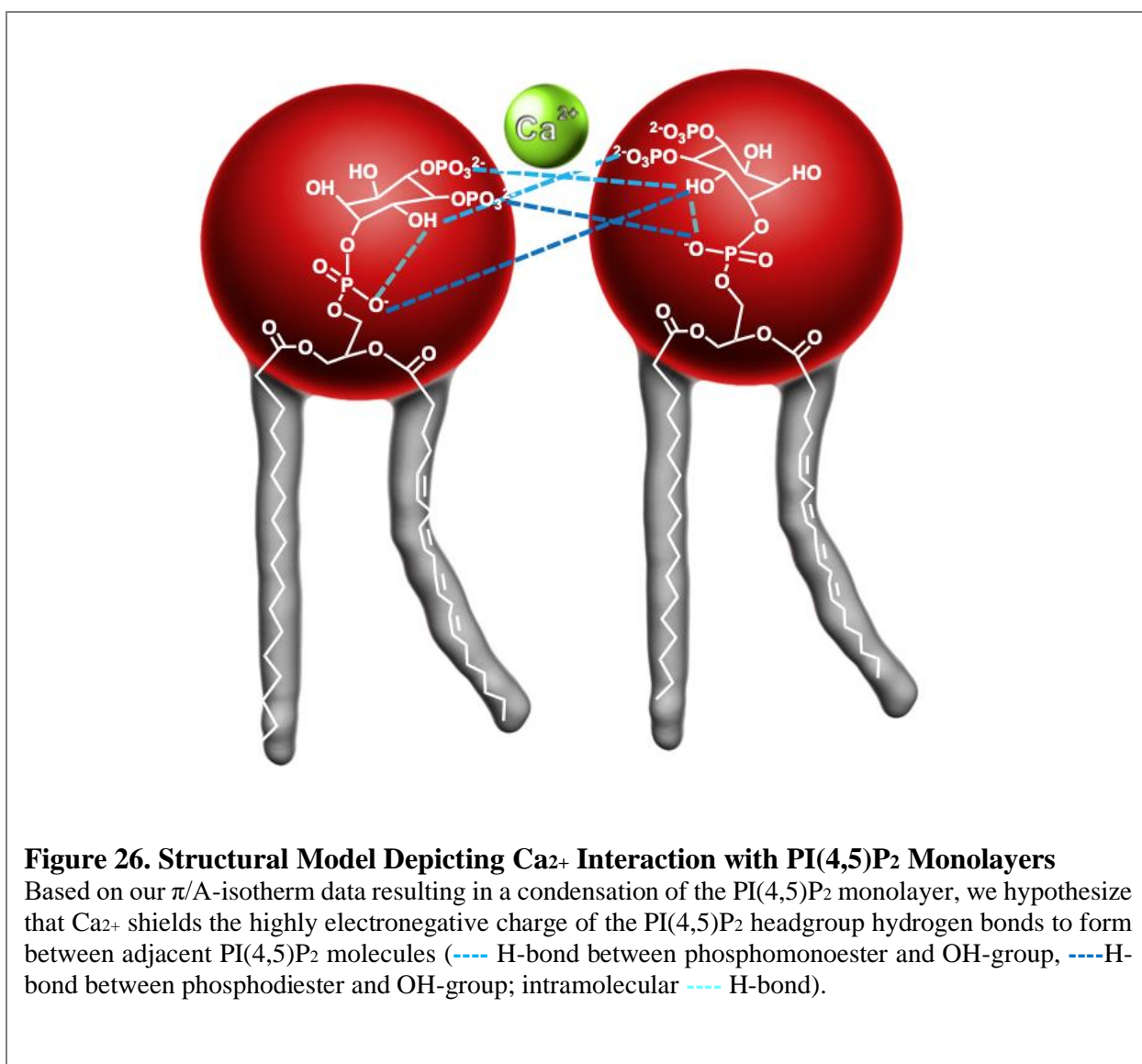
The PI(4,5)P<sub>2</sub> monolayer in the absence of  $\text{Ca}^{2+}$  ions showed an expanded  $\pi/A$ -isotherm with a transition from a LE/G state at low surface pressures to an LE state at higher surface pressures (**Figure 30**). The  $\pi/A$ -isotherm also indicated that the monolayer collapsed at low pressures ( $\sim 35$  mN/m), which was likely from the instability of pure PI(4,5)P<sub>2</sub> to form stable monolayers. PI(4,5)P<sub>2</sub> has a highly unsaturated acyl-chain composition and negative headgroups repulsing one another, which leads PI(4,5)P<sub>2</sub> to slip under the barriers of the Langmuir trough. The isotherm of an unstable monolayer in the absence of  $\text{Ca}^{2+}$  was not surprising because previous epifluorescent data showed no macroscopically discernible domains (King 2016). At the lowest concentration of  $\text{Ca}^{2+}$  0.01 mM, there was a significant condensation of the monolayer (lower area/molecule) compared to  $\text{Ca}^{2+}$  free subphase. The  $\pi/A$ -isotherm also showed an increase in the collapse pressure ( $\sim 38$  mN/m) upon the addition of the 0.01 mM  $\text{Ca}^{2+}$ , showing that a physiologically relevant  $\text{Ca}^{2+}$  concentration stabilizes the monolayer and clusters PI(4,5)P<sub>2</sub> (**Figure 30**). This data agreed with the epifluorescence images at 0.01 mM  $\text{Ca}^{2+}$ , which revealed macroscopically discernible domains at pressures up to 38 mN/m (King 2016).





Increasing the Ca<sub>2+</sub> concentration to 0.1 mM resulted in an even further condensation of the monolayer and a higher collapse pressure (~50 mN/m), indicating a higher stability of the monolayer. Once the Ca<sub>2+</sub> concentration was increased to 1 mM, the  $\pi$ /A-isotherm showed an additional condensation at low surface pressures (<15 mN/m). However, at a surface pressure of ~20 mN/m, there was crossover in which the  $\pi$ /A-isotherm for 0.1 mM Ca<sub>2+</sub> shifted to a higher area/molecule (expanded) than the one for 1 mM Ca<sub>2+</sub>. This crossover at higher surface pressures, could be the result of reduced stability of the PI(4,5)P<sub>2</sub> monolayers at low concentrations (i.e. repulsion of highly negative headgroups). The  $\pi$ /A-isotherm performed on a subphase containing 2 mM Ca<sub>2+</sub> showed the same condensation effects as 1 mM Ca<sub>2+</sub>, suggesting that the presence of an additional 1 mM Ca<sub>2+</sub> does not further cluster PI(4,5)P<sub>2</sub>. Similar clustering behavior for 1 mM

and 2 mM  $\text{Ca}^{2+}$  was also observed with previous epifluorescent images; however, images were not obtained since the Top Fluor® PI(4,5)P<sub>2</sub> fluorophore used for imaging seemed to form clusters by itself at higher pressures (King 2016). The  $\pi/A$ -isotherm data obtained confirmed that the presence of low concentrations of  $\text{Ca}^{2+}$  (0.01-2 mM) leads to a condensation of the PI(4,5)P<sub>2</sub> monolayer, revealing that the PI(4,5)P<sub>2</sub> molecules must pack more tightly. Based on this data, we further hypothesize that  $\text{Ca}^{2+}$  shields the highly negatively charged PI(4,5)P<sub>2</sub> headgroups leading to  $\text{Ca}^{2+}$ -bridged clusters that are further stabilized by hydrogen-bonding networks (**Figure 31**).

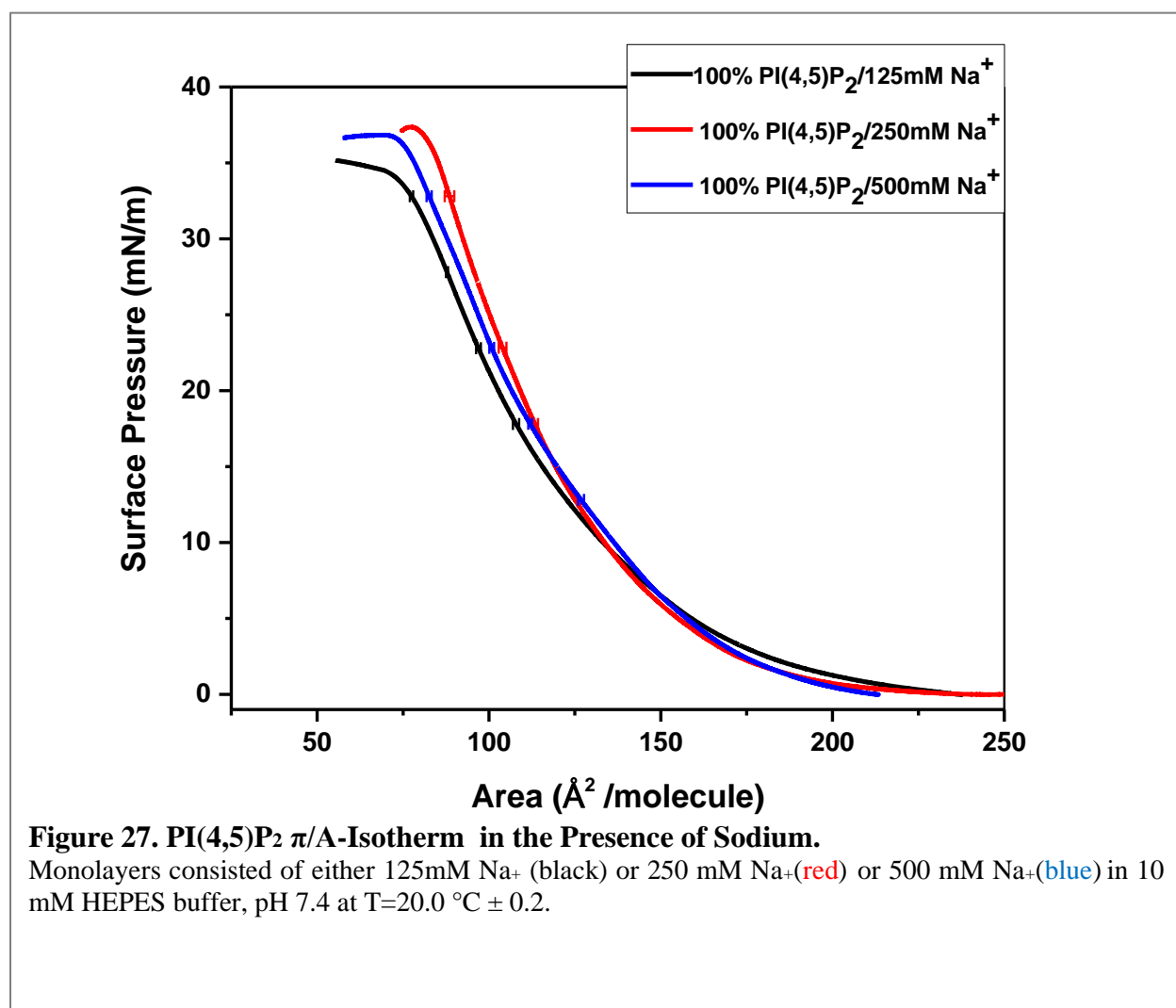


## 2.1.4 Investigating the Role of Cations on PI(4,5)P<sub>2</sub> Clustering in

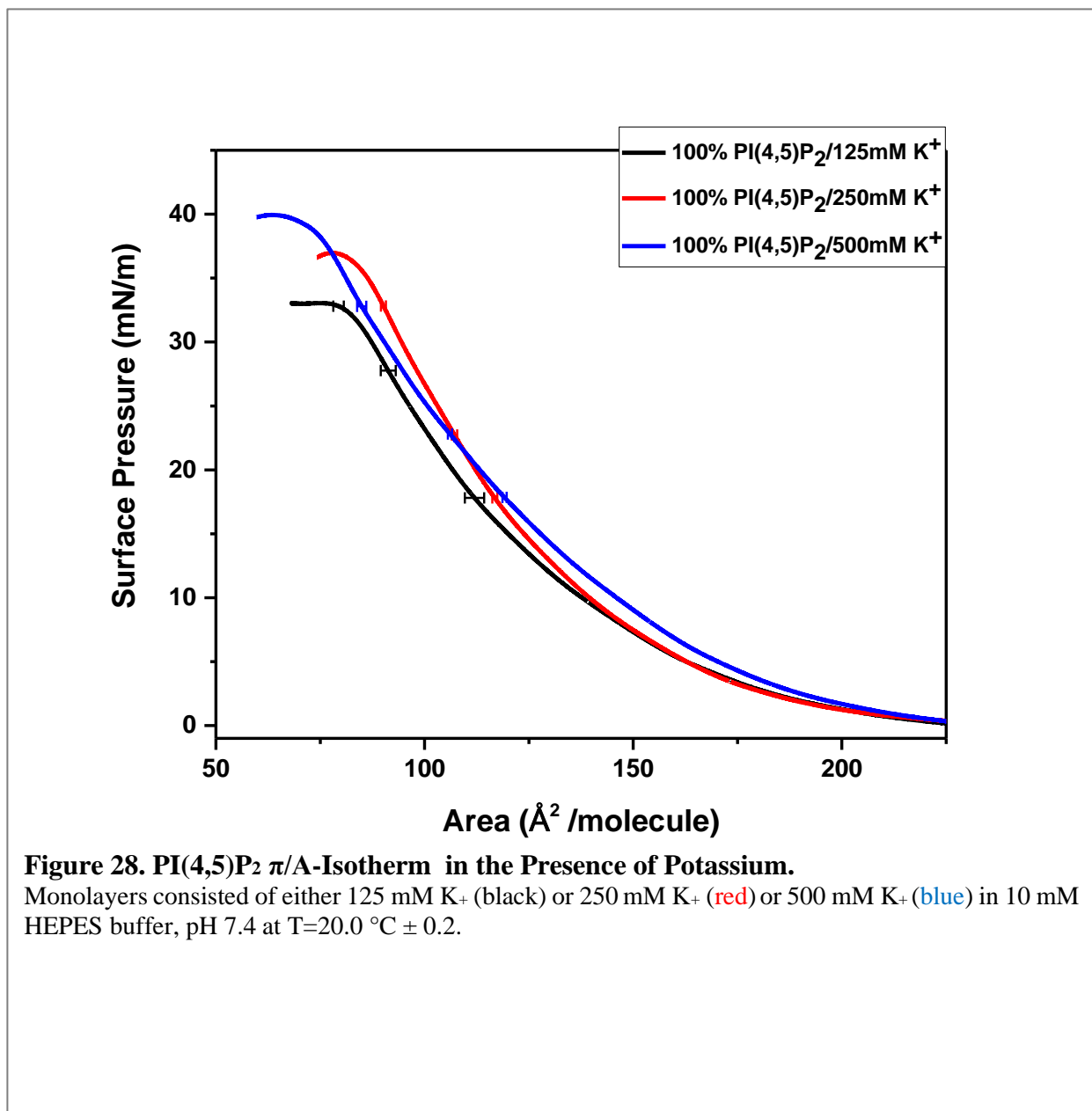
### Langmuir Films

Many biological processes are driven by processes at the plasma membrane, continuously shuttling ions (Na<sup>+</sup>, K<sup>+</sup>, Ca<sup>2+</sup>, and Cl<sup>-</sup>) across the membrane generating ion gradients and electric potential. However, the role of two principle monovalent ions, Na<sup>+</sup> and K<sup>+</sup>, on clustering of phosphoinositides in the membrane, in particular PI(4,5)P<sub>2</sub>, and their involvement in regulating the resting membrane potential (-60 to -90 mV) has been studied much less. Some spectroscopic studies have suggested that changes in the PI(4,5)P<sub>2</sub> lateral distribution in model membranes are different depending on the ion, and not simply related to the net charge. One study, in particular, showed that even though the binding constants for Ca<sup>2+</sup> and Mg<sup>2+</sup> for PI(4,5)P<sub>2</sub> are similar, only Ca<sup>2+</sup> is able to induce local PI(4,5)P<sub>2</sub> clustering (Wang, Collins et al. 2012). This is interesting since the two cations are similar in size and carry the same charge; therefore, the clustering difference is possibly due to the Ca<sup>2+</sup> having a smaller hydration shell than Mg<sup>2+</sup> allowing Ca<sup>2+</sup> to easily interact with PI(4,5)P<sub>2</sub> headgroups. Based on previous studies showing a difference with similarly charged cations, we are interested in studying the effect of monovalent cations (Na<sup>+</sup>, K<sup>+</sup>) with similar charge densities to better understand the specific ionic environment required for PI(4,5)P<sub>2</sub> clustering. The physiological concentration of the K<sup>+</sup> concentration is intracellularly higher (~ 150 mM intracellular, ~20 mM extracellular), while the Na<sup>+</sup> concentration is extracellularly higher (~ 12 mM intracellular, ~150 mM extracellular) (Degreve 1996, Mancinelli 2007). Therefore, in these Langmuir monolayer studies, a subphase using the high bulk concentrations (125 mM-500 mM) was physiological relevant.

At the three bulk concentrations (125 mM, 250 mM and 500 mM), PI(4,5)P<sub>2</sub>  $\pi$ /A- isotherms in the presence of Na<sup>+</sup> had nearly identical area/molecule typical of a LE/G state isotherm at low surface pressures (<15 mN/m); however, as the surface pressure increased the 250 mM and 500 mM Na<sup>+</sup> concentrations showed an expansion in comparison to the 125 mM Na<sup>+</sup> (Figure 32). This shift is due to the higher stability of the PI(4,5)P<sub>2</sub> monolayer, which results in less leakage through the barriers and less partial collapse.



Not surprisingly, the  $\pi/A$ -isotherms for  $K^+$  were very similar to  $Na^+$  with a typical LE/G state at low surface pressures to an LE state at higher surface pressures (**Figure 33**). However, at surface pressure  $\sim 20$  mN/m a cross over was observed between the 125 mM and 250 mM at surface pressure  $\sim 20$  mN/m, which was likely the result of monolayer film instability.



Since the monolayer film at the bulk concentrations >125 mM was unstable, the 125 mM concentrations were used for comparison to understand the specific ion effect on PI(4,5)P<sub>2</sub> clustering. When comparing  $\pi/A$ -isotherms of PI(4,5)P<sub>2</sub> in the presence of either 125 mM Ca<sub>2+</sub>, 125 mM Na<sup>+</sup> or 125 mM K<sup>+</sup> (

**Figure 34**), Ca<sub>2+</sub> had the greatest condensing effect on the PI(4,5)P<sub>2</sub> monolayers (note: at this concentration of Ca<sub>2+</sub> the monolayer was still somewhat expanded due to the high concentration). Ca<sub>2+</sub> showed the strongest mediated PI(4,5)P<sub>2</sub> condensation followed by Na<sup>+</sup> and

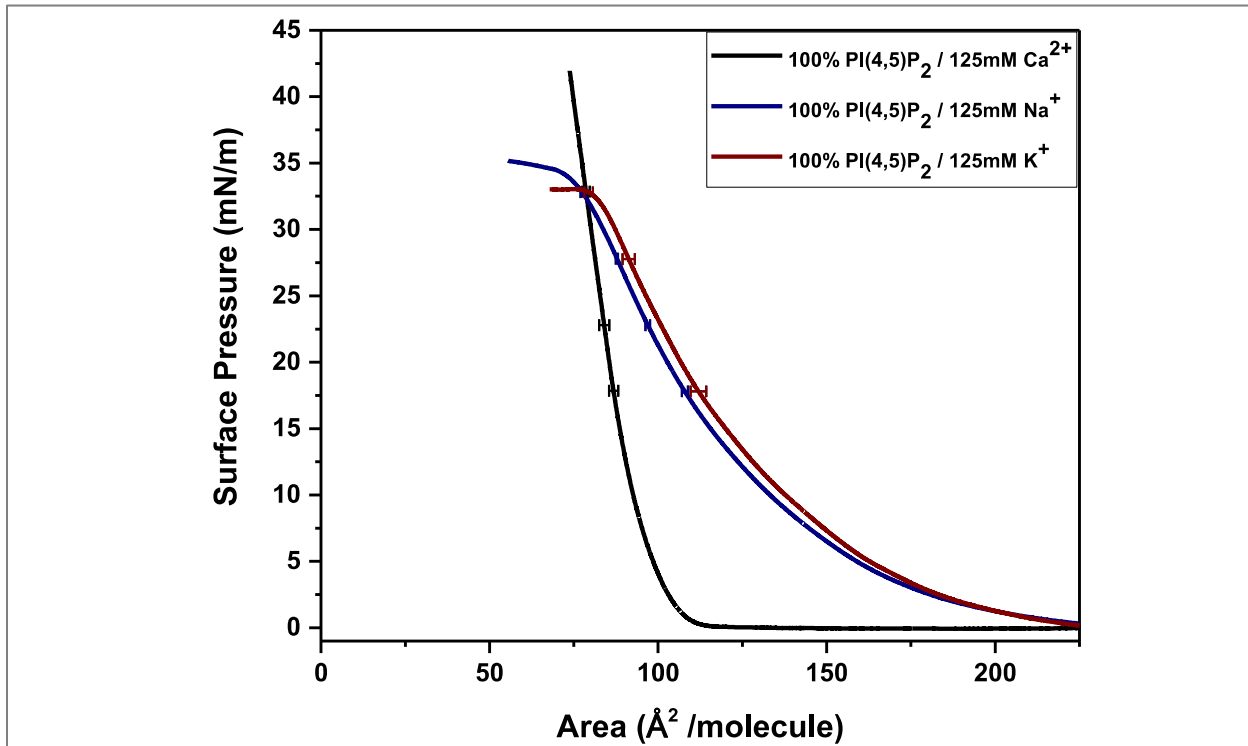
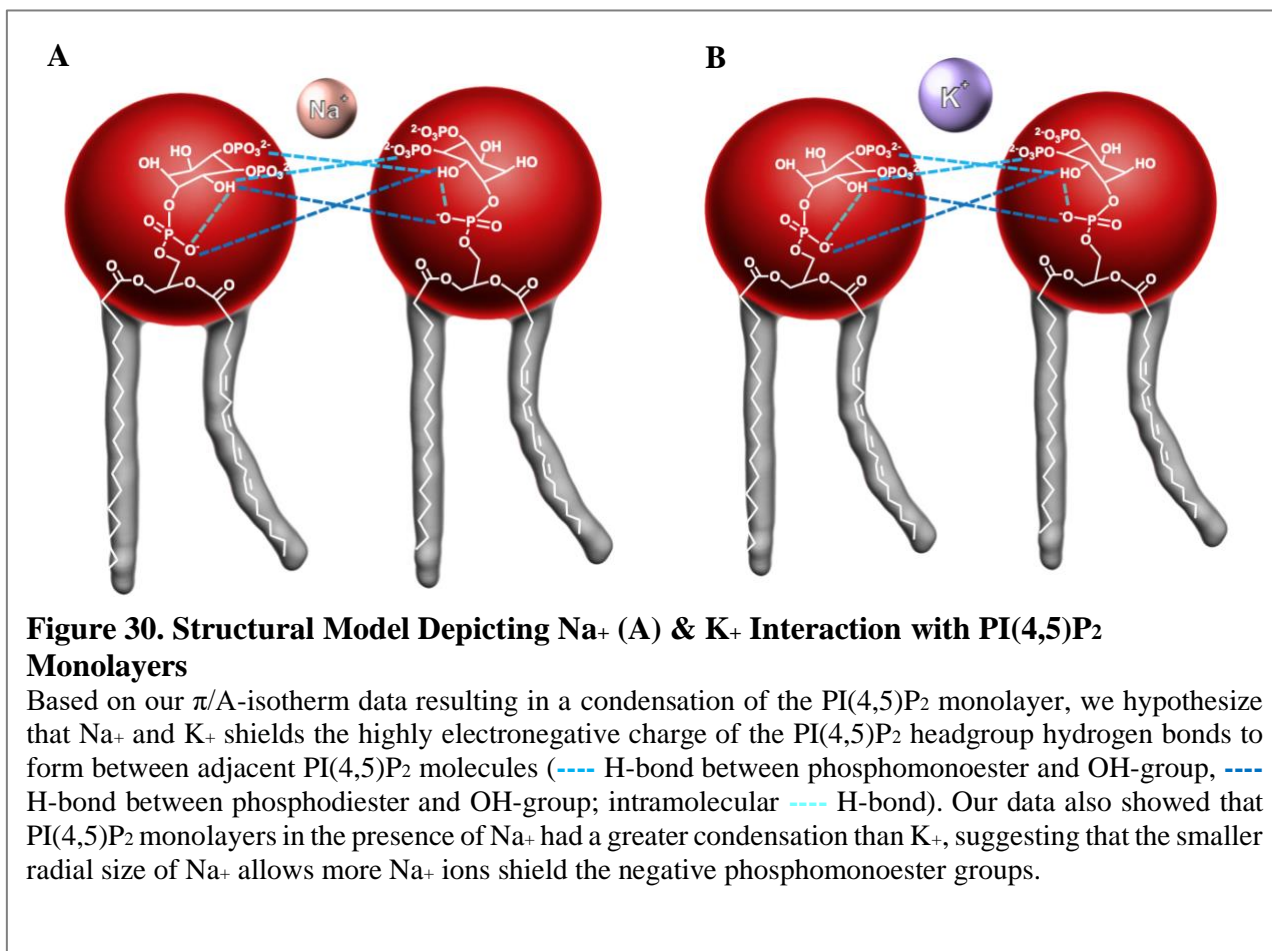


**Figure 29. Comparing the Specific Ion Effect on PI(4,5)P<sub>2</sub>  $\pi/A$ -Isotherm Behavior.**

Monolayers consisted of either 125 mM Ca<sub>2+</sub> (black), 125 mM Na<sup>+</sup> (navy) or 250 mM K<sup>+</sup> (wine) in 10 mM HEPES buffer, pH 7.4 at T=20.0 °C ± 0.2. \*In the presence of Ca<sub>2+</sub> the monolayer became very stiff, resulting in incorrect surface tension measurements of the Wilhelmy plate in the highly compressed state (low surface tensions).

then  $K^+$  ( $Ca^{2+} > Na^+ > K^+$ ). This trend was observed both experimentally with  $\pi/A$ -isotherms and theoretically with all-atom molecular dynamics (MD) simulations (performed by our collaborators). We postulated that  $Ca^{2+}$  would have the strongest condensation effect since it has the most charge and the ability to accept more electrons from the phosphate groups, whereas monovalent  $Na^+$  had a greater effect than  $K^+$  due to  $Na^+$  having a smaller ionic radius (102 pm) compared to  $K^+$  (138 pm). It is possible that the larger radial size of  $K^+$  only allows one  $K^+$  to bind, still leaving a negatively charged phosphate. It is also possible that the binding of  $K^+$  on one phosphomonoester group on PI(4,5)P<sub>2</sub> affected the binding of another  $K^+$  to the adjacent phosphomonoester group; however, further studies are required to understand the preferential binding of each phosphate group (**Figure 35**).

Based upon our thermodynamic data, we hypothesize that the cations shield the electronegative headgroups reducing the overall electron density allowing intermolecular hydrogen bonds to form between adjacent PI(4,5)P<sub>2</sub> molecules. In particular we believe that  $Ca^{2+}$  has preferential binding to the phosphomonoesters located on the 4- and 5-position of the inositol ring, which has been proposed previously (Graber, Jiang et al. 2012, Graber, Gericke et al. 2014, Graber, Wang et al. 2015). However, it was not possible to verify this notion experimentally using spectroscopic or diffraction techniques (NMR and Neutron Diffraction) due to resolution limitations, therefore we lacked the structural information required to understand the exact positioning of these ions on the PI(4,5)P<sub>2</sub> headgroup. In order to understand the structural binding of these ions on PI(4,5)P<sub>2</sub> headgroups, we collaborated with Richard Pastor & Kyungreem Han at NIH. The all-atom (MD) simulations modeled PI(4,5)P<sub>2</sub> clustering under the same experimental conditions, thus allowing us to compare our area/molecule data with our collaborators at specific



surface tensions. Please note for convenience of comparing the two studies, our surface pressure ( $\pi$ ) values were converted to surface tension ( $\gamma$ ) values using  $\pi = \gamma_0 - \gamma$ , where  $\gamma_0$  was the surface tension of pure water ( $\sim 73$  mN/m at 20 °C) (**Table 1**).

Considering all the experimental hurdles, such as, PI(4,5)P<sub>2</sub> purity and accurate concentration determination, PI(4,5)P<sub>2</sub> monolayer instability and PI(4,5)P<sub>2</sub> leakage under the barriers, as well as the theoretical hurdles of box specifications required for the all-atom MD simulations, it is remarkable how closely the two sets of data agree. The all-atom MD simulations also found that Ca<sup>2+</sup> had a stronger clustering tendency followed by Na<sup>+</sup> then K<sup>+</sup> confirming there is a specific ion effect even for the monovalent cations. Additionally, the all-atom MD simulations were able to validate our structural hypothesis by proving that Ca<sup>2+</sup> is attracted to the 4,5-

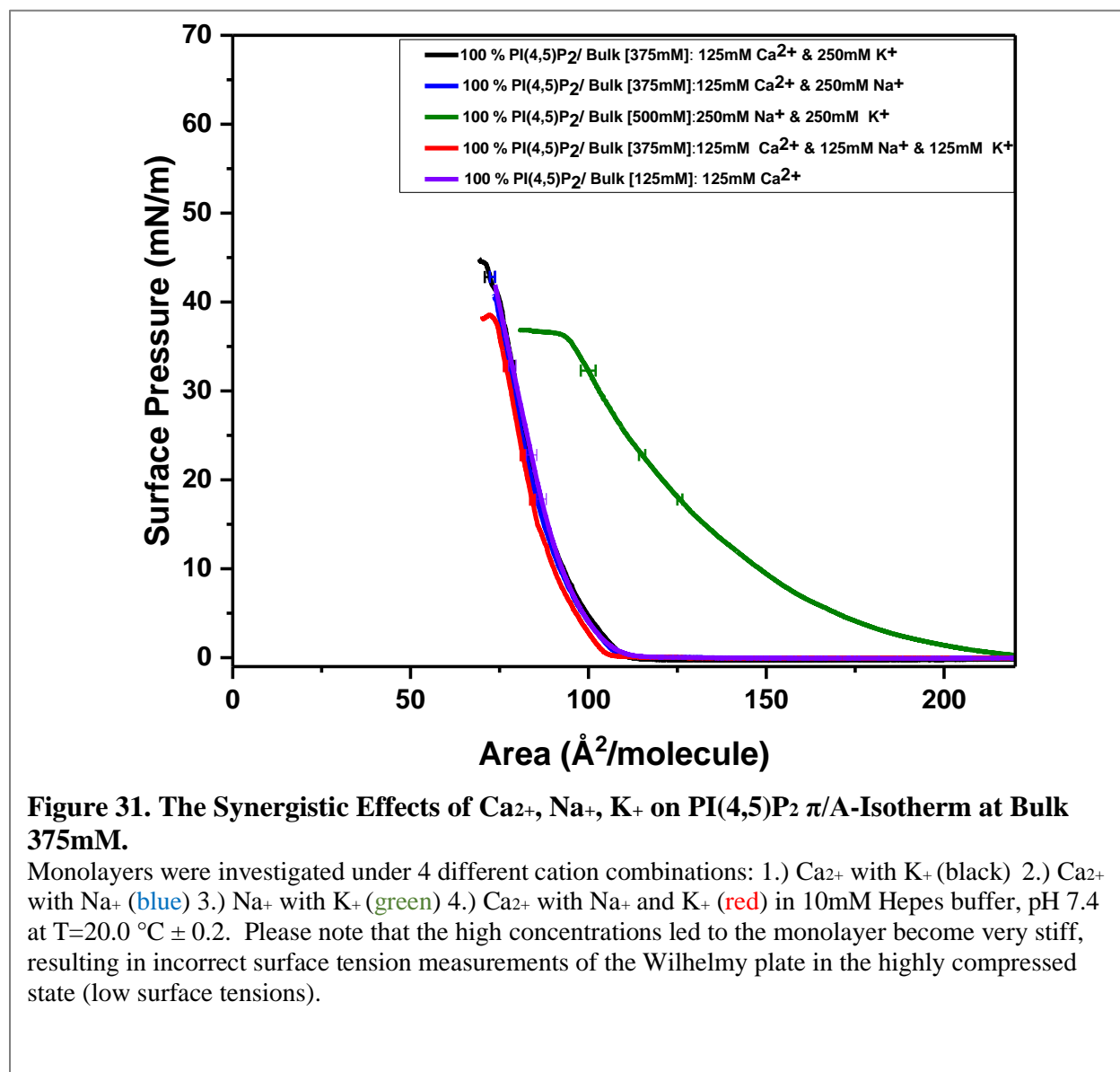


phosphate monoester regions with its binding affinity being maximal near the non-protonated 4,5-phosphomonoester groups. The simulations also provided information on Na<sup>+</sup> and K<sup>+</sup> positioning, showing that these two ions do not have a preferential binding site; Na<sup>+</sup> binds promiscuously, but with high affinity to the 4,5-phosphomonoester and to 1-phosphodiester groups whereas K<sup>+</sup> binds only to the 1-phosphodiester (Figure 31). The relative binding affinity for 4,5-phosphomonoester groups was the strongest with Ca<sup>2+</sup> followed by Na<sup>+</sup>, then very weakly K<sup>+</sup> (Ca<sup>2+</sup> > Na<sup>+</sup> >>> K<sup>+</sup>) and for the 1-phosphodiester K<sup>+</sup>, then Na<sup>+</sup>, followed by Ca<sup>2+</sup> (K<sup>+</sup> > Na<sup>+</sup> > Ca<sup>2+</sup>) (unpublished). The agreement between our experimental  $\pi/A$ -isotherms and theoretical all-atom molecular dynamics (MD) simulations has allowed us to confirm with confidence that the structural models obtained from the MD simulations are an accurate representation of Ca<sup>2+</sup>, Na<sup>+</sup>, K<sup>+</sup> ion effects on PI(4,5)P<sub>2</sub> clustering.

### **2.1.5 The Synergistic Cation Effects on PI(4,5)P<sub>2</sub> Clustering in Langmuir Monolayers**

The aim of this chapter was to understand the ionic environment required for PI(4,5)P<sub>2</sub> clustering. In the above sections, we investigated the individual effects of Ca<sup>2+</sup>, Na<sup>+</sup>, K<sup>+</sup> on molecular packing of PI(4,5)P<sub>2</sub> monolayers; however at any given time all of these ions are present at the plasma membrane; thus, it is highly likely that these cations work together to induce PI(4,5)P<sub>2</sub> clustering. To compare these synergistic effects, we evaluated PI(4,5)P<sub>2</sub> Langmuir monolayers under 4 different cation combinations: 1.) Ca<sup>2+</sup> with K<sup>+</sup>, 2.) Ca<sup>2+</sup> with Na<sup>+</sup>, 3.) Na<sup>+</sup> with K<sup>+</sup>, 4.) Ca<sup>2+</sup> with Na<sup>+</sup> and K<sup>+</sup>. As in the experiments above, the total bulk (molar) concentration was investigated at 375 mM, 200 mM, and 125 mM. Looking first at the 500 mM

bulk concentration, the  $\pi/A$ -isotherm's conditions that included  $\text{Ca}^{2+}$  with another counter cation, either  $\text{Na}^+$  or  $\text{K}^+$  or both, all resulted in an identical isotherms (**Figure 36**). There was a clear condensation of these monolayers shifting from  $\sim 130 \text{ \AA}^2/\text{molecule}$  in  $\text{Ca}^{2+}$ -free scenario to  $\sim 90 \text{ \AA}^2/\text{molecule}$  at surface pressure of  $10 \text{ mN/m}$ . At the  $375 \text{ mM}$  bulk concentrations, the concentration of  $\text{Ca}^{2+}$  present was  $125 \text{ mM}$ ; therefore, the multi-cation systems were compared with  $125 \text{ mM}$   $\text{Ca}^{2+}$   $\pi/A$ -isotherm to see if any other cations participated in the condensation. The  $125 \text{ mM}$   $\text{Ca}^{2+}$



$\pi/A$ -isotherm overlayed with all synergistic systems containing  $\text{Ca}_{2+}$ , which suggests that the addition of either  $\text{Na}_{+}$  or  $\text{K}_{+}$  did not cause a further condensation. However, since the  $\text{Ca}_{2+}$  concentrations were very high and beyond physiological range, it was hard to discern if any other cations interacted with such stiff films. When the synergistic effects of  $\text{Ca}_{2+}$ ,  $\text{Na}_{+}$ ,  $\text{K}_{+}$  were investigated for bulk concentration 200 mM, the  $\text{Ca}_{2+}$  with  $\text{K}_{+}$  and  $\text{Ca}_{2+}$  with  $\text{Na}_{+}$  systems resembled that of 375 mM concentration, however the  $\pi/A$ -isotherm for  $\text{Ca}_{2+}$  with  $\text{Na}_{+}$  and  $\text{K}_{+}$  shifted to a higher area/molecule and the  $\pi/A$ -isotherm for  $\text{Na}_{+}$  with  $\text{K}_{+}$  resembled an instable monolayer (**Figure 37**). The inconsistencies in the 375 mM and 200 mM data were likely the result of high cation concentrations; therefore, similar to the individual cation scenarios, we used the 125mM bulk concentration to explore the synergistic role in more depth. The  $\text{Ca}_{2+}$ -free scenario of  $\text{Na}_{+}$  and  $\text{K}_{+}$  transitioned from a LE/G state at low surface pressures to an LE state at higher surface pressures, and collapsed at a low surface pressure  $\sim 30$  mN/m. This data heavily suggested that  $\text{Ca}_{2+}$  is required in the ionic environment needed for PI(4,5) $\text{P}_2$  clustering. At low surface pressures ( $< 20$  mN/m), the  $\pi/A$ -isotherm system of  $\text{Ca}_{2+}$  with the addition of  $\text{K}_{+}$  had the greatest condensation effect, suggesting that  $\text{K}_{+}$  may participate with  $\text{Ca}_{2+}$  in PI(4,5) $\text{P}_2$  clustering (**Figure 37**). This was confirmed with all-atom (MD) simulations revealing a structural synergistic effect, in which  $\text{K}_{+}$  penetrated deeper into the headgroup region toward the 1-phosphodiester group while  $\text{Ca}_{2+}$  was attracted to the 4,5-phosphomonoester regions shielding the negative headgroups (unpublished).

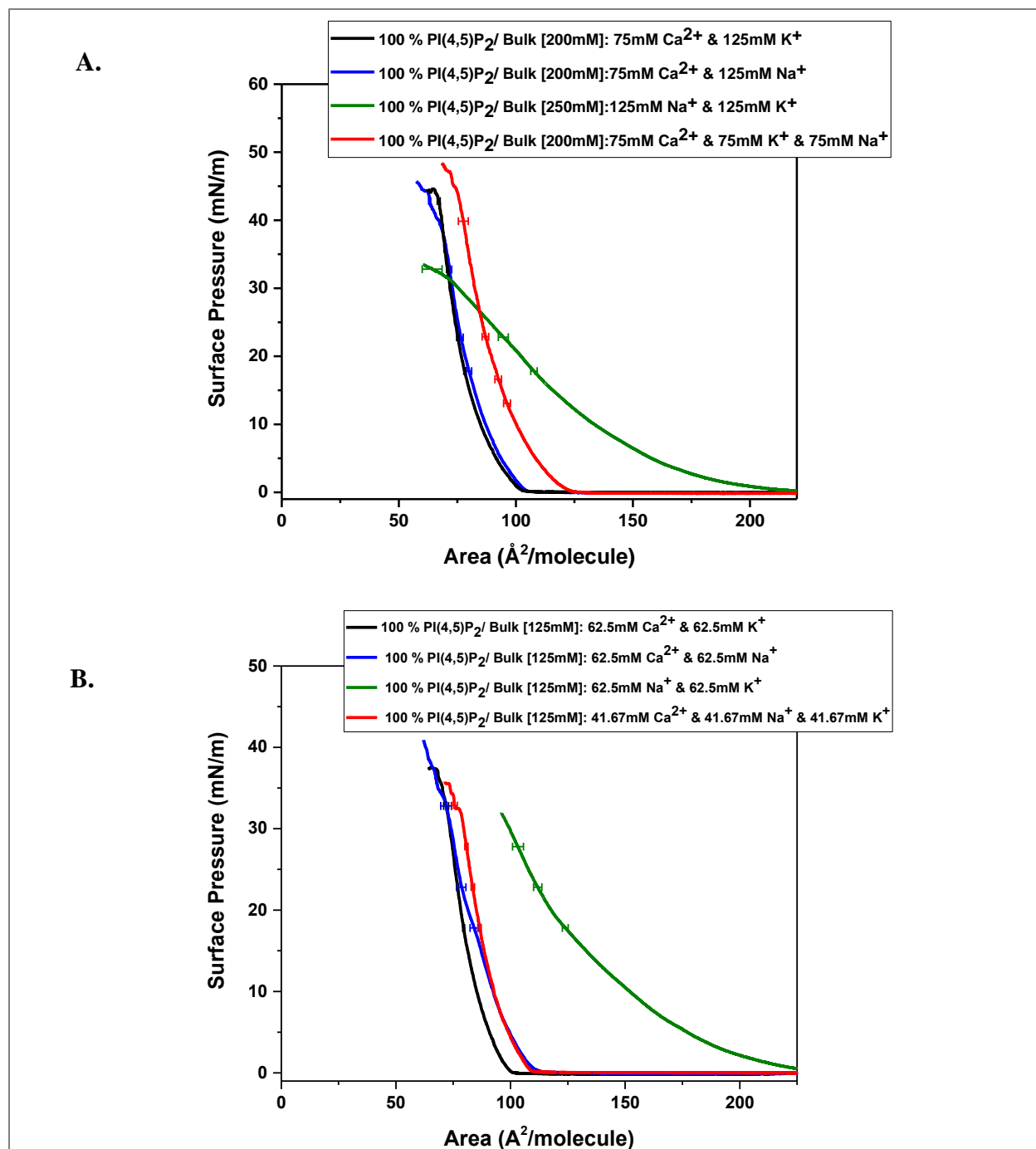


**Figure 32. The Synergistic Effects of Ca<sup>2+</sup>, Na<sup>+</sup>, K<sup>+</sup> on PI(4,5)P<sub>2</sub>  $\pi$ /A-Isotherm at Bulk 200mM (A) and 125mM (B).**

Monolayers were investigated under 4 different cation combinations: 1.) Ca<sup>2+</sup> with K<sup>+</sup> (black). 2.) Ca<sup>2+</sup> with Na<sup>+</sup> (blue) 3.) Na<sup>+</sup> with K<sup>+</sup> (green) 4.) Ca<sup>2+</sup> with Na<sup>+</sup> and K<sup>+</sup> (red) in 10mM HEPES buffer, pH 7.4 at T=20.0 °C  $\pm$  0.2. Please note that the high concentrations led to the monolayer become very stiff, resulting in incorrect surface tension measurements of the Wilhelmy plate in the highly compressed state (low surface tensions).

Ions	Type of Monolayer	$\gamma$ mN/m	Experimental Results		Simulation Results	
			Area (PI(4,5)P <sub>2</sub> ) Å <sup>2</sup> /molecule	SE	Area (PI(4,5)P <sub>2</sub> ) Å <sup>2</sup> /molecule	SE
125 mM Ca <sup>2+</sup>	100% PI(4,5)P <sub>2</sub>	65	95.3	±1.5		
		60	90.3	±1.4	90.5	±0.2
		55	86.7	±1.4	83.2	±0.2
		50	83.5	±1.5	80.3	±0.1
		45	80.9	±1.5	77.2	±0.3
		40	78.1	±1.0	74.7	±0.2
125 mM Na <sup>+</sup>	100% PI(4,5)P <sub>2</sub>	55	108.6	±0.9	93.2	±0.1
		50	97.6	±0.7	84.0	±0.1
		45	88.4	±0.6	81.2	±0.3
		40	80.0	±0.5	75.1	±0.1
125 mM K <sup>+</sup>	100% PI(4,5)P <sub>2</sub>	52	108.2	±2.0	103.8	±0.8
		50	104.0	±1.9	95.9	±0.1
		45	94.2	±1.8	88.4	±0.1
		40	80.8	±1.3	81.8	±0.2
41.67mM Ca <sup>2+</sup> 41.67mM Na <sup>+</sup> 41.67mM K <sup>+</sup>	100% PI(4,5)P <sub>2</sub>	60	89.7	±1.1	99.5	±0.5
		55	85.5	±0.7	89.5	±0.2
		50	82.3	±0.7	83.4	±0.1
		45	81.9	±0.7	76.6	±0.1
		40	75.9	±1.2	74.8	±0.2

**Table 1: Comparison of Experimental & Computationally Derived Surface Tension Data**

Please note that a low surface tension corresponds to the compressed state of the monolayer (high surface pressure in the isotherms). The standard error (SE) for the experimental data were obtained from the variation of the repeat  $\pi/A$ -isotherm measurements for the respective system. In particular for low surface tensions (high surface pressures), phosphoinositide monolayer tends to show a lack of surface pressure stability, which can be attributed to film material loss due to slippage underneath and around the barriers used for the compression of the film.

### 1.19 Conclusion:

Although the effect of cations on PI(4,5)P<sub>2</sub> lateral organization has been previously studied, a molecular understanding of PI(4,5)P<sub>2</sub> clustering remains unclear due to the complex dynamics of the phosphoinositide headgroup/cation interactions. In this study we aimed to understand the unique ionic environment required for electrostatic PI(4,5)P<sub>2</sub> cluster formation. We discovered that calcium individually and calcium along with potassium had a greater effect on PI(4,5)P<sub>2</sub> cluster formation than sodium and potassium, individually and combined. Our results showed that

PI(4,5)P<sub>2</sub> monolayer stability was increased by the lipid packing and ordering in the presence of calcium, suggesting that calcium shields the negative charge of the PI(4,5)P<sub>2</sub> headgroup and bridges adjacent PI(4,5)P<sub>2</sub> headgroups by interacting with the respective phosphomonoester groups. The mutual PI(4,5)P<sub>2</sub> interaction is further stabilized by a hydrogen bond network formed between the PI(4,5)P<sub>2</sub> headgroups. Recently performed experiments in our lab have shown that the thermal stability of PI(4,5)P<sub>2</sub> clusters increase in the presence of presence of Ca<sup>2+</sup>, the cluster/non-cluster transition of pure PI(4,5)P<sub>2</sub> in mixed lipid bilayers with PC was ~25 °C and upon the addition of 100 uM Ca<sup>2+</sup> the transition increased to >52 °C (5% PI(4,5)P<sub>2</sub>/95% POPC) . This increase in thermal stability is further evidence that Ca<sup>2+</sup> not only shields the negative headgroup charge but also bridges adjacent headgroups. Our  $\pi/A$ -isotherm experimental data showed a strong agreement with our collaborators all-atom (MD) simulations combined with graph-theoretic analysis, allowing us to faithfully represent the ion-specific nature of intermolecular interactions of the phosphate headgroup. The all-atom simulations were able to pinpoint the exact molecular location of the cations' interaction with the phosphate groups, a discovery that will lay the physical foundation in understanding electrostatic PI(4,5)P<sub>2</sub> clustering. It was discovered that calcium is strongly attracted to the 4,5-phosphomonoester regions, while Na<sup>+</sup> binds promiscuously, but with high affinity to the 4,5-phosphomonoester and to 1-phosphodiester and K<sup>+</sup> binds only to 1-phosphodiester. This discovery of the electrostatics and molecular positioning of cations required for stabilization of PI(4,5)P<sub>2</sub> clustering will help us understand aspects of PI(4,5)P<sub>2</sub> mediated signaling events, such as the temporal control of proteins that bind PI(4,5)P<sub>2</sub> clusters to enhance their function.

## Chapter 4: Role of Cholesterol in PI(4,5)P<sub>2</sub> Cluster Formation

### 1.20 Introduction

Local PI(4,5)P<sub>2</sub> clusters are thought to be mediated by signaling events; however a lingering question in understanding this mechanism: What are the factors that fine-tune PI(4,5)P<sub>2</sub> cluster formation in space and time? One important spatiotemporal modulator that affects the local concentration of PI(4,5)P<sub>2</sub> pools is cholesterol, a steroid present in large quantities (30-40 mole%) within the plasma membrane (Lindblom and Oradd 2009, Maxfield and van Meer 2010, Wood, Igbavboa et al. 2011). Cholesterol has gained much attention because of its involvement in the formation of raft-like structures, dense L<sub>o</sub> phase domains (10–100 nm) that are enriched in cholesterol and gel phase forming sphingolipids, which are found in the outer leaflet of the membrane (Edidin 2003, Lingwood 2010) (refer to section **Error! Reference source not found.**). The general model for formation of lipid rafts is well-established for the outer leaflet of the plasma membrane where L<sub>o</sub> domains can form. In contrast inner leaflet domain formation is poorly understood since it lacks a sufficient quantity of lipid species that form L<sub>o</sub> phases at physiological temperatures. However, there have been several studies that observed PI(4,5)P<sub>2</sub> mediated signaling events to be affected by cholesterol levels, which has led to the hypothesis that PI(4,5)P<sub>2</sub> partitions into lipid rafts (Elhyany 2004, Cinar 2007, Lasserre). In model membranes mimicking a raft lipid composition, it has been found that raft resident PI(4,5)P<sub>2</sub> binding proteins or peptides are required for PI(4,5)P<sub>2</sub> partitioning into lipid rafts (Tong 2008). However, it is important to note here that it is highly unlikely that PI(4,5)P<sub>2</sub> partitions into L<sub>o</sub> domains, since PI(4,5)P<sub>2</sub> favors more of a disordered and fluid environment than what is found in lipid raft domains. This makes the interaction between PI(4,5)P<sub>2</sub> and cholesterol somewhat puzzling and therefore poorly understood.

While it is tempting to simply link cholesterol dependent signaling to outer membrane lipid rafts, cholesterol impacting inner membrane phosphoinositide domains in the absence of raft formation has been found in vitro (Jiang, Redfern et al. 2014). Cholesterol has been observed to promote clustering of both phosphatidylinositol and PIPs as well as to stabilize phosphoinositide vesicles that will not form by themselves (20% cholesterol) (Jiang, Redfern et al. 2014). These studies have provided us with a first glimpse that cholesterol modulates phosphoinositide domain formation, despite the rigid sterol ring structure and the disordered PI(4,5)P<sub>2</sub> acyl chain structure. However, the mystery still remains in understanding exactly how cholesterol enhances cluster formations. There are two main hypothesis for the mechanism of PI(4,5)P<sub>2</sub> cluster formation 1) the “indirect” accumulation of PI(4,5)P<sub>2</sub> from the lack of physical space due to being excluded from cholesterol-rich domains or 2) the “direct” accumulation in which cholesterol directly interacts with functional groups in the PI(4,5)P<sub>2</sub> headgroup region (Daly, Wang et al. 2011, Jiang, Redfern et al. 2014, Krause, Daly et al. 2014, Brown 2015, Bennett, Shea et al. 2018)

The latter of the two hypotheses has been strongly supported by experiments showing that sterols lacking the hydroxyl group do not promote domain formation, revealing that the hydroxyl group of cholesterol is essential for this domain formation (Jiang, Redfern et al. 2014). Considering the importance of the cholesterol hydroxyl group, it was further hypothesized that the hydroxyl group of cholesterol is a potential hydrogen-bond donor and may interact with the PI(4,5)P<sub>2</sub> headgroup through hydrogen-bond formation. Further <sup>31</sup>P NMR studies showed that cholesterol hydroxyl group does not directly interact with the phosphomonoesters of PI(4,5)P<sub>2</sub>, suggesting that it may interact with the phosphodiester group or even the hydroxyl groups on the inositol ring (Graber, Gericke et al. 2014). Interestingly this cholesterol cluster formation was also



found for phosphatidylinositol. In contrast, PC, which like PI contains a phosphodiester group, does not cluster in the presence of cholesterol. The fact that not only PIPs cluster in the presence of cholesterol but also PI, suggest that the PIP phosphomonoester may modulate the cholesterol induced clustering but are not required. This not surprising considering that even for a PI(4,5)P<sub>2</sub> inositol ring that is tilted towards the bilayer, the cholesterol OH-group would need to be positioned deep in the polar headgroup region to interact directly with the phosphomonoester groups, a highly unlikely scenario considering the non-polar nature of the sterol ring structure. Therefore, it was additionally speculated that the cholesterol hydroxyl group interacts with the hydroxyl groups in the 2- or 6-position of the inositol ring, suggesting that cholesterol moves close to the PI(4,5)P<sub>2</sub> headgroup region. Even this movement would position the cholesterol much deeper in the headgroup region than it is found in the presence of any of the other phospholipids. This positioning of cholesterol would also allow cholesterol to fully participate in PI(4,5)P<sub>2</sub> hydrogen bond network; however, without structural data confirming the positioning of the cholesterol these are just educated speculations.

The question still remains: What permits such a rigid sterol ring of cholesterol to interact with the highly unsaturated arachidonoyl chain of PI(4,5)P<sub>2</sub>? One suggestion is that other modulation factors that promote clustering, such as cations, may synergistically work with cholesterol to form domains. One study has shown that Ca<sup>2+</sup> enhanced PI(4,5)P<sub>2</sub> domain formation in the presence of cholesterol, while this was confirmed with another study showing that the interactions between the phosphomonoesters of PI(4,5)P<sub>2</sub> and the divalent Ca<sup>2+</sup> is additive to the effect induced by cholesterol (Jiang, Redfern et al. 2014, Graber, Wang et al. 2015, Wen, Vogt et al. 2018). However, additional studies are required to understand if and how cholesterol

participates in a  $\text{Ca}^{2+}/\text{PI}(4,5)\text{P}_2$  complex. Therefore, we have again collaborated with Richard Pastor and Hank Kyungreem from the NIH, to run all-atom molecular dynamics (MD) simulations that will enrich our thermodynamic studies to gain insight into the synergistic effects of cations and cholesterol on  $\text{PI}(4,5)\text{P}_2$  cluster formation. In this study, we used the Langmuir trough experiments to monitor the molecular packing of  $\text{PI}(4,5)\text{P}_2$  in the presence of ( $\text{Ca}^{2+}$ ,  $\text{Na}^+$ ,  $\text{K}^+$ ) and cholesterol. Our results along with our collaborators structural data will provide a deeper understanding on the structural association of cholesterol in  $\text{PI}(4,5)\text{P}_2$ -cation cluster formation.

## **1.21 Results:**

### **3.1.1 Effects of cholesterol on $\text{PI}(4,5)\text{P}_2$ clustering**

In this chapter we aim to understand the synergistic effects of cholesterol on  $\text{PI}(4,5)\text{P}_2$  clustering in the presence of cations ( $\text{Ca}^{2+}$ ,  $\text{Na}^+$ ,  $\text{K}^+$ ), given the cation-headgroup interaction is essential for screening the highly negative charged headgroup. To analyze the clustering behavior in a simple planar model membrane, we used Langmuir trough experiments to monitor the compression of a  $\text{PI}(4,5)\text{P}_2$  monolayer in the presence of 20 % cholesterol with a subphase composed of either a  $\text{Ca}^{2+}$ ,  $\text{Na}^+$  or  $\text{K}^+$  ions. In the previous chapter, we studied the purely electrostatic role of cation-clustering experiments, therefore in order to understand the additive effect of including cholesterol we kept the experiment conditions the same. We hypothesize that the addition of cholesterol in the presence of the cations will lead to a further condensation of monolayers as a result of the cholesterol OH group interacting with the functional groups in the  $\text{PI}(4,5)\text{P}_2$  headgroup region and through participation in the  $\text{PI}(4,5)\text{P}_2$  H-bond network. Please

note that the area/molecule in the  $\pi/A$ -isotherms does not include the area for cholesterol, which is typical for monolayer studies since the cholesterol molecule typically is not making contact with the water surface and is usually embedded in the hydrophobic acyl chain region. Even though it turns out that cholesterol for a PI(4,5)P<sub>2</sub> monolayer is actually situated between the headgroups (see below), we follow here the established procedure for monolayers, thus cholesterol was treated like an impurity.

When investigating the additive effect of cholesterol on PI(4,5)P<sub>2</sub> monolayer condensation, the bulk concentration of the cations was kept the same as for the pure PI(4,5)P<sub>2</sub> monolayer systems, 125 mM, 250 mM and 500 mM. In our previous studies we observed Ca<sup>2+</sup> mediated PI(4,5)P<sub>2</sub> condensation is strongest followed by Na<sup>+</sup> and then K<sup>+</sup> (Section 0). We believe that Ca<sup>2+</sup> had the strongest condensation effect due its divalent charge significantly reducing the electrostatic repulsion and bridging the negatively charged phospholipid headgroups. In the presence of cholesterol, Ca<sup>2+</sup> has been shown to enhance PI(4,5)P<sub>2</sub> domain, however it is currently not understood whether cholesterol participates in the cluster formation (Jiang, Redfern et al. 2014). In this study, the effect of 20 % cholesterol on PI(4,5)P<sub>2</sub> molecular packing in subphases containing either 250 mM or 125 mM Ca<sup>2+</sup> was investigated. We hypothesize that the addition of cholesterol to a Ca<sup>2+</sup> containing monolayer, will lead to a further condensation than in the absence of cholesterol due Ca<sup>2+</sup> reducing the electrostatic repulsion between PI(4,5)P<sub>2</sub> molecules allowing the OH-group of cholesterol to H-bond with the PI(4,5)P<sub>2</sub> headgroup. It was not surprising when an expanded monolayer was observed for cholesterol in the presence of 250 mM Ca<sup>2+</sup>, since PI(4,5)P<sub>2</sub> monolayer subphases containing high Ca<sup>2+</sup> concentrations caused the monolayer to be too stiff and therefore impossible to observe molecular packing changes. Therefore, we compared the 125mM Ca<sup>2+</sup> system in the presence of cholesterol to the pure PI(4,5)P<sub>2</sub>, in which the cholesterol containing

$\pi/A$ -isotherm shifted to lower area/molecule. Since the area of cholesterol was not included in the  $\pi/A$ -isotherm, this suggested that the further condensation must be the result of cholesterol and  $\text{Ca}^{2+}$  additively working together to reduce the area/molecule (**Figure 38**). Based on our results, we hypothesize that  $\text{Ca}^{2+}$  shields the negatively charged headgroups allowing adjacent PI(4,5) $\text{P}_2$  molecules to participate in H-bonding networks, while cholesterol stabilizes this interaction by

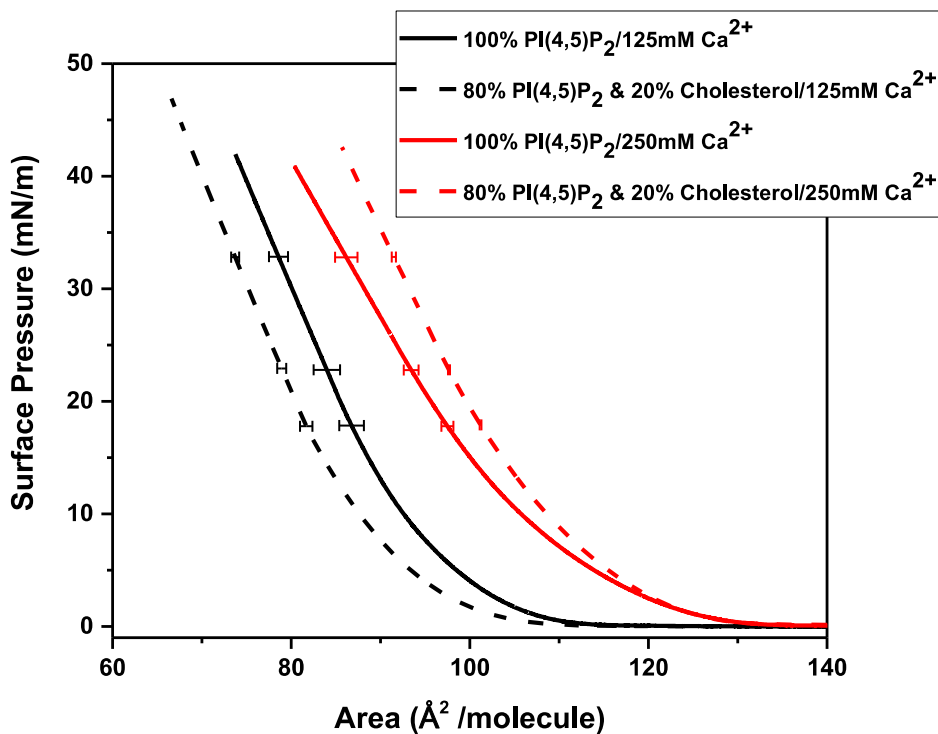


**Figure 33. PI(4,5)P<sub>2</sub>  $\pi/A$ -Isotherm in the Presence of High Molar Concentration of Calcium**

Monolayers consisted of either 125mM  $\text{Ca}^{2+}$  (black, solid) or 250mM  $\text{Ca}^{2+}$  (red, solid) in the absence of cholesterol, compared 125mM  $\text{Ca}^{2+}$  (black, dashed) or 250mM  $\text{Ca}^{2+}$  (red, dashed) in the presence of cholesterol, in 10mM HEPES buffer, pH 7.4 at  $T=20.0\text{ }^\circ\text{C} \pm 0.2$ . Please note that in the presence of high  $\text{Ca}^{2+}$  concentrations the monolayer become very stiff, resulting in incorrect surface tension measurements of the Wilhelmy plate in the highly compressed state (low surface tensions). In particular for low surface tensions (high surface pressures), phosphoinositide monolayer tend to show a lack of surface pressure stability, which can be attributed to film material loss due to slippage underneath and around the barriers used for the compression of the film. This is less pronounced for the PI(4,5) $\text{P}_2$  monolayer in the presence of cholesterol.

participating in the H-bond network through the OH-group interacting with the phosphodiester group or the OH-groups in the 2- or 6-position of the inositol ring.

There was an altogether different observation for cholesterol in the presence of Na<sup>+</sup>, which had the second strongest effect on PI(4,5)P<sub>2</sub> cluster formation (section 0). We hypothesize that PI(4,5)P<sub>2</sub> isotherms in the presence of Na<sup>+</sup> exhibited a stronger condensation effect than in the presence of the similarly charged K<sup>+</sup> due to the smaller ionic radius of Na<sup>+</sup> being more favorable to interact with the phosphate groups. However, all PI(4,5)P<sub>2</sub> isotherms in the presence of Na<sup>+</sup> and cholesterol exhibited an expanded  $\pi/A$ -isotherm when compared to the absence of cholesterol (**Figure 39**). Without knowing the association strengths of Na<sup>+</sup> to the phosphate groups, it is hard to explain why this happened. One explanation might be that Na<sup>+</sup> has a stronger affinity for the phosphodiester group and a weaker affinity for the phosphomonoester groups, causing cholesterol to act as spacer to keep optimal distance between negative charged headgroup. The K<sup>+</sup> exhibited the weakest electrostatic effect on PI(4,5)P<sub>2</sub> cluster formation possibly due to its larger radius only allowing one K<sup>+</sup> molecule to bind to phosphate group, thereby leaving behind a partial negative charge that repels nearby phosphate groups. All K<sup>+</sup> containing systems in the presence of cholesterol led to a further condensed monolayer than in the absence of cholesterol (**Figure 40**). This is likely the result of cholesterol by itself inducing the cluster formation through its OH-group interacting with either the phosphodiester group or the OH-groups of the inositol ring.

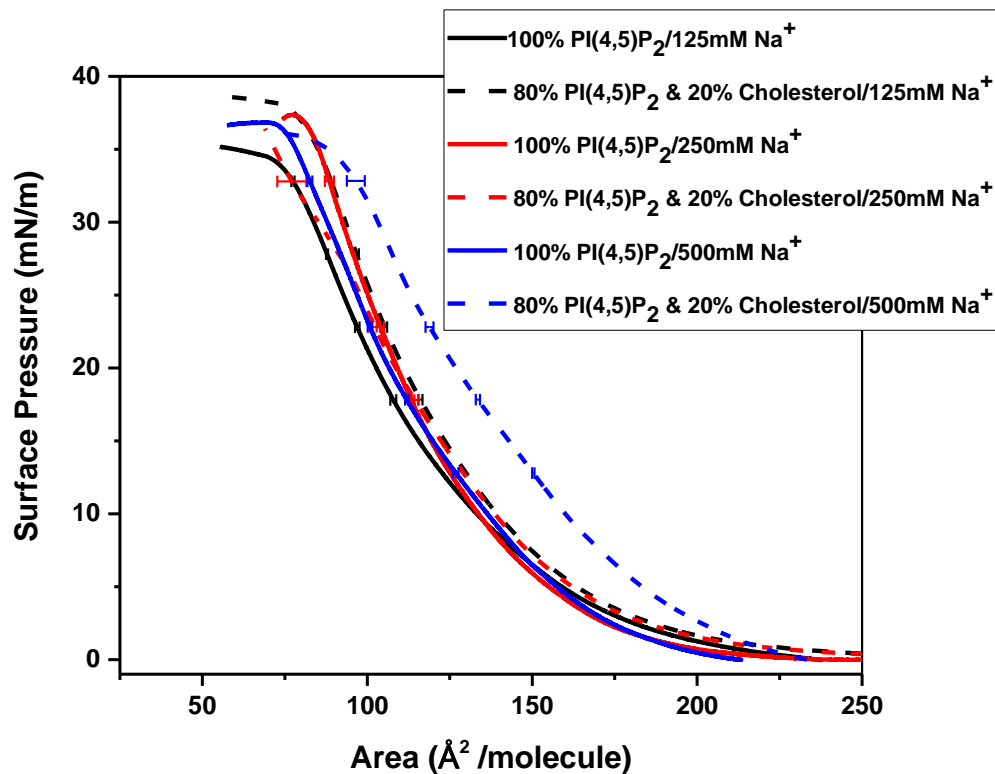


**Figure 34. PI(4,5)P<sub>2</sub>  $\pi$ /A-Isotherm in the Presence of High Molar Concentration of Sodium.**

Monolayers consisted of either 125mM Na<sup>+</sup> (black, solid) or 250mM Na<sup>+</sup> (red, solid) or 500mM Na<sup>+</sup> (blue, solid) in the absence of cholesterol, compared 125mM Na<sup>+</sup> (black, dashed) or 250mM Na<sup>+</sup> (red, dashed) or 500mM Na<sup>+</sup> (blue, dashed) in the absence of cholesterol, in 10mM HEPES buffer, pH 7.4 at T=20.0 °C  $\pm$  0.2.

In the plasma membrane at any given time it is likely that Ca<sup>2+</sup>, Na<sup>+</sup>, K<sup>+</sup> ions will be present at physiological concentrations, therefore we hypothesized that these cations work together to induce PI(4,5)P<sub>2</sub> clustering. Our studies performed in the previous chapter, revealed that Ca<sup>2+</sup> along with K<sup>+</sup> had the greatest electrostatic effect on PI(4,5)P<sub>2</sub> cluster formation (see section 2.1.5). Therefore, we looked synergistically at these ions to understand if a specific ionic environment in the presence of cholesterol would lead to an increase in PI(4,5)P<sub>2</sub> condensation. The synergistic effects of these 4 different cation combinations in the presence of cholesterol were evaluated for

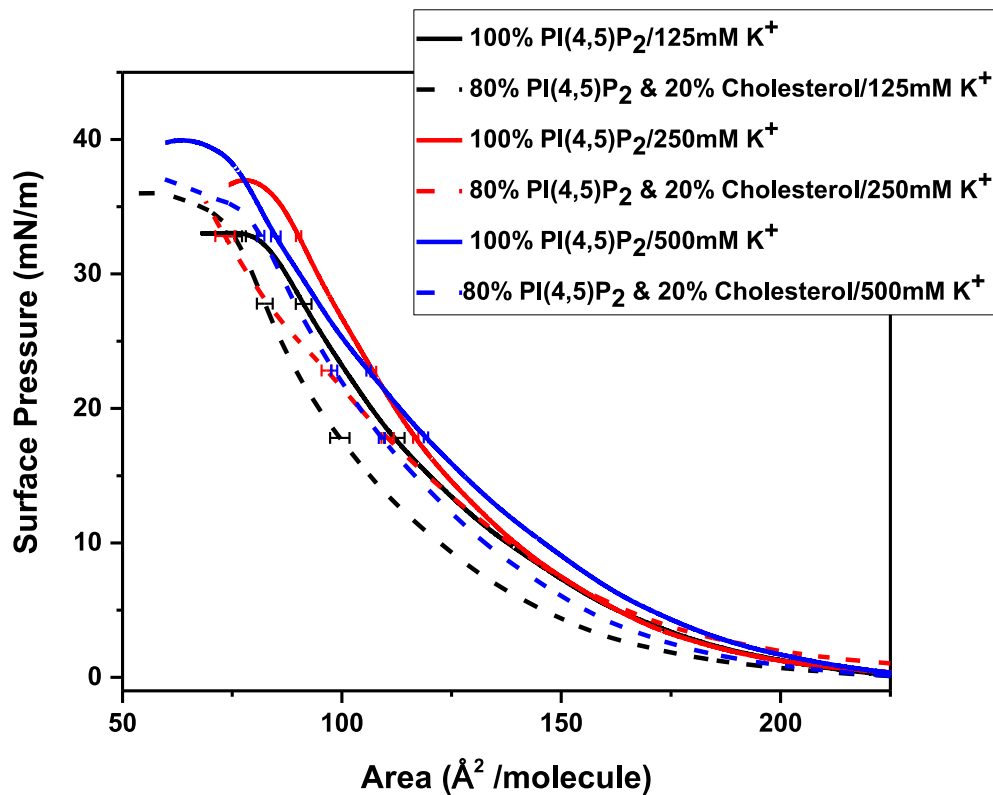


**Figure 35. PI(4,5)P<sub>2</sub>  $\pi$ /A-Isotherm in the Presence of High Molar Concentration of Potassium**

Monolayers consisted of either 125 mM K<sup>+</sup> (black, solid) or 250mM K<sup>+</sup> (red, solid) or 500 mM K<sup>+</sup> (blue, solid) in the absence of cholesterol, compared 125 mM K<sup>+</sup> (black, dashed) or 250mM K<sup>+</sup> (red, dashed) or 500 mM K<sup>+</sup> (blue, dashed) in the absence of cholesterol, in 10 mM HEPES buffer, pH 7.4 at T=20.0 °C  $\pm$  0.2.

changes in PI(4,5)P<sub>2</sub> monolayer packing: 1.) Ca<sub>2+</sub> with K<sup>+</sup>, 2.) Ca<sub>2+</sub> with Na<sup>+</sup>, 3.) Na<sup>+</sup> with K<sup>+</sup>, 4.) Ca<sub>2+</sub> with Na<sup>+</sup> and K<sup>+</sup>. The effects of cholesterol on the PI(4,5)P<sub>2</sub> monolayer in the presence of these ion combinations were investigated for the same total molar ion concentration (500 mM, 250 mM, and 125 mM), however as previously observed in the pure PI(4,5)P<sub>2</sub> monolayers, the high cation concentrations (especially, 500 mM and 250 mM) caused the film to be too stiff for a proper

function of the Wilhelmy plate, therefore for simplicity only the 125mM systems were considered

Ions	Type of Monolayer	$\gamma$ mN/ m	Experimental Results		Simulation Results		
			Area (PI(4,5)P <sub>2</sub> ) Å <sup>2</sup> /molecule	SE	Area (PI(4,5)P <sub>2</sub> ) Å <sup>2</sup> /molecule	SE	
125 mM Ca <sup>2+</sup>	100% PI(4,5)P <sub>2</sub>	65	95.3	±1.5	N/A		
		60	90.3	±1.4	90.5	±0.2	
		55	86.7	±1.4	83.2	±0.2	
		50	83.5	±1.5	80.3	±0.1	
		45	80.9	±1.5	77.2	±0.3	
		40	78.1	±1.0	74.7	±0.2	
	80% PI(4,5)P <sub>2</sub> / 20% cholesterol	65	88.5	±1.2	104.9	±0.2	
		60	83.8	±0.9	94.1	±0.1	
		55	80.1	±0.7	88.3	±0.1	
		50	77.2	±0.5	83.5	±0.1	
		45	74.7	±0.4	82.1	±0.1	
		40	72.6	±0.5	81.0	±0.1	
	125 mM Na <sup>+</sup>	100% PI(4,5)P <sub>2</sub>	55	108.6	±0.9	93.2	±0.1
			50	97.6	±0.7	84.0	±0.1
45			88.4	±0.6	81.2	±0.3	
40			80.0	±0.5	75.1	±0.1	
80% PI(4,5)P <sub>2</sub> / 20% cholesterol		55	115.4	±0.6	93.0	±0.3	
		50	104.5	±0.7	87.0	±0.3	
		45	96.3	±0.7	81.4	±0.4	
		40	89.4	±0.8	77.9	±0.1	
125 mM K <sup>+</sup>	100% PI(4,5)P <sub>2</sub>	52	108.2	±2.0	103.8	±0.8	
		50	104.0	±1.9	95.9	±0.1	
		45	94.2	±1.8	88.4	±0.1	
		40	80.8	±1.3	81.8	±0.2	
	80% PI(4,5)P <sub>2</sub> / 20% cholesterol	52	91.10	±2.0	96.6	±1.0	
		50	87.8	±1.9	93.7	±0.1	
		45	80.9	±2.0	85.1	±0.1	
		40	74.9	±1.8	81.8	±0.3	
41.67mM Ca <sup>2+</sup> 41.67mM Na <sup>+</sup> 41.67mM K <sup>+</sup>	100% PI(4,5)P <sub>2</sub>	60	89.7	±1.1	99.5	±0.5	
		55	85.5	±0.7	89.5	±0.2	
		50	82.3	±0.7	83.4	±0.1	
		45	81.9	±0.7	76.6	±0.1	
		40	75.9	±1.2	74.8	±0.2	
	80% PI(4,5)P <sub>2</sub> / 20% cholesterol	60	95.8	±0.4	92.2	±0.2	
		55	91.8	±0.2	84.4	±0.3	
		50	88.5	±0.2	81.6	±0.2	
		45	85.5	±0.03	79.3	±0.2	
		40	82.7	±0.3	77.5	±0.2	

(Figure 41,

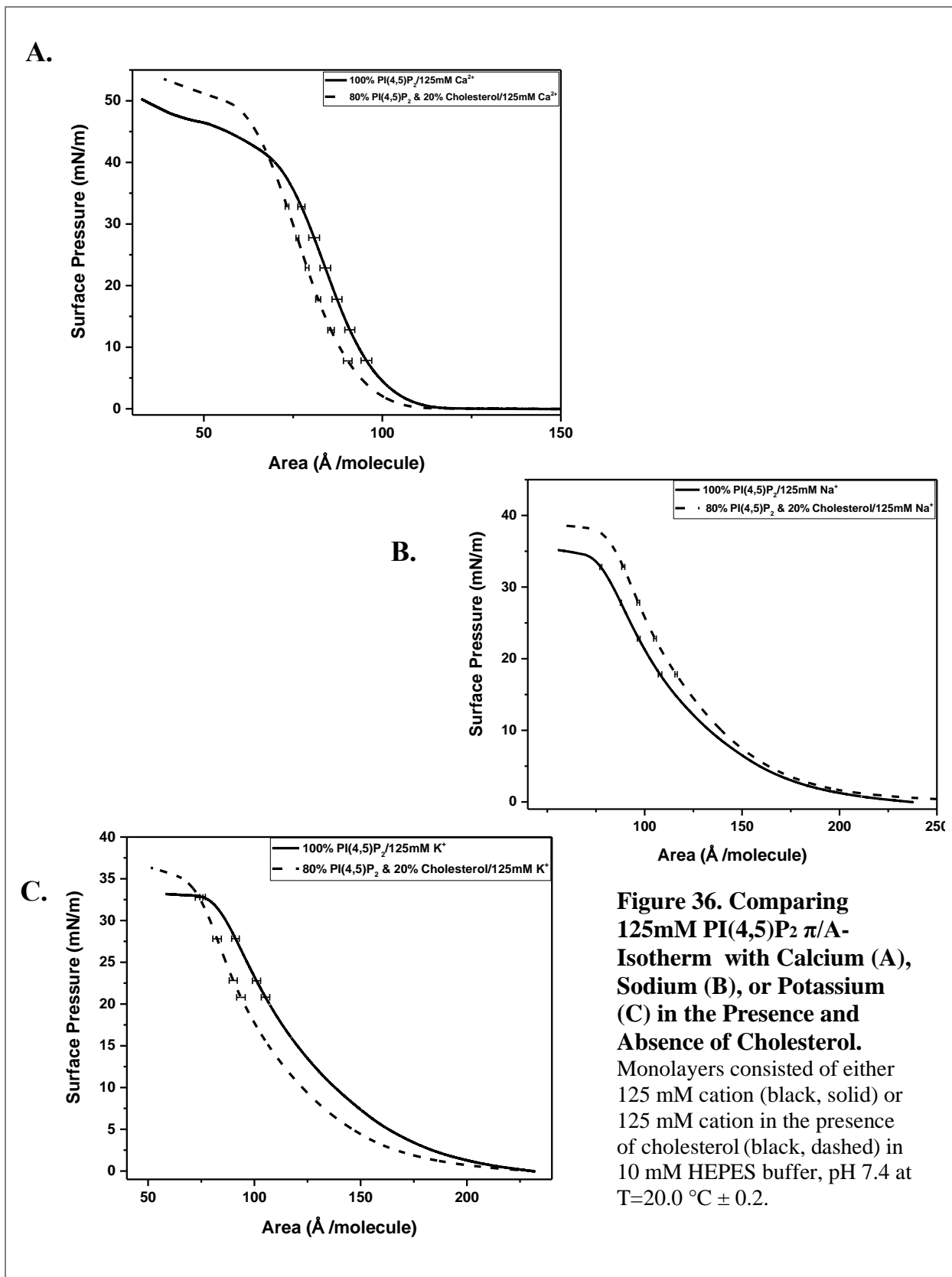
Table 2). At 125 mM concentrations, the 1.) Ca<sup>2+</sup> with K<sup>+</sup>, 2.) Ca<sup>2+</sup> with Na<sup>+</sup>, 3.) Na<sup>+</sup> with K<sup>+</sup> all exhibited an expansion in the presence of cholesterol, suggesting the concentration of ions is still too high not allowing cholesterol to interact and causing cholesterol to act as a spacer (Figure 41). Therefore, in order to gain a better understanding of the synergistic cation effects in the presence of cholesterol, lower total molar concentrations will need to be used.



Ions	Type of Monolayer	$\gamma$ mN/ m	Experimental Results		Simulation Results	
			Area (PI(4,5)P <sub>2</sub> ) Å <sup>2</sup> /molecule	SE	Area (PI(4,5)P <sub>2</sub> ) Å <sup>2</sup> /molecule	SE
125 mM Ca <sup>2+</sup>	100% PI(4,5)P <sub>2</sub>	65	95.3	±1.5	N/A	
		60	90.3	±1.4	90.5	±0.2
		55	86.7	±1.4	83.2	±0.2
		50	83.5	±1.5	80.3	±0.1
		45	80.9	±1.5	77.2	±0.3
	80% PI(4,5)P <sub>2</sub> / 20% cholesterol	40	78.1	±1.0	74.7	±0.2
		65	88.5	±1.2	104.9	±0.2
		60	83.8	±0.9	94.1	±0.1
		55	80.1	±0.7	88.3	±0.1
		50	77.2	±0.5	83.5	±0.1
125 mM Na <sup>+</sup>	100% PI(4,5)P <sub>2</sub>	45	88.4	±0.6	81.2	±0.3
		40	80.0	±0.5	75.1	±0.1
		55	115.4	±0.6	93.0	±0.3
		50	104.5	±0.7	87.0	±0.3
	80% PI(4,5)P <sub>2</sub> / 20% cholesterol	45	96.3	±0.7	81.4	±0.4
		40	89.4	±0.8	77.9	±0.1
		52	108.2	±2.0	103.8	±0.8
		50	104.0	±1.9	95.9	±0.1
125 mM K <sup>+</sup>	100% PI(4,5)P <sub>2</sub>	45	94.2	±1.8	88.4	±0.1
		40	80.8	±1.3	81.8	±0.2
		52	91.10	±2.0	96.6	±1.0
		50	87.8	±1.9	93.7	±0.1
	80% PI(4,5)P <sub>2</sub> / 20% cholesterol	45	80.9	±2.0	85.1	±0.1
		40	74.9	±1.8	81.8	±0.3
		60	89.7	±1.1	99.5	±0.5
41.67mM Ca <sup>2+</sup> 41.67mM Na <sup>+</sup> 41.67mM K <sup>+</sup>	100% PI(4,5)P <sub>2</sub>	55	85.5	±0.7	89.5	±0.2
		50	82.3	±0.7	83.4	±0.1
		45	81.9	±0.7	76.6	±0.1
		40	75.9	±1.2	74.8	±0.2
		60	95.8	±0.4	92.2	±0.2
	80% PI(4,5)P <sub>2</sub> / 20% cholesterol	55	91.8	±0.2	84.4	±0.3
		50	88.5	±0.2	81.6	±0.2
		45	85.5	±0.03	79.3	±0.2
		40	82.7	±0.3	77.5	±0.2

**Table 2: Comparison of Experimental & Computational Derived Surface Tension Data in Presence of Cholesterol.**

The PI(4,5)P<sub>2</sub>  $\pi$ /A-isotherms at various surface tensions with corresponding area/molecule. The standard error (SE) for the experimental data were obtained from the variation of the repeat  $\pi$ /A-isotherm measurements for the respective system. Please note that the area/molecule in the  $\pi$ /A-isotherms does not include the area for cholesterol, which is typical for monolayer studies since the cholesterol molecule is small and takes a smaller space than PI(4,5)P<sub>2</sub> in the monolayer, thus cholesterol is treated like an impurity.



## 1.22 Conclusion

In this chapter, we used thermodynamic studies to gain insight into the synergistic effects of cations and cholesterol on PI(4,5)P<sub>2</sub> cluster formation. In the presence of cholesterol, Ca<sup>2+</sup> or K<sup>+</sup> had a strong condensation effect on the PI(4,5)P<sub>2</sub> monolayer, therefore reducing the area/molecule and increasing the connectivity between the PI(4,5)P<sub>2</sub> headgroups (

Ions	Type of Monolayer	$\gamma$ mN/ m	Experimental Results		Simulation Results	
			Area (PI(4,5)P <sub>2</sub> ) Å <sup>2</sup> /molecule	SE	Area (PI(4,5)P <sub>2</sub> ) Å <sup>2</sup> /molecule	SE
125 mM Ca <sup>2+</sup>	100% PI(4,5)P <sub>2</sub>	65	95.3	±1.5	N/A	
		60	90.3	±1.4	90.5	±0.2
		55	86.7	±1.4	83.2	±0.2
		50	83.5	±1.5	80.3	±0.1
		45	80.9	±1.5	77.2	±0.3
		40	78.1	±1.0	74.7	±0.2
	80% PI(4,5)P <sub>2</sub> / 20% cholesterol	65	88.5	±1.2	104.9	±0.2
		60	83.8	±0.9	94.1	±0.1
		55	80.1	±0.7	88.3	±0.1
		50	77.2	±0.5	83.5	±0.1
		45	74.7	±0.4	82.1	±0.1
		40	72.6	±0.5	81.0	±0.1
125 mM Na <sup>+</sup>	100% PI(4,5)P <sub>2</sub>	55	108.6	±0.9	93.2	±0.1
		50	97.6	±0.7	84.0	±0.1
		45	88.4	±0.6	81.2	±0.3
		40	80.0	±0.5	75.1	±0.1
	80% PI(4,5)P <sub>2</sub> / 20% cholesterol	55	115.4	±0.6	93.0	±0.3
		50	104.5	±0.7	87.0	±0.3
		45	96.3	±0.7	81.4	±0.4
		40	89.4	±0.8	77.9	±0.1
125 mM K <sup>+</sup>	100% PI(4,5)P <sub>2</sub>	52	108.2	±2.0	103.8	±0.8
		50	104.0	±1.9	95.9	±0.1
		45	94.2	±1.8	88.4	±0.1
		40	80.8	±1.3	81.8	±0.2
	80% PI(4,5)P <sub>2</sub> / 20% cholesterol	52	91.10	±2.0	96.6	±1.0
		50	87.8	±1.9	93.7	±0.1
		45	80.9	±2.0	85.1	±0.1
		40	74.9	±1.8	81.8	±0.3
41.67mM Ca <sup>2+</sup> 41.67mM Na <sup>+</sup> 41.67mM K <sup>+</sup>	100% PI(4,5)P <sub>2</sub>	60	89.7	±1.1	99.5	±0.5
		55	85.5	±0.7	89.5	±0.2
		50	82.3	±0.7	83.4	±0.1
		45	81.9	±0.7	76.6	±0.1
		40	75.9	±1.2	74.8	±0.2
	80% PI(4,5)P <sub>2</sub> / 20% cholesterol	60	95.8	±0.4	92.2	±0.2
		55	91.8	±0.2	84.4	±0.3
		50	88.5	±0.2	81.6	±0.2
		45	85.5	±0.03	79.3	±0.2
		40	82.7	±0.3	77.5	±0.2

Table 2). Our collaborator's all-atom molecular dynamics (MD) simulations also exhibited a more pronounced condensation for these systems (unpublished). The strong agreement has allowed us to trust the structural representation obtained from the theoretical simulations of cholesterol's interaction with PI(4,5)P<sub>2</sub>. The all-atom molecular dynamics (MD) simulations were

able to confirm our hypothesis and verified structurally that cholesterol OH interacts via H-bonding with the phosphodiester group as well as the PI(4,5)P<sub>2</sub> - OH groups in the 2- and 6-position (**Figure 42**) (unpublished). The cholesterol moving closer to the PI(4,5)P<sub>2</sub> headgroup region is a unique interaction that has only been suggested for phosphoinositides, since the interaction of the cholesterol hydroxyl group and PC has been found to happen at the lipid carbonyl groups. Our thermodynamic data along with our collaborator's modeling has lead us to pinpoint a "direct" interaction between cholesterol and PI(4,5)P<sub>2</sub>. Additionally, this study has confirmed that PI(4,5)P<sub>2</sub> cluster formation in the presence of cholesterol is enhanced by the presence of cations; however, it is impossible to determine from our studies if cholesterol directly or indirectly influences cation binding to the phosphate groups and this should be further explored experimentally and theoretically. Cholesterol along with cations are major modulators of PI(4,5)P<sub>2</sub> domain formation, thus the results from our studies provide a deeper understanding of these modulators at the atomic

level. These studies furthered our understanding of dependent environmental factors required for PI(4,5)P<sub>2</sub> clustering, thus shedding light on phosphoinositide mediated signaling events.

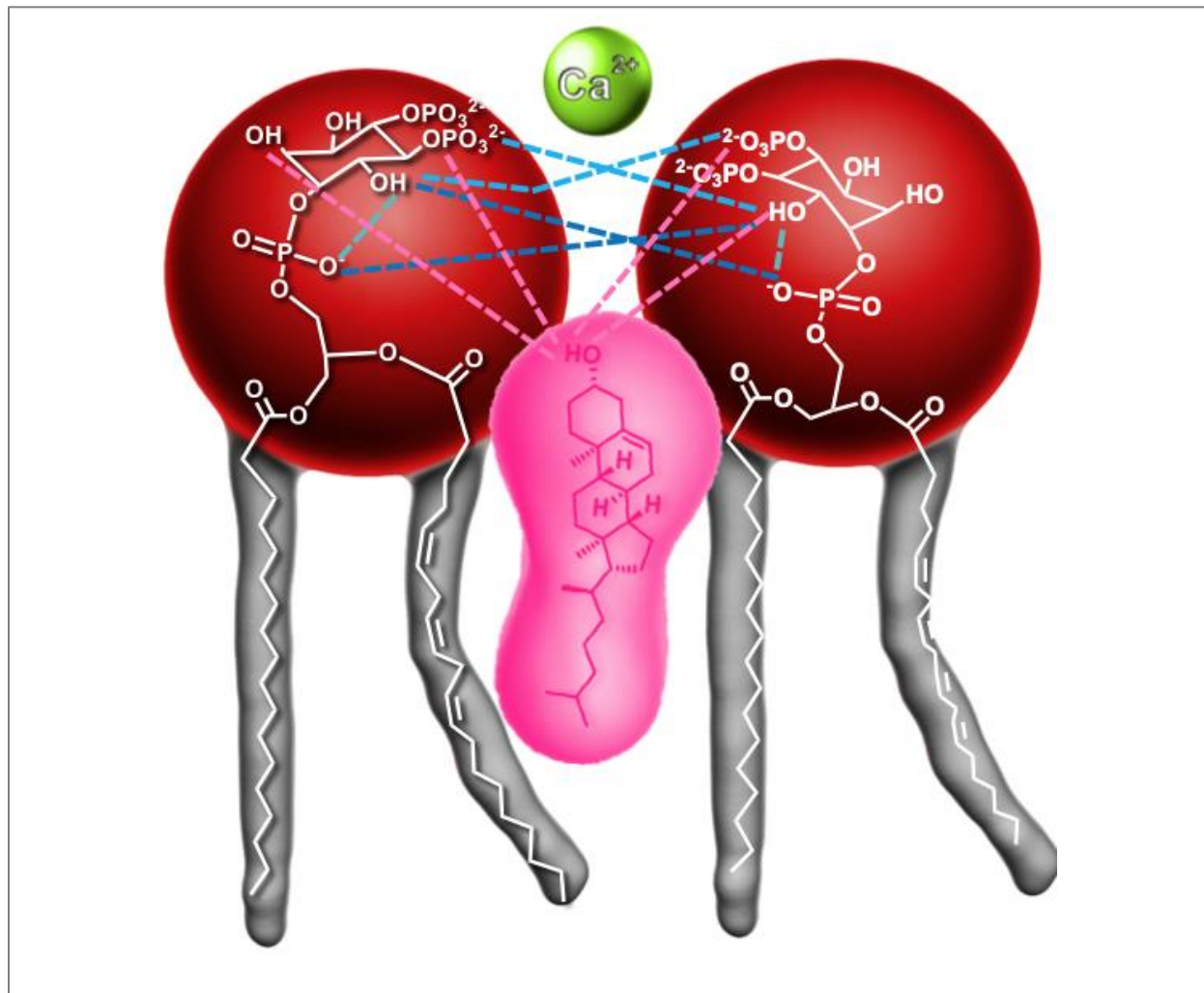


**Figure 37. Model of Cholesterol Participating in PI(4,5)P<sub>2</sub> Hydrogen Bond Network.**

We hypothesize that cholesterol OH interacts via H-bonding with the phosphodiester group as well as the PI(4,5)P<sub>2</sub> - OH groups on the inositol ring (-----), thus participating in PI(4,5)P<sub>2</sub> H-bond network (- - - - H-bond between phosphomonoester and OH-group, - - - - H-bond between phosphodiester and OH-group; intramolecular - - - - H-bond). Our thermodynamic data along with our collaborator’s modeling has led us to pinpoint a “direct” interaction between cholesterol and PI(4,5)P<sub>2</sub>. The all-atom MD simulated that cholesterol OH interacts directly with the phosphodiester group as well as the PI(4,5)P<sub>2</sub> - OH groups in the 2- and 6-position. The cholesterol moving closer to of PI(4,5)P<sub>2</sub> headgroup region is a unique interaction that has only been suggested for phosphoinositides, since the interaction with cholesterol and PC has been found to happen at the lipid carbonyl groups.

## Chapter 5: The Effect of Calcium on Mixed PI/ PI(4,5)P<sub>2</sub> and PS/ PI(4,5)P<sub>2</sub>

### Langmuir Films

#### 1.23 Introduction:

In the previous chapters, we have shown how plasma membrane modulators, such as cholesterol and cations, directly participate in PI(4,5)P<sub>2</sub> cluster formation and stabilization of its H-bond network. PI(4,5)P<sub>2</sub> clusters are targeted and retained by polycationic proteins to the PM; however, this lipid species is only present in quantities of about 1 % of total plasma membrane lipids. Therefore, it is highly likely that other anionic phospholipid species interact with PI(4,5)P<sub>2</sub> to form inner leaflet domains, in particular anionic lipids found in high abundance, such as phosphatidylinositol (PI, ~ 6-10 % total PM) and phosphatidylserine (PS, ~10 to 20 % total PM). These two lipids have a net negative charge at physiologic pH and are predominately responsible for generating a significant difference in charge and membrane asymmetry between the two leaflets of the lipid bilayer. Therefore, the high concentration of PI or PS would provide a large negatively charged platform for non-specific electrostatic protein binding, while co-localized PI(4,5)P<sub>2</sub> would provide specificity along with providing an additional electrostatic environment for protein binding. Additionally, previous <sup>31</sup>P-NMR ionization studies have assessed the deprotonation for PI(4,5)P<sub>2</sub> is inhibited by the presence of the anionic lipids, such as PS and PI. The presence of these anionic lipids increased the negative surface potential, thus decreasing interfacial pH, which suggests that PI(4,5)P<sub>2</sub> can overcome the mutual electrostatic repulsion and form intermolecular hydrogen-bonds (Graber, Jiang et al. 2012).

PI is of particular interest because of its role as a precursor to PIPs which participate in a broad range of signaling pathways. The phosphorylation at the 3 position of PI by PI3-Kinase (PI3K) leads to the formation of PI(3)P, a cell signaling lipid involved in endocytosis and vesicular trafficking events (Herman 1990, Odorizzi 2000). While phosphorylation at the 4 position of PI by PI4-Kinase (PI4K) leads to the formation PI(4)P, a particularly important lipid involved in vesicle and endosomal trafficking in the Golgi (Wang 2007, Tan and Brill 2014). The third monophosphate, PI(5)P, which is produced by PI5-Kinase (PI5K), is responsible for setting the threshold of T-cell activation, thus maintaining T-cell homeostasis (Guittard, Mortier et al. 2010). The PI kinases have been found to be localized in phosphoinositide lipid domains; however, the spatial and temporal organization of such domains remains understood. *In vitro* studies with giant unilamellar vesicles (GUVs) have shown that PI and PI(4,5)P<sub>2</sub> cooperatively form macroscopic domains enriched in PI and PI(4,5)P<sub>2</sub>. Strikingly under these conditions, neither of these lipids form macroscopic domains individually with PC, they must both be present for the formation of macroscopic domains. Taking this into account, it is tempting to think PI(4,5)P<sub>2</sub> domains enriched in PI may provide a physiologically relevant platform for peripheral protein binding that has dual specificity for anionic lipids. Therefore, in this study we aimed to understand if PI along with PI(4,5)P<sub>2</sub> is able to form a stable phosphoinositide domain.

Membrane PS regulates surface charge and provides an abundant electrostatic environment for protein binding (Yeung 2008, Yeung, Heit et al. 2009). PS is found preferentially in the inner leaflet of the plasma membrane; however, the appearance of PS on the outer leaflet of the cell membrane is an indication of a loss of membrane integrity (Leventis and Grinstein 2010, Bevers and Williamson 2016). Thus, many of the studies have analyzed the role of PS when exposed on the

surface of apoptotic cells, in which PS targets them for phagocytosis signaling. By contrast, the intracellular role of PS has been studied less extensively due in part to the lack of a suitable probe to monitor PS intracellularly (Kay 2012). However, studies have revealed that PS along with  $\text{Ca}^{2+}$  is required for the proper localization and/or activation of important intracellular proteins that have C2 or gamma-carboxyglutamic domains, such as protein kinase C (Cho 2006, Cassilly and Reynolds 2018). In order for the C2-domains to bind to PS, it has been suggested that the presence of sizable pools of PS on the cytosolic leaflet are used as docking sites (Menke 2005). The effective PM recruitment of these cellular proteins may require PS and other phosphoinositides, such as  $\text{PI}(4,5)\text{P}_2$ , to work synergistically. However, based on  $^{31}\text{P}$  NMR data, PS and  $\text{PI}(4,5)\text{P}_2$  do not interact and further studies with GUV's suggested that PS does not induce macroscopic  $\text{PI}(4,5)\text{P}_2$  domain formation (Graber, Jiang et al. 2012). However, it is very possible that microscopic domains form that are below the diffraction limit of microscopy. The environments in biological membranes are significantly more complex than in these model systems, thus raising the question whether  $\text{PI}(4,5)\text{P}_2$  and PS are co-localized in cell membranes. This idea was first proposed when it was discovered that PTEN, a protein part of the PI3K signaling pathway, was able to bind both PS and  $\text{PI}(4,5)\text{P}_2$  synergistically (Shenoy, Shekhar et al. 2012, Gericke, Leslie et al. 2013). Therefore, in order to further understand spatiotemporal regulation of cell membrane signaling pathways there is a critical need to understand if PS and  $\text{PI}(4,5)\text{P}_2$  form stable phosphoinositide domains.

While previous studies in this dissertation have focused on looking at the physicochemical behavior of  $\text{PI}(4,5)\text{P}_2$  clustering, this part of the study focuses on determining anionic lipid partners that stabilize  $\text{PI}(4,5)\text{P}_2$  clustering. Our previous work has showed that  $\text{Ca}^{2+}$  had the strongest ion-



mediated condensation effect on PI(4,5)P<sub>2</sub>, when compared to Na<sup>+</sup> and K<sup>+</sup> (see section 0) Therefore, using Langmuir trough monolayer films we will compare the interaction of PI or PS on PI(4,5)P<sub>2</sub> cluster formation in the absence and presence of Ca<sup>2+</sup>. We hypothesize that in the absence of Ca<sup>2+</sup>, PI will have a stronger condensation effect due the inositol ring of PI's headgroup having a richer hydrogen bond capability than the serine group of PS. However, we believe that the ability of Ca<sup>2+</sup> to shield the negative charge on the headgroups will lead to hydrogen bond formation in both of these anionic lipids. Understanding the properties of both PI and PS interaction with PI(4,5)P<sub>2</sub> will not only help us identify lipid partners that may lead to stabilization of PI(4,5)P<sub>2</sub> domains, but will also provide us with physiological cues about temporal control of the spatially resolved protein activity.

## **1.24 Results:**

### **4.1.1 The Effect of Ca<sup>2+</sup> on Individual PI or PS $\pi/A$ -Isotherms**

Before we begin to investigate whether PI or PS participate in PI(4,5)P<sub>2</sub> cluster formation in the presence of Ca<sup>2+</sup>, we need to first explore the effects of Ca<sup>2+</sup> on individual PI or PS Langmuir monolayer films. We will use the same experimental conditions that were used to investigate the role of Ca<sup>2+</sup> on PI(4,5)P<sub>2</sub> monolayers. The buffer subphase was composed of 10 mM Tris, and 150 mM NaCl at pH 7.4 with varying concentrations of Ca<sup>2+</sup> (0.01 mM, 0.1 mM, 1 mM, or 2 mM) or in the case of 0 mM Ca<sup>2+</sup>, 0.1mM EDTA was used to chelate any Ca<sup>2+</sup> leached from the glassware. The  $\pi/A$ -Isotherm of PI in the absence of Ca<sup>2+</sup> was characteristic of an expanded monolayer (Figure 43) which was expected considering the headgroup charge repulsion and the unsaturated nature of the acyl chains. Our data confirmed previous epifluorescence images that showed no

domain formation or contrast throughout the compression of the PI monolayer in the absence of  $\text{Ca}^{2+}$  (King 2016). The addition of 0.01 mM and 0.1 mM  $\text{Ca}^{2+}$  to the subphase had no effect on the shape and placement of the  $\pi/A$ -isotherm (Figure 43). This was also consistent with previous epifluorescent data showing no visible domain formation at higher surface pressures and round domains typical for LE/G co-existence region at low pressures (King 2016). However, once the subphase concentration was increased to 1mM & 2mM (Figure 43), the  $\pi/A$ -isotherm expanded suggesting  $\text{Ca}^{2+}$  sits between the headgroup and interacts with phosphodiester. There could be

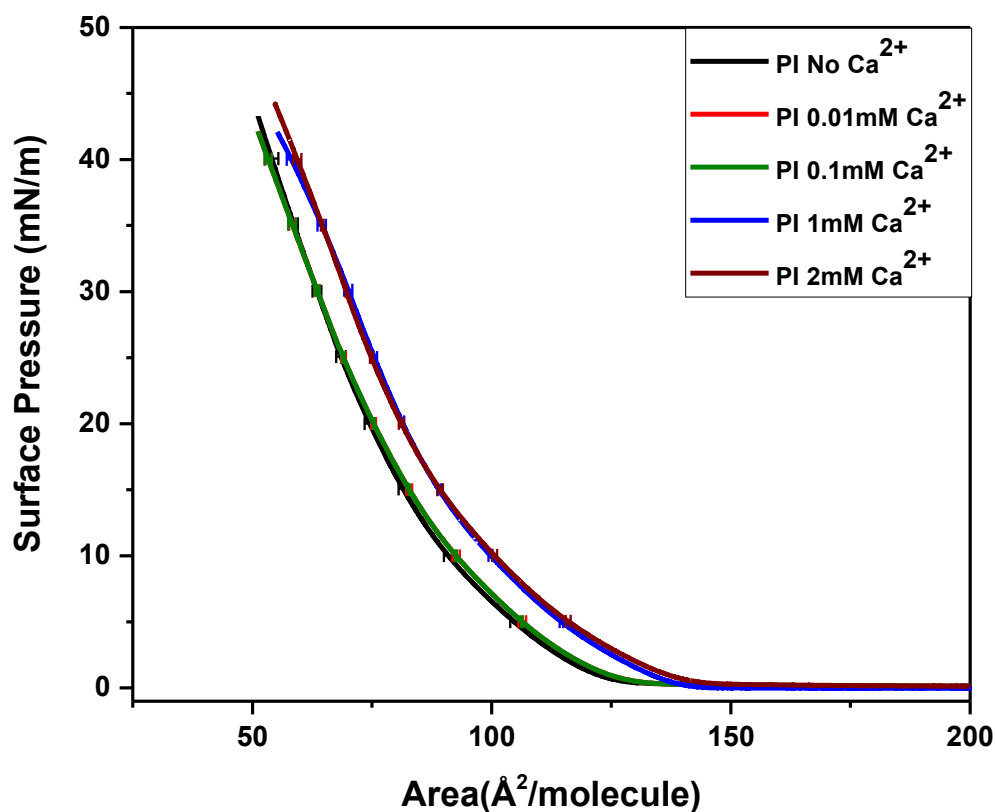


**Figure 38. PI  $\pi/A$ -Isotherm in the Presence of Low Molar Calcium Concentrations.** Monolayers consisted of varying subphase concentrations: 0 mM  $\text{Ca}^{2+}$  (black), 0.01 mM  $\text{Ca}^{2+}$  (red), 0.1 mM  $\text{Ca}^{2+}$  (green), 1 mM  $\text{Ca}^{2+}$  (blue), or 2 mM  $\text{Ca}^{2+}$  (wine), in 10mM Tris buffer containing 150 mM NaCl, pH 7.4 at  $T=25.0\text{ }^{\circ}\text{C} \pm 0.2$ .

competition between the monolayer condensing effect of the  $\text{Ca}^{2+}$  due to headgroup bridging and monolayer expansion due to insertion of the cation between the headgroup (Figure 45).

For PS, the  $\pi/A$ -Isotherm in the absence of  $\text{Ca}^{2+}$  was characteristic of an expanded monolayer just like PI (Figure 44). However, in contrast to PI upon addition of 0.01 mM  $\text{Ca}^{2+}$  the  $\pi/A$ -Isotherm shifted to lower areas/molecule showing a condensation of the monolayer. Additionally previously performed epifluorescence data showed PS domains at lower pressures (Pinderi 2017). This suggests that  $\text{Ca}^{2+}$  is screening the negative headgroup charge, thus reducing

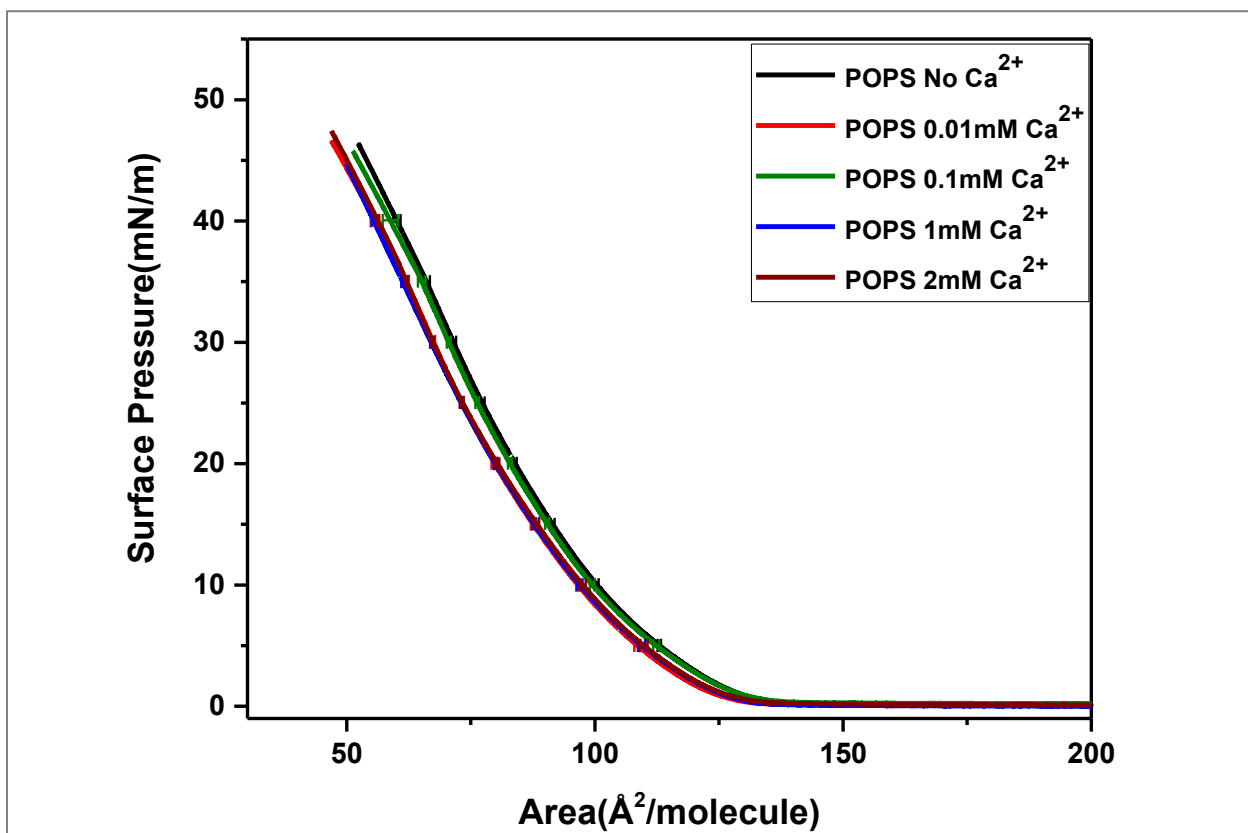


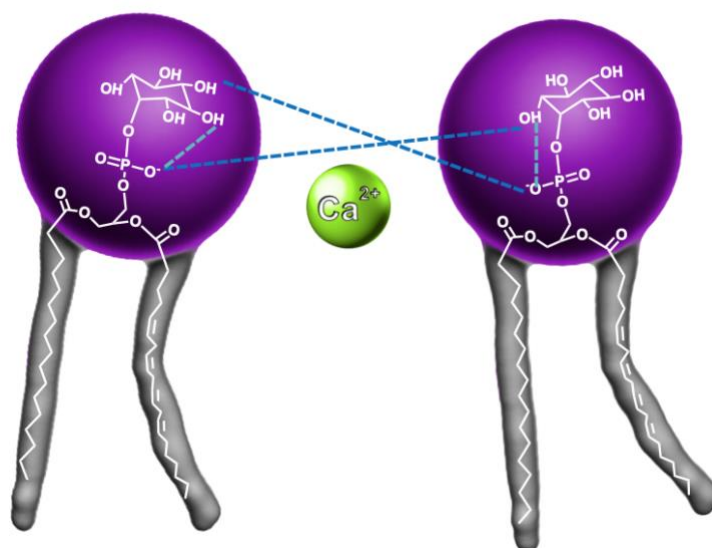
**Figure 39. POPS  $\pi/A$ -Isotherm in the Presence of Low Molar Calcium Concentrations.** Monolayers consisted of varying subphase concentrations: 0 mM  $\text{Ca}^{2+}$  (black), 0.01 mM  $\text{Ca}^{2+}$  (red), 0.1 mM  $\text{Ca}^{2+}$  (green), 1 mM  $\text{Ca}^{2+}$  (blue), or 2 mM  $\text{Ca}^{2+}$  (wine), in 10mM Tris buffer containing 150 mM NaCl, pH 7.4 at  $T=25.0\text{ }^\circ\text{C} \pm 0.2$ .

the repulsive forces (which would lead to a small condensation of the film). It appears, like in the case of PI(4,5)P<sub>2</sub>, that the observed condensation is predominantly due to bridging of the headgroup by Ca<sup>2+</sup>. The addition of higher concentrations of Ca<sup>2+</sup> (1 mM and 2 mM) exhibited the same condensing effect in the PS monolayer as it was observed for 0.01 mM Ca<sup>2+</sup> (Figure 44) this suggests that the higher concentration does not further stabilize PS monolayers. This was further supported with previous epifluorescence images showing that domains at 1 mM and 2 mM Ca<sup>2+</sup> looked similar to the 0.01 mM Ca<sup>2+</sup> at low surface pressures (Pinderi 2017).

Overall, in the absence of Ca<sup>2+</sup> both PI and PS monolayers are characterized by an expanded  $\pi/A$ -Isotherm typical for a transition from an LE/G state at low surface pressures to an LE state at high pressures. However, the presence of Ca<sup>2+</sup> resulted in different packing behavior for PI than PS. At low concentrations of Ca<sup>2+</sup> (0.01 mM), the lipid packing of PI did not change, whereas PS lipids packed more tightly evident by the condensation. Higher concentrations of Ca<sup>2+</sup> (1 mM and 2 mM) had the opposite effects on PI than PS, the PI  $\pi/A$ -isotherm moved to higher areas/molecule while the isotherm for the PS monolayer stayed similarly condensed as observed for the 0.01 mM Ca<sup>2+</sup>. We hypothesize that for high concentrations, the Ca<sup>2+</sup> sits between PI headgroup and interacts with phosphodiester (**Figure 45, A**). For the case of PS monolayers we hypothesize that Ca<sup>2+</sup> screens and bridges the negatively charged headgroup allowing H-bond formation between the OH-group on the amine and the phosphodiester group on adjacent PS (**Figure 45, B**).

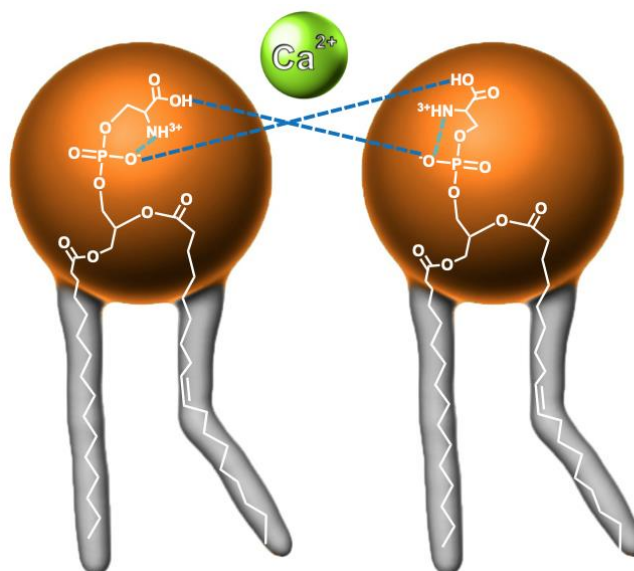
**Figure 40. Structural Model of A.) PI interaction with  $\text{Ca}^{2+}$  and B.) PS Interaction with  $\text{Ca}^{2+}$**

**A.  
PI interaction  
with  $\text{Ca}^{2+}$**



Based on the expansion of the  $\pi/A$ -isotherm at high concentrations of  $\text{Ca}^{2+}$  (1-2 mM), we hypothesize that  $\text{Ca}^{2+}$  sits between PI headgroup and interacts with phosphodiester. We further hypothesize that the inositol ring of PI's headgroup interacts with an adjacent phosphodiester group (----) forming H-bond networks that stabilize PI cluster formation (intramolecular ---- H-bond).

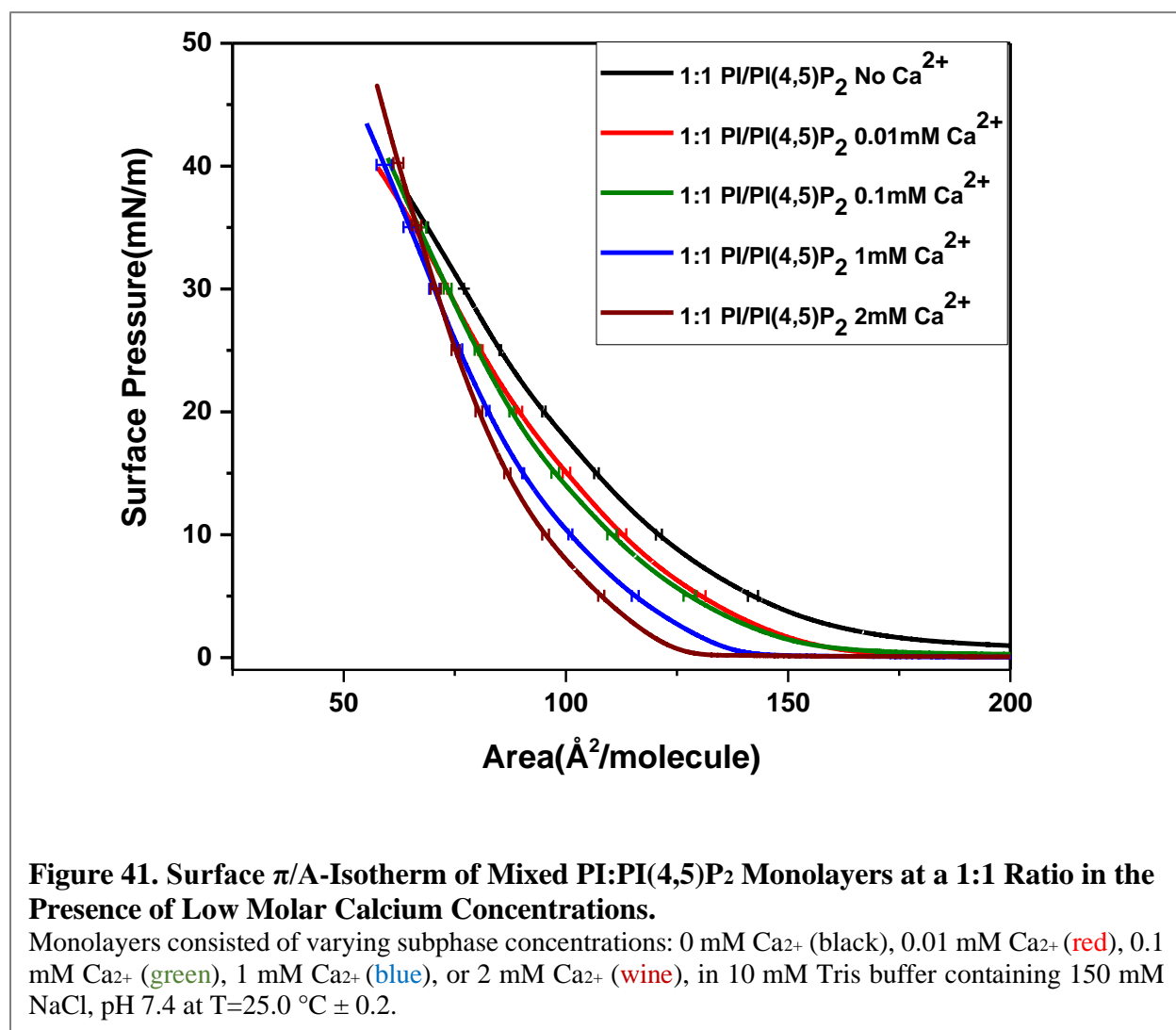
**B.  
PS interaction  
with  $\text{Ca}^{2+}$**



In the presence of high concentration of  $\text{Ca}^{2+}$  (1-2 mM) there was a condensation of the monolayer, thus we hypothesize  $\text{Ca}^{2+}$  screens and bridges the negatively charged headgroup of PS allowing the hydroxyl group of the amine to H-bond with an adjacent phosphodiester group (----) (intramolecular ---- H-bond).

### 4.1.2 Effect of $\text{Ca}^{2+}$ on Mixed PI/ PI(4,5)P<sub>2</sub>

Before we began to investigate whether  $\text{Ca}^{2+}$  acts as modulator to stabilize PI/PI(4,5)P<sub>2</sub> interaction, we needed to have an understanding of PI's interaction with PI(4,5)P<sub>2</sub>; therefore, we investigated both a 1:1 ratio and 2:1 ratio of PI/ PI(4,5)P<sub>2</sub>. In the absence of  $\text{Ca}^{2+}$ , the  $\pi/A$ -Isotherm of the 1:1 PI/ PI(4,5)P<sub>2</sub> monolayer resulted in an isotherm that is directly in between the pure PI and pure PI(4,5)P<sub>2</sub>  $\pi/A$ -isotherms, which suggested that 1:1 PI/PI(4,5)P<sub>2</sub> resulted in a well-mixed system (**Figure 46**). This observation is in agreement with the previous GUV PC/PI/PI(4,5)P<sub>2</sub>



microscopy experiments that showed PI/PI(4,5)P<sub>2</sub> demixing from PC (Jiang, Redfern et al. 2014). We hypothesized that PI & PI(4,5)P<sub>2</sub> participate in H-bonding between the OH-group of PI & phosphomonoester groups of PI(4,5)P<sub>2</sub>, which resulted in a condensed monolayer when compared to pure PI(4,5)P<sub>2</sub>. The more accurate representation of the global PI/PI(4,5)P<sub>2</sub> concentration found in biological membranes was investigated with a 2:1 ratio. The  $\pi/A$ -Isotherm of the 2:1 PI/PI(4,5)P<sub>2</sub> resulted in an expanded monolayer in comparison to the 1:1 ratio, but a condensation when compared to pure PI(4,5)P<sub>2</sub> monolayer (**Figure 47**). These results suggested that the best mole ratio for a PI/PI(4,5)P<sub>2</sub> mixed phase is 1:1. For a 2:1 mixture, the packing is less efficient.

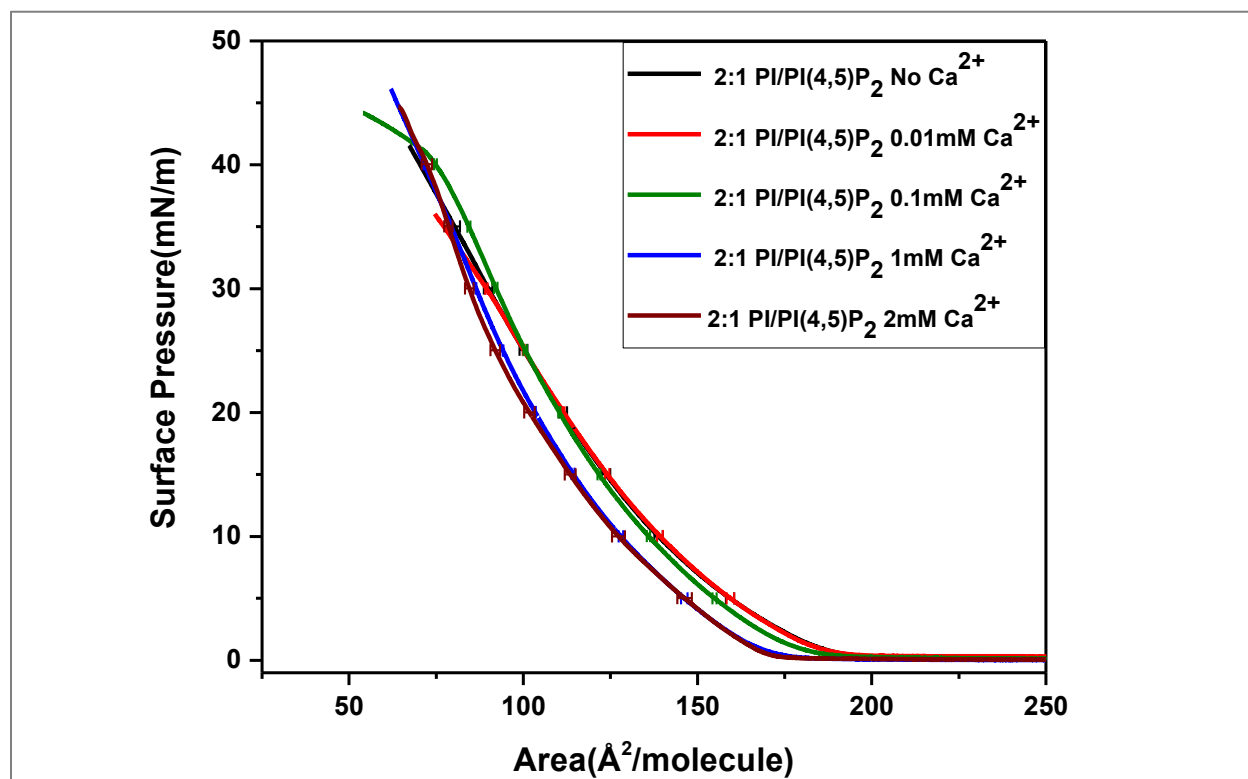


**Figure 42. Surface  $\pi/A$ -Isotherm of Mixed PI:PI(4,5)P<sub>2</sub> Monolayers at a 2:1 Ratio in the Presence of Low Molar Calcium Concentrations.**

Monolayers consisted of varying subphase concentrations: 0 mM Ca<sub>2+</sub> (black), 0.01 mM Ca<sub>2+</sub> (red), 0.1 mM Ca<sub>2+</sub> (green), 1 mM Ca<sub>2+</sub> (blue), or 2 mM Ca<sub>2+</sub> (wine), in 10 mM Tris buffer containing 150 mM NaCl, pH 7.4 at T=25.0 °C ± 0.2.

Next the effect of  $\text{Ca}^{2+}$  on further stabilizing PI/PI(4,5) $\text{P}_2$  cluster formation was investigated. For the 1:1 ratio, the addition of  $\text{Ca}^{2+}$  to the subphase led to a systematic increase in the monolayer condensation (**Figure 46**). We hypothesized that the condensation of the monolayer in the presence of  $\text{Ca}^{2+}$  is the result of  $\text{Ca}^{2+}$  shielding the head group of PI(4,5) $\text{P}_2$  & bridging the PI/PI(4,5) $\text{P}_2$  phosphodiester or the PI phosphodiester w/ PI(4,5) $\text{P}_2$  phosphomonoester with adjacent OH-groups. For the 2:1 ratios, the addition of 0.01 mM and 0.1 mM  $\text{Ca}^{2+}$  did not have any observable effect in comparison to the  $\pi/A$ -Isotherm in the absence of  $\text{Ca}^{2+}$ ; however, 1 mM  $\text{Ca}^{2+}$  led to a condensation of monolayer. The presence of additional 1 mM  $\text{Ca}^{2+}$  (total 2 mM) did not further condense the monolayer (**Figure 46**). Previously performed epifluorescence measurements confirmed the presence of small domains characterized by circular monolayer free “bubbles” for both 1:1 and 2:1 PI/PI(4,5) $\text{P}_2$  (King 2016). When comparing the area/molecule for the 2:1 to the 1:1, the 2:1 was always more expanded than 1:1 with characteristics of an expanded isotherm (Figure 47).

Interestingly, even in the absence of  $\text{Ca}^{2+}$  the 2:1 PI/PI(4,5) $\text{P}_2$  remained more expanded than the 1:1 PI/PI(4,5) $\text{P}_2$ . (**Figure 47**). Therefore, 1:1 ratio of PI/PI(4,5) $\text{P}_2$  in the presence and absence of  $\text{Ca}^{2+}$  led to a more efficient molecular packing than it is found for the 2:1 ratio. This data suggests that the best stoichiometry for the PI/PI(4,5) $\text{P}_2$  interaction is 1:1, therefore it is probable to assume that the optimal cellular ratio of PI/PI(4,5) $\text{P}_2$  domains would also be similar, but of course this would depend on the biochemical alternations that could shift this ratio in one direction or another. Overall, our thermodynamic data suggests that the presence of  $\text{Ca}^{2+}$  shields the head group of PI(4,5) $\text{P}_2$  and bridging the PI/PI(4,5) $\text{P}_2$  phosphodiester or the PI phosphodiester with the PI(4,5) $\text{P}_2$  phosphomonoester, forming a stabilized monolayer (**Figure 49**).



### 4.1.3 Effect of $\text{Ca}_{2+}$ on Mixed PS/ PI(4,5)P<sub>2</sub>

The effects of  $\text{Ca}_{2+}$  on mixed PS/ PI(4,5)P<sub>2</sub> systems were investigated similarly to the PI/ PI(4,5)P<sub>2</sub> systems. Before we began to investigate whether  $\text{Ca}_{2+}$  acts as a modulator to stabilize PS/ PI(4,5)P<sub>2</sub> interaction, we investigated the interaction of PS with PI(4,5)P<sub>2</sub> in a 1:1 ratio. In the absence of  $\text{Ca}_{2+}$  the  $\pi/A$ -isotherm of the 1:1 PS/ PI(4,5)P<sub>2</sub> resulted in a condensed isotherm in comparison to the one for a pure PI(4,5)P<sub>2</sub> monolayer. The area/molecule for a 1:1 PS/ PI(4,5)P<sub>2</sub> was half way in between the area/molecule of pure PS and pure PI(4,5)P<sub>2</sub> isotherms. The 1:1 PS/PI(4,5)P<sub>2</sub> resulted in a  $\pi/A$ -isotherm in between the pure PS and pure PI(4,5)P<sub>2</sub>  $\pi/A$ -isotherms. There are two likely explanations either the 1:1 PS/PI(4,5)P<sub>2</sub> is a well-mixed system, similarly to the 1:1 PI/PI(4,5)P<sub>2</sub> system, suggesting PS may also stabilize PI(4,5)P<sub>2</sub> domain formation or PS is demixed from PI(4,5)P<sub>2</sub>. We hypothesized that PS & PI(4,5)P<sub>2</sub> participate in H-bonding between the OH-group of PS and phosphomonoester groups of PI(4,5)P<sub>2</sub>, which resulted in a condensed monolayer when compared to pure PI(4,5)P<sub>2</sub> (**Figure 48**).

The effect on  $\text{Ca}_{2+}$  on PS/PI(4,5)P<sub>2</sub> interaction showed a systematic increase in condensation corresponding to  $\text{Ca}_{2+}$  concentration (**Figure 48**). We hypothesize that the condensation of the monolayer in the presence of  $\text{Ca}_{2+}$  is the result of  $\text{Ca}_{2+}$  shielding the negative phosphodiester group of PS and phosphomonoester groups of PI(4,5)P<sub>2</sub> and bridging the group of PS and PI(4,5)P<sub>2</sub> headgroups. This would enable interaction between the PS OH group and the PI(4,5)P<sub>2</sub> phosphodiester or phosphomonoester groups and the  $\text{NH}_3^+$  of PS with either the phosphodiester or phosphomonoester of PI(4,5)P<sub>2</sub>. The 2:1 ratio was not explored for PS/PI(4,5)P<sub>2</sub> systems, but based on the similarity between PS and PI  $\pi/A$ -isotherm it is acceptable to assume

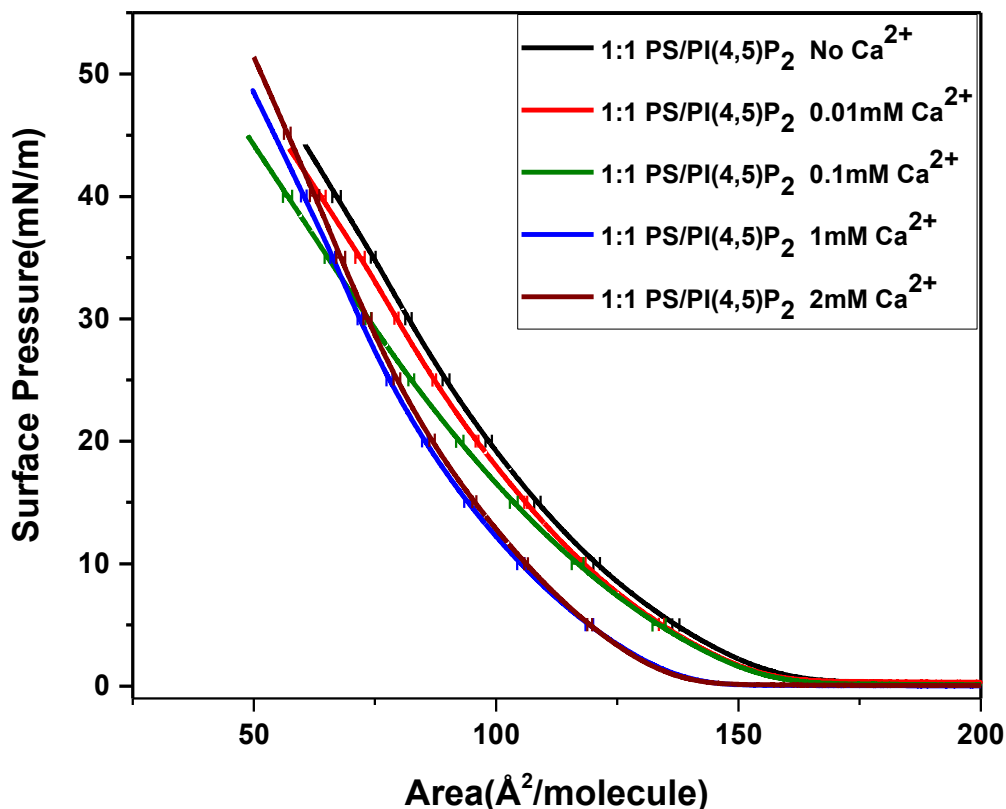


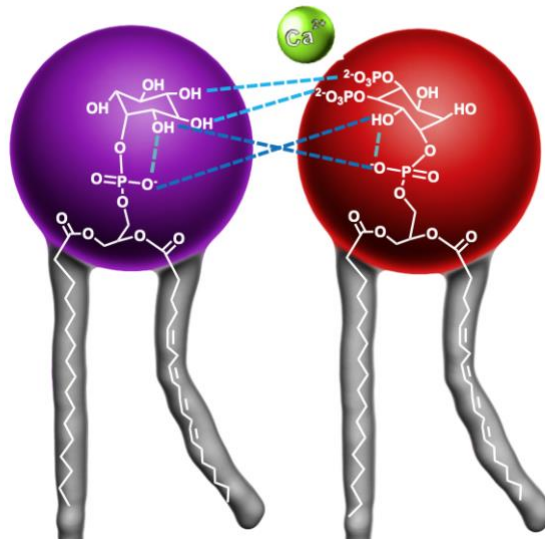
**Figure 43. Surface  $\pi/A$ -Isotherm of Mixed PS:PI(4,5)P<sub>2</sub> Monolayers at a 1:1 Ratio in the Presence of Low Molar Calcium Concentrations.**

Monolayers consisted of varying subphase concentrations: 0 mM Ca<sub>2+</sub> (black), 0.01 mM Ca<sub>2+</sub> (red), 0.1 mM Ca<sub>2+</sub> (green), 1 mM Ca<sub>2+</sub> (blue), or 2 mM Ca<sub>2+</sub> (wine), in 10mM Tris buffer containing 150 mM NaCl, pH 7.4 at T=25.0 °C ± 0.2.

the 1:1 ratio is a best representation of cellular PS/PI(4,5)P<sub>2</sub> interactions as well; however the effects of Ca<sub>2+</sub> on 2:1 PS/PI(4,5)P<sub>2</sub> isotherm films should be explored to confirm the biologically relevant ratio. Overall, our thermodynamic data suggests that presence of Ca<sub>2+</sub> does induce a stable PS/ PI(4,5)P<sub>2</sub> domain by shielding the negatively charged headgroups and allowing the OH-group and the NH<sub>3+</sub> of the reactive amine of PS to hydrogen bond with PI(4,5)P<sub>2</sub> phosphodiester or phosphomonoesters groups (**Figure 49**).

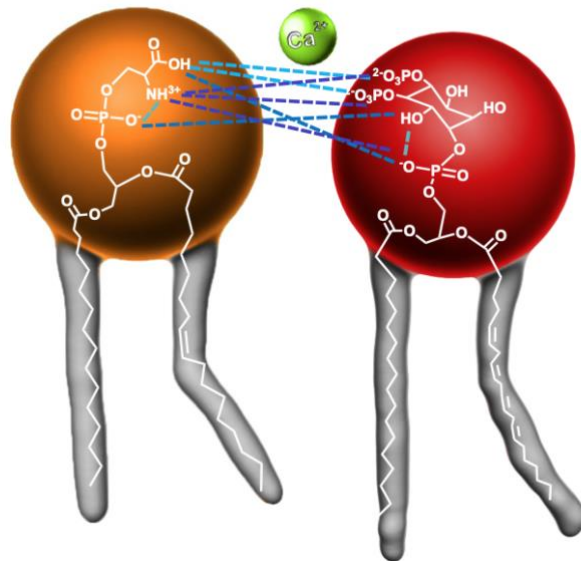
**Figure 44. Structural Model of A.) PI interaction with PI(4,5)P<sub>2</sub> and B.)PS Interaction with PI(4,5)P<sub>2</sub>**

**B. PI interaction with PI(4,5)P<sub>2</sub> in the Presence of Ca<sup>2+</sup>**



The addition of Ca<sup>2+</sup> lead to a condensation of the PI/PI(4,5)P<sub>2</sub> monolayers, thus we hypothesize that Ca<sup>2+</sup> shields the negative head group of PI(4,5)P<sub>2</sub> & bridges PI/PI(4,5)P<sub>2</sub> through H-bond formation, the phosphodiester of PI or PI(4,5)P<sub>2</sub> can H-bond with adjacent OH-groups and the PI(4,5)P<sub>2</sub> phosphomonoester can H-bond with adjacent PI OH-group (---- H-bond between phosphomonoester and OH-group, ----H-bond between phosphodiester and OH-group; intramolecular ---- H-bond).

**A. PS interaction with PI(4,5)P<sub>2</sub> in the Presence of Ca<sup>2+</sup>**

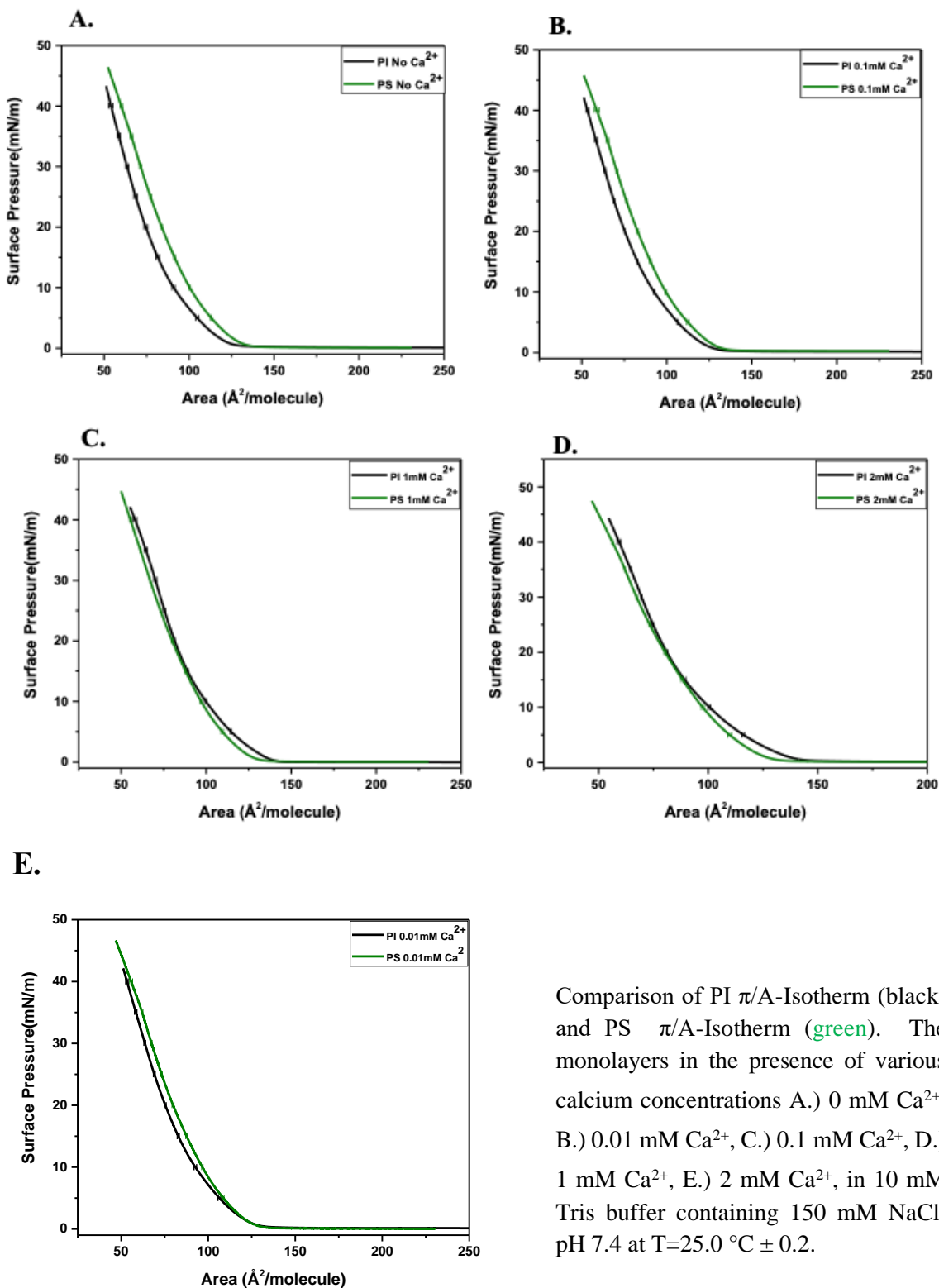


The addition of Ca<sup>2+</sup> led to a condensation of the PS/PI(4,5)P<sub>2</sub> monolayers, thus we hypothesize that Ca<sup>2+</sup> shields the negative head group of PI(4,5)P<sub>2</sub> & bridges PS/PI(4,5)P<sub>2</sub>. The NH<sub>3</sub><sup>+</sup> group of PS can interact with the phosphodiester or phosphomonoester of an adjacent PI(4,5)P<sub>2</sub> (----), the phosphodiester of PI(4,5)P<sub>2</sub> can H-bond with adjacent PS OH-groups (----) and the PI(4,5)P<sub>2</sub> phosphomonoester can H-bond with adjacent PI OH-group (----).

#### 4.1.4 Comparing PI and PS interaction with PI(4,5)P<sub>2</sub>

Both PS and PI are similarly charged anionic lipids found in high abundance in the inner leaflet of the PM, therefore it is suspected that both PS and PI have similar ability to provide an electrostatic environment for protein binding. Based on this we hypothesize that the  $\pi/A$ -isotherm characteristics of PI interaction with PI(4,5)P<sub>2</sub> would be similar to PS interaction with PI(4,5)P<sub>2</sub>. Before, we investigated the interaction of PI and PS with PI(4,5)P<sub>2</sub> in the presence of Ca<sup>2+</sup>, we compared the interaction of PS and PI individually in the presence of Ca<sup>2+</sup>. The  $\pi/A$ -Isotherm of PI is slightly shifted to a lower area/molecule when compared to the PS  $\pi/A$ -Isotherm, which suggests that the PI molecules are able to pack more tightly than the PS molecule (**Figure 50**). We hypothesize this is because the six OH groups inositol ring of participation in H-bonds is stronger than the reactive amine (NH<sub>3</sub>) and OH group participation in H-bonding. Furthermore, the chair conformation of the PI headgroup can pack very efficiently as long as the “chairs” line up appropriately. This has been observed previously for lipid with sugar ring headgroup that also can assume a very tight packing. Upon the addition of 0.01 mM and 0.1 mM Ca<sup>2+</sup>, the  $\pi/A$ -isotherm for PI was slightly more condensed than PS  $\pi/A$ -isotherm, suggesting that PI molecules pack a bit more tightly. However, upon the addition of higher Ca<sup>2+</sup> concentrations (1 mM and 2 mM), the PI  $\pi/A$ -isotherm expanded suggesting that Ca<sup>2+</sup> at high concentrations sits between the headgroups shielding the phosphodiester group. Unlike the PS at these concentrations which resulted in the  $\pi/A$ -isotherm being a bit more condensed bringing the smaller less bulky serine headgroups closer together. However, at the various Ca<sup>2+</sup> concentrations the PS and PI  $\pi/A$ -isotherm's were characteristically very similar showing that these lipids pack together similarly, thus suggesting they will interact similarly with PI(4,5)P<sub>2</sub>.

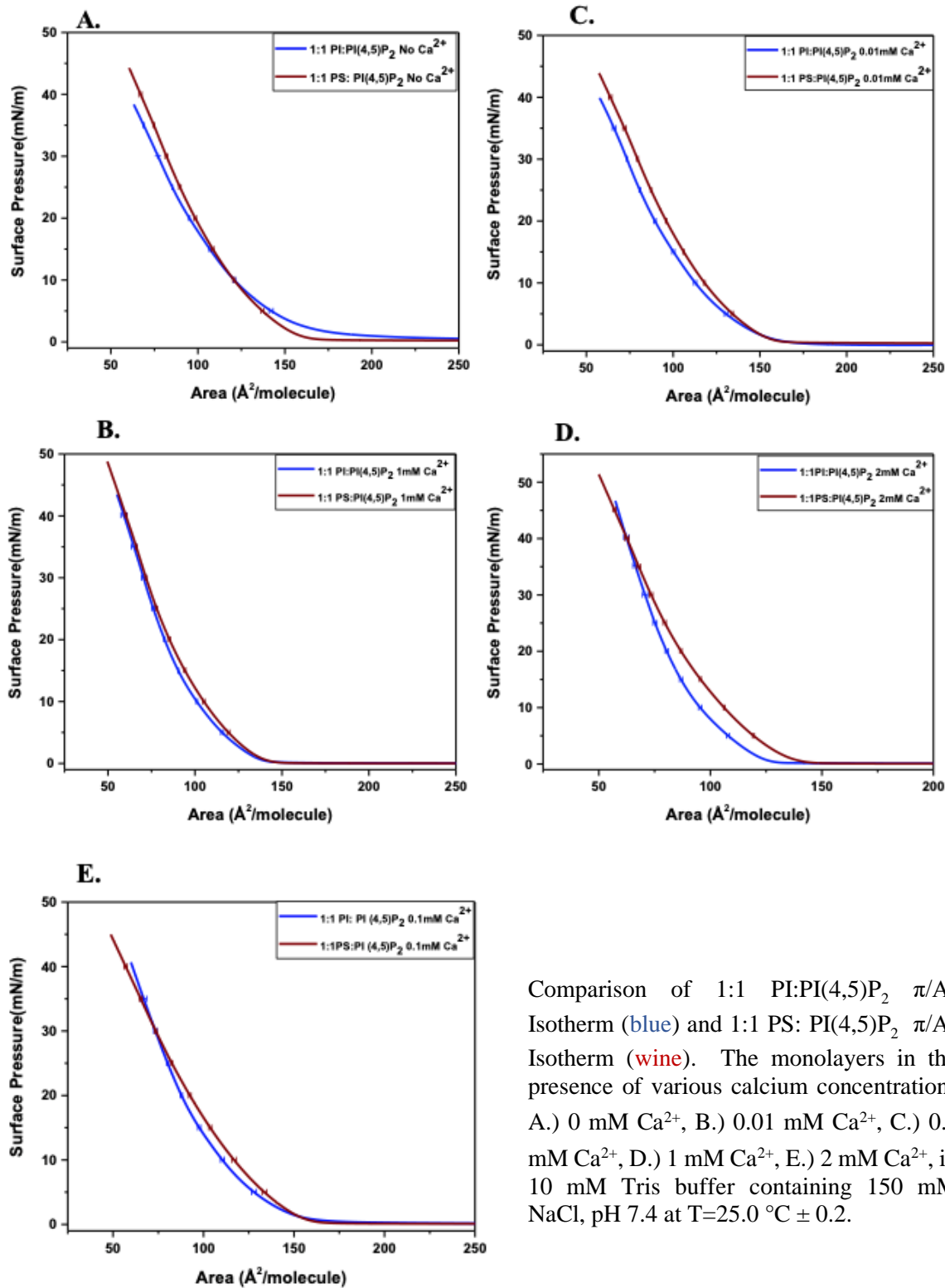
**Figure 45. Comparison of Surface  $\pi/A$ -Isotherm of PI and PS Monolayers in the Presence of Low Molar Calcium Concentrations.**



Comparison of PI  $\pi/A$ -Isotherm (black) and PS  $\pi/A$ -Isotherm (green). The monolayers in the presence of various calcium concentrations A.) 0 mM  $\text{Ca}^{2+}$ , B.) 0.01 mM  $\text{Ca}^{2+}$ , C.) 0.1 mM  $\text{Ca}^{2+}$ , D.) 1 mM  $\text{Ca}^{2+}$ , E.) 2 mM  $\text{Ca}^{2+}$ , in 10 mM Tris buffer containing 150 mM NaCl, pH 7.4 at  $T=25.0\text{ }^\circ\text{C} \pm 0.2$ .

In the presence of PI(4,5)P<sub>2</sub>, but the absence of Ca<sup>2+</sup> we hypothesize that PI will have a stronger condensation effect due the inositol ring of PI's headgroup having a richer hydrogen bond capability and the more efficient packing than the amine group of PS. The  $\pi/A$ -isotherm of 1:1 PI/PI(4,5)P<sub>2</sub> was similar to PI/PI(4,5)P<sub>2</sub> at low surface pressure (within each's other standard error) (Figure 51). However, at higher surface pressure (>10 mN/m), PI in the presence of PI(4,5)P<sub>2</sub> packed more tightly (lower area/molecule) than PS in the presence of PI(4,5)P<sub>2</sub> (**Figure 51**). This results was in line with our hypothesis, which suggests that PI's headgroup interacts more effectively with PI(4,5)P<sub>2</sub> H-bond network. In the presence of all Ca<sup>2+</sup> concentrations (0.01 mM, 0.1 mM, 1 mM, and 2 mM) the  $\pi/A$ -isotherm's of PS in the presence of PI(4,5)P<sub>2</sub> were all slightly more expanded than PI (**Figure 51**). However, both PI and PS shifted slightly to a lower area/molecule than in the absence of Ca<sup>2+</sup>, suggesting that Ca<sup>2+</sup> shields the negative charge on the headgroups lending each of these anionic lipids to interact in PI(4,5)P<sub>2</sub> hydrogen bond network. Overall, comparing both PI and PS in the presence of PI(4,5)P<sub>2</sub> and Ca<sup>2+</sup> showed characteristically similarly  $\pi/A$ -isotherm, suggesting that PI and PS interact can interact with PI(4,5)P<sub>2</sub> H-bond network to form stable domains. Understanding both PI and PS interaction with PI(4,5)P<sub>2</sub> helped us identify that these two readily abundant lipids further stabilize PI(4,5)P<sub>2</sub> domains. However, more studies are required to further understand if these domains are found naturally in the biological membrane.

**Figure 46. Comparison of Surface  $\pi/A$ -Isotherm of PI or PS with PI(4,5)P<sub>2</sub> Monolayers in the Presence of Low Molar Calcium Concentrations.**



Comparison of 1:1 PI:PI(4,5)P<sub>2</sub>  $\pi/A$ -Isotherm (blue) and 1:1 PS:PI(4,5)P<sub>2</sub>  $\pi/A$ -Isotherm (wine). The monolayers in the presence of various calcium concentrations A.) 0 mM Ca<sup>2+</sup>, B.) 0.01 mM Ca<sup>2+</sup>, C.) 0.1 mM Ca<sup>2+</sup>, D.) 1 mM Ca<sup>2+</sup>, E.) 2 mM Ca<sup>2+</sup>, in 10 mM Tris buffer containing 150 mM NaCl, pH 7.4 at T=25.0 °C ± 0.2.

## 1.25 Conclusion

In this part of the study we aimed to better understand whether other anionic lipids, in particular PI and PS, participated and strengthened PI(4,5)P<sub>2</sub>-Ca<sup>2+</sup> cluster formation. Since PI(4,5)P<sub>2</sub> is only found at ~1 % of total lipids in the PM, it is high likely that other anionic lipid species participate in cluster formation. We were particularly interested in PI and PS because both are found at high abundance, ~6-10 % and ~10-20 % respectively, and both are found to electrostatically bind peripheral proteins. Previous studies have found that PI cooperatively forms macroscopic domains with PI(4,5)P<sub>2</sub>, conversely PS did not induce macroscopic domain formation all though there may be microscopic PI(4,5)P<sub>2</sub> domains below the diffraction limit of the microscopy technique (Graber, Jiang et al. 2012, King 2016, Pinderi 2017). Our previous studies in this dissertation (chapter 2) showed that Ca<sup>2+</sup> leads to a further stabilization of PI(4,5)P<sub>2</sub> monolayer likely to due to the ability of the cationic species to interact with the negative charge of the headgroup and shifting the balance between repulsive charge interactions. In the presence of Ca<sup>2+</sup> both 1:1 PI/PI(4,5)P<sub>2</sub> and PS/PI(4,5)P<sub>2</sub> equally showed a systematic increase in condensation corresponding to Ca<sup>2+</sup> concentration. This suggests that Ca<sup>2+</sup> further stabilized both PI and PS cluster formation with PI(4,5)P<sub>2</sub>. In comparing the interaction of PI and PS with PI(4,5)P<sub>2</sub>, the  $\pi/A$ -isotherm showed very similar area/molecule, which suggest that PI and PS interact similarly with PI(4,5)P<sub>2</sub>. The  $\pi/A$ -isotherm for PI/PI(4,5)P<sub>2</sub> were shifted to a slightly lower area/molecule suggesting that PI is slightly more attracted to PI(4,5)P<sub>2</sub> than PS. We hypothesize that PI is able interact more strongly with PI(4,5)P<sub>2</sub> as a result of its inositol ring headgroup have a higher propensity for H-bonding than the serine headgroup of PS (Figure 49). Our results confirm previous ionization studies suggesting that PI(4,5)P<sub>2</sub> can overcome the mutual electrostatic repulsion and form intermolecular hydrogen-bonds with anionic lipid species PS and PI (Graber,



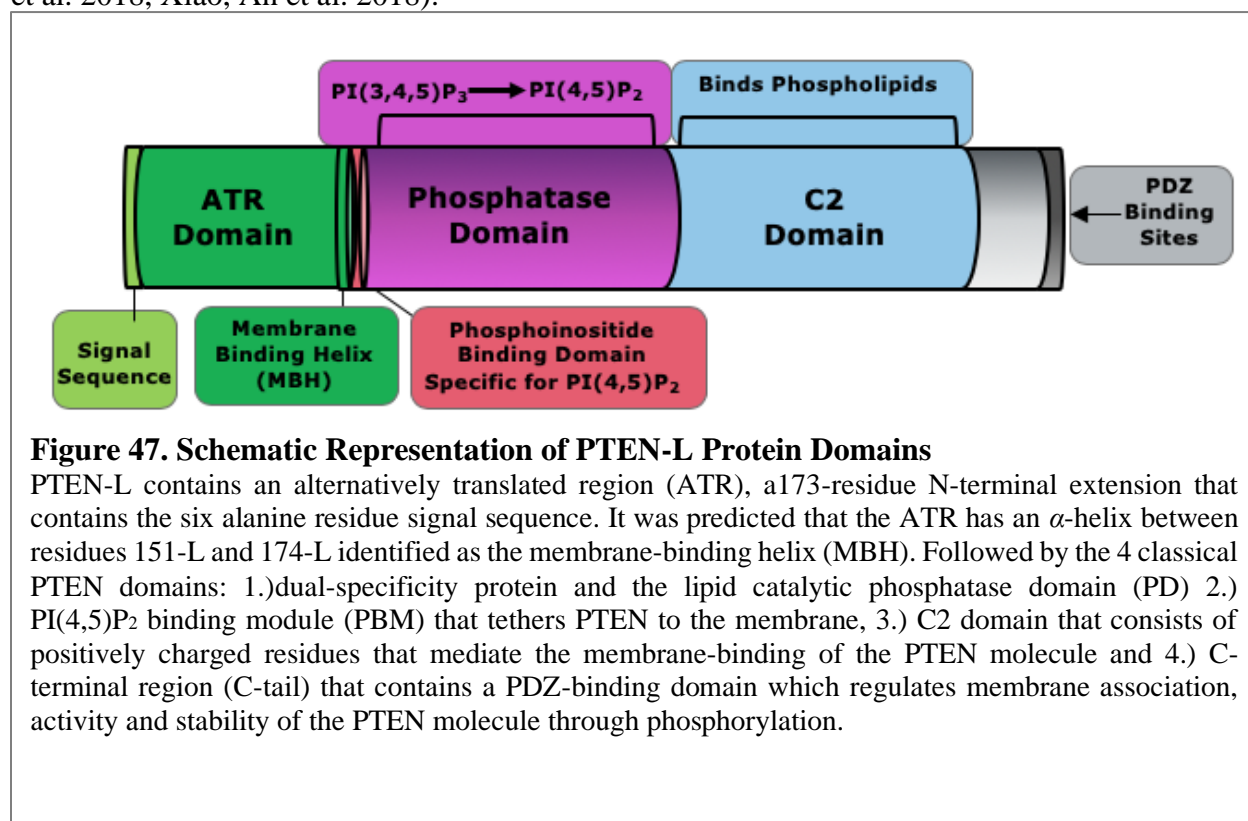
Jiang et al. 2012). Since both PI and PS equally stabilize PI(4,5)P<sub>2</sub> cluster formation, it is highly likely that these lipids interact *in vivo* to form stabilize electrostatic domains required for protein binding. This data confirms that the presence of other anionic lipid are involved in PI(4,5)P<sub>2</sub> cluster formation, thus furthering our knowledge on the environment involved in spatially regulating phosphoinositide clustering.

## Chapter 6: ATR-Domain of PTEN-Long Membrane Binding Preferences

### 1.26 Introduction

In the previous chapters we aimed to understand the spatial control of PI(4,5)P<sub>2</sub> clustering by investigating the effects of cations, cholesterol, and other anionic lipid partners on PI(4,5)P<sub>2</sub> phase behavior. In this chapter we will analyze the temporal regulation by investigating PI(4,5)P<sub>2</sub> protein interactions, in particular a translation variant of PTEN. PTEN (phosphatase and tensin homolog deleted on chromosome 10) is primarily studied for its role as a lipid phosphatase that dephosphorylates PI(3,4,5)P<sub>3</sub> in the PI3K/Akt pathway preventing signaling by inhibiting PI(3,4,5)P<sub>3</sub> dependent processes, such as the membrane recruitment and activation of AKT, thus regulating cell growth, survival and proliferation (Georgescu 2010, Hemmings and Restuccia 2012, Bermudez Brito, Goulielmaki et al. 2015). To date, the COSMIC cancer database currently lists > 5,000 mutations in PTEN tumor suppressor gene, and these mutations have been found in a variety of cancers including brain, prostate, endometrial, glioblastoma, and breast. The PTEN mutations have also been linked to PTEN hereditary tumor syndromes (PHTS), including Cowden disease, Bannayan–Riley–Ruvalcaba syndrome, Proteus syndrome, and Proteus-like syndrome, and have also been associated with macrocephaly and autism spectrum disorder (Ming and He 2012, Ortega-Molina and Serrano 2013, Milella, Falcone et al. 2015, Nguyen, Yang et al. 2015, Pulido 2015, Wang, Cao et al. 2018, Eissing, Ripken et al. 2019). The involvement of PTEN in maintaining proper cellular signaling has led to decades of research on understanding the modes of PTEN protein regulation such as protein–protein interactions, post-translational modifications, and secretion out of the cell (Gericke, Munson et al. 2006, Tamguney and Stokoe 2007, Wang and Jiang 2008, Leslie 2012, Fragoso and Barata 2015, Leslie, Kriplani et al. 2016, Lee 2018).

This exploration led to the recent discovery of a translational variant of PTEN that arises from an alternative translation start site 519 base-pairs upstream of the ATG initiation sequence, adding 173 N-terminal amino acids to the normal PTEN open reading frame (Hopkins, Fine et al. 2013). The alternative translation termed PTEN-Long encodes a 173–amino acid domain (~17 kDa) at its N-terminus, known as the alternative translation region (ATR), followed by the classical 403 amino acids of PTEN (~ 55 kDa) (**Figure 52**). Interestingly, cellular studies have shown that PTEN-L is able to act as a lipid phosphatase and is able to down regulate PI3K signaling, suggesting that it behaves similarly to PTEN. Therefore, studies over the last several years have been geared towards understanding the differences and/or similarities between PTEN and PTEN-L (Hopkins, Fine et al. 2013, Hopkins, Hodakoski et al. 2014, Hodakoski, Fine et al. 2015, Johnston and Raines 2015, Zhang, Yin et al. 2015, Masson, Perisic et al. 2016, Wang, Cho et al. 2018, Xiao, An et al. 2018).



The PTEN structure has been extensively studied revealing that PTEN has four distinct functional domains: 1.) dual-specificity protein and the lipid catalytic phosphatase domain (PD) 2.) PI(4,5)P<sub>2</sub> binding module (PBM) that tethers PTEN to the membrane, 3.) C2 domain that consists of positively charged residues that mediate the membrane-binding of the PTEN molecule and 4.) C-terminal region (C-tail) that contains a PDZ-binding domain which regulates membrane association, activity and stability of the PTEN molecule through phosphorylation (Figure 52) (Lee 1999, Sun 1999, Georgescu 2000, Murray 2002, Odriozola, Singh et al. 2007, Song, Salmena et al. 2012, Frago and Barata 2015, Chen, Dempsey et al. 2016). The main structural difference between PTEN and PTEN-L is the additional 173 amino acids (ATR- domain), thus most studies have revolved around exploring the effects of this addition. Intriguingly studies have revealed that the ATR-domain contains a secretion signal sequence with a predicted cleavage site at amino acid 22 that allows PTEN-L to be secreted from cells, thus mutating the signal sequence abolishes secretion (Hopkins, Fine et al. 2013, Malaney, Uversky et al. 2013, Masson, Perisic et al. 2016). Even more surprising was the discovery that PTEN-L can enter back into cells, which has been suggested through the presence of a poly-arginine stretch in the ATR domain that behaves similarly to cell-penetrating peptides, in particular HIV transactivator of transcription (TAT) protein. The effect of PTEN-L in mouse tumor models revealed that PTEN-L induced and inhibited tumor growth, suggesting PTEN-L alters PI3K signaling through its ability to enter back into cells (Hopkins, Fine et al. 2013, Hopkins, Hodakoski et al. 2014). This ability may provide a means to restore a functional tumor-suppressor protein to tumor cells, suggesting PTEN-L may have therapeutic uses as a deliverable tumor suppressor protein. The mechanism by which PTEN-L and not PTEN can enter cells is currently a mystery, thus more detailed research on PTEN-L molecular interactions, both biophysical and biochemical are necessary.

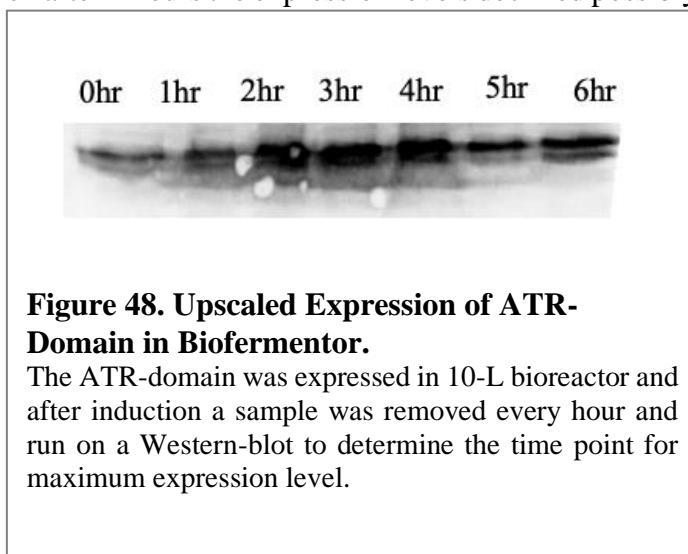
In this study, we aimed to understand the biological role of PTEN-L in cellular membrane processes by investigating the plasma membrane lipid binding preferences of the alternative translated region (ATR) of PTEN-L. Currently, most of the studies on PTEN-L have neglected to investigate the specific protein-protein and protein-lipid interactions thereby leaving a major gap in understanding the biological significance of PTEN-L. Thus, it was evident to us that biophysical studies are needed to understand the ATR-domain/lipid interactions. We began our study by cloning and optimizing expression and purification conditions of the ATR-domain. Since the ATR-domain was a low-yield expressing protein, we upscaled the expression using a Bioreactor, which resulted in a much higher yield of protein. Next, we investigated the interactions of ATR-domain with lipid partners in the plasma membrane to gain insight into how PTEN-L can exit and enter the plasma membrane. We used attenuated total reflection-Fourier transformation infrared (ATR-FTIR) spectroscopy (refer to methods 1.15) to monitor the structural change of ATR-domain upon lipid binding to inner leaflet lipids. In order to understand if any structural changes were present, we first determined the secondary structure of ATR-domain using both circular dichroism (CD) and FTIR spectroscopy. Since the ATR region contains a polyarginine stretch with homology to other cell permeable peptides (such as Tat in HIV), this suggests that PTEN-L may be able to traverse the plasma membrane passively, a process that is dependent on the composition of membrane lipids and proteins. Our studies will help to delineate the lipid binding preferences of the ATR, allowing us to better understand the involvement of PTEN-L in the PI3K/Akt signaling pathway.

## 1.27 Results:

The isoform of the translational variant of PTEN, PTEN-L has an additional 173 amino acids at its N-terminus (ATR-domain) than normal PTEN. Previously performed studies have shown that the ATR-domain (N-173) is required for PTEN-L secretion and transport to adjacent cells, which suggests that the ATR-domain has the potential to act as a drug delivery system for PTEN. An extensive analysis of the ATR-domain is warranted to better exploit its structural and biophysical peculiarities for drug delivery applications. In this chapter, we herein analyze the structural properties and membrane binding preferences of the ATR-domain of PTEN-L.

### 5.1.1 ATR-Domain Protein Expression and Purification

During cloning, expression and purification of ATR domain, we experienced many scientific challenges like low-yield protein expression, not obtaining > 90 % pure protein, and not enough protein to carry out experiments. To alleviate the expression and protein yield problems, we successfully upscaled the expression in a 10-L biofermentor. The maximum expression level was obtained after 3-4 hours of induction, then after 4 hours the expression levels declined possibly due to the ATR protein being toxic to the bacterial cells (**Figure 53**). Next, we established a reproducible protocol to purify the ATR-domain (~17 kDa) in higher yields (~5mg per 1L cell paste). The western blot (A) and SDS-PAGE (B) analysis confirmed the purification



resulted in an ATR-domain with > 95 % purity (17 kDa protein) (Figure 21). The higher yields of purified protein allowed us to carry out *in-vitro* characterizations of ATR domain lipid binding preferences (~10 mg/mL needed for biophysical studies, such as ATR-FTIR). Refer to chapter 1 section 1.1.9 for specifics on the protein expression and purification methodology

### 5.1.2 Investigation of ATR-Domain Secondary Structure

Once the ATR-domain was successfully purified, we wanted to gain insight into the secondary structure of the protein. A comprehensive bioinformatics analysis using several PONDR disorder predictors suggested that the ATR-domain of PTEN-L is likely intrinsically disordered with protein-binding sites and post-translational modifications (PTMs), indicating its probable role in PTEN-L function and transport across cells (Malaney, Uversky et al. 2013, Masson, Perisic et al. 2016). However, this has yet to be confirmed experimentally, thus we used both circular dichroism (CD) and Fourier transformation infrared (FTIR) spectroscopy to assess the conformational properties of the ATR-domain. The CD spectra of proteins in the far ultraviolet (UV) range (180-250 nm) depends strongly on the backbone conformation, and therefore the secondary structure can be determined by the signals. A typical CD spectrum for an  $\alpha$ -helix structure possesses two minima at 208 nm and 220 nm with the same intensity, while  $\beta$ -sheet proteins show a characteristic signal with only one minimum around 217 nm and a maximum near 198 nm, and random coil shows a minimum around 200 nm. The CD spectra of the ATR-domain showed only a minimum peak around 200 nm, which suggested ATR-domain was random coiled with no defined structural (**Figure 54**) These results were confirmed using FTIR showing an amide I peak at  $\sim 1644\text{ cm}^{-1}$ , which is typical for a random coil structure (**Figure 55**). To further confirm

the presence of an unfolded protein structure thermal denaturation (**Figure 57 A**) and renaturation runs (**Figure 57 B**) using CD-spectroscopy were performed, in which both showed a lack of conformation change in the secondary structure typical for a structure that is already disordered.

A random coiled structure is the main characteristic for intrinsically disordered proteins (IDPs), therefore our results confirm that the ATR-domain is an intrinsically disordered region of PTEN-L. The sequence of the ATR-domain is primarily enriched in disorder-promoting polar amino acids (specifically serine and arginine) and hydrophobic and structure-breaking proline (

**Figure 56**). The distortedness of IDPs is linked to the peculiarities in amino acid sequence, which are generally enriched in polar and charged residues, and are depleted of hydrophobic residues (Ile, Leu

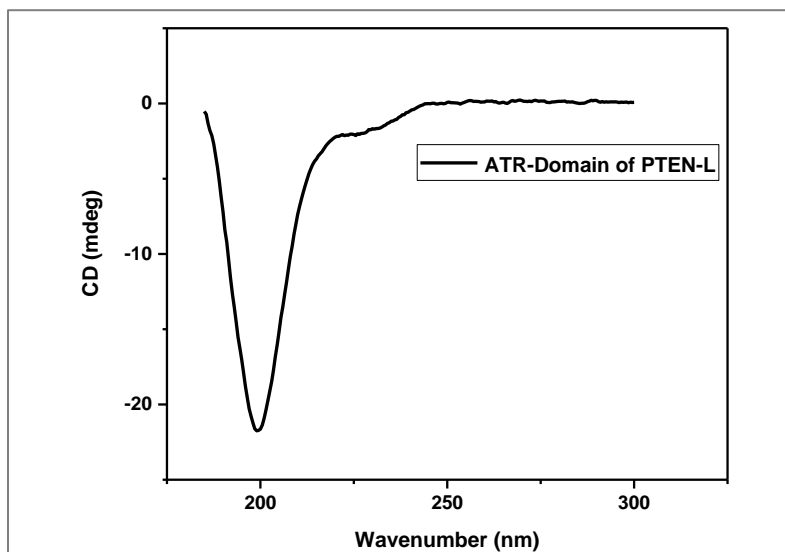


**Figure 49. CD spectra of the ATR-Domain**

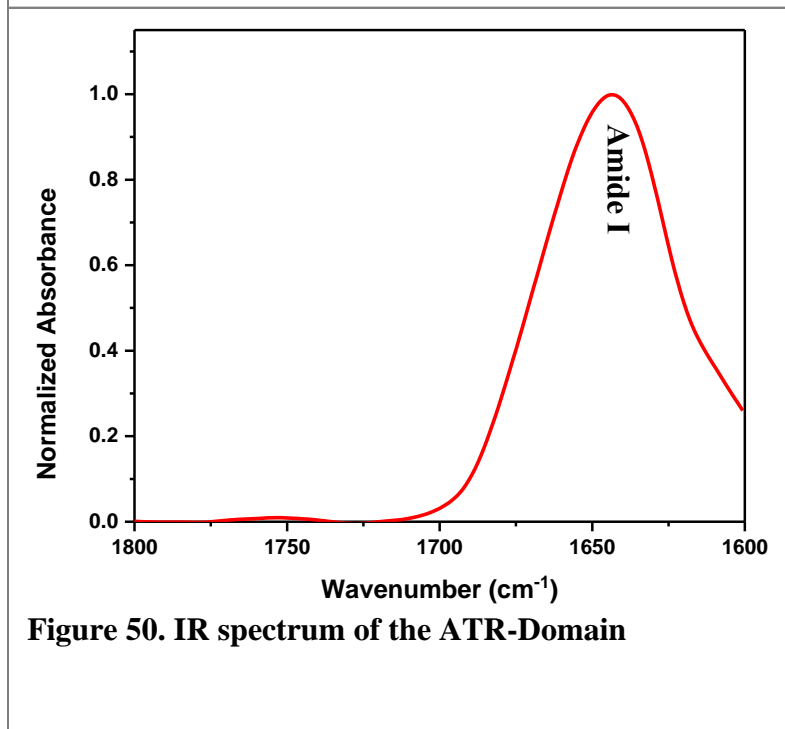
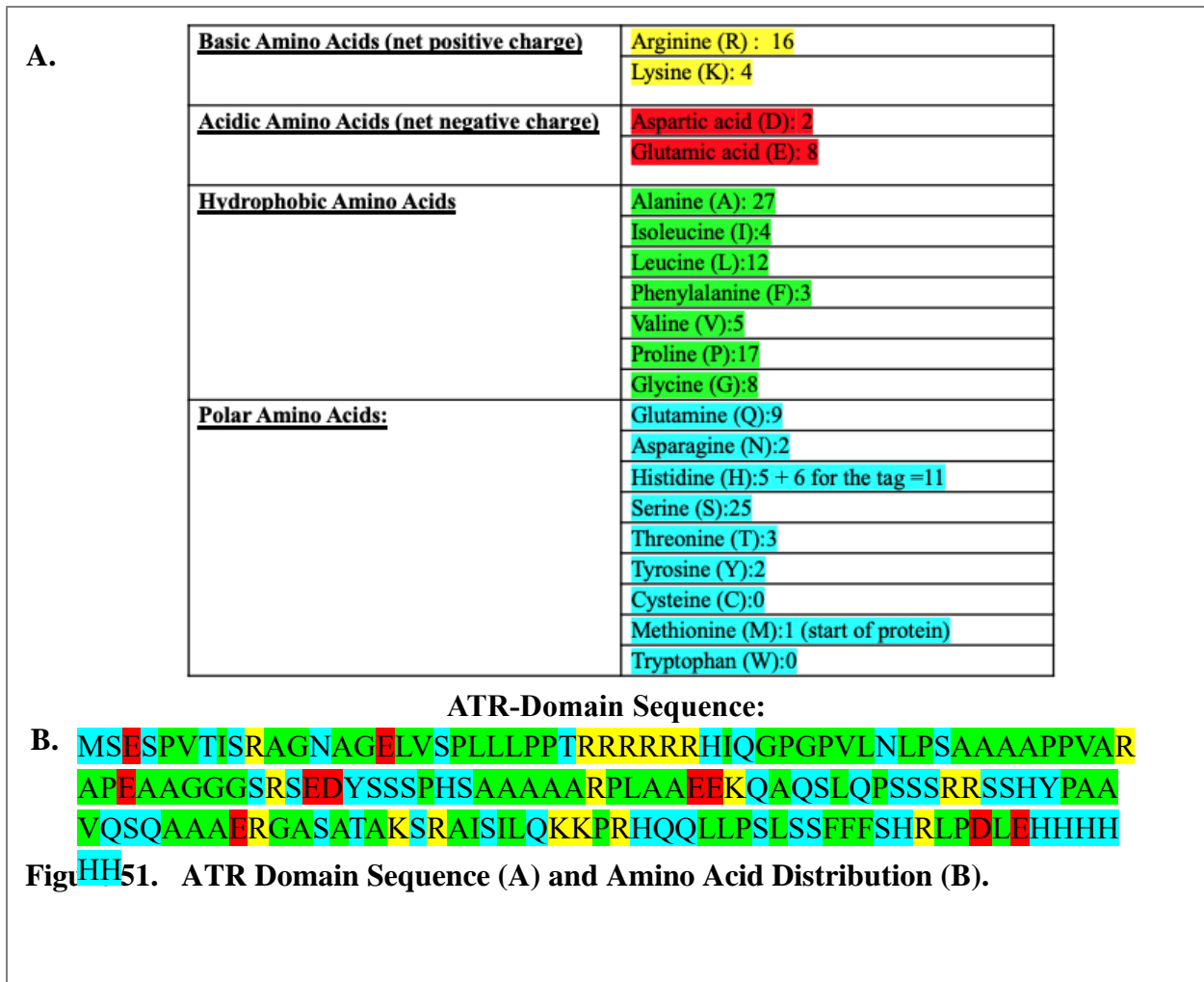


**Figure 50. IR spectrum of the ATR-Domain**





and Val) and aromatic amino acid residues (Trp, Tyr and Phe), which would normally form the hydrophobic core of a folded globular protein. The ATR-domain also contains positively charged polyarginine stretch (6 Arginine residues) that has homology to other intrinsically disordered cell permeable peptides (such as Tat in HIV). This suggests that the amino acid composition and the flexibility of its intrinsically disordered nature is likely what facilitates entry across the anionic and hydrophobic layers of the plasma membrane (in the case of direct transport of PTEN-L across the membrane) or into phospholipid transport vesicles (in the case of vesicular transport of PTEN-

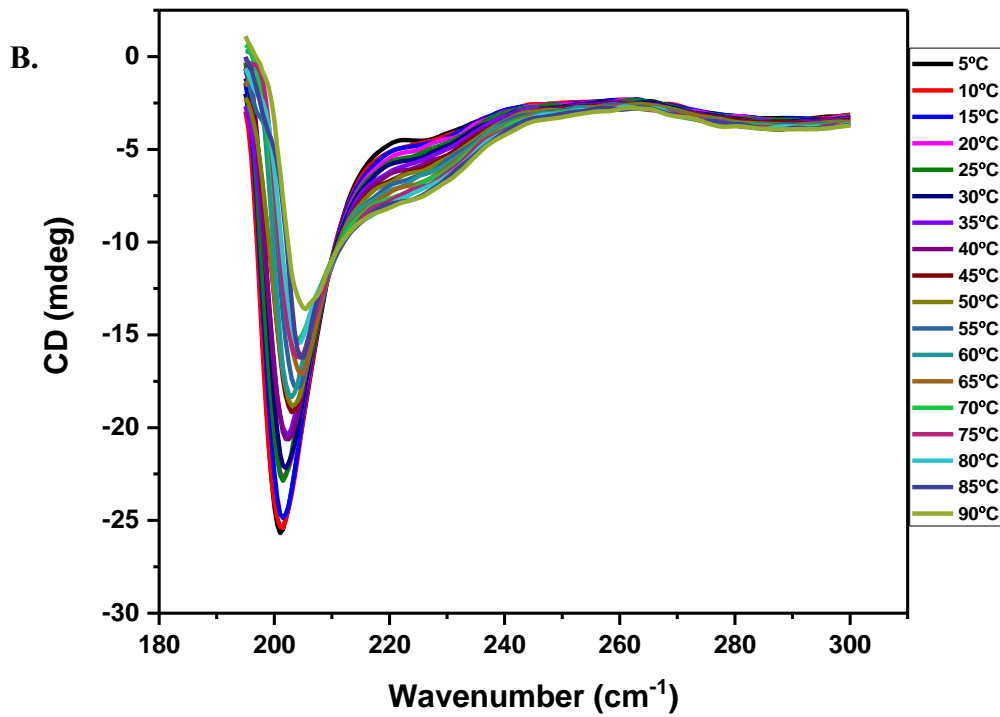
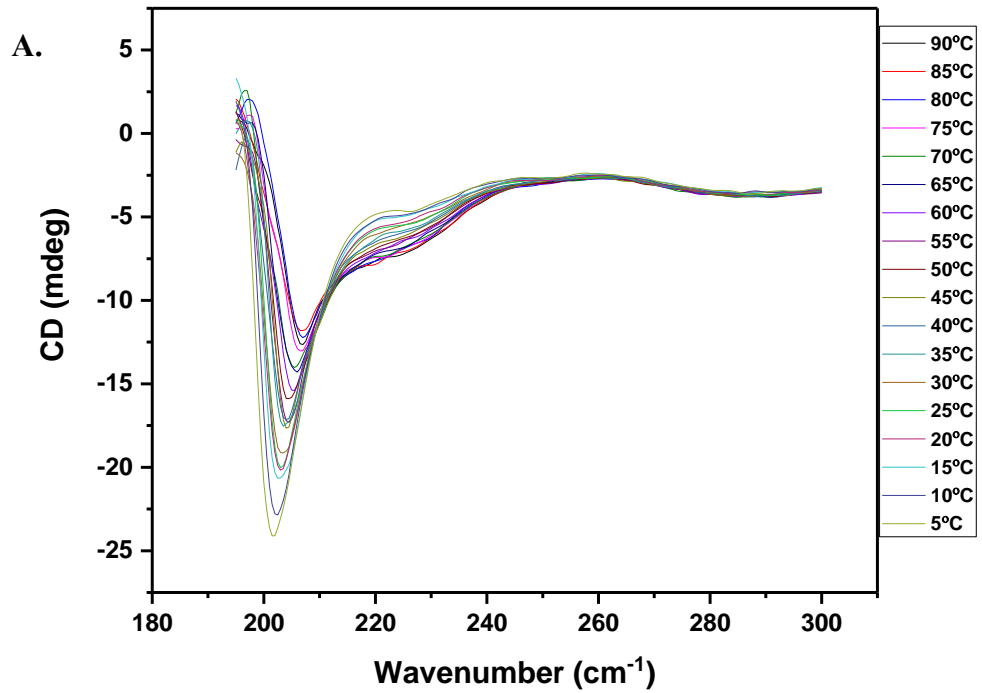


**Figure 52. Thermal Denaturation (A) and Thermal Renaturation (B) CD Spectra for ATR-Domain**

L across cells). These studies support that the ATR-domain is required for the secretion of PTEN-L, however further studies are required to understand if this it is passive or active transport mechanism.

### 5.1.3 Investigation of ATR-Domain Lipid Binding Preferences

Now that we have experimentally confirmed that the ATR-domain is intrinsically disordered, the next thing we were interested in exploring was the lipid binding preferences of ATR-domain to understand how it associates with the plasma membrane. To preliminarily investigate the lipid binding preferences of the ATR-domain we used Avanti Inositol Snoopers®. The inositol snoopers consisted of 13 different lipid species spotted individually on a solid support that mimics the bilayer, which was a major advantage over the one-dimensional PIP strips available from other manufacturers. The ATR-domain recognized PI(3,4,5)P<sub>3</sub>, PI(3,4)P<sub>2</sub>, PI(4,5)P<sub>2</sub> with slightly higher specificity than the other anionic lipids (**Figure 58**, → ). This data suggests that these phosphoinositide derivatives are involved in ATR-domain PM interaction; however, confirmation was required with lipid bilayer-based assays, thus we used ATR-FTIR spectroscopy experiments.

ATR-FTIR spectroscopy was used to monitor secondary structure changes in the presence of different inner leaflet lipid compositions through varying the presence anionic phospholipids. When the protein is in different conformations, the amide I band vibrations occur at different frequencies causing an amide I shift that can easily be monitored. The first lipid composition tested was zwitterionic POPC. The IR-spectra of the ATR-domain in the presence of 100 % POPC



Ref.	18:1 PI (3,5)P <sub>2</sub>	18:1 PI (4,5)P <sub>2</sub>	18:1 PI (3,4,5)P <sub>2</sub>	DMPC
16:0 PI	18:1 PI	18:1 PI(3)P	18:1 PI(5)P	18:1 PI(3,4)P <sub>2</sub>
Ref.	Liver PI	Soy PI	Brain PI(4)P	Brain PI(4,5)P <sub>2</sub>

**Figure 54.** Avanti Inositol Snoopers® were used to preliminarily investigate ATR-Domain Interactions with 13 Different Lipids Species.

Each spot contains 1 µg of the highest quality pure lipid and were used to investigate ATR-domain lipid interactions. The higher specificity interactions are indicated with →.

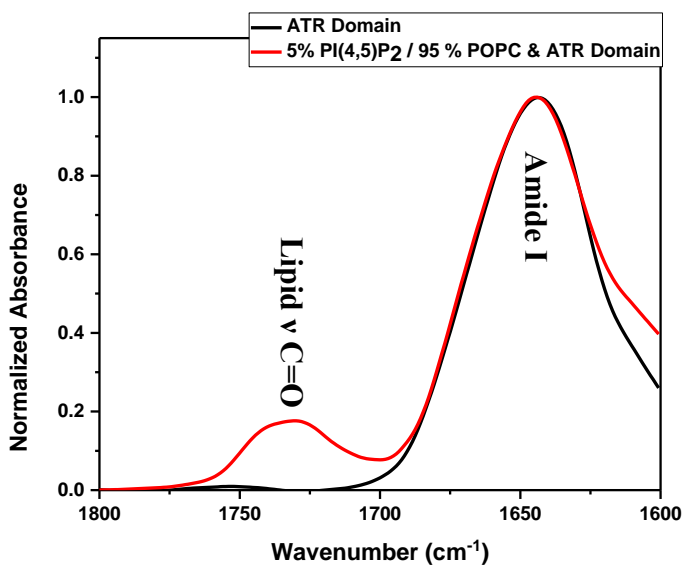
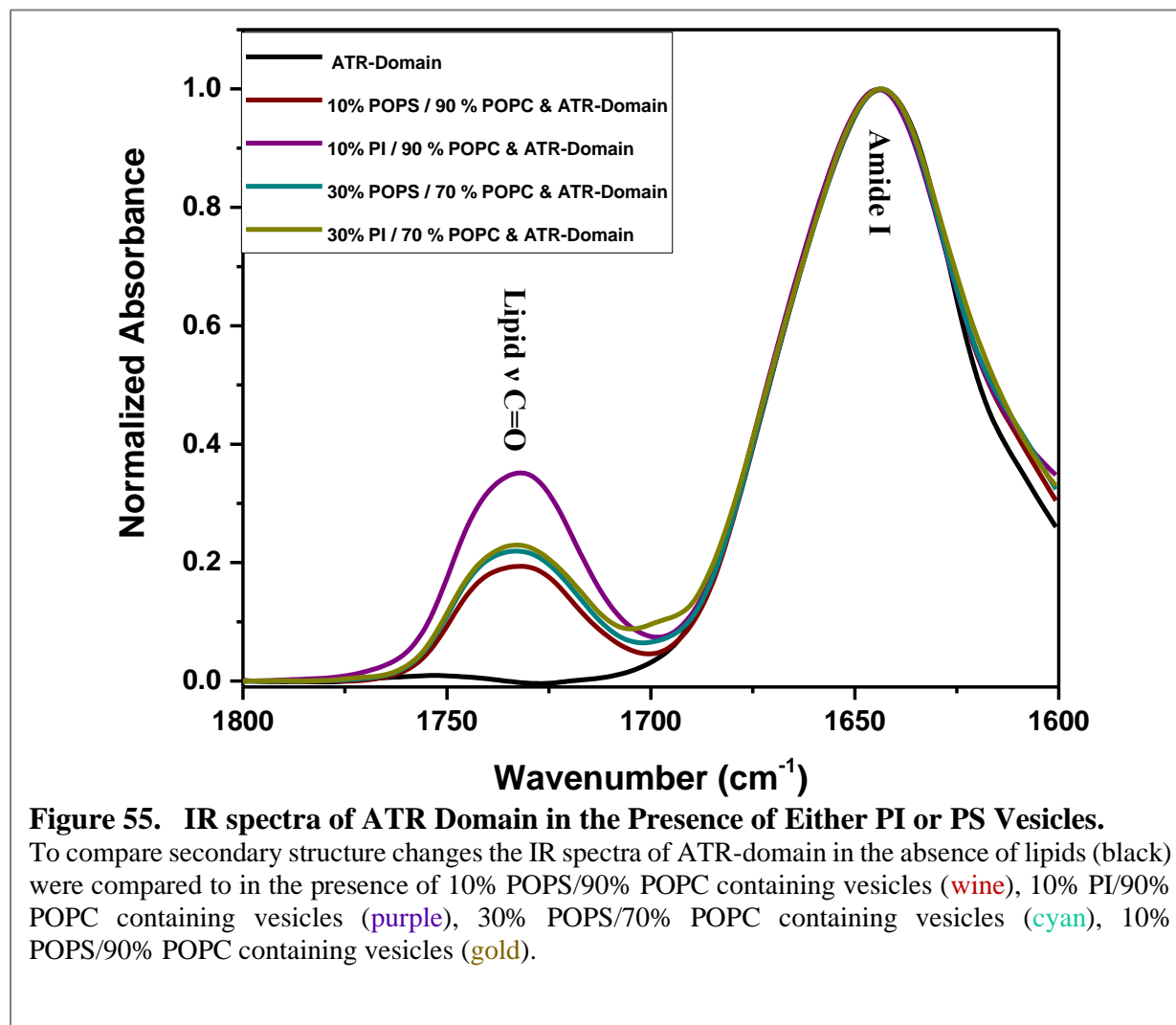


**Figure 53.** IR spectra of ATR-Domain in the Presence of 5% PI(4,5)P<sub>2</sub> Vesicles.

To compare secondary structure changes the IR spectra of ATR domain in the absence of lipids (black) was compared to in the presence of 5% PI(4,5)P<sub>2</sub>/95% POPC containing vesicles (red).

resulted in no shift in the amide I peak compared to ATR-domain in the absence of lipids (Error! Reference source not found.). This was likely due to the lack of charge in POPC headgroup not forming electrostatic associations with the ATR-domain, thus POPC lipid composition was used as a control. Next we tested the ATR-domain in the presence of 5% PI(4,5)P<sub>2</sub> vesicles, and there also was not an observable secondary change (**Figure 59**), which was surprising since PI(4,5)P<sub>2</sub> induced a structural change in PTEN (Redfern 2008). This suggests that ATR-domain may provide PTEN-L with lipid binding mechanisms different from PTEN. Previously published data has reported that PTEN is able to bind PS and PI(4,5)P<sub>2</sub> synergistically (Redfern 2008, Shenoy, Shekhar et al. 2012, Gericke, Leslie et al. 2013), thus we investigated the effects of PS as a electrostatic lipid binding partner of the ATR-domain. The structure of ATR domain did not change in the presence of 10% nor 30% POPS (**Figure 60**), however to our surprise in the presence of 100% POPS vesicles the lipid carbonyl peak was not visible in the spectra (~1730 cm<sup>-1</sup>) and the sample was extremely cloudy (data not shown). This suggested that ATR domain was causing the POPS lipids to fall apart or aggregate; this was further investigated with membrane integrity studies (see section 0). Based on our monolayer studies confirming that PI behaves similarly to PS (see section 4.1.4), the effect of PI on ATR-domain secondary structure was investigated. As similarly observed with PS, 10 % nor 30 % PI showed no structural difference in the amide I peak (**Figure 60**). Interestingly, the same phenomena that was observed with 100% PS effecting the lipid integrity was not observed with 100 % PI, which suggests the ATR-domain interacts differently with PS than with PI.

Next, we investigated the synergistic effects of anionic lipid compositions to understand if a specific lipid environment induces a structural change. Our monolayer studies showed that PI(4,5)P<sub>2</sub> packs more tightly in the presence of both PS and PI (see section 4.1.4), which suggests



that PS and/or PI may provide a rich electrostatic environment for protein binding; thus we investigated the association of ATR-domain to both PI/PI(4,5)P<sub>2</sub> and PS/PI(4,5)P<sub>2</sub> lipid compositions. The ATR-domain in presence of both 5 % PI(4,5)P<sub>2</sub>/10% POPS or 5% PI(4,5)P<sub>2</sub>/10 % PI did not exhibit any change in the amide I peak (Figure 61); however, in the presence of 5 % PI(4,5)P<sub>2</sub>/30 % POPS the amide I peak shifted to ~ 1633 cm<sup>-1</sup> (Figure 61, Table 3). This shift suggests a more  $\beta$ -sheet composition upon interaction with PS/PI(4,5)P<sub>2</sub> containing vesicles.

Further experiments are needed to verify whether this increased  $\beta$ -sheet content is due to protein aggregation at the bilayer surface. However,  $\beta$ -sheet aggregation usually gives rise to a

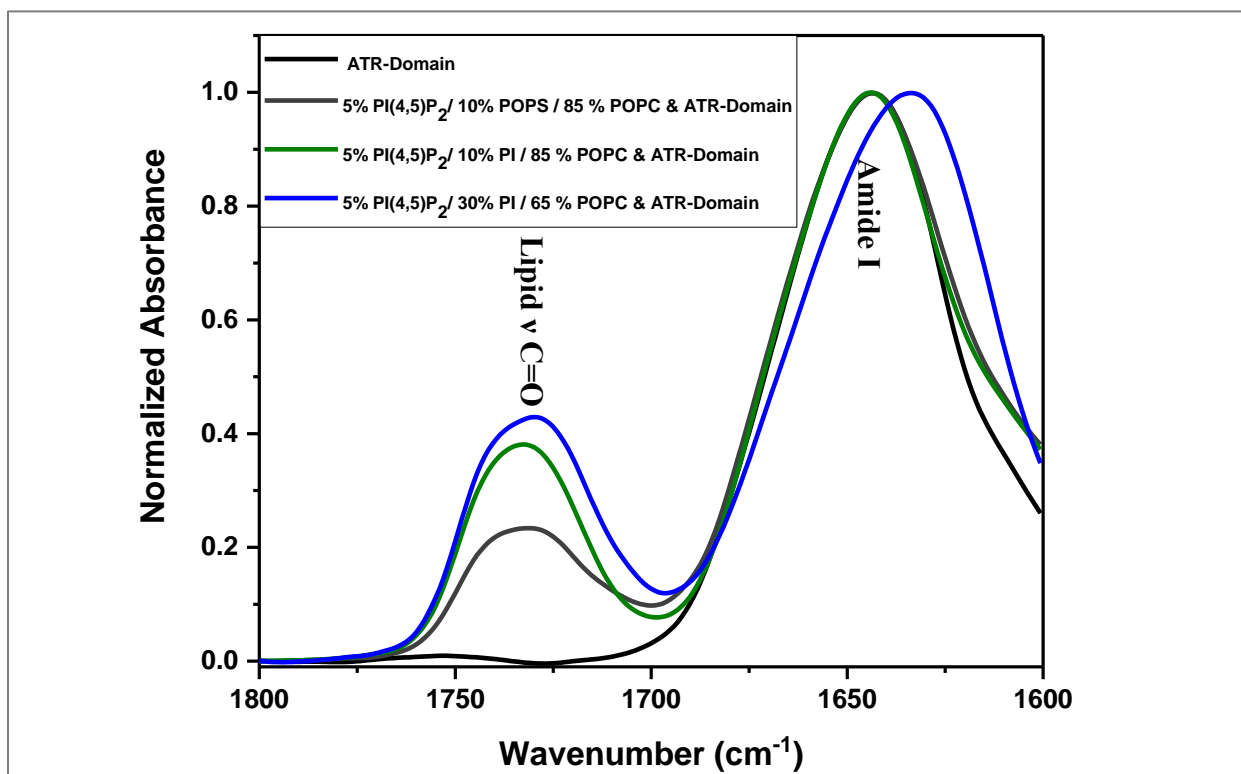


**Figure 56. IR spectra of ATR Domain in the Presence of Either PI/PI(4,5)P<sub>2</sub> or PS/PI(4,5)P<sub>2</sub> Vesicles**

To compare secondary structure changes the IR spectra of ATR-domain in the absence of lipids (black) were compared to in the presence of 5%PI(4,5)P<sub>2</sub>/10% POPS/85% POPC containing vesicles (gray), 5%PI(4,5)P<sub>2</sub>/10% PI/85% POPC containing vesicles (green), 5%PI(4,5)P<sub>2</sub>/30% POPS/65% POPC containing vesicles (royal blue).

band centered at  $\sim 1619 \text{ cm}^{-1}$ , while the observed band is found at  $\sim 1632 \text{ cm}^{-1}$ , which is a band position typical for a non-aggregated  $\beta$ -sheet protein.

A study using hydrogen/deuterium exchange mass spectrometry (HDX-MS) identified a membrane-binding helix (MBH) of PTEN-L in the presence of the bilayer suggesting the ATR-domain changes confirm to exhibit an  $\alpha$ -helix structure that binds to the membrane (Masson, Perisic et al. 2016). Therefore, the structure of the MBH peptide (amino acids 150–162) was investigated in the presence of anionic lipids using FTIR spectroscopy. First, the structure of the MBH peptide in the absence of lipids was determined via CD spectroscopy, the spectra of the MBH was nearly identical to the ATR-domain showing that the MBH-domain is also unstructured

(Figure 62). Next, the MBH peptide was investigated in the presence of PS, since we observed that ATR-domain was affecting lipids composed of PS. The IR-spectra of MBH in the presence of both 30 % (Figure 64) and 100 % POPS (Figure 64)

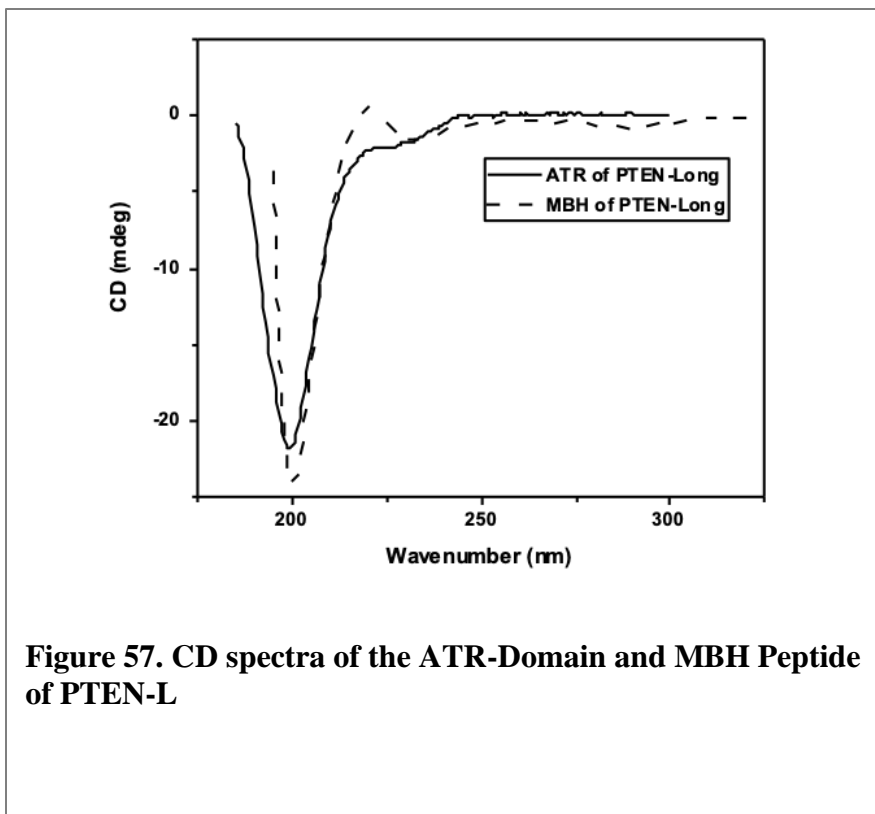


**Figure 57. CD spectra of the ATR-Domain and MBH Peptide of PTEN-L**

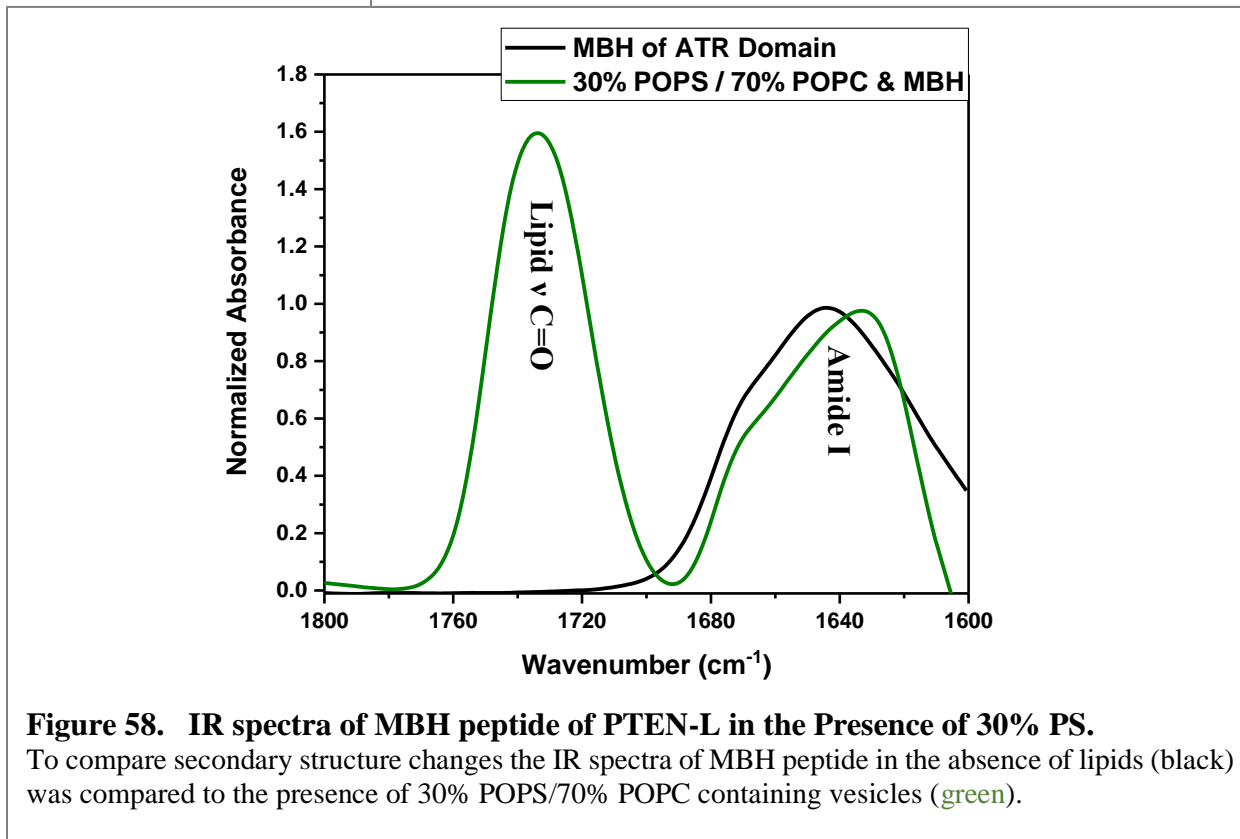


**Figure 58. IR spectra of MBH peptide of PTEN-L in the Presence of 30% PS.**

To compare secondary structure changes the IR spectra of MBH peptide in the absence of lipids (black) was compared to the presence of 30% POPS/70% POPC containing vesicles (green).



vesicles showed a shift in the amide I peak from  $\sim 1644\text{ cm}^{-1}$  (random coiled) to  $\sim 1632\text{ cm}^{-1}$  and  $\sim 1631\text{ cm}^{-1}$  respectively, which is evident of a  $\beta$ -sheet structure. This data suggests that the MBH in the presence of anionic lipid PS induces a secondary structure change to an  $\beta$ -sheet, thus providing the otherwise unstructured N-terminal elongation of PTEN-L with order. Interestingly, a previous study showed that the MBH resembles a PTEN family member, the transmembrane S4-helix of voltage-sensitive phosphatase Ci- VSP, which changes conformation upon membrane depolarization (Li 2014). Our studies provide information on the specific anionic lipid environment required for membrane association, however whether the MBH is a transmembrane helix or lies against the membrane surface has yet to be determined. Thus, the exact mechanism of how this conformational change affects the rest of PTEN-L structure and function is not understood. Further studies defining the MBH and ATR-domain interfacial plasma membrane kinetics would provide us with a better understanding of PTEN-L membrane association.

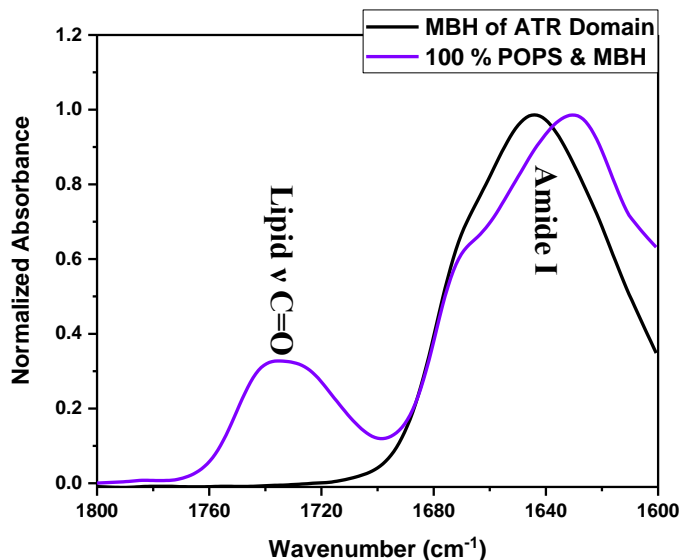


**Figure 59. IR spectra of MBH peptide of PTEN-L in the Presence of 100% PS.**

To compare secondary structure changes the IR spectra of MBH peptide in the absence of lipids (black) was compared to the presence of 30% POPS/100% POPC containing vesicles (purple).

**Table 3: FTIR Amide I Peaks for ATR-Domain (A) & MBH Peptide (B) in the Presence of Anionic Lipid Vesicles**

**A.**

<b>ATR-Domain &amp; Anionic Lipids</b>	<b>Amide I Peak Wavenumber (cm-1)</b>
ATR-Domain Only	1644.1
100% POPC	1645.9
5% PI(4,5)P <sub>2</sub> / 95% POPC	1644.1
10% PI / 90% POPC	1646.9
10% POPS / 90% POPC	1644.1
30% POPS / 70% POPC	1643.1
30% PI / 70% POPC	1644.1
5% PI(4,5)P <sub>2</sub> / 10% PI / 85% POPC	1644.1
5% PI(4,5)P <sub>2</sub> / 10% POPS / 85% POPC	1644.1
5% PI(4,5)P <sub>2</sub> / 30% POPS / 85% POPC	1633.5

**B.**

<b>MBH Peptide &amp; Anionic Lipids</b>	<b>Amide I Peak Wavenumber (cm-1)</b>
MBH Peptide Only	1644.1
5% PI(4,5)P <sub>2</sub> / 95% POPC	1644.1
30% PI(4,5)P <sub>2</sub> / 95% POPC	1646.9
30% POPS / 70% POPC	1632.5
100% POPS / 70% POPC	1630.6

## 5.1.4 Investigation of the Effect of ATR-Domain on Membrane Integrity

### Integrity

Based on the FTIR studies revealing that PS containing vesicles were affected by the addition of ATR-domain, we wanted to further investigate these changes in lipid integrity. We used DLS to monitor the changes in the size of 100nm extruded vesicles when the ATR-domain was titrated in. The ATR-domain was titrated at 44 ug/mL, 88 ug/mL, 132 ug/mL, 176 ug/mL and 200 ug/mL. The first experiment performed was using zwitterionic unilamellar POPC vesicles, which was used as control since POPC did not induce any observable ATR-domain structure change. In the presence of 100% POPC, the addition of all concentrations of the ATR-domain did not affect the size distribution of the 100nm vesicles, which was expected (**Figure 66**). Next, the

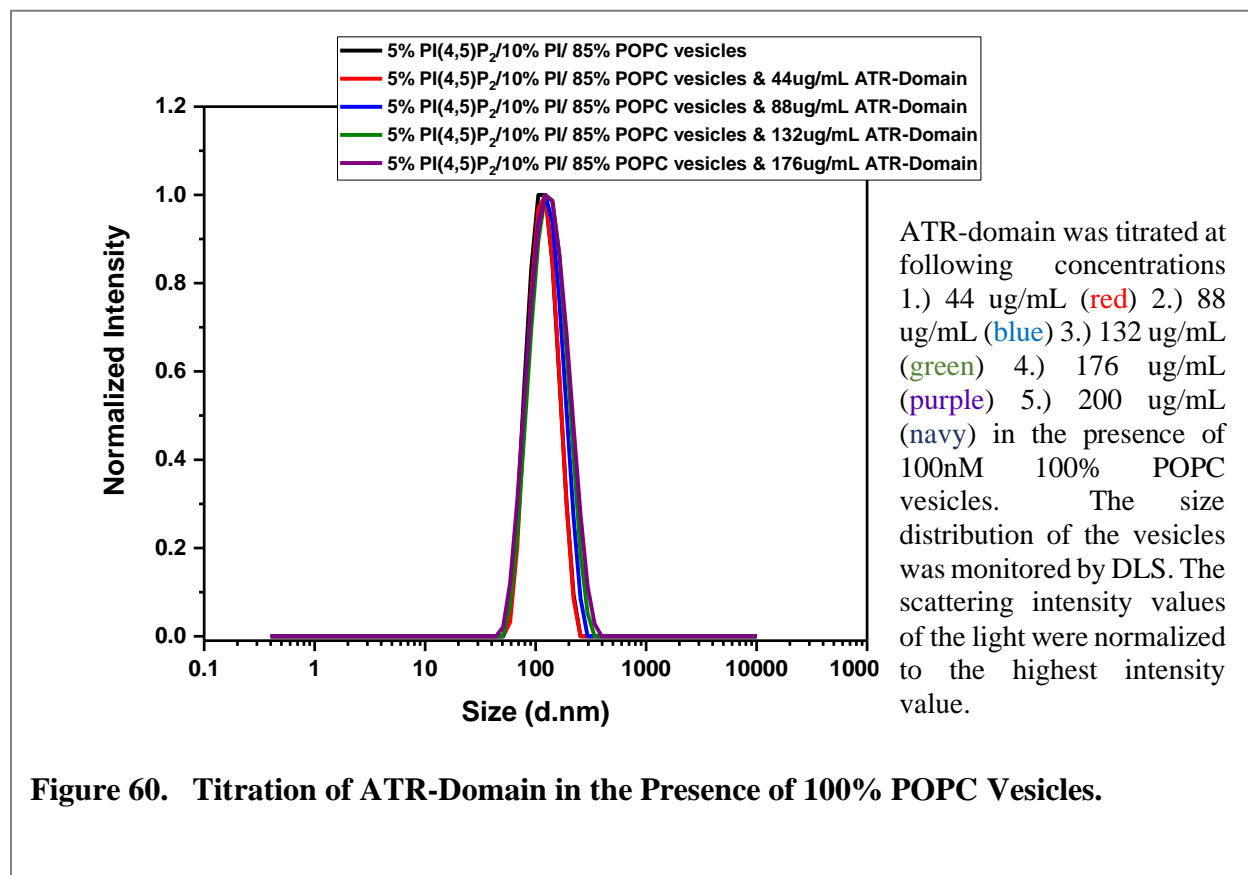
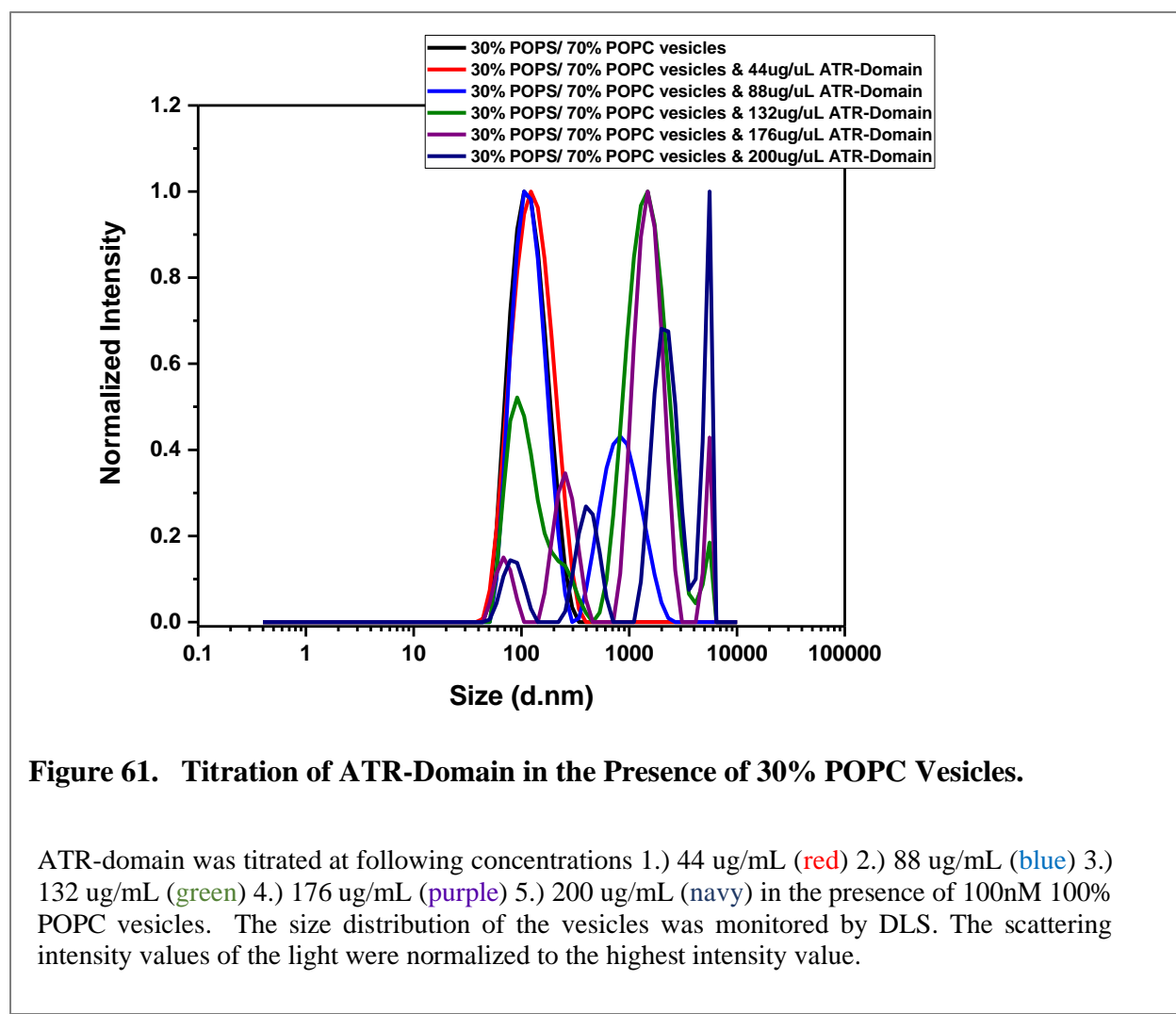


**Figure 60. Titration of ATR-Domain in the Presence of 100% POPC Vesicles.**

ATR-domain was titrated into a suspension of 30%POPS/70% POPC unilameallar vesicles. Upon the addition of 44 ug/uL ATR, there was not an observable change in the size of the vesicles, however as more ATR-domain was titrated (88-200 ug/mL) there was a shift in the size of the vesicles to a mixture of higher sized particles (100-100,000 nm) (**Figure 67**). This suggests that the ATR-domain is either causing the 30%POPS/70% POPC vesicles to fall apart or aggregate. To understand what is happening further membrane permeabilization studies are needed. Since PS and PI are suspected to behave similarly the effect of the ATR-domain on 10%PI/90% POPC vesicles was investigated (**Figure 68**). The addition of the ATR-domain to 10% PI did not affect



the vesicle integrity, however, higher concentrations of PI should be investigated to confirm the effects.

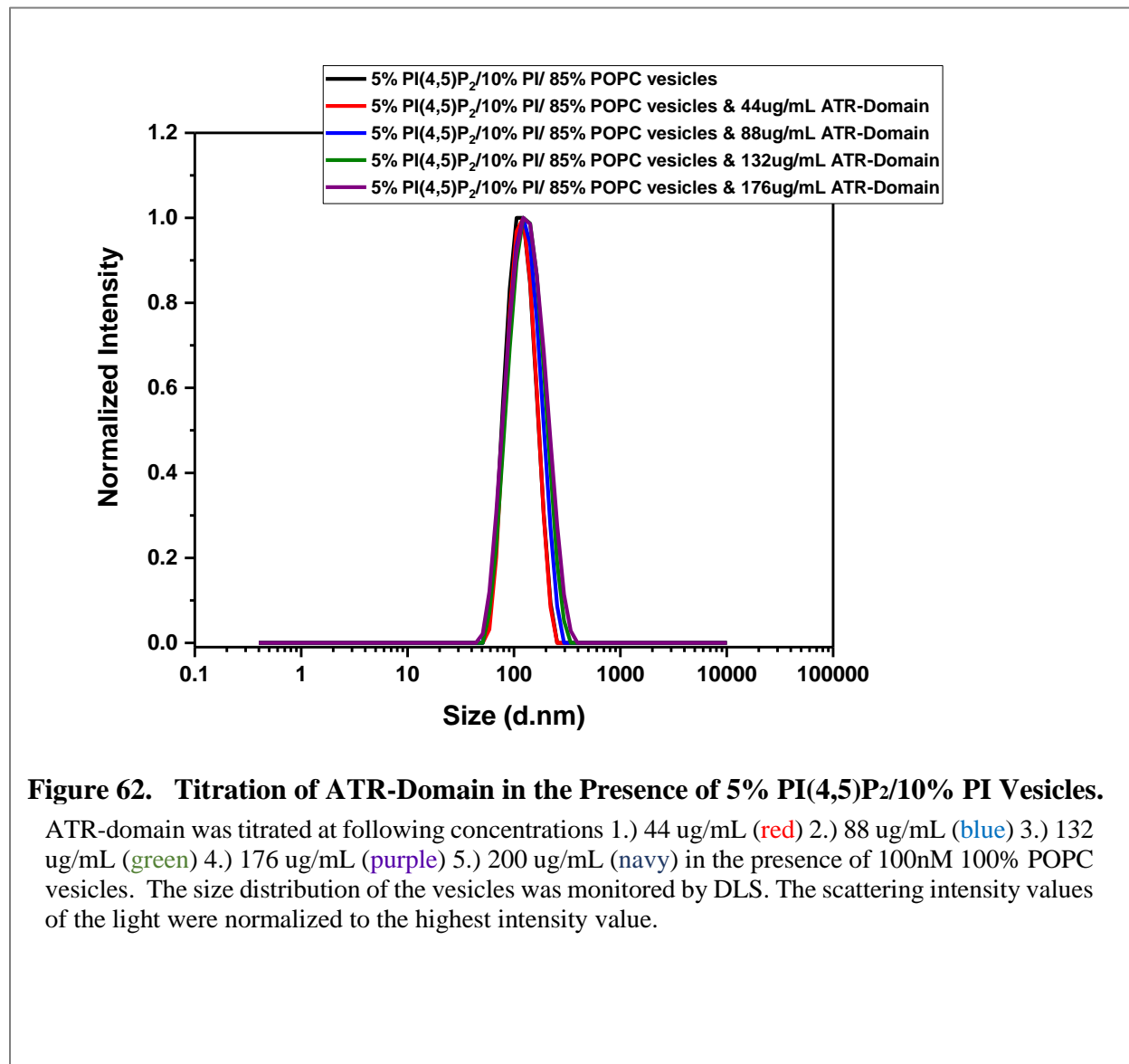


**Figure 62. Titration of ATR-Domain in the Presence of 5% PI(4,5)P<sub>2</sub>/10% PI Vesicles.**

ATR-domain was titrated at following concentrations 1.) 44 ug/mL (red) 2.) 88 ug/mL (blue) 3.) 132 ug/mL (green) 4.) 176 ug/mL (purple) 5.) 200 ug/mL (navy) in the presence of 100nM 100% POPC vesicles. The size distribution of the vesicles was monitored by DLS. The scattering intensity values of the light were normalized to the highest intensity value.

## 1.28 Conclusion:

In this chapter, we aimed to understand the lipid interaction of the ATR-domain that is part of the translation variant of PTEN. The ATR-domain is a 173-amino acid domain (~17 kDa) found on the N-terminus of PTEN-Long responsible for the structural difference between PTEN and PTEN-L. The ATR-domain is also likely responsible for the observed cellular ability of PTEN-L to exit and enter back into cells, whereas PTEN lacks this ability. Our studies focused on understanding the specific lipid interactions of the ATR-domain with the goal of providing insight into the lipid environment required for PTEN-L to exit and enter through the plasma membrane. When we initially began this study, our goal was to compare the lipid binding preferences of the ATR-domain to full length PTEN-L; however, the full length PTEN-L protein was extremely unstable and nearly impossible to purify; thus, our experiments relied solely on the ATR-domain to understand the PTEN-L lipid interactions. We successfully cloned and upscaled the expression and purification of the ATR-domain with > 95% purity. The ATR-domain structure was analyzed with both CD and FTIR spectroscopy showing the ATR-domain is unstructured in solution. The lack of structure and the polyarginine stretch homology to cell permeable peptides (such as Tat in HIV) suggests that the ATR-domain facilitates entry across the anionic and hydrophobic layers of the plasma membrane (in the case of direct transport of PTEN Long across the membrane) or into phospholipid transport vesicles (in the case of vesicular transport of PTEN Long across cells). Thus, we began to investigate secondary structure changes of the ATR-domain in the presence of various anionic lipid compositions. Our FTIR studies with lipid bilayers containing either PC, PS, PI and PI(4,5)P<sub>2</sub> did not reveal an observable structural change to ATR-domain upon lipid binding. However, when both PS and PI(4,5)P<sub>2</sub> lipids are present, we observed an increase in  $\beta$ -sheet content suggesting these lipids are required for ATR-domain interaction with the PM. The

positioning of this shifts suggests the shift is unlikely due to protein aggregation at the bilayer surface (protein aggregation gives rise to a band centered at  $\sim 1619$   $\text{cm}^{-1}$ , while the observed band is found at  $\sim 1632$   $\text{cm}^{-1}$ , which is a band position typical for a non-aggregated  $\beta$ -sheet protein). Based on the lack of the carbonyl peak with 100% POPS in the presence of the ATR-domain it was assumed that the lipid bilayer integrity was compromised. Therefore, lipid vesicle integrity was investigated showing that the ATR-domain caused 30%POPS/100%POPC lipid vesicles to aggregate and/or fall apart. This suggests that PTEN-L ATR affects the integrity of anionic lipid vesicles, in particular PS and further studies with the MBH peptide suggested the MBH may drive ATR-domain across the membrane through  $\beta$ -sheet conformational change. We are currently performing membrane permeabilization studies using GUVs and monolayer films to better understand the effects of ATR-domain on anionic lipid species. This study thus far provides us with information on ATR-domain lipid binding preferences aiding in our understanding of the biological and functional role of PTEN-L as a deliverable tumor suppressor protein.

## Chapter 7: Summation of Dissertation

### 1.29 Discussion

Local PI(4,5)P<sub>2</sub> clusters are thought to be mediated by signaling events; however, a molecular understanding on how modulation factors (cholesterol, cations, anionic lipids, proteins) affect PI(4,5)P<sub>2</sub> clustering remains unclear due to the complex dynamics of the phosphoinositide headgroup. Therefore in this dissertation we aimed to experimentally understand the physiological relevant environment required for PI(4,5)P<sub>2</sub> cluster formation, so our collaborators could computationally model the structural interactions that these modulation factors have with the PI(4,5)P<sub>2</sub> headgroup. Since PI(4,5)P<sub>2</sub> is constantly exposed to cytosolic cations it is highly likely that the formation of PI(4,5)P<sub>2</sub> clusters is dependent on the local cation concentrations. As a gateway to understanding clustering of PI(4,5)P<sub>2</sub> in membranes, our group along with our collaborators (Richard Pastor & Kyungreem Han, NIH) investigated clustering of monomethyl phosphate dianion (MMP<sub>2</sub><sup>-</sup>) in solutions of K<sup>+</sup>, Ca<sup>2+</sup> (Han, Venable et al. 2018). This study provided us with a starting point to align the experimental and theoretical conditions required to understand cation-dependent clustering of lipids with phosphomonoester groups like phosphoinositides or phosphatidic acid (PA).

Now we were ready to systematically investigate PI(4,5)P<sub>2</sub> cluster stabilization in the presence of cations (Ca<sup>2+</sup>, K<sup>+</sup>, Na<sup>+</sup>). We explored several cation concentrations (125 mM-500 mM for Na<sup>+</sup> and K<sup>+</sup> and 0.1-125 mM Ca<sup>2+</sup>), as well as mixed cation systems to determine how PI(4,5)P<sub>2</sub> monolayer packing was electrostatically influenced. We discovered that Ca<sup>2+</sup> individually and Ca<sup>2+</sup> along with K<sup>+</sup> had a greater effect on PI(4,5)P<sub>2</sub> cluster formation than Na<sup>+</sup> and K<sup>+</sup>, individually and combined. These results suggest that Ca<sup>2+</sup> is required for PI(4,5)P<sub>2</sub> cluster



stability, which is likely the result of the divalent cation shielding the negative charge of the PI(4,5)P<sub>2</sub> headgroup allowing the attractive forces like intermolecular hydrogen-bonds to cluster the molecules. The incredibly close agreement between the experimental and theoretical studies gave us faith in the structural data provided by the all-atom molecular dynamics (MD) simulations. The all-atom simulations were able to pinpoint the exact molecular location of each cation's interaction with the phosphate groups, a discovery that will lay the physical foundation in understanding electrostatic PI(4,5)P<sub>2</sub> clustering. It was discovered that Ca<sup>2+</sup> is strongly attracted to the 4,5-phosphomonoester regions, while Na<sup>+</sup> binds promiscuously, but with high affinity to the 4,5-phosphomonoester and to 1-phosphodiester and K<sup>+</sup> binds only to 1-phosphodiester group. However, the synergistic binding of cations to PI(4,5)P<sub>2</sub> not only depends on the local charge, but also on average electrostatic potential implying that the binding of an ion to one monoester phosphate group on PI(4,5)P<sub>2</sub> may also affect the binding of ions to the adjacent monoester phosphate. Therefore, we investigated the synergistic effects of different cation combinations, our results indicated that Ca<sup>2+</sup> with the addition of K<sup>+</sup> had the greatest condensation effect on PI(4,5)P<sub>2</sub> clustering.

Another important spatiotemporal modulator that affects the local concentration of PI(4,5)P<sub>2</sub> is cholesterol, however it is unclear how a rigid sterol ring structure can associate with a disordered PI(4,5)P<sub>2</sub> acyl chain structure. It has been suggested that cholesterol-dependent PI(4,5)P<sub>2</sub> cluster formation is either a 1) “indirection interaction due to the accumulation of PI(4,5)P<sub>2</sub> from the lack of physical space due to being excluded from cholesterol-rich domains or 2) a “direct” interaction in which cholesterol directly interacts with functional groups in the PI(4,5)P<sub>2</sub> headgroup region. The interaction between PI(4,5)P<sub>2</sub> and cholesterol is somewhat

puzzlingly and therefore poorly understood, even though studies have suggested that a specific interaction with the phosphoinositide headgroups not the phosphodiester group must drive cholesterol-dependent PI(4,5)P<sub>2</sub> clusters, especially since cluster formation does not occur with phosphatidylcholine (PC). Based on our cation study showing an increase in PI(4,5)P<sub>2</sub> molecular packing, we highly suspected that the presence of cations along with cholesterol would have an additive effect on PI(4,5)P<sub>2</sub> clustering, which was confirmed with our  $\pi/A$ -isotherm experimental data. Not including the area of cholesterol in the  $\pi/A$ -isotherm and observing a condensation of the monolayer film suggested that cholesterol is directly interacting with PI(4,5)P<sub>2</sub> in the presence of Ca<sup>2+</sup>. However, it was impossible to verify experimentally using spectroscopic or diffraction techniques (NMR and Neutron Diffraction), therefore we relied heavily on our collaborator's all-atom simulations to determine the exact positioning of cholesterol with PI(4,5)P<sub>2</sub>. Since the experimental Langmuir film data of PI(4,5)P<sub>2</sub> in the presence of cholesterol and cations (Ca<sup>2+</sup>, K<sup>+</sup>, Na<sup>+</sup>) also resulted in a strong agreement with the theoretical data, we have confidence in the structural data provided by the simulations. The results of the all-atom MD simulations showed that the cholesterol hydroxyl interacts via H-bonding with the phosphodiester group as well as the PI(4,5)P<sub>2</sub> hydroxyl- groups in the 2- and 6-position. This finding that cholesterol moves closer to the PI(4,5)P<sub>2</sub> headgroup region is a unique interaction, since the interaction with cholesterol and PC has been found to happen at the lipid carbonyl groups. This suggests that cholesterol participating in the PI(4,5)P<sub>2</sub> hydrogen-bond network is a direct interaction that stabilizes PI(4,5)P<sub>2</sub> cluster formation.

In order to understand the predominant interactions of PI(4,5)P<sub>2</sub> in biological membranes, there was a need to increase the complexity of our model membrane systems. This led us to explore PI(4,5)P<sub>2</sub> cluster formation in the presence of other inner leaflet anionic lipids and the

divalent cation,  $\text{Ca}^{2+}$ . Based on the high abundance of PI (~ 6-10% total lipids in PM) and PS (~10 to 20% total lipids in the PM), it is highly likely these anionic phospholipid species interact with PI(4,5)P<sub>2</sub> to form inner leaflet clusters. In the presence of  $\text{Ca}^{2+}$  both 1:1 PI/PI(4,5)P<sub>2</sub> and PS/PI(4,5)P<sub>2</sub> equally showed a systematic increase in condensation corresponding to  $\text{Ca}^{2+}$  concentration. This suggests that  $\text{Ca}^{2+}$  further stabilized both PI and PS cluster formation with PI(4,5)P<sub>2</sub>. Interestingly, our data strongly suggest that PI and PS interact cooperatively with PI(4,5)P<sub>2</sub> to form clusters, even though studies have suggested that PS does not induce macroscopic PI(4,5)P<sub>2</sub> domain formation. Therefore, our results strongly suggest that microscopic domains form and are below the diffraction limit of microscopy. When comparing the interaction of PI and PS with PI(4,5)P<sub>2</sub>, the  $\pi/A$ -isotherm showed very similar area/molecule, which suggests that PI and PS interact similarly with PI(4,5)P<sub>2</sub>. Since both PI and PS equally stabilize PI(4,5)P<sub>2</sub> cluster formation, it is likely that these lipids interact *in vivo* to form stabilize electrostatic domains required for protein binding. Therefore, we hypothesize that a high concentration of PI or PS would provide a large negatively charged platform for non-specific electrostatic protein binding, while co-localized PI(4,5)P<sub>2</sub> would provide high specificity along with providing an additional electrostatic environment for protein binding.

The principal role of these distinct PI(4,5)P<sub>2</sub> clusters is to regulate intricate spatiotemporal control of protein function. Thereby we were interested in investigating proteins that act as modulators of local PI(4,5)P<sub>2</sub> concentration. Our lab had previously investigated PTEN, a phosphatase that regulates the dynamic metabolism and localization between PI(4,5)P<sub>2</sub> and PI(3,4,5)P<sub>3</sub> in the PI3K-AKT pathway. The membrane dynamics studies from our lab have shown that PTEN uses its multiple lipid binding domains to interact synergistically with anionic lipid

membranes and efficiently localize to its substrate. Hence, when a paper was published showing a translational variant of PTEN called PTEN-L acts as a lipid phosphatase, is able to down regulate PI3K signaling similarly to PTEN and can exit and enter the cells (Hopkins, Fine et al. 2013), we were interested in understanding PTEN-L membrane association. For our experiments we relied on the main structural difference between PTEN and PTEN-L, the additional 173 amino acids called the ATR- domain. Most of the studies performed on PTEN-L have neglected to investigate the specific protein-lipid interactions leaving us to understand the mechanism in which PTEN-L facilitates entry across the anionic and hydrophobic layers of the plasma membrane (in the case of direct transport of PTEN-L across the membrane) or into phospholipid transport vesicles (in the case of vesicular transport of PTEN-L across cells). Our CD and FTIR spectroscopy showed the ATR-domain lacks secondary structure, which is common for cell permeable peptides (such as Tat in HIV) suggesting that the ATR-domain facilitates entry across the anionic and hydrophobic layers of the plasma membrane. Thus, we began to investigate secondary structure changes of the ATR-domain in the presence of various anionic lipid compositions. Our FTIR studies with lipid vesicles containing either PC, PS, PI and PI(4,5)P<sub>2</sub> did not reveal an observable structural change to ATR-domain upon lipid binding; however when both PS and PI(4,5)P<sub>2</sub> lipids were present, we observed an increase in  $\beta$ -sheet content. Additionally, the membrane binding helix (MBH) of the ATR-domain showed a  $\beta$ -structure change in the presence of PS. Our data suggests that PS and PI(4,5)P<sub>2</sub> are required for ATR-domain association with the plasma membrane. Further studies investigating anionic lipid vesicles membrane integrity revealed that the ATR-domain affects the stability of PS lipids, this suggests that the interaction with PS may drive ATR-domain across the membrane. However, additional membrane permeabilization studies are required to verify the specific anionic environment required for ATR-domain transport.

Overall the studies in this dissertation strongly demonstrate that modulation factors work synergistically to fine-tune PI(4,5)P<sub>2</sub> cluster formation in space and time. The ability of cations, cholesterol, and anionic lipids to interact with PI(4,5)P<sub>2</sub> headgroups strongly suggests that strengthening the H-bond formation leads to stabilized PI(4,5)P<sub>2</sub> clusters. It is highly likely in the that synergistic interaction with PI(4,5)P<sub>2</sub> modulator factors are required in the complex biological environment in order to regulate local concentration of PI(4,5)P<sub>2</sub>, and thus provide spatiotemporal control and regulation of signaling events. This dissertation unites nearly two decades worth of research by shedding light on the physiological environment required for PI(4,5)P<sub>2</sub> cluster formation, thus helping the scientific community understand the specific clustering environment required for the temporal control of the spatially resolved protein activity.

### **1.30 Future Work**

We found strong evidence that Ca<sup>2+</sup>, cholesterol, and anionic lipids PS and PI stabilize the formation of PI(4,5)P<sub>2</sub> clusters. The mechanism that PI(4,5)P<sub>2</sub> cluster formation has on phosphoinositide signaling, in particular regulating the PI3K/signaling pathway needs to be investigated; however, the complexity of the PI3K/signaling pathway makes studying *in vivo* interactions nearly impossible. Therefore, it is important that the complexity of model membranes is increased in order to characterize how these interactions can effect PI(4,5)P<sub>2</sub> mediated signaling pathways. The use of asymmetric GUVs with complex membrane composition should be used to investigate the effects of cations, cholesterol, anionic lipids and proteins on PI(4,5)P<sub>2</sub> clusters. This will provide us with a more accurate model of the actual cellular membrane.

To understand the structural interaction of PS and PI with PI(4,5)P<sub>2</sub> cluster formation, it would be helpful to run MD simulations including PS and PI; however, this will probably make the simulations complicated and lengthy. Lastly, membrane permeabilization studies of the ATR-domain are needed to explore the effects of the ATR-domain on lipid integrity. Thus, experiments such as injecting the ATR-domain under lipid monolayer films would allow us to characterize the ATR-domain adsorption in lipid monolayers. Additionally, for our experiments, we focused on inner leaflet lipid composition, however it is known that the ATR-domain can also enter back into cells. Thus, the membrane binding preferences of outer leaflet lipids (SM, PE, PC) should be investigated to provide insight into the lipid association required for entry back into the cell. We could also use single-molecule total internal reflection fluorescence microscopy (TIRFM) to investigate if the ATR-domain alters the membrane binding mechanism of PTEN-L compared to PTEN.

## References

- Arrondo, J. L. R. M., A.; Castresana, J.; Goni, F.M. (1992). "Quantitative studies of the structure of proteins in solution by Fourier-Transform Infrared Spectroscopy." *Prog. Biophys. molec. Biol.* **59**: 23-56.
- Balla, T. (2013). "Phosphoinositides: tiny lipids with giant impact on cell regulation." *Physiol Rev* **93**(3): 1019-1137.
- Barr, F. A. and U. Gruneberg (2007). "Cytokinesis: placing and making the final cut." *Cell* **131**(5): 847-860.
- Barth, A. and C. Zscherp (2003). "What vibrations tell about proteins." *Quarterly Reviews of Biophysics* **35**(4): 369-430.
- Bartlett, G. R. (1958). "Phosphorus Assay Chromatography." *J. Biol. Chem.* **234**: 466-468.
- Bennett, W. F. D., J. E. Shea and D. P. Tieleman (2018). "Phospholipid Chain Interactions with Cholesterol Drive Domain Formation in Lipid Membranes." *Biophys J* **114**(11): 2595-2605.
- Bermudez Brito, M., E. Goulielmaki and E. A. Papakonstanti (2015). "Focus on PTEN Regulation." *Front Oncol* **5**: 166.
- Bevens, E. M. and P. L. Williamson (2016). "Getting to the Outer Leaflet: Physiology of Phosphatidylserine Exposure at the Plasma Membrane." *Physiol Rev* **96**(2): 605-645.
- Bilkova, E., R. Pleskot, S. Rissanen, S. Sun, A. Czogalla, L. Cwiklik, T. Rog, I. Vattulainen, P. S. Cremer, P. Jungwirth and U. Coskun (2017). "Calcium Directly Regulates Phosphatidylinositol 4,5-Bisphosphate Headgroup Conformation and Recognition." *J Am Chem Soc* **139**(11): 4019-4024.
- Blin, G., E. Margeat, K. Carvalho, C. A. Royer, C. Roy and C. Picart (2008). "Quantitative analysis of the binding of ezrin to large unilamellar vesicles containing phosphatidylinositol 4,5 bisphosphate." *Biophys J* **94**(3): 1021-1033.
- Brown, D. A. (2015). "PIP2 Clustering: From model membranes to cells." *Chem Phys Lipids* **192**: 33-40.

Brown, D. A. and E. London (2000). "Structure and function of sphingolipid- and cholesterol-rich membrane rafts." *J Biol Chem* **275**(23): 17221-17224.

Brunet, A. e. a. (1999). "Akt Promotes Cell Survival by Phosphorylating and Inhibiting a Forkhead Transcription Factor." *Cell* **96**: 857-868.

Cain, R. J. and A. J. Ridley (2009). "Phosphoinositide 3-kinases in cell migration." *Biol Cell* **101**(1): 13-29.

Campbell, R. B., F. Liu and A. H. Ross (2003). "Allosteric activation of PTEN phosphatase by phosphatidylinositol 4,5-bisphosphate." *J Biol Chem* **278**(36): 33617-33620.

Carney, D. S., D.L.; Gordon, E.A.; LaBelle, E.F. (1995). "Phosphoinositides in mitogenesis-neomycin inhibits thrombin-stimulated phosphoinositide turnover and initiation of cell proliferation." *Cell* **42**: 479-488.

Carvalho, K., L. Ramos, C. Roy and C. Picart (2008). "Giant unilamellar vesicles containing phosphatidylinositol(4,5)bisphosphate: characterization and functionality." *Biophys J* **95**(9): 4348-4360.

Cassilly, C. D. and T. B. Reynolds (2018). "PS, It's Complicated: The Roles of Phosphatidylserine and Phosphatidylethanolamine in the Pathogenesis of *Candida albicans* and Other Microbial Pathogens." *J Fungi (Basel)* **4**(1).

Cauvin, C. and A. Echard (2015). "Phosphoinositides: Lipids with informative heads and mastermind functions in cell division." *Biochim Biophys Acta* **1851**(6): 832-843.

Chen, Z., D. R. Dempsey, S. N. Thomas, D. Hayward, D. M. Bolduc and P. A. Cole (2016). "Molecular Features of Phosphatase and Tensin Homolog (PTEN) Regulation by C-terminal Phosphorylation." *J Biol Chem* **291**(27): 14160-14169.

Cho, W. (2006). "Building signaling complexes at the membrane." *Sci STKE* **321**: pp. pe7.

Cinar, B. M., N.K.; et al (2007). "Phosphoinositide 3-kinase-independent non- genomic signals transit from the androgen receptor to Akt1 in membrane raft microdomains." *J Biol Chem* **282**(40): 29584-29593.



Daly, T. A., M. Wang and S. L. Regen (2011). "The origin of cholesterol's condensing effect." *Langmuir* **27**(6): 2159-2161.

Das, S., J. E. Dixon and W. Cho (2003). "Membrane-binding and activation mechanism of PTEN." *Proc Natl Acad Sci U S A* **100**(13): 7491-7496.

Dasgupta, U., T. Bamba, et al. (2009). "Ceramide kinase regulates phospholipase C and phosphatidylinositol 4, 5, bisphosphate in phototransduction." *Proc Natl Acad Sci U S A* **106**(47): 20063-20068.

Datta, S. R. B., A.; Greenberg, M.E. (1999). "Cellular survival: a play in three Akts." *Gene & Development* **13**: 2905–2927.

Davis, B. M., J. L. Richens and P. O'Shea (2011). "Label-free critical micelle concentration determination of bacterial quorum sensing molecules." *Biophys J* **101**(1): 245-254.

De Matteis, M. A. G., A. (2004). "PI-losing membrane traffic." *Nature Cell Biology* **6**: 487-492.

Degreve, L. V., S.M.; Junior C.Q. (1996). "The hydration structure of the Na<sup>+</sup> and K<sup>+</sup> ions and the selectivity of their ionic channels." *Biochem Biophys Acta* **1274**: 149-156.

Demchenko, A. P. (2012). "Modern views on the structure and dynamics of biological membranes." *Biopolymers and Cell* **28**(N 1): 24–38

Devreotes, P. and A. R. Horwitz (2015). "Signaling networks that regulate cell migration." *Cold Spring Harb Perspect Biol* **7**(8): a005959.

Di Paolo, G. and P. De Camilli (2006). "Phosphoinositides in cell regulation and membrane dynamics." *Nature* **443**(7112): 651-657.

Dickson, E. J. and B. Hille (2019). "Understanding phosphoinositides: rare, dynamic, and essential membrane phospholipids." *Biochem J* **476**(1): 1-23.

Do Heo, W. e. a. (2006). "PI(3,4,5)P3 and PI(4,5)P2 Lipids Target Proteins with Polybasic Clusters to the Plasma Membrane." *Science* **314**.

Dong, A. H., P.; Caughey, W.S. (1990). "Protein secondary structures in water from 2nd-derivative Amide I Infrared spectra." *Biochemistry* **29**: 3303-3308.

Edidin, M. (2003). "The state of lipid rafts: from model membranes to cells." *Annu Rev Biophys Biomol Struct* **32**: 257-283.

Eissing, M., L. Ripken, G. Schreibelt, H. Westdorp, M. Ligtenberg, R. Netea-Maier, M. G. Netea, I. J. M. de Vries and N. Hoogerbrugge (2019). "PTEN Hamartoma Tumor Syndrome and Immune Dysregulation." *Transl Oncol* **12**(2): 361-367.

Elhyany, S. A.-K., E. et al (2004). "The integrity of cholesterol-enriched microdomains is essential for the constitutive high activity of protein kinase B in tumour cells." *Biochem Soc Trans* **32**.

Ellenbroek, W. G., Y. H. Wang, D. A. Christian, D. E. Discher, P. A. Janmey and A. J. Liu (2011). "Divalent cation-dependent formation of electrostatic PIP2 clusters in lipid monolayers." *Biophys J* **101**(9): 2178-2184.

Escriba, P. V. and G. L. Nicolson (2014). "Membrane structure and function: relevance of lipid and protein structures in cellular physiology, pathology and therapy." *Biochim Biophys Acta* **1838**(6): 1449-1450.

Fahy, E., M. Sud, D. Cotter and S. Subramaniam (2007). "LIPID MAPS online tools for lipid research." *Nucleic Acids Res* **35**(Web Server issue): W606-612.

Falke, J. J. and B. P. Ziemba (2014). "Interplay between phosphoinositide lipids and calcium signals at the leading edge of chemotaxing ameboid cells." *Chem Phys Lipids* **182**: 73-79.

Fernandes, F., L. M. Loura, A. Fedorov and M. Prieto (2006). "Absence of clustering of phosphatidylinositol-(4,5)-bisphosphate in fluid phosphatidylcholine." *J Lipid Res* **47**(7): 1521-1525.

Flanagan, L. A. C., C.; Chen, J., Prestwich, G.D.; Kosik, K. and Janmey, P. (1997). "The Structure of Divalent Cation-induced Aggregates of PIP2 and Their Alteration by Gelsolin and Tau." *Biophysical Journal* **73**: 1440-1447.

Fragoso, R. and J. T. Barata (2015). "Kinases, tails and more: regulation of PTEN function by phosphorylation." *Methods* **77-78**: 75-81.

Fruman, D. A., H. Chiu, B. D. Hopkins, S. Bagrodia, L. C. Cantley and R. T. Abraham (2017). "The PI3K Pathway in Human Disease." *Cell* **170**(4): 605-635.

Fujita, A. (2009). "A distinct pool of phosphatidylinositol 4,5-bisphosphate in caveolae revealed by a nanoscale labeling technique." *Proceedings of the National Academy of Sciences* **106**(28): 11818.11812-11818.

Gambhir, A. e. a. (2004). "Electrostatic Sequestration of PIP2 on Phospholipid Membranes by Basic/Aromatic Regions of Proteins." *Biophysical Journal* **86**: 2188-2207.

Gamper, N. and M. S. Shapiro (2007). "Target-specific PIP(2) signalling: how might it work?" *J Physiol* **582**(Pt 3): 967-975.

Gao, X., P. R. Lowry, X. Zhou, C. Depry, Z. Wei, G. W. Wong and J. Zhang (2011). "PI3K/Akt signaling requires spatial compartmentalization in plasma membrane microdomains." *Proc Natl Acad Sci U S A* **108**(35): 14509-14514.

Georgescu, M. M. (2000). "Stabilization and Productive Positioning Roles of the C2 Domain of PTEN Tumor Suppressor." *Cancer Research* **60**: 7033-7038.

Georgescu, M. M. (2010). "PTEN Tumor Suppressor Network in PI3K-Akt Pathway Control." *Genes Cancer* **1**(12): 1170-1177.

Gericke, A. (2018). "Is Calcium Fine-Tuning Phosphoinositide-Mediated Signaling Events Through Clustering?" *Biophys J* **114**(11): 2483-2484.

Gericke, A., N. R. Leslie, M. Losche and A. H. Ross (2013). "PtdIns(4,5)P2-mediated cell signaling: emerging principles and PTEN as a paradigm for regulatory mechanism." *Adv Exp Med Biol* **991**: 85-104.

Gericke, A., M. Munson and A. H. Ross (2006). "Regulation of the PTEN phosphatase." *Gene* **374**: 1-9.

Glaser, M. e. a. (1996). "Myristoylated Alanine-rich C Kinase Substrate (MARCKS) Produces Reversible Inhibition of Phospholipase C by Sequestering Phosphatidylinositol 4,5-Bisphosphate in Lateral Domains." *The Journal of Biological Chemistry* **271**(42): 26187-26191.

Glassford, S. E., B. Byrne and S. G. Kazarian (2013). "Recent applications of ATR FTIR spectroscopy and imaging to proteins." *Biochim Biophys Acta* **1834**(12): 2849-2858.

Golebiewska, U., A. Gambhir, G. Hangyas-Mihalyne, I. Zaitseva, J. Radler and S. McLaughlin (2006). "Membrane-bound basic peptides sequester multivalent (PIP<sub>2</sub>), but not monovalent (PS), acidic lipids." *Biophys J* **91**(2): 588-599.

Goni, F. M. (2014). "The basic structure and dynamics of cell membranes: an update of the Singer-Nicolson model." *Biochim Biophys Acta* **1838**(6): 1467-1476.

Graber, Z. T., A. Gericke and E. E. Kooijman (2014). "Phosphatidylinositol-4,5-bisphosphate ionization in the presence of cholesterol, calcium or magnesium ions." *Chem Phys Lipids* **182**: 62-72.

Graber, Z. T., Z. Jiang, A. Gericke and E. E. Kooijman (2012). "Phosphatidylinositol-4,5-bisphosphate ionization and domain formation in the presence of lipids with hydrogen bond donor capabilities." *Chem Phys Lipids* **165**(6): 696-704.

Graber, Z. T., W. Wang, G. Singh, I. Kuzmenko, D. Vaknin and E. E. Kooijman (2015). "Competitive cation binding to phosphatidylinositol-4,5-bisphosphate domains revealed by X-ray fluorescence." *RSC Advances* **5**(129): 106536-106542.

Grabon, A., D. Khan and V. A. Bankaitis (2015). "Phosphatidylinositol transfer proteins and instructive regulation of lipid kinase biology." *Biochim Biophys Acta* **1851**(6): 724-735.

Guittard, G., E. Mortier, H. Tronchere, G. Firaguay, A. Gerard, P. Zimmermann, B. Payrastra and J. A. Nunes (2010). "Evidence for a positive role of PtdIns5P in T-cell signal transduction pathways." *FEBS Lett* **584**(11): 2455-2460.

Hammond, G. R. (2016). "Does PtdIns(4,5)P<sub>2</sub> concentrate so it can multi-task?" *Biochem Soc Trans* **44**(1): 228-233.

Han, K., R. M. Venable, A. M. Bryant, C. J. Legacy, R. Shen, H. Li, B. Roux, A. Gericke and R. W. Pastor (2018). "Graph-Theoretic Analysis of Monomethyl Phosphate Clustering in Ionic Solutions." *J Phys Chem B* **122**(4): 1484-1494.

Haris, P. I. S., F. (1999). "FTIR spectroscopic characterization of protein structure in aqueous and non-aqueous media." *J Mol Catal B Enzym* **7**: 207-221.

Heath, R. J. and R. H. Insall (2008). "F-BAR domains: multifunctional regulators of membrane curvature." *J Cell Sci* **121**(Pt 12): 1951-1954.

Hemmings, B. A. and D. F. Restuccia (2012). "PI3K-PKB/Akt pathway." *Cold Spring Harb Perspect Biol* **4**(9): a011189.

Herman, P. K. E., S.D (1990). "Characterization of VPS34, a gene required for vacuolar protein sorting and vacuole segregation in *Saccharomyces cerevisiae*." *Mol Biol Cell* **10**(12): 6742-6754.

Hodakoski, C., B. Fine, B. Hopkins and R. Parsons (2015). "Analysis of intracellular PTEN signaling and secretion." *Methods* **77-78**: 164-171.

Holmes, A. B., et al. (2008). "The PI(3,5)P2 and PI(4,5)P2 Interactomes." *Journal of Proteome Research* **7**: 5295-5313.

Honigsmann, A., G. van den Bogaart, E. Iraheta, H. J. Risselada, D. Milovanovic, V. Mueller, S. Mullar, U. Diederichsen, D. Fasshauer, H. Grubmuller, S. W. Hell, C. Eggeling, K. Kuhnel and R. Jahn (2013). "Phosphatidylinositol 4,5-bisphosphate clusters act as molecular beacons for vesicle recruitment." *Nat Struct Mol Biol* **20**(6): 679-686.

Hope, H. R. P., L.J. (1996). "Phosphoinositides and Phosphoinositide-utilizing Enzymes in Detergent-insoluble Lipid Domains." *Molecular Biology of the Cell* **7**: 843-851.

Hopkins, B. D., B. Fine, N. Steinbach, M. Dendy, Z. Rapp, J. Shaw, K. Pappas, J. S. Yu, C. Hodakoski, S. Mense, J. Klein, S. Pegno, M. L. Sulis, H. Goldstein, B. Amendolara, L. Lei, M. Maurer, J. Bruce, P. Canoll, H. Hibshoosh and R. Parsons (2013). "A secreted PTEN phosphatase that enters cells to alter signaling and survival." *Science* **341**(6144): 399-402.

Hopkins, B. D., C. Hodakoski, D. Barrows, S. M. Mense and R. E. Parsons (2014). "PTEN function: the long and the short of it." *Trends Biochem Sci* **39**(4): 183-190.

Iijima, M., et al. (2015). "Opening the conformation is a master switch for the dual localization and phosphatase activity of PTEN." *Nature Scientific Reports* **5**: 1-14.

James, D. J., C. Khodthong, J. A. Kowalchuk and T. F. Martin (2008). "Phosphatidylinositol 4,5-bisphosphate regulates SNARE-dependent membrane fusion." *J Cell Biol* **182**(2): 355-366.

Jiang, Z., R. E. Redfern, Y. Isler, A. H. Ross and A. Gericke (2014). "Cholesterol stabilizes fluid phosphoinositide domains." *Chem Phys Lipids* **182**: 52-61.

Johnston, S. B. and R. T. Raines (2015). "Catalysis by the tumor-suppressor enzymes PTEN and PTEN-L." *PLoS One* **10**(1): e0116898.

Kaszuba, M., D. McKnight, M. T. Connah, F. K. McNeil-Watson and U. Nobbmann (2007). "Measuring sub nanometre sizes using dynamic light scattering." *Journal of Nanoparticle Research* **10**(5): 823-829.

Kay, J. G. e. a. (2012). "Phosphatidylserine dynamics in cellular membranes." *Mol Biol Cell* **23**(11).

Kazarian, S. G. and K. L. Chan (2013). "ATR-FTIR spectroscopic imaging: recent advances and applications to biological systems." *Analyst* **138**(7): 1940-1951.

King, K. E. (2016). *Phosphoinositide Phase Behavior in Complex Lipid Monolayer Systems*. PhD, Worcester Polytechnic Institute

Koldso, H., D. Shorthouse, J. Helie and M. S. Sansom (2014). "Lipid clustering correlates with membrane curvature as revealed by molecular simulations of complex lipid bilayers." *PLoS Comput Biol* **10**(10): e1003911.

Kooijman, E. E., K. M. Carter, et al. (2005). "What makes the bioactive lipids phosphatidic acid and lysophosphatidic acid so special?" *Biochemistry* **44**(51): 17007-17015.

Kooijman, E. E., K. E. King, M. Gangoda and A. Gericke (2009). "Ionization properties of phosphatidylinositol polyphosphates in mixed model membranes." *Biochemistry* **48**(40): 9360-9371.

Koreh, K. a. M., M.E. (1986). "The relationship of hormone-sensitive and hormone-insensitive phosphatidylinositol to phosphatidylinositol 4,5-bisphosphate in the WRK-1 cell." *J Biol Chem* **261**(1): 88-91.

Krause, M. R., T. A. Daly, P. F. Almeida and S. L. Regen (2014). "Push-pull mechanism for lipid raft formation." *Langmuir* **30**(12): 3285-3289.

Kunz, W. (2010). "Specific ion effects in colloidal and biological systems." *Current Opinion in Colloid & Interface Science* **15**(1-2): 34-39.

Kutateladze, T. G. (2010). "Translation of the phosphoinositide code by PI effectors." *Nat Chem Biol* **6**(7): 507-513.

Kwiatkowska, K. (2010). "One lipid, multiple functions: how various pools of PI(4,5)P(2) are created in the plasma membrane." *Cell Mol Life Sci* **67**(23): 3927-3946.

La Rovere, R. M., G. Roest, G. Bultynck and J. B. Parys (2016). "Intracellular Ca(2+) signaling and Ca(2+) microdomains in the control of cell survival, apoptosis and autophagy." *Cell Calcium* **60**(2): 74-87.

Laroche, G., E. J. Dufourc, J. Dufourcq and M. Pezolet (1991). "Structure and dynamics of dimyristoylphosphatidic acid/calcium complexes by 2H NMR, infrared, spectroscopies and small-angle x-ray diffraction." *Biochemistry* **30**(12): 3105-3114.

Lasserre, R. G., X. J.; et al. (2008). "Raft nanodomains contribute to Akt/PKB plasma membrane recruitment and activation." *Nat Chem Biol* **4**(9): 538-547.

Laux, T. F., K.; Thelen, M.; Golub, T.; Frey, D.; Caroni, P. (2000). "GAP43, MARCKS, and CAP23 modulate PI(4,5)P(2) at plasmalemmal rafts, and regulate cell cortex actin dynamics through a common mechanism." *J. Cell Biol* **149**: 1455-1472.

Lee, O. J. Y., H.; Georgescu, M.M.; Cristofano, A.D.; Maehama, T.; Shi, Y.; Dixon, J.E.; Pandolfi, P. and Pavletich, N.P. (1999). "Crystal Structure of the PTEN Tumor Suppressor-Implications for Its Phosphoinositide Phosphatase Activity and Membrane Association." *Cell* **99**: 323-334.

Lee, Y. C., M.; Pandolfi, P.P. (2018). "The functions and regulation of the PTEN tumour suppressor: new modes and prospects." *Nature Reviews* **19**: 547-562.

Lemmon, M. A. (2003). "Phosphoinositide Recognition Domains " *Traffic* **4**: 201–213.

Lemmon, M. A. (2003). "Phosphoinositide Recognition Domains." *Traffic* **4**: 201-213.

Lemmon, M. A. (2007). "Pleckstrin homology (PH) domains and phosphoinositides." *Biochem Soc Symp*(74): 81-93.

Lemmon, M. A. (2007). "Pleckstrin Homology (PH) domains and phosphoinositides." *Biochem Soc Symp. A* **74**: 81-93.

Lemmon, M. A. (2008). "Membrane recognition by phospholipid-binding domains." *Nat Rev Mol Cell Biol* **9**(2): 99-111.

Lemmon, M. A. and J. Schlessinger (2010). "Cell signaling by receptor tyrosine kinases." *Cell* **141**(7): 1117-1134.

Leslie, N. R. (2012). "PTEN: an intercellular peacekeeper?" *Sci Signal* **5**(250): pe50.

Leslie, N. R., N. Kriplani, M. A. Hermida, V. Alvarez-Garcia and H. M. Wise (2016). "The PTEN protein: cellular localization and post-translational regulation." *Biochem Soc Trans* **44**(1): 273-278.

Levental, I., A. Cebers and P. A. Janmey (2008). "Combined electrostatics and hydrogen bonding determine intermolecular interactions between polyphosphoinositides." *J Am Chem Soc* **130**(28): 9025-9030.

Levental, I., D. A. Christian, Y. H. Wang, J. J. Madara, D. E. Discher and P. A. Janmey (2009). "Calcium-dependent lateral organization in phosphatidylinositol 4,5-bisphosphate (PIP<sub>2</sub>)- and cholesterol-containing monolayers." *Biochemistry* **48**(34): 8241-8248.

Levental, I. C., A.; Janmey, P. (2008). "Combined Electrostatics and Hydrogen Bonding Determine Intermolecular Interactions Between Polyphosphoinositides." *JACS* **2008**(130): 9025-0230.

Leventis, P. A. and S. Grinstein (2010). "The distribution and function of phosphatidylserine in cellular membranes." *Annu Rev Biophys* **39**: 407-427.

Lewis, R. N. and R. N. McElhaney (2013). "Membrane lipid phase transitions and phase organization studied by Fourier transform infrared spectroscopy." *Biochim Biophys Acta* **1828**(10): 2347-2358.

Li, L., X. Shi, X. Guo, H. Li and C. Xu (2014). "Ionic protein-lipid interaction at the plasma membrane: what can the charge do?" *Trends Biochem Sci* **39**(3): 130-140.



- Li, Q. e. a. (2014). "Structural mechanism of voltage-dependent gating in an isolated voltage-sensing domain." *Nat Struct Mol Biol* **21**(244-252).
- Lindblom, G. and G. Oradd (2009). "Lipid lateral diffusion and membrane heterogeneity." *Biochim Biophys Acta* **1788**(1): 234-244.
- Lingwood, D. a. S., K. (2010). "Lipid Rafts As a Membrane- Organizing Principle." *Science* **327**: 46-50.
- Lucic, I., M. K. Rathinaswamy, L. Truebestein, D. J. Hamelin, J. E. Burke and T. A. Leonard (2018). "Conformational sampling of membranes by Akt controls its activation and inactivation." *Proc Natl Acad Sci U S A* **115**(17): E3940-E3949.
- Luckey, M. (2014). *Membrane Structural Biology, 2nd ed.*. Cambridge, United Kingdom, Cambridge University Press: University Printing House.
- Lumb, C. N. and M. S. Sansom (2013). "Defining the membrane-associated state of the PTEN tumor suppressor protein." *Biophys J* **104**(3): 613-621.
- Malaney, P., V. N. Uversky and V. Dave (2013). "The PTEN Long N-tail is intrinsically disordered: increased viability for PTEN therapy." *Mol Biosyst* **9**(11): 2877-2888.
- Mancinelli, R. B., A.; Bruni, F.; Ricci, M.A. (2007). "Hydration of Sodium, Potassium, and Chloride Ions in Solution and the Concept of Structure Maker/Breaker." *J.Phys.Chem* **111**: 13570-13577.
- Martin, I., E. Goormaghtigh and J. M. Ruysschaert (2003). "Attenuated total reflection IR spectroscopy as a tool to investigate the orientation and tertiary structure changes in fusion proteins." *Biochimica et Biophysica Acta (BBA) - Biomembranes* **1614**(1): 97-103.
- Masson, G. R., O. Perisic, J. E. Burke and R. L. Williams (2016). "The intrinsically disordered tails of PTEN and PTEN-L have distinct roles in regulating substrate specificity and membrane activity." *Biochem J* **473**(2): 135-144.
- Maxfield, F. R. and G. van Meer (2010). "Cholesterol, the central lipid of mammalian cells." *Curr Opin Cell Biol* **22**(4): 422-429.

McLaughlin, S., J. Wang, A. Gambhir and D. Murray (2002). "PIP(2) and proteins: interactions, organization, and information flow." *Annu Rev Biophys Biomol Struct* **31**: 151-175.

McLaughlin, S. a. M., D. (2005). "Plasma membrane phosphoinositide organization by protein electrostatics." *Nature* **438**: 605-611.

McMahon, H. T. and E. Boucrot (2011). "Molecular mechanism and physiological functions of clathrin-mediated endocytosis." *Nat Rev Mol Cell Biol* **12**(8): 517-533.

Mengistu, D. H. B., K. and May, S. (2009). "Binding of DNA to Zwitterionic Lipid Layers Mediated by Divalent Cations." *J. Phys. Chem.* **113**: 12277-12282.

Menke, M. G., V.; Steinmen, C. (2005). "Phosphatidylserine Membrane Domain Clustering Induced by Annexin A2/S100A10 Heterotetramer." *Biochemistry* **44**: 15296-15303.

Milella, M., I. Falcone, F. Conciatori, U. Cesta Incani, A. Del Curatolo, N. Inzerilli, C. M. Nuzzo, V. Vaccaro, S. Vari, F. Cognetti and L. Ciuffreda (2015). "PTEN: Multiple Functions in Human Malignant Tumors." *Front Oncol* **5**: 24.

Ming, M. and Y. Y. He (2012). "PTEN in DNA damage repair." *Cancer Lett* **319**(2): 125-129.

Modro, A. M. M., T. A (1992). "An Improved Synthesis of Monoesters of Phosphoric-Acid." *Org. Prep. Proced. Int.* **24**: 57-60.

Murray, D. e. a. (2002). "Electrostatic Control of the Membrane Targeting of C2 Domains." *Molecular Cell* **9**: 145-154.

Myers, M. P. S., J.P.; Eng, C.; Li, J.; Wang,S.I.; Wigler, M.H.; Parsons, R. and Tonks, N.K. (1997). "P-TEN, the tumor suppressor from human chromosome 10q23, is a dual-specificity phosphatase." *Proc Natl Acad Sci U S A* **94**: 9052-9057.

Nguyen, H. N., J. M. Yang, Jr., M. Rahdar, M. Keniry, K. F. Swaney, R. Parsons, B. H. Park, H. Sesaki, P. N. Devreotes and M. Iijima (2015). "A new class of cancer-associated PTEN mutations defined by membrane translocation defects." *Oncogene* **34**(28): 3737-3743.

Nicolson, G. L. (2014). "The Fluid-Mosaic Model of Membrane Structure: still relevant to understanding the structure, function and dynamics of biological membranes after more than 40 years." *Biochim Biophys Acta* **1838**(6): 1451-1466.

Odorizzi, G. B. M. E., S.D. (2000). "Phosphoinositide signaling and the regulation of membrane trafficking in yeast " Trends Biochem Sci.

Odriozola, L., G. Singh, T. Hoang and A. M. Chan (2007). "Regulation of PTEN activity by its carboxyl-terminal autoinhibitory domain." J Biol Chem **282**(32): 23306-23315.

Ohki, K. a. M., H. (2018). Physical Principles of Biomembranes and Cells. Springer Japan KK, Springer.

Ortega-Molina, A. and M. Serrano (2013). "PTEN in cancer, metabolism, and aging." Trends Endocrinol Metab **24**(4): 184-189.

Oy, K. N. B. S. (2013). Langmuir and Langmuir-Blodgett devices.

Parekh, A. B. (2008). "Ca<sup>2+</sup> microdomains near plasma membrane Ca<sup>2+</sup> channels: impact on cell function." J Physiol **586**(13): 3043-3054.

Picas, L., F. Gaits-Iacovoni and B. Goud (2016). "The emerging role of phosphoinositide clustering in intracellular trafficking and signal transduction." F1000Res **5**.

Picas, L. V., J.; Schauer, K., et al. (2014). "BIN1/M-Amphiphysin2 induces clustering of phosphoinositides to recruit its downstream partner dynamin." Nat Commun. **5**.

Pike, L. J. a. C., L. (1996). "Localization and Turnover of Phosphatidylinositol 4,5- Bisphosphate in Caveolin enriched Membrane Domains." Journal of Biological Chemistry **271**(43): 26453-26456.

Pike, L. J. a. M., J.M. (1998). "Cholesterol Depletion Delocalizes Phosphatidylinositol Bisphosphate and Inhibits Hormone-stimulated Phosphatidylinositol Turnover " The Journal of Biological Chemistry **273**(35): 22298-22304.

Pinderi, V. (2017). The Role of Phosphatidylserine as a Scaffold for Lipid/Protein Complexes. Bachelor of Science Major Qualifying Project, Worcester Polytechnic Insitute

Pulido, R. (2015). "PTEN: a yin-yang master regulator protein in health and disease." Methods **77-78**: 3-10.

Redfern, D. A. and A. Gericke (2005). "pH-dependent domain formation in phosphatidylinositol polyphosphate/phosphatidylcholine mixed vesicles." *JLipid Res* **46**(3): 504-515.

Redfern, D. G., A. (2004). "Domain Formation in Phosphatidylinositol Monophosphate/Phosphatidylcholine Mixed Vesicles." *Biophysical Journal* **86**: 2980-2992.

Redfern, R. e. a. (2008). "PTEN Phosphatase Selectively Binds Phosphoinositides and Undergoes Structural Changes." *Biochemistry* **47**: 2162-2171.

Rheenen, J. A., E.M; Janssen, H.; Calafat, J. and Jalink, K. (2005). "PIP2 signaling in lipid domains- a critical re-evaluation." *The EMBO Journal* **24**(9): 1664–1673.

Ross, A. H. and A. Gericke (2009). "Phosphorylation keeps PTEN phosphatase closed for business." *Proc Natl Acad Sci U S A* **106**(5): 1297-1298.

Saarikangas, J., H. Zhao and P. Lappalainen (2010). "Regulation of the actin cytoskeleton-plasma membrane interplay by phosphoinositides." *Physiol Rev* **90**(1): 259-289.

Saarikangas, J. Z., H.; Pykäläinen, A., et al. (2009). "Molecular mechanisms of membrane deformation by I-BAR domain proteins." *Curr Biol*. **19**(2): 95-107.

Salvemini, I. L., D. M. Gau, J. Reid, L. A. Bagatolli, A. Macmillan and P. D. Moens (2014). "Low PIP(2) molar fractions induce nanometer size clustering in giant unilamellar vesicles." *Chem Phys Lipids* **177**: 51-63.

Sarmiento, M. J., A. Coutinho, A. Fedorov, M. Prieto and F. Fernandes (2014). "Ca(2+) induces PI(4,5)P2 clusters on lipid bilayers at physiological PI(4,5)P2 and Ca(2+) concentrations." *Biochim Biophys Acta* **1838**(3): 822-830.

Schink, K. O., K. W. Tan and H. Stenmark (2016). "Phosphoinositides in Control of Membrane Dynamics." *Annu Rev Cell Dev Biol* **32**: 143-171.

Shenoy, S., P. Shekhar, F. Heinrich, M. C. Daou, A. Gericke, A. H. Ross and M. Losche (2012). "Membrane association of the PTEN tumor suppressor: molecular details of the protein-membrane complex from SPR binding studies and neutron reflection." *PLoS One* **7**(4): e32591.

Shi, S. H. J. L. Y. J., Y.N. (2003). "Hippocampal Neuronal Polarity Specified by Spatially Localized mPar3/mPar6

and PI 3-Kinase Activity." *Cell* **112**: 63-75.

Slochow, D. R., P. J. Huwe, R. Radhakrishnan and P. A. Janmey (2013). "Quantum and all-atom molecular dynamics simulations of protonation and divalent ion binding to phosphatidylinositol 4,5-bisphosphate (PIP2)." *J Phys Chem B* **117**(28): 8322-8329.

Slochow, D. R., Y. H. Wang, R. W. Tourdot, R. Radhakrishnan and P. A. Janmey (2014). "Counterion-mediated pattern formation in membranes containing anionic lipids." *Adv Colloid Interface Sci* **208**: 177-188.

Song, M. S., L. Salmena and P. P. Pandolfi (2012). "The functions and regulation of the PTEN tumour suppressor." *Nat Rev Mol Cell Biol* **13**(5): 283-296.

Stahelin, R. V., J. L. Scott and C. T. Frick (2014). "Cellular and molecular interactions of phosphoinositides and peripheral proteins." *Chem Phys Lipids* **182**: 3-18.

Stetefeld, J., S. A. McKenna and T. R. Patel (2016). "Dynamic light scattering: a practical guide and applications in biomedical sciences." *Biophys Rev* **8**(4): 409-427.

Stokoe, D. (1997). "Dual Role of Phosphatidylinositol-3,4,5-trisphosphate in the Activation of Protein Kinase B." *Science* **277**: 567-570.

Sud, M., E. Fahy, D. Cotter, A. Brown, E. A. Dennis, C. K. Glass, A. H. Merrill, Jr., R. C. Murphy, C. R. Raetz, D. W. Russell and S. Subramaniam (2007). "LMSD: LIPID MAPS structure database." *Nucleic Acids Res* **35**(Database issue): D527-532.

Sun, H. e. a. (1999). "PTEN modulates cell cycle progression and cell survival by regulating phosphatidylinositol 3,4,5,-trisphosphate and Akt/protein kinase B signaling pathway." *Proc Natl Acad Sci U S A* **96**: 6199-6204.

Surewicz, W. K. M., H.H. ; Chapman, D. (1992). "Determination of protein secondary structure by Fourier Transform Infrared Spectroscopy: A critical assessment." *Biochemistry* **32**(2): 390-394.

Surewicz, W. K. M., H.H.; Chapman,D. (1993). "Determination of protein secondary structure by Fourier-Transform Infrared spectroscopy — A critical assessment." *Biochemistry* **32**: 389-394.

Swairjo, M. A. B. A. S., B.A.; et al. (1994). "Effect of vesicle composition and curvature on the dissociation of phosphatidic acid in small unilamellar vesicles-a  $^{31}\text{P}$ -NMR study." *Biochim Biophys Acta* **1191**(2): 354-361.

Szymonowicz, K., S. Oeck, N. M. Malewicz and V. Jendrossek (2018). "New Insights into Protein Kinase B/Akt Signaling: Role of Localized Akt Activation and Compartment-Specific Target Proteins for the Cellular Radiation Response." *Cancers (Basel)* **10**(3).

Tahirovic, S. and F. Bradke (2009). "Neuronal polarity." *Cold Spring Harb Perspect Biol* **1**(3): a001644.

Tamguney, T. and D. Stokoe (2007). "New insights into PTEN." *J Cell Sci* **120**(Pt 23): 4071-4079.

Tan, J. and J. A. Brill (2014). "Cinderella story: PI4P goes from precursor to key signaling molecule." *Crit Rev Biochem Mol Biol* **49**(1): 33-58.

Tobias, D. J. a. H., J.C. (2008). "Getting Specific About Specific Ion Effects." *Science* **319**(5867): 1197-1198.

Toner, M., G. Vaio, A. McLaughlin and S. McLaughlin (2002). "Adsorption of cations to phosphatidylinositol 4,5-bisphosphate." *Biochemistry* **27**(19): 7435-7443.

Toner, M. V., G. ; et al. (1988). "Adsorption of cations to phosphatidylinositol 4,5-bisphosphate." *Biochemistry* **27**(19): 7435-7443.

Tong, J. N., L.; et al. (2008). "Role of GAP-43 in sequestering phosphatidylinositol 4,5-bisphosphate to Raft bilayers." *Biophys J* **94**(1): 125-133.

Tonks, N. K., et al. (1998). "The lipid phosphatase activity of PTEN is critical for its tumor suppressor function." *Proc. Natl. Acad. Sci. USA* **95**: 13513–13518.

van den Bogaart, G., K. Meyenberg, H. J. Risselada, H. Amin, K. I. Willig, B. E. Hubrich, M. Dier, S. W. Hell, H. Grubmuller, U. Diederichsen and R. Jahn (2011). "Membrane protein sequestering by ionic protein-lipid interactions." *Nature* **479**(7374): 552-555.

van Meer, G., D. R. Voelker and G. W. Feigenson (2008). "Membrane lipids: where they are and how they behave." *Nat Rev Mol Cell Biol* **9**(2): 112-124.

van Paridon, P. A. d. K., B.; et al. (1986). "Polyphosphoinositides undergo charge neutralization in the physiological pH range: a <sup>31</sup>P-NMR study." *Biochem Biophys Acta* **877**(1): 216-219.

van Rheenen, J., E. M. Achame, H. Janssen, J. Calafat and K. Jalink (2005). "PIP2 signaling in lipid domains: a critical re-evaluation." *EMBO J* **24**(9): 1664-1673.

Viaud, J., R. Mansour, A. Antkowiak, A. Mujalli, C. Valet, G. Chicanne, J. M. Xuereb, A. D. Terrisse, S. Severin, M. P. Gratacap, F. Gaits-Iacovoni and B. Payraastre (2016). "Phosphoinositides: Important lipids in the coordination of cell dynamics." *Biochimie* **125**: 250-258.

Wang, J. S., H.; Macia, E.; Kirchhausen, T.; Watson, H.; Bonifacino, J.S.; Yin, H.L. (2007). "PI4P promotes the recruitment of the GGA adaptor proteins to the trans-Golgi network and regulates their recognition of the ubiquitin sorting signal." *Molecular Biology of the Cell* **18**: 2646-2655.

Wang, L., Y. L. Cho, Y. Tang, J. Wang, J. E. Park, Y. Wu, C. Wang, Y. Tong, R. Chawla, J. Zhang, Y. Shi, S. Deng, G. Lu, Y. Wu, H. W. Tan, P. Pawijit, G. G. Lim, H. Y. Chan, J. Zhang, L. Fang, H. Yu, Y. C. Liou, M. Karthik, B. H. Bay, K. L. Lim, S. K. Sze, C. T. Yap and H. M. Shen (2018). "PTEN-L is a novel protein phosphatase for ubiquitin dephosphorylation to inhibit PINK1-Parkin-mediated mitophagy." *Cell Res* **28**(8): 787-802.

Wang, X., X. Cao, R. Sun, C. Tang, A. Tzankov, J. Zhang, G. C. Manyam, M. Xiao, Y. Miao, K. Jabbar, X. Tan, Y. Pang, C. Visco, Y. Xie, K. Dybkaer, A. Chiu, A. Orazi, Y. Zu, G. Bhagat, K. L. Richards, E. D. Hsi, W. W. L. Choi, J. H. van Krieken, J. Huh, M. Ponzoni, A. J. M. Ferreri, M. B. Moller, B. M. Parsons, J. N. Winter, M. A. Piris, S. Li, R. N. Miranda, L. J. Medeiros, Y. Li, Z. Y. Xu-Monette and K. H. Young (2018). "Clinical Significance of PTEN Deletion, Mutation, and Loss of PTEN Expression in De Novo Diffuse Large B-Cell Lymphoma." *Neoplasia* **20**(6): 574-593.

Wang, X. and X. Jiang (2008). "Post-translational regulation of PTEN." *Oncogene* **27**(41): 5454-5463.

Wang, Y. H., A. Collins, L. Guo, K. B. Smith-Dupont, F. Gai, T. Svitkina and P. A. Janmey (2012). "Divalent cation-induced cluster formation by polyphosphoinositides in model membranes." *J Am Chem Soc* **134**(7): 3387-3395.

Wang, Y. H., D. R. Slochower and P. A. Janmey (2014). "Counterion-mediated cluster formation by polyphosphoinositides." *Chem Phys Lipids* **182**: 38-51.

Wen, Y., V. M. Vogt and G. W. Feigenson (2018). "Multivalent Cation-Bridged PI(4,5)P<sub>2</sub> Clusters Form at Very Low Concentrations." *Biophys J* **114**(11): 2630-2639.

Wood, W. G., U. Igbavboa, W. E. Muller and G. P. Eckert (2011). "Cholesterol asymmetry in synaptic plasma membranes." *J Neurochem* **116**(5): 684-689.

Xiao, M., Y. An, F. Wang, C. Yao, C. Zhang, J. Xin, Y. Duan, X. Zhao, N. Fang and S. Ji (2018). "A chimeric protein PTEN-L-p53 enters U251 cells to repress proliferation and invasion." *Exp Cell Res* **369**(2): 234-242.

Yeung, T., B. Heit, J. F. Dubuisson, G. D. Fairn, B. Chiu, R. Inman, A. Kapus, M. Swanson and S. Grinstein (2009). "Contribution of phosphatidylserine to membrane surface charge and protein targeting during phagosome maturation." *J Cell Biol* **185**(5): 917-928.

Yeung, T. G., G.E.; Shi, J.; Silvius, J.; Kapus, A.; Grinstein, S. (2008). "Membrane Phosphatidylserine Regulates Surface Charge and Protein Localization." *Science* **319**: 210-213.

Yin, H. L. J., P. A. (2003). "Phosphoinositide regulation of the actin cytoskeleton." *Annu Rev Physiol* **65**: 761-789.

Zhang, X., B. Yin, F. Zhu, G. Huang and H. Li (2015). "A PTEN translational isoform has PTEN-like activity." *Chin J Cancer Res* **27**(5): 524-532.

Zhao, H. M., A.; Koskela, E.V., et al. (2013). "Membrane-sculpting BAR domains generate stable lipid microdomains." *Cell Rep.*(4): 1213-1223.